UNIVERSITY OF CALIFORNIA, MERCED

FRACTIONAL ORDER MODELING AND CONTROL OF MULTI-INPUT-MULTI-OUTPUT PROCESSES

By

Zhuo Li

A Dissertation

Submitted in partial satisfaction of the requirements for the degree of

Doctor of Philosophy

in

Electrical Engineering

Committee in Charge:

Professor YangQuan Chen, Chair
Professor Gerardo Diaz
Professor Stefano Carpin

2015

The dissertation of Zhuo Li is approved:

YangQuan Chen, Chair Date

Gerardo Diaz Date

Stefano Carpin Date

University of California, Merced

To my hopes.

Contents

List of Figures

List of Tables

Abstract

Fractional calculus is a mathematical tool for augmenting conventional integrals and derivatives. When introduced to control theory, it poses new opportunities and challenges for engineers. In the literature, pioneers have revealed the benefits brought to some general control theory by fractional order (FO) modeling and control techniques. Yet, there has not been a systematic study of such techniques for specific industrial processes. Therefore, this dissertation makes the efforts to fulfill the task. This research originates from the equipment control in the semi-conductor manufacturing industry, and most problems under discussion are very practical. Newly developed methodologies for solving these problems are exhibited: for example, the relay feedback identification of FO models, auto-decoupling of FO multi-input-multi-output (MIMO) processes, relative gain array of FO MIMO processes, feedback linearization of nonlinear FO systems, and the FO sliding-mode based extreme seeking control for impedance matching, etc. In addition, comprehensive literature surveys on relevant topics are provided; and an extensive review and evaluation of existing numerical tools for fractional calculus and FO controls are conducted. Novel concepts, such as the pseudo frequency response, are promoted; and potential future research opportunities are identified. Through these efforts, fractional order modeling and control are expected to receive wider adoption so that this powerful tool can be used more broadly for the development of modern industry.

Fractional calculus is like a mutated gene fragment which generates varieties of research spices when it is grafted to any research breed. Beside the research in the scope of pure FO modeling and control, a cadenza chapter is provided in the end of this dissertation, in which some interesting thinking, experimental results and hypothesis on miscellaneous research topics are presented. These discussions involve topics related to either fractional calculus or controls, such as Arduino based control demo gadgets for education, EtherCAT timing jitter characterization, Lévy distribution based random search, fractal analysis of the financial market, a Hurst exponent based technical indicator, etc.

Acknowledgments

I would first like to thank my advisor, Prof. YangQuan Chen, for the high-quality guidance he provided me with throughout my program of study. I wish to especially thank him for the great opportunities, for the stimulating learning environment, for the inspiring research resources, for the lavish laboratory legacy, for broadening my vision in research, for the influential passionate working style, and for everything else he has provided for me.

Thank you to my academic committee members, Prof. Gerardo Diaz and Prof. Stefano Carpin, for their devoted course teaching and time spent on advising me. Thank you to the department and campus staff, Ms. Heather Jackson, Ms. Tomiko Hale, Ms. Becky Mirza, Ms. Choua Moua, Ms. Pamela Leonard, *et al.* for their assistance on paperwork processing. Thank you to my undergraduate advisor Prof. Yong Wang in USTC, and master advisor Prof. Bai Li in Temple University, for their early guidance.

I wish also to express my gratefulness to my industrial mentors in Lam Research Corporation, Dr. Tao Zhang, Dr. John Daugherty, Dr. Jure Zaninovich and Dr. Fred Egley, *et al.*, for their kind supervision and funding support. The industrial platforms and practical problems provided by them further motivated my passion in doing this research.

Thank you to my lab colleagues, Dr. Chun Yin, Sina Dehghan, Tiebiao Zhao, Brendan Smith, Brandon Stark, Prof. Zhigang Lian, Prof. Jiacai Huang, Fudong Ge, Prof. Guimei Zhang, *et al.* Forgive me for not listing everyone's name since there are too many. With them, I know I'm not fighting alone in the countless days and nights.

A special thank you to my parents for their substantial and spiritual support. Thank you to my ex-girlfriend Meng Duan. If my life is compared to the shale, she lays the most gorgeous layer during its formation. I would love to borrow the following lyrics to thank all of those who helped me through out this process.

"I've never been stranded, abandoned
Or left here to fight alone
So I'm giving you control
...
If peace is a river let it sweep over me
If I'm under fire I know it's refining me
When I hear you calling out I follow now
Wherever the road may go
I know you're leading me home"
— "Lift my life up" lyrics by Unspoken

CURRICULUM VITAE

Education

- M.S. in Electrical Engineering, Temple University, Philadelphia, PA, USA, 2011.
- B.S. in Automation, University of Science and Technology of China (USTC), Hefei, China, 2009.

Publications

[1] Zhuo Li, Tiebiao Zhao and YangQuan Chen, "Fractional order model predictive control of a thermal process using hardware-in-the-loop RIOTS", To be submitted to Control Engineering Practice, 2015.

[2] Zhuo Li, Lu Liu, Sina Dehghan, YangQuan Chen and DingYu Xue, "A review and evaluation of numerical tools for fractional calculus and fractional order controls", Submitted to the International Journal of Control, 2015.

[3] Zhuo Li, Fudong Ge, YangQuan Chen and Chunhai Kou, "Fractional order feedback linearization", To be submitted to Journal of Process Control, 2015.

[4] Fudong Ge, YangQuan Chen, Chunhai Kou and Zhuo Li, "Stability analysis for a time fractional order anomalous diffusion equation with uncertain disturbance on the boundary", Submitted to Journal of Mathematical Analysis and Applications, 2015.

[5] Chun Yin, Yuhua Cheng, Shouming Zhong, J Cao and Zhuo Li, "Fractional-order sliding mode-extremum seeking control design with fractional-order PI sliding surface", In Proc. of the 34^{th} Chinese Control Conference (CCC), Hangzhou, China. 2015.

[6] Jiacai Huang, YangQuan Chen and Zhuo Li, "Mathematical model of human operator using fractional calculus for human-in-the-loop control", In Proc. of the 2015 ASME IDETC/CIE, Boston, MA, USA. Aug 2015.

[7] Zhigang Lian, Zhuo Li and YangQuan Chen, "A new cuckoo search method", Submitted to the 2015 ASME IDETC/CIE, Boston, MA, USA. Aug, 2015.

[8] Zhuo Li, Chun Yin, and YangQuan Chen, "Plasma impedance matching using fractional order sliding mode based extremum seeking control", In Proc. of the 53^{rd} IEEE Conference on Decision and Control (CDC), Los Angeles, CA, USA. 2014.

[9] Tiebiao Zhao, YangQuan Chen and Zhuo Li, "Fractional order nonlinear model predictive control using RIOTS_95", The International conference on fractional differentiation and its applications (ICFDA'14), Catania, Italy. 2014.

[10] Zhuo Li, Tiebiao Zhao and YangQuan Chen, "A low cost research platform for modeling and control of multi-input multi-output fractional order dynamic systems", In Proc. of the ICFDA'14, Catania, Italy. Aug, 2014.

[11] Zhuo Li, Chun Yin, YangQuan Chen and Jiaguo Liu, "Process identification using the relay feedback with a fractional order integrator", In Proc. of the 19^{th} IFAC World Congress. Cape Town, South Africa. Aug, 2014.

[12] Zhuo Li and YangQuan Chen, "Ideal, simplified and inverted decoupling of fractional order TITO processes", In Proc. of the 19^{th} IFAC World Congress. Cape Town, South Africa. Aug, 2014.

[13] Zhuo Li and YangQuan Chen, "Identification of linear fractional order systems using the relay feedback approach", In Proc. of the 2014 American Control Conference (ACC), Portland, OR, Jun, 2014.

[14] Chun Yin, Zhuo Li, YangQuan Chen and Shouming Zhong, "Fractional order sliding mode control based on fractional order reaching law: reaching condition analysis, and experimental validation", In Proc. of the 2013 ASME IDETC/CIE, Portland, OR, USA. Aug 2013.

[15] Brandon Stark, Zhuo Li, Brendan Smith, and YangQuan Chen, "Take-home mechatronics control labs: a low-cost personal solution and educational assessment", In Proc. of the 2013 ASME IDETC/CIE, Portland, OR, USA. 2013.

[16] Zhuo Li, Nathan Hoffer, Brandon Stark, and YangQuan Chen, "Design, modeling and validation of a T-tail unmanned aerial vehicle", Journal of Intelligent and Robotic Systems 69(1-4): pp. 91-107, 2013.

[17] Wenjing Li, Zhuo Li and Suyue Qin, "Simulation of a multi-agent based game model for financial credit risk of supply chain", System Engineering - Theory & Practice, Vol 32, 2012, (In Chinese).

[18] Zhuo Li, A multi-agent based approach for solving the redundancy allocation problems, M.S. Thesis, Department of Electrical and Computer Engineering, Temple University, Philadelphia, PA, USA. Aug 2011.

Working Experience

- May-Dec, 2012, Consultant, Lam Research Corp., Fremont, CA, USA.
- Jun-Jul, 2011, Intern, Mercury Systems Inc., Princeton, NJ, USA.
- Jun-Jul, 2010, Intern, China Unicom Co., Ltd., Zhengzhou, China.

ACRONYMS

AIC	Akaike information criterion
ARMA	Autoregressive-moving-average
BIBO	Bounded-input bounded-output
CCP	Capacitively coupled plasma
CRONE	The (French) acronym of Commande robuste d'ordre non-entier (Robust fractional order control)
CTRW	Continuous-time random walk
DF	Describing function
DSP	Digital signal processor
E-L	Euler-Lagrange
EMF	Electromagnetic force
ESC	Extremum seeking control
ESC_1	Electrostatic chucks
ESC_2	Electronic speed control
ETFs	Exchanged traded funds
EtherCAT	Ethernet for control automation technology
EVD	Electron velocity distribution
fBm	Fractional Brownian motion
FC	Fractional calculus
FF	Feed-forward
FKF	Fractional Kalman filter
FO	Fractional order
FPGA	Field-programmable gate array
FrFT	Fractional Fourier transform
FVO	Fractional variable order
G-L	Grünwald-Letnikov
HIL	Hardware-in-the-loop
IAE	Integral absolute error
ICP	Inductively coupled plasma
IED	Ion energy distribution
IIR	Infinite impulse response
ILC	Iterative learning control
IRID	Impulse response invariant discretization
ISIs	Inter-spike intervals
LMI	Linear matrix inequality
LTI	Linear time-invariant

MACD	Moving average convergence/divergenc
MEMS	Micro-electro-mechanical systems
MESA	Mechatronics, Embedded Systems and Automation
MFD	Matrix fractional description
MIMO	Multi-Input-Multi-Output
M-L	Mittag-Leffler
MPC	Model predictive control
MSD	Mean squared displacement
NILT	Numerical inverse Laplace transform
N-S	Navier-Stokes
NP	Nondeterministic polynomial time
ODE	Ordinary differential equation
OO	Object-oriented
pdf	Probability density function
PDF	Probability distribution function
PE	Persistent excitation
PFR	Pseudo frequency response
PID	Proportional-integral-derivative
PRBS	Pseudo-random binary sequence
PSO	Particle swarm optimization
RF	Radio frequency
RGA	Relative gain array
RIOTS	Recursive integration optimal trajectory solver
R-L	Riemann-Liouville
RL	Root locus
RMS	Root mean square
RTW	Real-time workshop
SISO	Single-Input-Single-Output
S-S	State-space
SVD	Singular value decomposition
TF	Transfer function
TITO	Two-Input-Two-Output
UAV	Unmanned arial vehicle
VIX	CBOE's S&P 500 volatility index
W-H	Wiener-Hammerstein
Z-N	Ziegler-Nichols

Chapter 1

Introduction

> "Being happy doesn't mean that everything is perfect. It means that you've decided to look beyond the imperfections."
>
> — Gerard Way

Control is just such a technique that trades off among stability, transient and steady state performance, time or fuel optimality, etc.

1.1 Background and motivation

Control is an old subject that has greatly advanced over time. It is like an ancient ancestor flowing young blood, which has always received intensive attention in the research field. Back to 2000 years ago, people in Greeks, Arabs and Ancient Rome had made cognition of the principle of feedbacks, based on which fantastic projects were built. The float valve level regulator for water clocks (figure 1.1(a)) and shower systems in the imperial palace, and the automatic gates in the temples are some of the brilliant works, [4]. In 132 A.D. (Han Dynasty), the Chinese polymath Zhang Heng invented the seismograph based on the "suspended pendulum" principle, which is another famous application containing the thoughts of control. The first formally adopted automatic control system in the modern sense should count James Watt's speed regulator for the steam engine in 1788 [5], as shown in figure 1.1(b).

Enjoying a long history, control has a vast application across all aspects in daily human life, from agriculture to industry, from healthcare to military, etc. The implementation of controls can be as simple as an auto-flush toilet or as complicated as the launch of a rocket. On the other hand, there are also limitations of this seemingly omnipotent methodology. It cannot guarantee to achieve arbitrary improvement with a given mechanical settings. This is one of the reasons why in the industry, companies sometimes tend to reconstruct the hardware structures rather than to upgrade an equivalently cost control. Nevertheless, control is still an indispensable modern technology. As expressed in the quote at the beginning of this chapter, control is a similar manner of seeking a balance among numerous performance indices under mutually constraining factor because "no pain no gain".

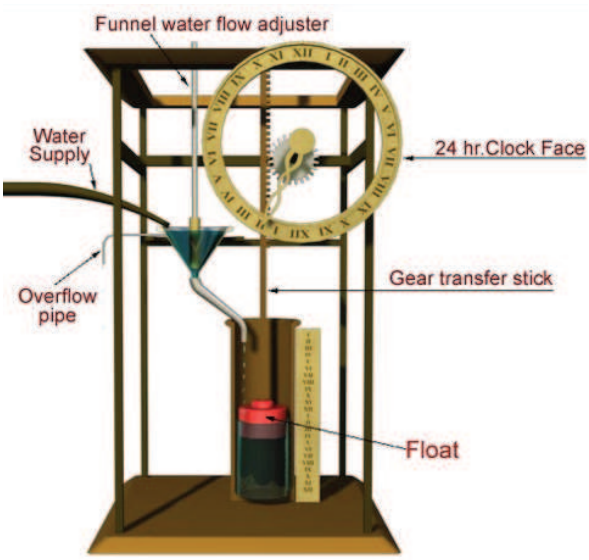

(a) The schematic of the water clock.

(b) Watt's centrifugal governor.

Figure 1.1: The ancient and modern automatic control systems.

The classification of controls can be diverse. As shown in table 1.1, it can be classified as open-loop and closed-loop control by mode. By direction, it can be classified into feed-forward, feedback and composite control. By the signal type, it can be classified as continuous control, discrete control, or hybrid. By mathematic models, it can be classified as linear, non-linear, time varying and time invariant controls, [5]. Finally, it can be classified into motion controls and process controls by the control objects under investigation.

Table 1.1: The classification of controls

Criteria	Classification		
Mode	Open-loop	Closed-loop	Hybrid
Direction	Feed-forward	Feedback	Hybrid
Signal type	Continuous (Analog)	Discrete (Digital)	Hybrid
Models	Linear/Non-linear	Time varying/invariant	Hybrid
Objects	Motion control	Process control	Hybrid

As the name implies, motion control deals with motions in most cases. The control objects usually involve the position, velocity and acceleration of electrical, hydraulic or pneumatic movable devices, such as motors, servos, solenoids, linea actuators, cylinders, pistons, and even crystal oscillators. Their advantages and applicable scenarios can be found in control related textbooks, e.g. [6, 7]. Motion control has changed people's life style in a great extent. The typical products such as automobile and industrial robots librate human beings from cumbersome labor work.

In contrast with motion controls whose objectives pursue the transient performance of reaction, process controls emphasize more on reliability and repeatability. Process control

is an engineering discipline that deals with architectures, mechanisms and algorithms for a specific process [8]. The control objects involved are often temperature, flame intensity, pressure, fluid flow, liquid level, *et. al.* Distinguishable characteristics of process controls usually include: 1) big nonlinearity, 2) big delay, 3) big lag, 4) big loop-interaction, and 5) big number of control variables. For example, thousands of control valves, countless pipelines and containers in a petroleum refining process are very normal. From this perspective, if the control of the motor driven or hydraulic valves in process control is treated as motion control, then, process control has a broader meaning [8].

Again, regarding reliability, process engineering has more diversified work to do than other industries such as information technology (IT). In those industries, it is not desired, yet is usually tolerable if the servers are down because reboot or alternate equipments can act as backups. Even scheduling an off-line maintenance during idle time, e.g. $2:00\text{am} \sim 4:00\text{am}$, will not cause disaster. However, it is not the case for process engineering. Many factories are designated to runs 24/7 continuously for years until an shut-down maintenance [5], such as the blast furnace. Hence, system breaking down is intolerable. In these circumstances, systematic and reliable process control theory reveals its importance.

As this old subject seemingly steps into its sunset age, new vitality is injected when the fractional calculus is introduced into the control theory. Factional calculus was born 300 years ago, and the research on fractional calculus experienced its boom in the past decades, especially in the field of controls. While the application of fractional order controls enjoyed a wide popularity, it spawned two major branches: fractional order (FO) modeling and fractional order control, which consequently formed three combinations in academic research and practical implementation:

1. Integer order control of fractional order process plants/models;
2. Fractional order control of integer order process plants/models;
3. Fractional order control of fractional order process plants/models.

Regarding these topics, many existing methodologies and principles are waiting to be augmented; meanwhile, dedicated new theory and methods need to be developed to deal with the sprouting circumstances. Motivated by these practical demands, the research in this dissertation is carried out, focusing on the following three aspects: 1.) characterizing specific industrial processes in higher accuracy using fractional order models; 2.) extending the existing integer order control techniques to fractional order cases; and 3.) developing novel FO control techniques dedicated to FO processes in the industry.

A larger hope behind the motivation of this dissertation is to push the FO control to broader implementation, so that one day, it is commonly utilized in off-the-shelf products that benefit the industry, since there has not yet been massive commercial products running FO control algorithms. For this purpose, the author chooses to organize the content with the modeling and control of a thermal process in the semiconductor manufacturing industry as a main thread, while many related topics are reviewed or explored during this procedure.

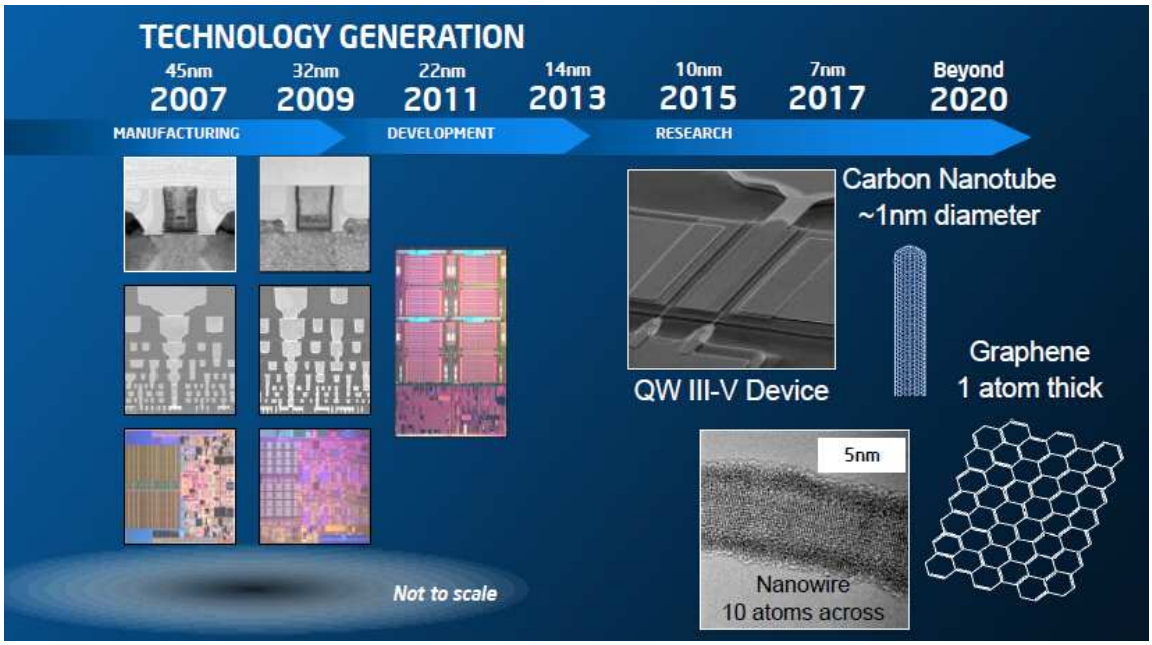

Figure 1.2: The technology generation of the semiconductor fabrication industry. Figure from [1].

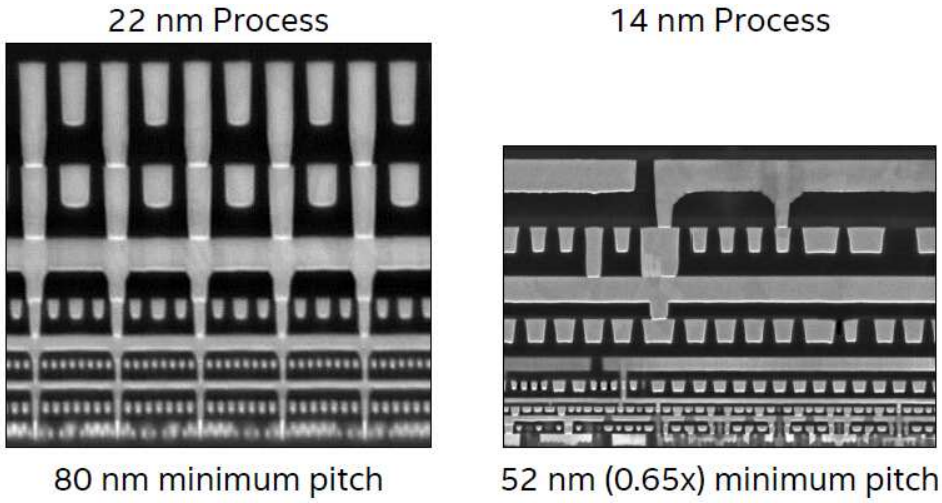

Figure 1.3: The pitch interconnects in Intel's 14 nm process. Figure from [1].

1.2 Applications

Process control is a crucial part in many conventional and emerging industries, such as steeling, petrochemical, winery, material processing, surface treatment, micro-electro-mechanical systems (MEMS) manufacturing, etc. In particular, this research originates from the practical problems posed in the recipe control of plasma etching processes, which is the most important key step in the semiconductor fabrication industry. Figure 1.2 displays the timeline of the technology generation of this industry. Some fantastic component samples produced by this state-of-the-art technology are shown in figure 1.3, such as Intel's 14nm tri-gate

transistor fins.

As one can imagine, such micro level chemical processes require high precision control of the process variables of the fabrication tool shown in figure 1.4. While the task is becoming more challenging, the fusion of fractional calculus into process control makes process engineers more equipped. Some results in this research have already revealed advantages and benefits, and are expected to further fulfill the performance improvement of this industrial process. Moreover, the developed methodologies are not narrowed to this industry, and the author would be more than pleased to see their wider application in other modern industrial areas wherever implementable.

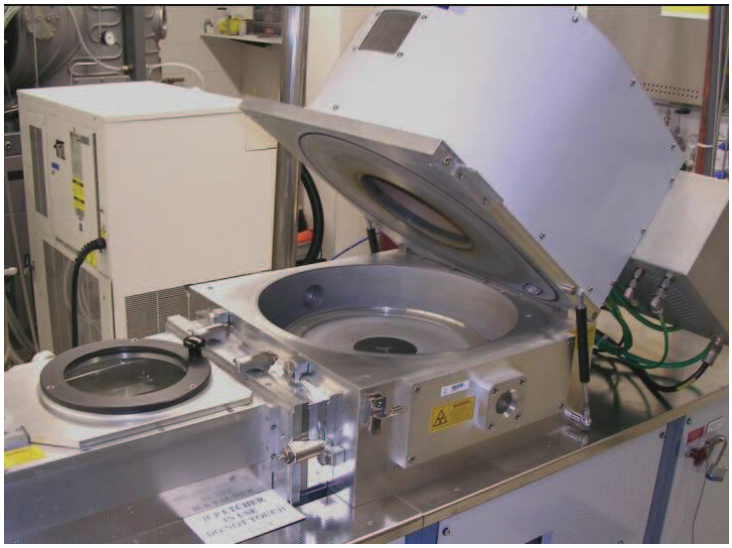

(a) Oxford ICP 100 Dry Etcher. [9].

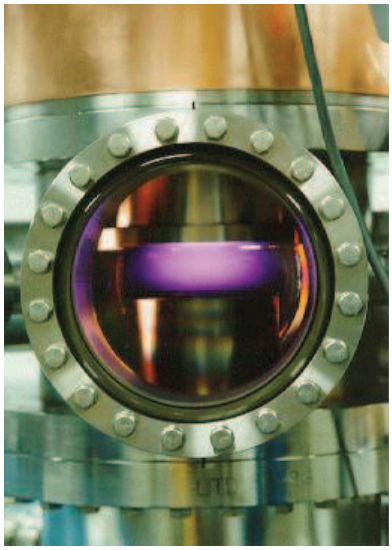

(b) ICP plasma. [10].

Figure 1.4: Photos of plasma etching tools.

1.3 Contributions

Besides a comprehensive literature review and the gathering of scattered relevant methodologies, the major contributions that distinguish this dissertation from other existing work are briefly highlighted below:

1. An extensive collection of Matlab based numerical tools for FC and FO controls are organized and documented; some basic evaluations are performed in order to provide a guidance for selecting the use of these tools; a very informative table (table 2.3) of these tools is created, in section 2.4;
2. The inverse response of FO transfer function models is explored for the first time based on real world observation and practical data; the condition for a class of fractional order LTI models to exhibit inverse response behavior is presented numerically; Time domain characteristics of such FO models are documented. See section 2.3;
3. Novel frequency domain parameter identification methods are developed for fractional order LTI models, including the relay feedback approach, and using relay with FO

integrator to identify integer or fractional order models; a pseudo frequency response (PFR) concept is proposed to unify the math operation of describing functions and transfer functions, which is used to analyze systems consist of both linear and nonlinear elements, in section 3.3;

4. The feedback linearizatin of autonomous nonlinear fractional order processes is proposed in section 3.4.3.
5. Auto-decoupling of fractional order MIMO processes is investigated; the frequency dependent relative gain array (RGA) for FO LTI models is derived, in section 4.2;
6. Simulation and/or implementation of the newly developed theory in real-world practice is presented, such as auto-decoupling FO processes, FO model predictive control (MPC) using RIOTS on a Peltier temperature control platform, FO extreme seeking control (ESC) for impedance matching, in Chapter 5;
7. A "potential model" concept is proposed for the identification and control of both fractional and integer order nonlinear processes, in section 5.5.
8. Multiple software "by-products" are developed along with the main thread of research, to name a few, the xPC-target based industrial data acquisition and analysis software suite, the Simulink block for Arduino I^2C communication, a Matlab function for plotting the root locus of FO transfer functions, in section 2.3, LevyPSO in section 6.1, etc. Some of them are shared in the relevant community, such as Matlab Central and Sparkfun Forums;
9. The use of FC in miscellaneous research fields are explored, such as random search, EtherCAT timing jitter characterization and financial market analysis, some interesting attempts and results are revealed, chapter 6.
10. New problems are identified as potential future research efforts, such as embedding the RIOTS and the fractional Rayleigh's differential equation, section 2.2.

A shortcoming of the current research on fractional order controls is that some methodology appears prior to the real application. They are developed from pure theoretical extension, but not originated from practical phenomenon. For example, the identification algorithms of fractional order Hammerstein models are documented in the literature, yet, there is no report of real-world implementation that utilize these algorithms up to now; a similar case is the fractional order non-minimum phase behavior. Hence, in addition to the theoretical development, a notable contribution of this dissertation resides in the supply of actual data that is able to support, verify or inspire the existing and further research in this area.

This dissertation covers a variety of topics across multiple academic disciplines due to the requirements of the sponsoring project. Hence, the contents in some chapters cross multiple disciplines. By and large, the rest of the dissertation are organized as follows. Chapter 2 provides math preliminaries for the following chapters, where related topics are reviewed, such as several selected typical fractional differential equations. The last two sections present survey summaries and provide new results. Chapter 3 focuses on the modeling and identification of fractional order processes, in which some novel theoretical developments and concepts are stated, such as the relay feedback identification of FO processes and fractional feedback

linearization. Chapter 4 addresses the control of fractional processes, including both SISO and MIMO processes. Novel topics such as fractional order auto-decoupling can be found in this chapter. All the simulation and experimental results are arranged to Chapter 5, which makes it "*data-heavy*". Many interesting problem descriptions, figures, outcomes and conclusions are put in this chapter. Chapter 6 is a cadenza chapter that serves like a back yard of related miscellaneous fruits behind the main field of research. The overall dissertation is summarized in Chapter 7, with the outlook of future research opportunities.

1.4 Literature review

Fractional calculus has been found application in a number of engineering disciplines, such as in electrical engineering [11, 12, 13], mechanical engineering [14, 15], environmental engineering [16], and bioengineering [17, 18], etc. Some general review papers and books on FC and FO controls can be found in [19], [20], [21], [22] and [23].

Up to now, introducing fractional calculus into the control theory is no long a brand new topic considering the earliest prototype work by Bode and Tustin *et al.*, [24], and the follow-ups in the 80s, [25] and [26]. As its advantages draw more and more attention, the publication volume on relevant research increases significantly, which witnessed its blossom in recent years. Figure 1.5 shows the publication histogram on Web of Sciences searched by the key words "fractional order control". Among the massive academically accessible publications, some notable and representative work are enumerated in this section for a relatively comprehensive review, with the main focus on fractional order modeling and control. More publications on specific and interesting topics are reviewed according to necessity within the individual sections where they are involved.

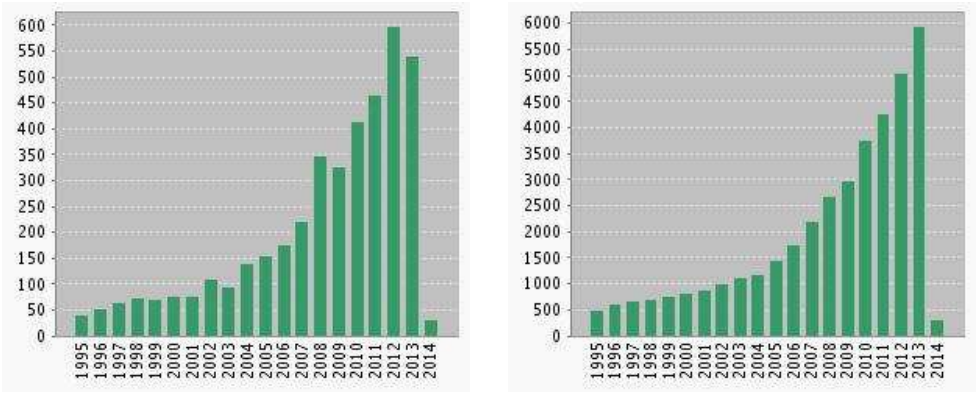

(a) The increase in publication. (b) The increase in citation.

Figure 1.5: The statistics of academic publication on FO controls [by Apr 2014].

Reviewed by Research Groups

The value of fractional order controls was discovered by more and more people after its debut. Among the pioneers, the contribution of Podlubny's group receives wide adoption. The paper [27] revealed the benefits of modeling dynamic systems with arbitrary real orders and proposed the concept of fractional order $PI^{\lambda}D^{\mu}$ controllers. A survey on stability of FO

systems with rational orders is presented in [28]. The analogue realizations of FO systems and FO controllers are studied in [29, 30, 31]. Besides the traditional scheme, advanced control technologies have also been explored for fractional order systems, e.g. [32] presented the Posicast control of fractional order processes; and the book [33] provides comprehensive investigation of fractional order nonlinear systems. They also conducted studies in modeling of some physical phenomena, such as in [34].

Chen's group is one of the leading contributors to the research field of fractional order control. To name a few, the monograph [35] and the tutorial in [36] are good resources for popularization of fractional order controls to the public who have not been familiar with fractional calculus and controls. Numerical approximation and practical implementation are also developed by Chen's group. The impulse response invariant discretization (IRID) invented by Li, Hu and Chen *et al.* is a superior method for approximating the fractional differential operators than those based on finite impulse responses (FIR), [37, 38, 39, 40]. The "flat phase" tuning rule for fractional order controllers based on the iso-damping property, [41, 42, 43, 44, 45], is proposed and received high volume of citation. The fractional order control are even applied on the flight control of unmanned arial vehicles (UAVs) [46], the control of hard-disc drive servos [47, 48], and extremum-seeking based cognitive lighting control [49, 50]. Other than these topics, their research also covers the distributed order dynamic systems [51], the stability of fractional order systems and controllers, [52, 53, 54], identification of nonlinear fractional order systems, [55], and so forth. Some unconventional control strategies are also taken into consideration. Yin *et al.* polished the adaptive sliding mode control of fractional order chaotic systems, [56]. Malek *et al.* explored maximum solar power point tracking using fractional order control scheme [57].

An important work that worth a mention is the monograph on fractional order motion controls [58], because it is one of the motivations of carrying out the present research work on process controls. In this book, numerous integer order modeling and control techniques are extended to fractional order cases, such as the the disturbance observer and "flat phase" PID tuning rule. The associated problems such as the stable region and feasible region are solved as well.

Another shining group is formed by Oustloop, Trigeassou, and Malti *et al.*, who are the members of the well-known CRONE team [59, 60]. CRONE is the French abbreviation for "Commande Robuste d'Ordre Non Entier" with the meaning of non-integer order robust control. The CRONE Toolbox developed by the group is one of the earliest (1995) Matlab/Simulink Toolbox dedicated to FO controls, based on which the CRONE control was proposed for the pursuit of fractal robustness, [61, 62, 63]. They also presented system identification approaches using fractional differentiation models [64, 65, 66, 67, 68, 69], the identification procedure for tuning robust fractional controller, [70], and nonlinear system identification using fractional Hammerstein models [71], and using fractional Volterra series, [72]. The resonance conditions of elementary fractional transfer functions are deeply investigated in [73]. [74] proposes a frequency domain method for the stability of FO differential equations based on Nyquist's theorem. [75] investigates the stability of non-integer order LTI systems, i.e. not limited to rational orders. [76] analyzes the stability of FO systems

using LMI tools.

Similar to the above group, the contribution of Valerio and Costa's group covers both theoretical analysis and numerical computation. For instance, the time domain implementation of fractional order controllers [77], and the identification of fractional models from frequency response data [22, 78]. The non-integer differentiator (ninteger) is one of the very few tools in the early days compatible with Simulink [79]. Without listing more of their work, a partial summary can be found in the book of the recent advances of fractional control [80].

Lorenzo, Hartley *et al.* are also authors making tremendous contribution. Some of their representative work are on the optimal fractional order damping in a mass-spring-damper setting [81, 82], and on finite-time controllability of FO systems [83]. They also looked into the energy consideration for mechanical "fractional-order elements" [84] which is a point of view that had seldom been touched by others. [85] is another contribution to FO system identification. Their efforts in exploring the application of fractional calculus in electrical engineering build the bridge between fractional calculus in math and engineering, [86, 87]. The implementation of fractional order operators on FPGAs (Field Programmable Gate Array) pushes the theory of FO control closer to industrial reality, [88].

Tavalzoe and Tavakoli's group addressed a lot of interesting and valuable aspects in this area. For example, the concept of viewing PI controllers as a weighting of error makes the fraction order PI controllers elegantly fit into the generalized PID forms, [89]; the energy efficiency of fractional controllers versus traditional integer order controllers is discussed in [90]; the minimal realizations for some classes of fractional order transfer functions is also studied in their work, [91].

Different identification methods for FO systems are reported by Wang's group. Specifically, [92, 93] presents the subspace identification for linear and nonlinear FO models, and [94] presents the identification of FO systems with frequency responses. The identification algorithm for MIMO FO systems in [95] provides a helpful resource for the research in this dissertation. Other than these, various topics are also explored in their publication. To list a few, in [96], a math operator called spatial product, where FO systems can be represented as a standard state space (S-S) form of partial differential equations, is proposed; the tracking differentiator based FO model reference adaptive control is discussed in [97]; in [98], sufficient and necessary condition for an FO system to be positive real is derived in terms of linear matrix inequalities (LMIs).

Lu *et. al* are another contributing group whose analysis on the robust and asymptotical stability and stabilization are remarkable [99, 100, 101].

Reviewed by Topics

Besides the enumerated work from the aforementioned groups, many well-known authors and notable works on related interesting topics are worth mentioning.

The stability analysis is always the most basic and important topic in signal, systems and controls. It is still true for fractional order scenarios. [102, 103, 104] are some relatively early research work on this topic by Matignon *et. at.* [105] discusses coprime factorizations and stability of fractional differential systems. [106] gives necessary and sufficient stability condition of FO interval linear systems. [54] investigates the Mittag-Leffler stability of

FO nonlinear dynamic systems. [107] proposed an algorithm for stabilizing FO time delay systems using FO PIDs, on which further research was carried out in [58]. [108] analyzes stability of discrete FO state-space models. Asymptotic stability analysis for SS models are studied in [109] and [110]. A numerical algorithm for stability testing of fractional delay systems is developed in [111]. [112] investigates the stability of linear FO systems with delays of the retarded type. In [113], a generalization of the Routh-Hurwitz criterion for FO systems is presented. Mikolaj *et. al* presents a frequency domain method for stability checking of the system with commensurate or non-commensurate orders described by the state equation with double fractional orders based on the Argument Principle, [114]. [115, 116] applied the similar approach on discrete FO systems with delays. Besides the work from Trigeassou and Lu *et al.* in the previous subsection, more results on robust stability for FO systems can be found in [117, 118, 119, 120, 121], etc. Other general and specific analysis can be found in [122]. For more related research results on FO system stabilities, refer to [123, 124, 125]

Talking about system stability, the root locus method cannot be skipped since it is a straightforward graphical tool in classic control. While the aforementioned publications study the stability of miscellaneous FO systems, root locus is devoted for LTI system stability analysis and compensator design. Along with the tide of extending advanced control techniques into fractional order, such a fundamental tool should not be forgotten, so as to gain traditional engineers more confidence to adopt FO control. In, [126, 127, 126], Bayat and Afshar *et al.* discussed about extending the classic root locus approach to FO models. [128] gives a computational approach for obtaining the root locus of fractional systems. A sample Matlab code is provided in the paper [129]. In [130], Machado *et al.* provides a set of practical rules for sketching root locus of FO systems by hand. They also exhibited a gallery of root locus of FO systems, [131]. [132] explored the root locus method for any fractional order commensurate system. A recent research on a new and simple method to construct root locus of general FO systems can be found in [133].

As a consisting part of system theory, modeling and identification is an essential step before carrying out most kind of controls. While many approaches for integer order systems have been extended to fractional order cases, new methodologies are under development. [134, 2, 135] and [136] list some of the existing FO system identification methods. [137] and [138] present the modeling techniques for FO systems. [139] illustrates the functional fractional calculus for system identification.

An academic theory would become gaudy if there is no way to realize it in practice. Hence, a lot of efforts have been made on the numerical computation of fractional operations, physical realization of FO electrical elements and implementation of FO controls, etc. To name a few in addition to the mentioned work in the previous subsection, analog realization of FO circuits [140], the reduced order approximation of MIMO FO systems [141] and realization of fractional order impedance by feedback control [142] are all the efforts on this direction. Regarding the numerical computation of fractional operations, various types of discretization and approximation methods have been proposed, such as the indirect methods for simulation of fractional systems using the diffusive representation in [143, 144], and the IIR type filter approximation in [145]. More dedicated review and detailed research are discussed in section

2.4. Implementation is also a hot topic. Besides the FPGA implementation and analogy realization mentioned above, the PLC implementation of a CRONE controller can be found in [146], and the FO controller for autonomous parking systems is presented in [147].

Topics on fractional order sliding mode control (SMC), nonlinear FO systems and MIMO FO systems are reviewed in later corresponding sections. Other than these, some control concepts with relatively narrower and specific application are also extended to FO. For instance, the variable fractional order dead-beat control of a robot arm [148]. The application of computational intelligence techniques in fractional order systems and control is explored in the book [149]

All in all, it is by no means possible to traverse all the published contribution on fractional order controls. However, through the above review, state-of-the-art status and the evolvement of research focus in this area are revealed. Holding this knowledge, comparing with the conventional integer order controls, what left to be exploited become clear. To the author's best knowledge, there has been no leading comprehensive monograph on FO MIMO process modeling and controls in the literature. Hence, this research is in hope of dedicating efforts into the "missing land", as is done for FO motion controls in [58].

Chapter 2

Preliminaries

> 'The future already exists. We do not exist in the majority of these times; in some you exist, and not I; in others I, and not you.'
>
> — Jorge. L. Borges, *A Garden of Forking Path*, 1941

The law of natural already exists, waiting for human to characterize.

2.1 Introduction to fractional calculus

The history of fractional calculus is almost as long as that of the ordinary calculus. It can date back to the $17th$ century, short after Newton and Leibniz invented the ordinary integration and differentiation [150]. In L'Hospital's letter to Leibniz [151], he questioned what if the order of the derivative were 0.5, which eventually led to the birth of the theory of derivatives and integrals of arbitrary order.

Similar analogies are commonly seen in the development of math. It is known that the history of mathematics is pushed forwards by paradoxes and crisis as civilization advances [152, 153, 154]. Taking the development of numbers as an example, the integers on the number axis are like isolated islands in the ocean where the majority of water is of fractional and non-rational numbers. Moving a step further, the proposal of complex number made people realize that the real numbers are like the planets in the vast universe which only occupy a negligibly tiny portion of the space.

By the same token, the advances of operations also experienced the journey from basic to complicated, namely, from plus/minus to powers/roots, and furthermore to integration/derivation and convolution. In the past 300 years, the development of fractional calculus makes the theory of operation even more complete. For a recent history of fractional calculus, refer to [155]. Fractional calculus is such a incredible tool that can explain many physics phenomena which traditional math could not. It is especially good at depicting phenomena with long memory, long range dependence, etc. For example, one of the most amazing use is the math description of various random walks, which can unify the macro and micro level of anomalous diffusion.

$$\mathbb{N}, \quad \mathbb{Z}, \quad \mathbb{R}, \quad \mathbb{C}$$
$$+ \quad - \quad \times \quad \div \quad \int \quad {}_0\boldsymbol{D}_t^{\boldsymbol{\alpha}}$$

The crisis	Cause (paradox)	About	Impact
I (370 A.D)	Pythagoras	Irrational number	Number theory
II (17th century)	Zeno's	Infinitesimal	Calculus
III (1897)	Russell's	Sets	Set theory

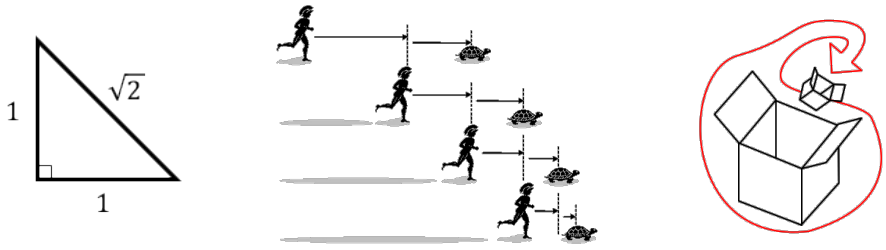

Figure 2.1: Crisis in the foundations of mathematics.

2.1.1 Definitions

Up to now, there are more than 10 types of definitions for fractional order integrals and differentiations [20]. For readers' convenience, several commonly used definitions are briefly listed below. More details can be found in [17].

A. Riemann-Liouville definition of FO integration

The Riemann-Liouville (R-L) definition of fractional order integration is:

$$ {}_0D_t^{-\alpha} f(t) = \frac{1}{\Gamma(\alpha)} \int_0^t \frac{f(\tau)}{(t-\tau)^{1-\alpha}} d\tau, \tag{2.1}$$

where $0 < \alpha < 1$, and $\Gamma(x)$ is the Gamma function $\Gamma(x) = \int_0^\infty e^{-u} u^{x-1} du$. When the initial integral limit changes from 0 to an arbitrary point a, this definition is generalized to the **Weyl** definition of FO integral:

$$ {}_aD_t^{-\alpha} f(t) = \frac{1}{\Gamma(\alpha)} \int_a^t \frac{f(\tau)}{(t-\tau)^{1-\alpha}} d\tau. \tag{2.2}$$

B. Riemann-Liouville definition of FO differentiation

The R-L definition of fractional order differentiation is based on the fractional integral and the ordinary derivatives:

$$ {}_0D_t^{\alpha} f(t) = \frac{d}{dt} [{}_0D_t^{-(1-\alpha)} f(t)]. \tag{2.3}$$

More specifically, there are left R-L and right R-L definitions for FO differentiation by distinguishing the lower and upper limits of the integration,

$$
\begin{aligned}
{}_aD_t^\alpha f(t) &= \frac{1}{\Gamma(n-\alpha)}\left(\frac{d}{dt}\right)^n \int_a^t (t-\tau)^{n-\alpha-1} f(\tau)d\tau, && (2.4)\\
{}_tD_b^\alpha f(t) &= \frac{1}{\Gamma(n-\alpha)}\left(-\frac{d}{dt}\right)^n \int_t^b (t-\tau)^{n-\alpha-1} f(\tau)d\tau. && (2.5)
\end{aligned}
$$

C. Caputo definition of FO differentiation

The Caputo definition of fractional order differentiation takes the integer order differentiation of the function first and then take a fractional order integration:

$$
{}_0^C D_t^\alpha f(t) = \frac{1}{\Gamma(1-\alpha)} \int_0^t \frac{f'(\tau)}{(t-\tau)^\alpha} d\tau. \tag{2.6}
$$

Under this definition, D and ${}_0D_t^{-(1-\alpha)}$ do not commute because the initial value needs be considered:

$$
{}_0^C D_t^\alpha f(t) = {}_0D_t^{-(1-\alpha)} f(t)[Df(t)] + \frac{f(0^+)t^{-\alpha}}{\Gamma(1-\alpha)}. \tag{2.7}
$$

D. Grünwald-Letnikov definition

The Grünwald-Letnikov (G-L) definition defines the fractional integration and differentiations in a unified way:

$$
{}_aD_t^\alpha f(t) = \lim_{h\to 0} \frac{1}{h^\alpha} \sum_{j=0}^{[(t-a)/h]} (-1)^j \begin{pmatrix} \alpha \\ j \end{pmatrix} f(t-jh). \tag{2.8}
$$

2.1.2 Important functions

Some important special functions which are frequently encountered in fractional calculus are listed below. For more details, refer to [17].

Gamma function

Gamma function is important because it is the fundamental element in most of the definitions of fractional integrals. It is usually treated as the factorial of non-integer numbers. The integral representation can be written as:

$$
\Gamma(x) = \int_0^\infty e^{-u} u^{x-1} du, \quad x \neq \mathbb{Z}_0^- . \tag{2.9}
$$

Some useful properties of the Gamma function are:

$$
\begin{aligned}
\Gamma(1) = 1; \qquad & \Gamma(n+1) = n! \ \ (n = 0, 1, 2\ldots)\\
\Gamma(\frac{1}{2}) = \sqrt{\pi}; \qquad & \Gamma(x+1) = x\Gamma(x).
\end{aligned}
$$

Similar to ordinary (integer order) calculus, the fractional order derivative of a variable's same fractional order power is a constant,

$$\frac{d^\alpha}{dx^\alpha}x^\alpha = \frac{\Gamma(\alpha+1)}{\Gamma(\alpha-\alpha+1)}x^{\alpha-\alpha} = \Gamma(\alpha+1).$$

Mittag-Leffler function

The Mittag-Leffler (M-L) function is a generalization of the exponential function which plays an important role in the solution of fractional differential equations as the exponential function does in ordinary differential equations. It has four forms [156, 157], and the most frequently used forms are the 1-parameter and 2-parameter representation [158]:

$$E_\alpha(x) = \sum_{k=0}^{\infty}\frac{x^k}{\Gamma(\alpha k+1)} \quad (\alpha>0); \tag{2.10}$$

$$E_{\alpha,\beta}(x) = \sum_{k=0}^{\infty}\frac{x^k}{\Gamma(\alpha k+\beta)} \quad (\alpha>0,\beta>0). \tag{2.11}$$

Some of the beautiful properties of M-L function are as follows,

$$E_{1,1}(x) = e^x; \tag{2.12}$$

$$E_{1,2}(x) = \frac{e^x-1}{x}. \tag{2.13}$$

Error function

The error function is a special function of the "S" shape, and is defined as:

$$erf(x) = \frac{2}{\sqrt{\pi}}\int_0^x e^{-u^2}du, \quad -\infty<x<\infty. \tag{2.14}$$

The error function has the following properties,

$$\begin{aligned} erf(0) &= 0 \\ erf(\infty) &= 1 \\ erf(x)+erfc(x) &= 1, \end{aligned}$$

where $erfc(x)$ is the so-called complementary error function.

Confluent hypergeometric function

A confluent hypergeometric function is a solution of a confluent hypergeometric equation, and is expressed in the following form,

$${}_1F_1(a;c;x) = \sum_{n=0}^{\infty}\frac{(a)_n}{(c)_n}\frac{x^n}{n!}, \quad -\infty<x<\infty, \tag{2.15}$$

where $(a)_n$ and $(c)_n$ are the Pochhammer symbols,

$$(\mathrm{a})_\mathrm{n} = \frac{\Gamma(a+n)}{\Gamma(a)}, \text{ and } (\mathrm{c})_\mathrm{n} = \frac{\Gamma(c+n)}{\Gamma(c)}, \ n=0,1,2,...$$

Some frequently used properties for the hypergeometric function are listed below,

$$\begin{aligned} {}_1F_1(1;1;x) &= e^x, \\ \frac{1}{\Gamma(\alpha+1)}{}_1F_1(a;\alpha+1;at) &= E_{1,\alpha+1}(at). \end{aligned}$$

In recent years, more functions are documented as handy instrument for FC and FO controls, [139]. To name a few, **Agarwal function** is a generalization of the Mittag-Leffler function; **Robotnov-Hartley** function is the "impulse response" of the fundamental fractional differential equation and is used for control system analysis; **Miller-Ross** function is introduced for the solution of fractional order initial value problems.

2.1.3 Laplace transform of fractional operators

To many people's unawareness, the Laplace transform not only applies on functions of integer powers of t, but also on functions of non-integer powers of t, as demonstrated in the following example, [17]:

$$\mathcal{L}[t^x] = \int_0^\infty e^{-st} t^x dt. \tag{2.16}$$

Let $u = st$, then,

$$\begin{aligned} \int_0^\infty e^{-u} \left(\frac{u}{s}\right)^x \frac{du}{s} &= \frac{1}{s^{x+1}} \int_0^\infty e^{-u} u^x du, \quad x > -1 \\ &= \frac{\Gamma(x+1)}{s^{x+1}}. \end{aligned} \tag{2.17}$$

A useful property of the Laplace transform for FO control is the integration property,

$$\mathcal{L}[{}_0D_t^{-\alpha} f(t)] = \frac{1}{s^\alpha} F(s) \quad (\alpha > 0), \tag{2.18}$$

which can also be interpreted as the Laplace transform of a time domain convolution,

$$\mathcal{L}[{}_0D_t^{-\alpha} f(t)] = \mathcal{L}\left[\frac{t^{\alpha-1}}{\Gamma(\alpha)} * f(t)\right] = \frac{1}{s^\alpha} F(s), \tag{2.19}$$

where $\frac{t^{\alpha-1}}{\Gamma(\alpha)}$ is usually called the kernel of fractional integration. The differentiation property is often encountered as well,

$$\mathcal{L}[{}_0D_t^{\alpha} f(t)] = s^\alpha F(s) \quad (\alpha > 0), \tag{2.20}$$

with zero initial conditions assumed, or,

$$\mathcal{L}[{}_0^C D_t^{\alpha} f(t)] = s^\alpha F(s) - \sum_{k=0}^{m-1} s^{\alpha-k-1} \left[\frac{d^k Y(t)}{dt^k}\right], \tag{2.21}$$

for non-zero initial condition using Caputo's definition. Several useful Laplace transform pairs in fractional calculus are listed below for readers' reference.

Table 2.1: Useful Laplace transform pairs in fractional calculus.

F(s)	$\frac{1}{s^\alpha}$	$\frac{1}{(s+a)^\alpha}$	$\frac{1}{\sqrt{s}+1}$	$\frac{1}{s^\alpha+a}$	$\frac{s^{\alpha-\beta}}{s^\alpha+a}$
f(t)	$\frac{t^{\alpha-1}}{\Gamma(\alpha)}$	$\frac{t^{\alpha-1}}{\Gamma(\alpha)}e^{-at}$	$\frac{1}{\sqrt{\pi t}} - e^t erfc[\sqrt{t}]$	$t^{\alpha-1}E_{\alpha,\alpha}(-at^\alpha)$	$t^{\beta-1}E_{\alpha,\beta}(-at^\alpha)$

Other than the regular definition of Laplace transform for fractional operators, there are several variants, for example, Laplace transform via Mittag-Leffler function and the modified Riemann-Liouville derivative [159], Laplace transforms of a k-Weyl fractional integral and derivative [160], etc.

2.1.4 The fractional Fourier transform

The Laplace transform can be applied on FO integration/differentiation, so does the Fourier transform. The fractional Fourier transform (FrFT) is a generalization of the integer order Fourier transform. The signal produced by FrFT can be considered as a rotated time-frequency representation of the original signal. The FrFT is defined as, [161]:

$$X_\alpha(u) = \mathcal{F}_\alpha(x(t)) = \int_{-\infty}^{\infty} x(t)K_\alpha(t,u)dt, \tag{2.22}$$

where $K_\alpha(t,u)$ represents the kernel function:

$$K_\alpha(t,u) = \begin{cases} \sqrt{\frac{1-j\cot\alpha}{2}} & \\ \times e^{j(u^2/2)\cot\alpha} e^{j(t^2/2)\cot\alpha - jut\cos(ec\alpha)} & \text{if } \alpha \neq 2\pi \\ \delta(t-u) & \text{if } \alpha = 2\mathrm{n}\pi \\ \delta(t+ut) & \text{if } \alpha = (2\mathrm{n}-1)\pi, \end{cases} \tag{2.23}$$

when $\alpha = \pi/2$, the FrFT degrades to standard Fourier transform, and when α is multiple of π, FrFT degenerates to parity and identity operator. For interesting and useful properties of the FrFT, refer to [40, 162, 163].

FrFT has a broad application in many fields, such as communication, signal processing and pattern recognition, etc, among which a widely acclaimed application is filtering. A fractional filter can be written as a generalization of the conventional filter:

$$x_o(t) = \mathcal{F}_{-a}\mathcal{R}_\alpha x_i(t) \cdot H_\alpha(u), \tag{2.24}$$

where $H_\alpha(u) = \mathcal{F}(h(t))$, $x_i(t)$, $x_o(t)$ and $h(t)$ refer to the input signal, output signal and the filter's impulse response, respectively. Briefly, the Wigner distribution of a signal $f(t)$ and that of its α^{th} order FrFT staggers an angle of $-\alpha$:

$$(\mathcal{W}f_a)(t,u) = \mathcal{R}_{-a}(\mathcal{W}f)(t,u), \tag{2.25}$$

where $\alpha = a\pi/2$, $f_a = \mathcal{F}_a f$, and $\mathcal{R}_{-a}$ represent a clockwise rotation of the variables (t,u) over angle α. Hence, fractional filters give more freedom to the selection of domain in which

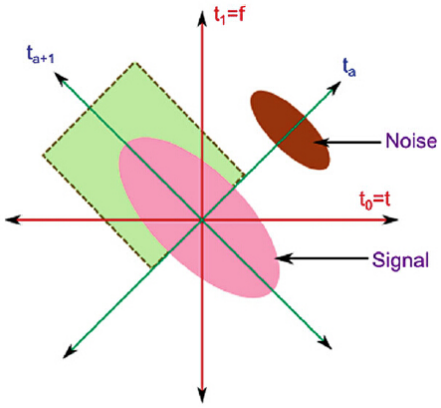

Figure 2.2: The schematic illustration of fractional filters based on FrFT

signal and noise could be separated, which would be overlapped on either time or frequency domain using integer order filters, as shown in figure 2.2.

Besides filtering, FrFT based estimation methods have been used to analyze the long range dependence in time series. For example, Hurst exponent calculated by FrFT based methods have been shown to be better than others, [164], like wavelet based methods. For numerical computation of FrFT, a Matlab based tool is available in [165, 166].

2.2 Fractional order differential equations

Fractional order differential equations (FODEs) are the foundation for describing FO dynamic systems. Any type of fractional order system analysis, time domain, s-domain and complex frequency domain, are all built on the basis of FODEs. Hence, their importance needs no more emphasis. This section reviews some properties of FODEs such as stability, solution structures and so on. Several selected ordinary differential equations (ODEs) are presented with their fractional order form for the reference in later chapters. The fractional order Rayleigh differential equation is proposed and briefly studied.

2.2.1 Fractional version of typical differential equations

2.2.1.1 Linear FODEs

Linear FOEDs are commonly used in fractional order controls due to their simplicity and regularity. The general expression takes the following form:

$$\begin{aligned} &a_1 D^{\alpha_1} y(t) + a_2 D^{\alpha_2} y(t) + \cdots + a_n D^{\alpha_n} y(t) \\ &= b_1 D^{\beta_1} u(t) + b_2 D^{\beta_2} u(t) + \cdots + b_m D^{\beta_m} u(t), \end{aligned} \tag{2.26}$$

where the orders, $\alpha_i,\ \beta_j\ (i,j = 1,2,...)$, can be arbitrary real numbers, i.e. $\alpha_i,\ \beta_j \in \mathbb{R}$. If α_i and β_j are integer multiples of a common factor, the equation is called having commensurate order; and is of non-commensurate order if no common factor exists [167].

The fractional Langevin equation The original Langevin equation describes the Brownian motion of a particle in a fluid,

$$m\frac{d^2x}{dt^2} = -\lambda\frac{dx}{dt} + \eta(t), \tag{2.27}$$

where x is the particle's position and m denotes the particle's mass. The noise term $\eta(t)$ represents the effect of the collisions with the molecules of the fluid, and has a Gaussian probability distribution with the following correlation function:

$$Corr(\eta_i(t), \eta_j(t')) = 2\lambda k_b T \delta_{i,j}\delta(t-t'),$$

where k_b is Boltzmann's constant, T is the temperature, and δ is the Dirac's function.

However, the above equation of motion does not completely capture the hydrodynamics because it ignores the effects of the added mass and the retarded viscous force due to the acceleration of the particle. Thus, the fractional Langevin equation is promoted to supplement the missing dynamics, [168],

$$m\frac{dx}{dt} = -\frac{m}{\sigma_e}[1 + \sqrt{T_*}D_0^{1/2}]x(t) + \eta(t), \tag{2.28}$$

where the description of the coefficients can be found in [168]. For the above fractional Langevin equation, the random force $\eta(t)$ cannot be represented uniquely by a white noise. Instead, it can be represented by a superposition of the white noise with a "fractional" noise. Consequently, the added mass and the fractional noise slow down the velocity correlation function from exponential decay to algebraic or power law decay.

2.2.1.2 Nonlinear FODEs

In this subsection, several specific nonlinear fractional differential equations are visited. Some of them are selected due to the necessity of the latter content; others are chosen according to the author's interest because they are not as accessible as the general discussions in the literature.

The fractional Van der Pol equation The Van der Pol (VDP) equation was originally proposed by Van der Pol in the 1920s to depict the self-sustaining oscillation in electrical circuits employing vacuum tubes, [169]. It is one of the first discovered instances of deterministic chaos, and can be expressed by the following nonlinear ODE:

$$\ddot{x} + \mu(x^2-1)\dot{x} + x = 0. \tag{2.29}$$

It can also describe a wide variety of phenomena, such as a mass-spring-damper system with a nonlinear position-dependent damping coefficient, or an RLC electrical circuit with a negative-nonlinear resistor.

Later, a number of variant VDP equations were proposed, for example, Mickens *et al.* investigated the following two equations in [170, 171],

$$\ddot{x} + \mu(x^2-1)\dot{x} + x^{1/3} = 0, \tag{2.30}$$

$$\ddot{x} + \mu(x^2-1)(\dot{x})^{1/3} + x = 0, \tag{2.31}$$

which was referred to as fractional VDP. However, these dynamics only contains the fractional power of the state variables rather than fractional order derivatives, which are not fractional order in the sense of calculus. In 2004, Pereira *et al.* considered the following fractional derivative version VDP by substituting the capacitance with a "fractance" in a nonlinear RLC circuit model, [172],

$$D^{\alpha}x + \mu(x^2 - 1)\dot{x} + x = 0, \quad 1 < \alpha < 2. \tag{2.32}$$

In [173], Barbosa *et al.* introduced the following fractional VDP with both derivatives being fractional order,

$$D^{1+\alpha}x + \mu(x^2 - 1)D^{\alpha}x + x = 0, \quad 0 < \alpha < 1. \tag{2.33}$$

In [174], Diaz *et al.* investigated the dynamics and control of the variable order VDP equation originated from the physical model of an oscillating mass on a non-uniform viscoelastic film,

$$\ddot{x} + \mu(\beta D^{q(x)}x) + x = 0, \tag{2.34}$$

where $\beta = \pm 1$ and $q(x)$ is the variable order in the range of $(0.5, 1)$, e.g. $q(x) = (1 + x^2)/2$. The value of $q(x)$ is determined while solving the identity equation,

$$(y^2 - 1)\dot{y} = \beta D^{q(x)}x. \tag{2.35}$$

The graphical analysis of the limit cycles of fractional VDP equations can be found in [175] and [176], where the forced fractional VDP is also investigated.

The fractional Rayleigh differential equation A numerical Matlab toolbox, RIOTS, will be described in section 4.3.1.1 which uses the Rayleigh's problem as a demonstrative example. Hence, a brief description is inserted here. The Rayleigh's differential equation, named after Lord Rayleigh (John William Strutt), [177], takes the following simplified form,

$$\ddot{x} + \mu(\dot{x}^2 - 1)\dot{x} + x = 0. \tag{2.36}$$

It is known that the ordinary Van der Pol equation can be derived from the Rayleigh differential equation by differentiating x,

$$\dddot{x} + 2\mu\dot{x}\ddot{x}\dot{x} + \ddot{x}\mu\dot{x}^2 - \mu\ddot{x} + \dot{x} = 0, \tag{2.37}$$

and substituting $\dot{x}$ by y,

$$\ddot{y} + \mu(3y^2 - 1)\dot{y} + y = 0. \tag{2.38}$$

Let $y^{(\alpha)}$ denotes the α^{th} derivative of y with regard to t. If the above integer order directives are replaced by fractional order ones in the similar manner for equation (2.33), the fractional Rayleigh's equation can be obtained as,

$$y^{(1+\alpha)} + \mu[(y^{(\alpha)})^2 - 1]y^{(\alpha)} + y = 0, \quad 0 < \alpha < 1; \quad \text{or} \tag{2.39}$$

$$y^{(2\alpha)} + \mu[(y^{(\alpha)})^2 - 1]y^{(\alpha)} + y = 0, \quad 0.5 < \alpha < 1; \quad \text{or} \tag{2.40}$$

$$y^{(\beta)} + \mu[(y^{(\alpha)})^2 - 1]y^{(\alpha)} + y = 0, \quad 0 < \alpha < 1 < \beta < 2; \quad \text{or} \tag{2.41}$$

$$y^{(\beta)} + \mu[(y^{(\alpha)})^2 - 1]y^{(\lambda)} + y = 0, \quad 0 < \alpha, \lambda < 1 < \beta < 2. \tag{2.42}$$

However, since the chain rule applies on fractional derivatives only on specific conditions, the fractional VDP cannot be derived from the equation. Instead, other forms of fractional differential equation can be obtained. Let $x_1 = y$ and $x_2 = x_1^{(\alpha)}$. The phase portrait for equation (2.40) is plotted in figure 2.3, with $\mu = 1.2$ and fractional orders and initial conditions (IC) labeled in the legends of the sub-figures respectively. It can be seen from sub-figure one that if α violates the limit which makes the highest order happen to be 1, then, the origin becomes a stable focus whereas it is an unstable focus otherwise. Related discussion on the fractional Rayleigh's differential equation has not appeared in the literature, which hence, could be potential future research opportunities.

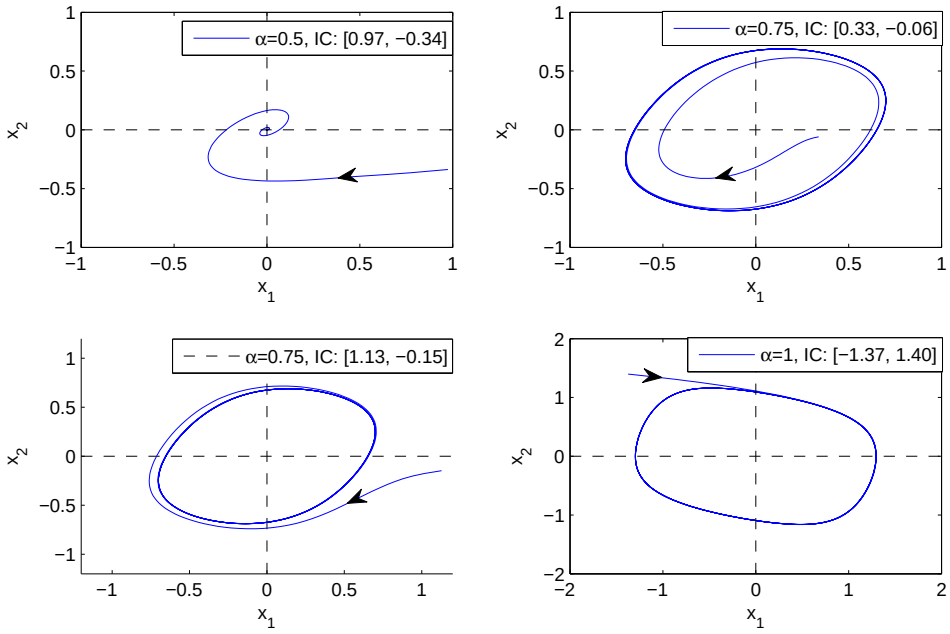

Figure 2.3: The phase portraits of equation (2.40) with different α and IC.

Duffing equation with FO damping Duffing's equation, introduced by Georg Duffing in 1918, is used to depict certain damped and driven oscillators. It is a well known simple model that yields chaos. The standard form of the Duffing's equation is,

$$\ddot{x} + \delta\dot{x} + ax + bx^3 = \gamma\cos(\omega t). \tag{2.43}$$

There are two different fractional order versions of the above equation derived. A simple form is to replace the 1^{st} order directive by a fractional order damping term, [178, 179, 180, 181],

$$\frac{d^2}{dt^2}x(t) + \delta\ {}_0D_t^{\alpha}x(t) + ax(t) + bx^3 = \gamma\cos(\omega t); \tag{2.44}$$

the complicated version is to change both the 1^{st} and 2^{nd} derivatives to fractional order derivatives of two coupled Duffing's equations, [137], and is more clearly expressed by the

the state equation:

$$\begin{aligned} {}_0D_t^{\alpha_1} x(t) &= y(t), \\ {}_0D_t^{\alpha_2} y(t) &= -ax(t) - bx^3(t) - \delta y(t) + \gamma \cos(\omega t). \end{aligned} \tag{2.45}$$

A recent study of the response of a Duffing-Rayleigh system with a fractional derivative under Gaussian white noise excitation can be found in [182].

The fractional Bernoulli's equation The ordinary Bernoulli differential equation is of the following form,

$$\frac{dy}{dx} + f(x)y = g(x)y^n. \tag{2.46}$$

When $n = 0$ or 1, it is a linear ODE; otherwise, it is nonlinear. In [183], Hristov promoted the fractional-time Bernoulli equation for the problem arising in a transient conduction with a non-linear boundary heat flux,

$${}_0D_t^{0.5}\theta_s = A + B\theta_s + C\theta_s^4, \tag{2.47}$$

where $\theta_s = T_s/T_a$ denotes the ratio of the surface temperature to the ambient temperature in the considered scenario. Following this format, a more general fractional Bernoulli equation can be expressed as follows,

$$\frac{d^\alpha y}{dx^\alpha} + f(x)y = g(x)y^n, \quad (0 < \alpha < 2). \tag{2.48}$$

The fractional pendulum equation The classic pendulum differential equation describes the swing motion of a mass attached to the end of a rigid pole with consideration of the air friction:

$$ml\ddot{\theta}(t) = -mg\sin\theta(t) - k\dot{\theta}(t), \tag{2.49}$$

where $\theta(t)$ is the angle of the pendulum with respect to the direction of gravity, m is the mass of the pendulum, k is the coefficient of friction at the pivot point, and l is the radius of the rigid pole. The variants include the double pendulum which has two segments of the poles connected by a joint, and cascaded multiple pendulum.

In [184], dynamics of multi-pendulum with fractional order creep elements is discussed. The fractional Lagrangian function is studied for two electric pendulum in [185],

$$L^F = \frac{1}{2}m[({}_aD_t^\alpha q_1)^2 + ({}_aD_t^\alpha q_2)^2] - \frac{1}{2}\frac{mg}{l}(q_1^2 + q_2^2) - \frac{e^2}{d + q_2 - q_1}, \tag{2.50}$$

where e is the electron charge, q_1 and q_2 represent the position of the two electric pendulum. The fractional order analysis of ordinary double pendulum is presented in [186].

2.2.1.3 Fractional order partial differential equations

The anomalous diffusion equation The famous diffusion equation is a succinct mathematical description of the diffusion phenomenon. As the science develops, broadened physical observation and sophisticated math methods led to the generalized diffusion equation, [187, 188],

$$ {}_tD_*^{\beta}u(x,t) = {}_xD_{\theta}^{\alpha}u(x,t), \quad -\infty < x < +\infty, \quad t \geq 0, \tag{2.51} $$

where ${}_xD_{\theta}^{\alpha}$ is the Riesz-Feller fractional derivative, $0 < \alpha < 2, \beta = 1$ refers to the strictly *space fractional* diffusion, $\alpha = 2, 0 < \beta < 1$ refers to the strictly *time fractional* diffusion, and $0 < \alpha < 2, 0 < \beta < 1$ refers to the strictly *space-time* fractional diffusion.

It is known that the ordinary diffusion equation can be interpreted as the evolution of Gaussian probability density function (pdf) in space with time, which depicts the random walk of particles performing the Brownian motion. The generalized diffusion equation can interpret more types of random walks with different pdfs, which are related to anomalous diffusions. As noted in [189], the mean squared displacement (MSD) of the particles doing random walk has the following relation with time,

$$ \langle x^2(t) \rangle \sim Kt^{\alpha}. \tag{2.52} $$

When $\alpha = 1$, it characterizes the normal diffusion; $0 < \alpha < 1$ characterizes the sub-diffusion; $1 < \alpha < 2$ characterizes the super-diffusion and $\alpha = 2$ characterizes the ballistic diffusion. More dedicated research reviews on anomalous transport and diffusion processes can be found in [190] and [191].

The fractional Navier-Stokes equation The Navier-Stokes (N-S) equation is also considered of its fractional order form in the literature. The expression and solution are investigated by Kumar *et al.*, [192, 193],

$$ D_t^{\alpha}u(r,t) = P + v(D_r^2 u + \frac{1}{r}D_r u), \quad 0 < \alpha \leq 1, \tag{2.53} $$

where $P = \frac{1}{\rho}\frac{\partial p}{\partial z}$, and v denotes the kinematic viscosity.

More FO PDEs can be found in [104] and the references therein.

2.2.2 Pseudo state-space representation

Many modern control concepts and methodologies are still applicable to the dynamic systems possessing "FO" behaviors. The state-space (S-S) representation is such a powerful tool. If an FODE has commensurate order, it can be generally expressed as the following by defining appropriate state variables,

$$ \begin{aligned} {}_0D_t^{\alpha}x(t) &= f(x,u,t) \\ y(t) &= g(x). \end{aligned} \tag{2.54} $$

where $x \in R^n$ is the state vector of dimension n, and $0 < \alpha < 2$ is the common factor of the differentiation orders. For linear FODEs in equation (2.26), the above equation can be

simplified as:

$$\begin{aligned} {}_0D_t^{\alpha}x(t) &= Ax(t) + Bu(t) \\ y(t) &= Cx(t), \end{aligned} \tag{2.55}$$

where A, B and C are system, input and output matrices, respectively.

For integer order state space models, the exponential matrix, $\Phi(t) = e^{At}$ is known as the state transition matrix. It can be analogized accordingly that the generalized exponential matrix using M-L function, $E_\alpha(At^\alpha)$, plays the same role for fractional order S-S models. It is called the fractional order state transition matrix and can be obtained by [35],

$$\Phi(t) = \mathcal{L}^{-1}\{(s^\alpha I - A)^{-1}\}. \tag{2.56}$$

The following property for state transition from the origin is inherited from integer order,

$$x(t) = \Phi(t)x(0) + \Phi(t) * [Bu(t)] = \Phi(t)x(0) + \int_0^t \Phi(t-\tau)Bu(\tau)d\tau. \tag{2.57}$$

However, the semigroup property of the state transition matrix is lost for fractional S-S models due to the failure of the chain rule on fractional derivatives. That is why the attribute "pseudo" is used in some literature to differentiate the S-S representation of fractional order from integer orders, [194].

2.2.3 Stability of fractional differential equations

2.2.3.1 The stability of linear FODEs

System stability is always a big concern in control theory due to its importance. There are numerous notions and criteria for different kinds of stabilities, such as bounded-input-bounded-output (BIBO) stability, exponential stability, asymptotic stability, Lyapunov stability, robust stability, etc. For FO systems, these criteria need to be extended, and new stability types are proposed, such as the Mittag-Leffler stability, [54]. As mentioned in the literature review in chapter 1, some of these stability criteria have been defined and can be referred to accordingly. Two usually used criteria for the BIBO stability of FO TFs are stated in section 2.3.

2.2.3.2 The stability of nonlinear FODEs

The stability of nonlinear FODEs can be much more complicated than integer order case and linear fractional order case. Yet, some stability criteria can be simply extended such as the asymptotic stability. Consider the FO system:

$$D^\alpha \mathbf{x} = f(\mathbf{x}), \tag{2.58}$$

where $0 < \alpha < 1$ and $\mathbf{x} \in \mathbb{R}^n$. The equilibrium points $\mathbf{x_0}$, obtained by $f(\mathbf{x}) = 0$, are asymptotically stable if all the eigenvalues λ_j, $(j = 1, 2, \ldots, n)$ of the Jacobian matrix $\mathbf{J}|_{\mathbf{x}=\mathbf{x_0}} = \partial f/\partial \mathbf{x}$ satisfies the condition:

$$|\angle(eig(\mathbf{J}))| = |\angle(\lambda_j)| > \alpha\frac{\pi}{2}. \tag{2.59}$$

This is the same as the integer order case except the range on the plane where the eigenvalues could be. [195] gives a Lyapunov approach for nonlinear FODEs. Mittag-Leffler stability are extensively studied by Li *et al.* [54]. This type of stability will be used in the derivation in section 3.4.4. Besides the mentioned works in the literature review (section 1.4), more stability related discussion can be referred to the two survey articles, [196, 28], and the book [137], chapter 1.

2.2.4 Solutions to fractional differential equations

Solution to FODEs is no more rigorous than its integer order counterpart, with regard to the existence, uniqueness, and periodicity. For example, the periodicity is an actively debated topic on which *contradictory* results have been reported in the literature [197, 198, 199, 200]. The Laplace transformation is a popular technique for obtaining analytical solutions, and "short-memory principle" is popular for the approximate numerical evaluations.

Definition 1 (Short-memory principle [80])**.** *When the R-L or G-L definition is used, if* $|f(t)| < M, \forall t > c$*, then the approximation error* ε *for* ${}_cD_t^\alpha f(t) \approx_{t-L} D_t^\alpha f(t)$ *(*$t > c + L, \alpha > 0$*), is bounded by:*

$$|\varepsilon| < \frac{M}{L^\alpha |\Gamma(1-\alpha)|}. \tag{2.60}$$

This means the behavior of $f(t)$ in only the "recent past" is considered.

Other than these two methods, Mellin transform, power series expansion using fractional Green's function, Babenko's symbolic method, orthogonal polynomial method, Reisz fractional potential method, method with Wright's function, and finite-part integral method are other mathematical tools for obtaining the solution of FODEs. For more dedicated results on the solution to specific types of FODEs, refer to [201, 202].

2.2.5 Fractional variational problems

The fractional variation problem provides theoretical support to fractional order optimal control which will be encountered in section 4.3.1.1. It is a problem in which either the objective functional or the constraint equation or both contain at least one fractional derivative term. The math definition of two such problems, i.e. the simplest fractional variational problem and the fractional variational problem of Lagrange, can be found in [203]. The formulation and study of **fractional Euler-Lagrange (E-L) equation** can be found in [204, 205].

2.3 Fractional order transfer functions

2.3.1 Obtaining fractional order transfer functions

Transfer function (TF) is an important tool to represent the input and output relationship of linear time-invariant (LTI) systems. Employing the Laplace transform for fractional differentiation introduced in section 2.1.3, the linear FODE in equation (2.26) can be mapped into the s-domain:

$$G(s) = \frac{\mathcal{L}[y(t)]}{\mathcal{L}[u(t)]} = \frac{b_1 s^{\beta_1} + b_2 s^{\beta_2} + \cdots + b_m s^{\beta_m}}{a_1 s^{\alpha_1} + a_2 s^{\alpha_2} + \cdots + a_n s^{\alpha_n}}. \tag{2.61}$$

Another way to obtain a fractional order transfer function is to convert from fractional order pseudo state-space expressions, [35]. Consider the pseudo S-S representation in equation (2.55), assuming zero initial conditions, and taking Laplace transformation gives,

$$s^{\alpha} X(s) = AX(s) + BU(s) \tag{2.62}$$

$$Y(s) = CX(s). \tag{2.63}$$

Then, the transfer function $G(s) = Y(s)/U(s)$ can be derived through:

$$G(s) = C(s^{\alpha} I - A)^{-1} B. \tag{2.64}$$

If B is a multi-column matrix and/or C is a multi-row matrix, then the resulting $G(s)$ is an FO transfer function matrix rather than a single FO transfer function. A transfer function matrix builds relation among multiple inputs and multiple outputs, which is the so-called MIMO process. Dedicated discussion on MIMO is in sections 3.5 and 4.2.

Similar to that for the ODEs, the TF simplifies the analysis of linear FODEs in a great extent by reducing the operations to algebraic, which, otherwise, contains much tedious integrals and differentiation of transcendental functions.

2.3.2 Root locus of fractional order transfer functions

The root locus method, developed by Walter R. Evans in the 1940s [206], is a graphical tool for examining the movement of a system's roots on the complex plane with variation of a certain system parameter, commonly the gain within a feedback system, e.g. the K change in the standard closed-loop system under unit feedback proportional control as shown in the block diagram in figure 2.4. It has been well studied for the classic integer order LTI systems. A survey in the early years is available in [207]. However, additional difficulties are posed when used onto FO TFs. For example, how to determine the number of zeros and poles, how to solve them, which poles and zeros are to be plotted on a certain plane, what is the uniform way of dealing with different TF structures, which poles affect the stability, etc.

Remark: the FO TFs discussed in this section narrowly refer to those of pure fractional orders, and irrational orders are not considered. Since any fraction is the quotation of two integers, in this sense, non-commensurate order TFs does not exist for FO systems. Similar conclusion can be found in [28]. Actually, the usual numerical approach for pole computation (used for instance in CRONE Toolbox) is to truncate the fractional orders to a given number of digits, according to [75]. Afshar and Bayat *et. al* also states that since numbers stored

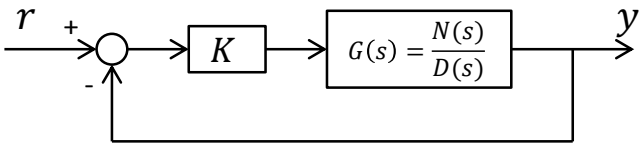

Figure 2.4: The block diagram of a standard unit feedback system.

in the computer memory/registers physically have finite precision, it is always possible to treat them as fractions, [127, 208]. The only inconvenience is that the denominator or the common denominator could be too large for computation. The following context provides the essential procedure for plotting basic root locus for FO TFs.

2.3.2.1 Determining the poles and zeros.

To proceed, the following notation and definitions are provided.

Definition 2 (FO polynomials)**.** *The function* $Q(s) = a_1 s^{\alpha_1} + a_2 s^{\alpha_2} + \cdots + a_n s^{\alpha_n}$ *is an FO polynomial if and only* $\alpha_i \in \mathbb{Q}_0^+,\ a_i \in \mathbb{R}$ *for* $i = 1, \ldots, n$.

Thus, an FO TF is composed of a numerator FO polynomial and a denominator FO polynomial: $G(s) = \frac{N(s)}{D(s)}$. Poles and zeros are the roots of the equation $D(s) = 0$ and $N(s) = 0$, respectively.

Definition 3 (Fundamental order and Fractional degree)**.** *Rewrite the above FO polynomial:*

$$Q(s) = a_1 s^{\frac{\lambda_1}{\lambda}} + a_2 s^{\frac{\lambda_2}{\lambda}} + \cdots + a_n s^{\frac{\lambda_n}{\lambda}}, \tag{2.65}$$

where $\lambda \in \mathbb{N}$ *is the least common denominator of* $\alpha_1, \ldots, \alpha_n$*, and* $\lambda_i \in \mathbb{N}$*.* $\frac{1}{\lambda}$ *is called the fundamental order. The fractional degree of* $Q(s)$ *is defined as* $fdeg\{Q(s)\} = \max\{\lambda_1, \ldots, \lambda_n\}$.

With this definition, the fundamental order is confined inside the interval of $(0, 1]$ (where it degrades to an integer order polynomial when $\lambda = 1$). Thus, a consistent mapping from the integer order s-plane to a proper fractional w-plane ($w = s^{\frac{1}{\lambda}}$) can be drawn.

Theorem 1 (Number of roots)**.** *Let* $Q(s)$ *be an FO polynomial with* $fdeg\{Q(s)\} = n$*. Then, the characteristic equation* $Q(s) = 0$ *has exactly* n *roots on* n *Riemann sheets.*

The proof can be found in [127]. Description of the Riemann surface can be found in [209]. In this context, the first Riemann sheet is denoted by $\mathcal{P} := \{re^{i\theta} | r > 0, -\pi < \theta \leq \pi\}$. In fact, since $w = s^\alpha$ is a multi-valued function, FO polynomials have infinite roots. This definition simplifies the analysis by concerning only about practically meaningful number of roots.

There are other definitions for the fundamental order, e.g. in [210, 118], where the greatest common divisor (not limited to integers) is selected to be the fundamental order. This consequently affects the number of roots.

Let $j\omega$ substitute the Laplace variable s, it can be seen that the mapping from $j\omega$ to $(j\omega)^{\frac{1}{\lambda}}$ in definition 3 always expands the s-plane to λ sheets of Riemann surface, while other definitions either compress or expand the s-plane depending on the selected fundamental order.

Example 2.3.1: Consider the FO TF below:

$$G(s) = \frac{1}{s^{2.6} + s^{1.3} + 1}. \tag{2.66}$$

According to the definition mentioned in [118], let the fundamental order be $\alpha = 1.3$. Then, the mapping compresses $s \to w_1$ where $w_1 = s^{1.3}$, as shown in figure 2.5(a). In contrast, according to definition 3, its fundamental order is $\frac{1}{\lambda} = \frac{1}{10}$. This mapping expands the s-plane on the w_2-plane, where $w_2 = s^{\frac{1}{10}}$. Hence, it has 26 roots. The TF in equation (2.66) is expressed in the following two forms, respectively:

$$G_1(w_1) = \frac{1}{w_1^2 + w_1 + 1}, \ (1) \qquad \mathrm{G_2(w_2)} = \frac{1}{\mathrm{w_2^{26}} + \mathrm{w_2^{13}} + 1}, \ (2). \tag{2.67}$$

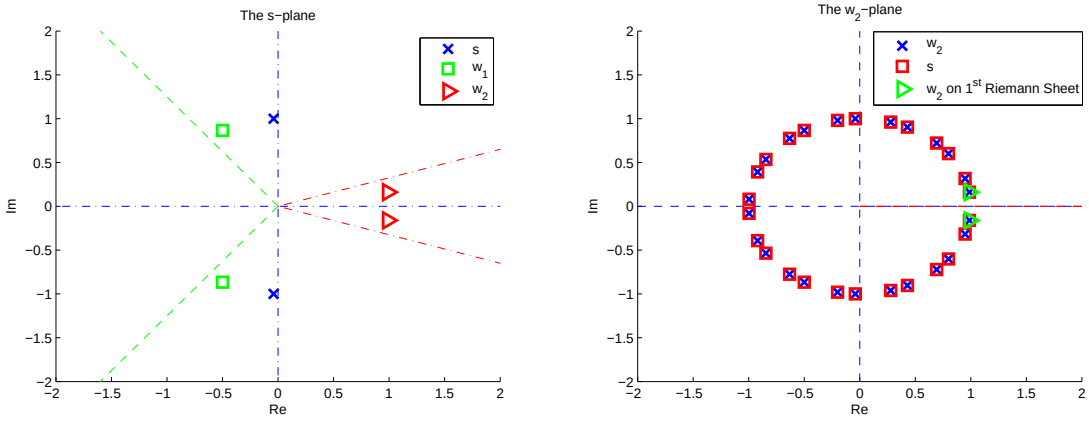

(a) On s-plane. (b) On w_2-plane.

Figure 2.5: The roots of eqn (2.66) and (2.67) on different planes.

From figure 2.5(b), it can be seen that the expansion of s-plane pushes the left sector to the upper sheets of Riemann surface, as if it squeezes and folds that sector when the two edges of the imaginary axis of w_2 are stretched flat and perpendicular to the real axis. Along with the expanded sector, multiple roots located on the left sector are pushed to other sheets as well. From the 2-D top view, the roots appear to be overlapped, which are actually located on the different sheets of the Riemann surface, as shown in figure 2.6. (The graph is generated with the help in [211].) It is important to notice that among the 26 poles, only one pair of complex conjugate poles locate on the first Riemann sheet, $\mathcal{P}$, i.e. $(-\pi, \pi]$ on the s-plane, or equivalently, the sector between $(-\frac{\pi}{10}, \frac{\pi}{10}]$ on the w_2-plane. This can be seen from table 2.2, which lists the 26 roots on the w_2-plane and the expanded s-plane, along with their corresponding angles. (Note that the signs of some roots are flipped after rotation.)

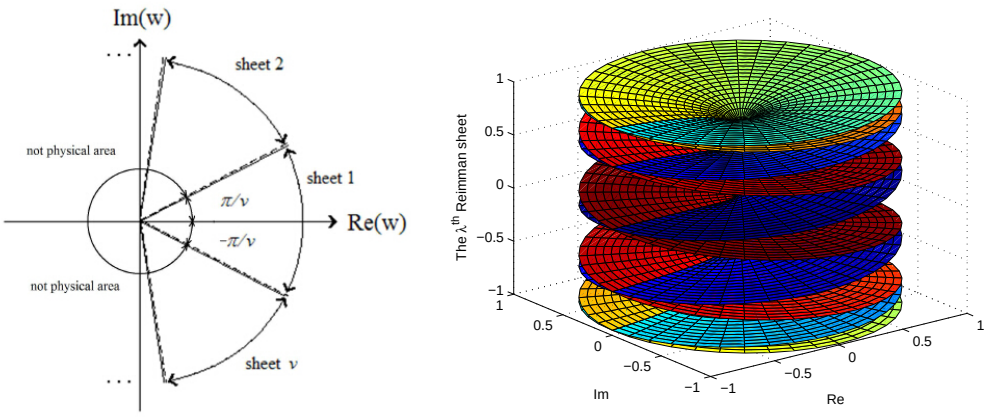

(a) 2-D plane. (b) Riemann surface.

Figure 2.6: The graphical view of expanding a 2-D plane containing 10 sectors to the Riemann surface with 10 sheets.

In the generalized root locus analysis, only the plot on $\mathcal{P}$ is concerned because the time domain behavior and stability properties of the closed-loop system are determined only by that [103]. For example, the behavior of the system $G(s) = \frac{1}{s+1}$ and $\hat{G}(s) = \frac{1}{s^{1.01}+1}$ are almost identical. However, $G(s)$ has one pole while $\hat{G}(s)$ has 100 poles according to definition 3, distributed on 100 Riemann sheets.

Table 2.2: The poles of TF in equation (2.67-2) on different planes.

w_2	arg (rad)	s	arg (rad)	mod(arg, π)
$-0.9968 \pm 0.0805i$	± 3.0610	$0.6927 \mp 0.7212i$	± 30.6104	∓ 0.8055
$-0.9200 \pm 0.3920i$	± 2.7388	$-0.6324 \pm 0.7746i$	± 27.3882	± 2.2555
$-0.8452 \pm 0.5345i$	± 2.5777	$0.7994 \pm 0.6007i$	± 25.7772	± 0.6444
$-0.6324 \pm 0.7746i$	± 2.2555	$-0.8452 \mp 0.5345i$	± 22.5550	∓ 2.5777
$\mathbf{-0.5000 \pm 0.8660i}$	$\mathbf{\pm 2.0944}$	$-0.5000 \pm 0.8660i$	± 20.9440	± 2.0944
$-0.2000 \pm 0.9798i$	± 1.7722	$0.4287 \mp 0.9035i$	± 17.7218	∓ 1.1278
$-0.0403 \pm 0.9992i$	± 1.6111	$-0.9200 \mp 0.3920i$	± 16.1107	∓ 2.7388
$0.2782 \pm 0.9605i$	± 1.2889	$0.9485 \pm 0.3167i$	± 12.8886	± 0.3222
$0.4287 \pm 0.9035i$	± 1.1278	$0.2782 \mp 0.9605i$	± 11.2775	∓ 1.2889
$0.6927 \pm 0.7212i$	± 0.8055	$-0.2000 \pm 0.9798i$	± 8.0554	± 1.7722
$0.9871 \pm 0.1604i$	± 0.1611	$\mathbf{-0.0403 \pm 0.9992i}$	$\mathbf{\pm 1.6111}$	$\mathbf{\pm 1.6111}$
$0.9485 \pm 0.3167i$	± 0.3222	$-0.9968 \mp 0.0805i$	± 3.2221	∓ 3.0610
$0.7994 \pm 0.6007i$	± 0.6444	$0.9871 \pm 0.1604i$	± 6.4443	± 0.1611

Definition 4 (Properness)**.** *The transfer function*

$$G(s) = \frac{N(s)}{D(s)} = \frac{b_m s^{\frac{\beta_m}{\lambda}} + b_{m-1} s^{\frac{\beta_{m-1}}{\lambda}} + \cdots + b_1 s^{\frac{\beta_1}{\lambda}} + 1}{a_n s^{\frac{\alpha_n}{\lambda}} + a_{n-1} s^{\frac{\alpha_{n-1}}{\lambda}} + \cdots + a_1 s^{\frac{\alpha_1}{\lambda}} + 1} \tag{2.68}$$

where β_i and $\alpha_j \in \mathbb{N}$ are the power of $s^{\frac{1}{\lambda}}$ in the descending order, is strictly proper for $\alpha_n > \beta_m$; bi-proper for $\alpha_n = \beta_m$; and improper for $\alpha_n < \beta_m$.

To generate the correct root locus, the selection of the fundamental order for numerator and denominator polynomials needs to be unified. Otherwise, tedious re-mapping is needed. For example, consider the TF below,

$$G(s) = \frac{s^{1.2} + s^{0.8} + s^{0.4} + 1}{s^{1.6} + s^{0.8} + 1}. \tag{2.69}$$

If 0.4 is chosen as the fundamental order for the numerator polynomial while 0.8 is chosen for the denominator, then the TF has three zeros and two poles. It is improper in the conventional intuition. Nevertheless, following definition 3, $\frac{1}{\lambda} = \frac{1}{5}$, then it has 8 poles and 6 zeros, and it is strictly proper.

2.3.2.2 Asymptotes and branches.

Theorem 2 (Asymptotes)**.** *Asymptotes of the root locus plot are straight lines which intersect the real axis at* $\left(\frac{b_m - a_n}{\alpha_n - \beta_m}\right)^{\lambda}$ *and their directions are given by:*

$$\varphi_h = \frac{(2h+1)\lambda}{\alpha_n - \beta_m} 180^\circ, \ \textit{where}$$
$$h = [\frac{\beta_m - \alpha_n - \lambda}{2\lambda}] + 1, \ldots, [\frac{\beta_m - \alpha_n - \lambda}{2\lambda}] + \alpha_n - \beta_m.$$

Asymptotes give direction of the trace of RL. Hence, it is convenient for field engineers when there is no computer aid available. Before the enumeration of more examples, the following facts are worth mentioning.

1. For the root locus plot of $G(w)$ on w-plane, there is possibility that some branches on $\mathcal{P}$ do not start from open-loop poles and terminate at open-loop zeros. They might initiate from and enter into other Riemann sheets. This is demonstrated in example 2.3.3.
2. If $\lambda > \alpha_n - \beta_m$ then there is no asymptote on $\mathcal{P}$.
3. If $\lambda > \alpha_n$, i.e. the highest order is between (0, 1), then there is no pole on $\mathcal{P}$. Take the half order system $G(s) = \frac{1}{s^{0.5}+1}$ for instance, the pole in the main value range, $e^{2\pi j}$, is located on the second Riemann sheet according to the definition of Riemann sheet's branch cut. **Remark:** Actually, the expression $G(s) = \frac{1}{s^{0.5}+1}$ lacks of mathematic rigor because $s^{0.5} + 1 = 0$ has no roots. The commonly treated root $e^{2\pi j}$ is one of the roots of $s^{0.5} + e^{2n\pi j} = 0, (\ n \neq 0)$. Although $e^{2n\pi j}$ and $e^{2 \cdot 0 \cdot \pi j}$ have the same modulus, they have different geometric meaning. That is why $\sqrt{e^{2 \cdot 0 \cdot \pi j}} = \sqrt{1} = 1$, but $\sqrt{e^{2n\pi j}} = e^{n\pi j} = -1$.

2.3.2.3 Case studies

A Matlab based script, `forlocus()`, is created to perform the root locus plot of FO TFs, and is available at [212]. A better technique is used to plot the lines instead of the unevenly spaced dots used in [213] and [129]. As a refinement, the overview of the RL on the whole s-plane is also plotted in order to provide a straightforward feeling about where the RL on $\mathcal{P}$ locates globally. It prompts users in case there is no zeros or poles on $\mathcal{P}$ rather than rendering a blank figure. A baseline verification of the correctness is made in example 2.3.2. Several representative TF structures are selected for demonstration.

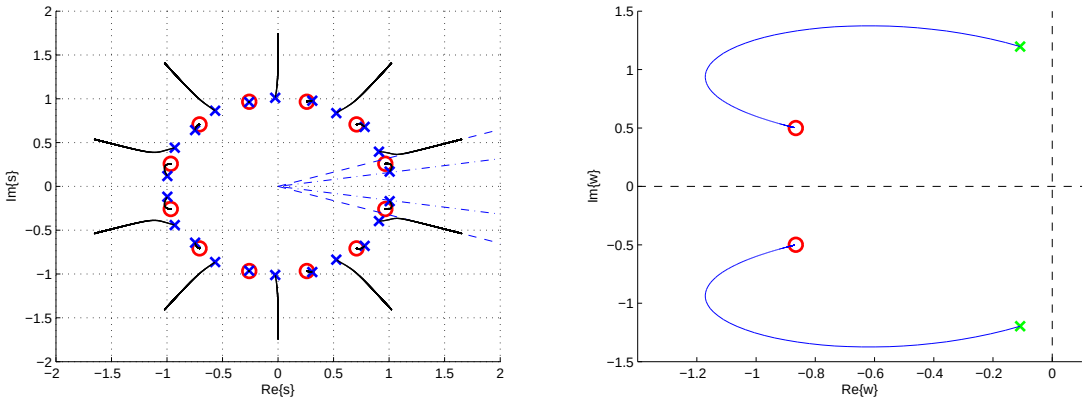

(a) On s-plane. (b) On w-plane.

Figure 2.7: The RL plot of equation (2.70) on different planes.

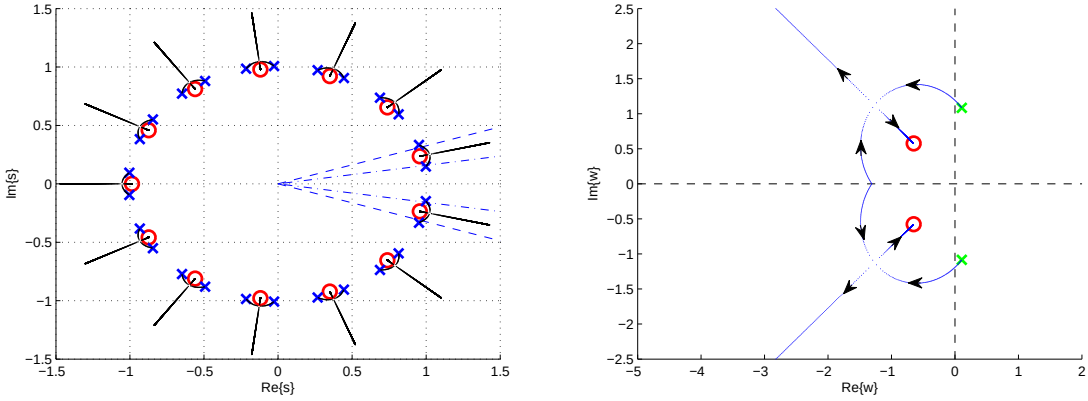

(a) On s-plane. (b) On w-plane.

Figure 2.8: The RL plot of equation (2.71) on different planes.

Example 2.3.2: The following TF is used as a demo in [213]. It is used here to test the created Matlab function, and is plotted in figure 2.7.

$$G(s) = \frac{s^{1.2} + 1}{0.8s^{2.2} + 0.5s^{0.9} + 1}. \tag{2.70}$$

Example 2.3.3: The root locus of the following TF is plotted in figure 2.8.

$$G(s) = \frac{1.2s^{1.3} + 1}{0.8s^{2.6} + 0.6s^{1.3} + 1}. \tag{2.71}$$

A closer view of the 2^{nd} quadrant in figure 2.8(b) tells that the RL in this example has two branches on $\mathcal{P}$. One starts from the pole marked in green, and the other from the next Riemann sheet. Along with the variation of the K gain, they aggregate at $(-1.25 + 1.1i)$ and then bifurcate. One approaches to the open loop zero marked in red and the other goes to infinity.

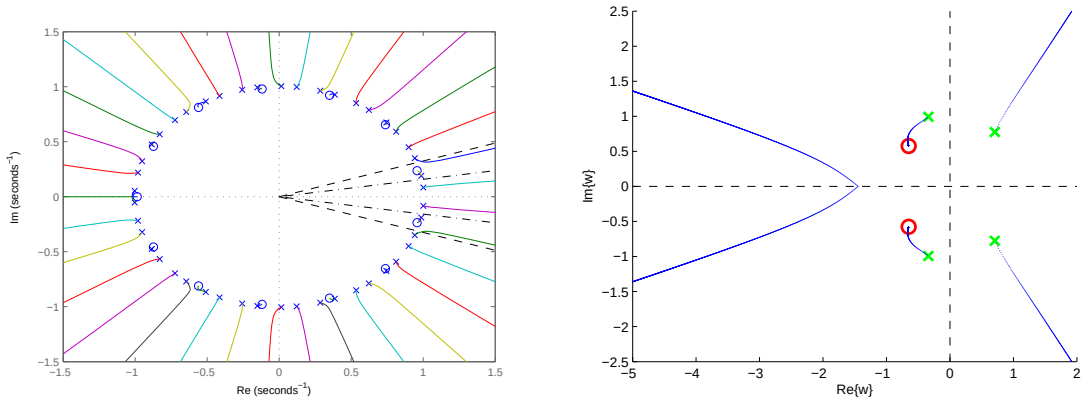

(a) On s-plane. (b) On w-plane.

Figure 2.9: The RL plot of equation (2.72) on different planes.

Example 2.3.4: The RL for the following TF is plotted in figure 2.9.

$$G(s) = \frac{1.2s^{1.3} + 1}{0.8s^{4.6} + 0.6s^{2.3} + 1}. \tag{2.72}$$

It can be seen that this TF has four poles and six zeros on $\mathcal{P}$, (including the infinite zeros). An interesting phenomenon can be observed that there are two branches coming from the 2^{nd} Riemann sheet as if they were not originated from any poles. Moreover, this TF has two open-loop poles on the right half plane on $\mathcal{P}$; thus, it is unstable. The stability of FO TFs are discussed in the next section.

Example 2.3.5: The root locus for the TF in equation (2.69) are plotted in figure 2.10. In comparison to figure 2.9, the RL of this TF contains two branches start from the open loop poles on $\mathcal{P}$ and spread into the next Riemann sheet.

Alternatively, if definition 3 is not followed but definition 10 is chosen for the fundamental order, more poles are generated, as shown in figure 2.11(a), but the RL on $\mathcal{P}$ is the same, see figure 2.11(b).

2.3.3 The stability of fractional order transfer functions

As a complement to the stability discussions in section 2.2.3, this section discusses the BIBO stability and lists two criteria dedicated for FO TFs, namely the extended RL method and a simplified Nyquist criterion.

Definition 5 (BIBO stability - time domain)**.** *A causal LTI system is BIBO stable if and only if its impulse response, $h(t)$, satisfies [103]:*

$$\int_0^\infty ||h(\tau)||d\tau < \infty. \tag{2.73}$$

This is the same with that for integer order systems. It has an equivalent proposition in frequency domain which is different from that for integer order TFs.

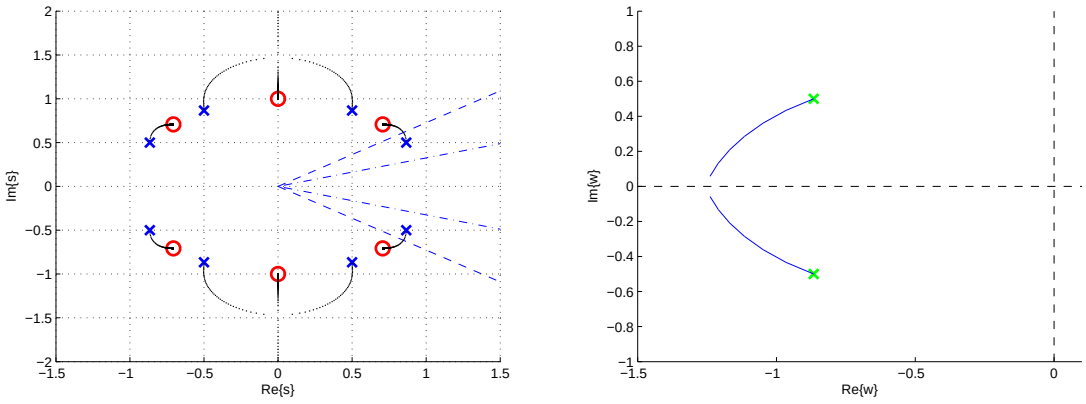

(a) On s-plane. (b) On w-plane.

Figure 2.10: The RL plot of equation (2.69) on different planes using $\lambda = 5$.

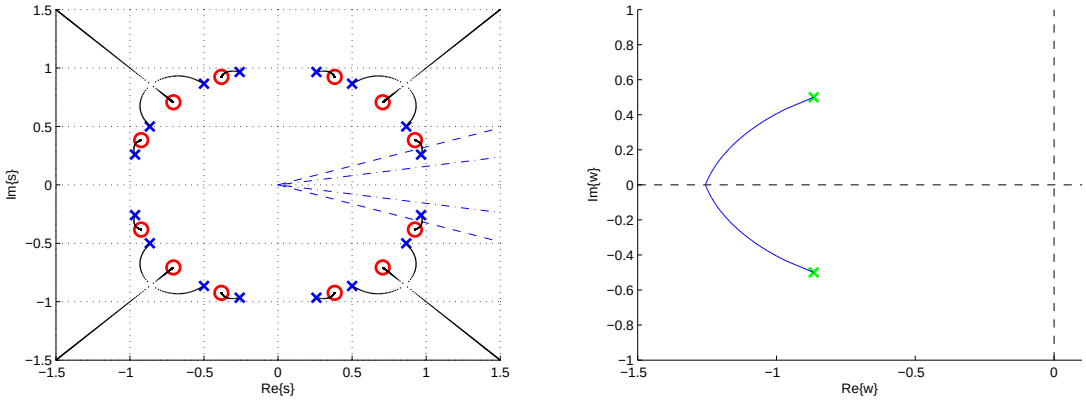

(a) On s-plane. (b) On w-plane.

Figure 2.11: The RL plot of eq (2.69) on different planes using $\lambda = 10$.

Proposition 1 (BIBO stability - s-domain)**.** *An FO TF is BIBO stable if and only if (iff) its transfer function has no pole in the closed right half complex plane, ([105]).*

To be more precise, it should be stated that an FO TF is BIBO stable iff no pole stays on the right half side of $\mathcal{P}$, which is the projection of s-plane on w-plane; or equivalently, no pole stays between $[-\frac{\pi}{2}\frac{1}{\lambda}, \frac{\pi}{2}\frac{1}{\lambda}]$ on the s-plane. The sub-figures in figures 2.5 $\sim$ 2.10 illustrate the s-plane and w-plane, respectively. The stable region plot for FO TFs can be well found in the literature, e.g. [28].

The extended FO root locus method illustrated in the previous section is not only a good graphical tool for evaluating the BIBO stability and the stabilization of unstable FO TFs, but also a visible way of improving system performance to some extent. However, it is for unit feedback with P control only. For systems that can not be stabilized using only P control, such as the one shown in figure 2.9, other compensation methods need to be employed, for example, the fractional order phase-lead/lag compensators, $C(s) = K(\frac{a\tau s+1}{\tau s+1})^{\mu}$, [214, 35].

The next proposition gives a simplified Nyquist criterion for FO TFs, proposed by Trigeassou *et. al*:

Proposition 2 (The Nyquist criterion)**.** *Let $s = j\omega$. If the Nyquist diagram of the open loop transfer function $H(jw)$ is situated at the "right side" of the critical point on the complex frequency domain $(-1, j0)$, then the system $H(s)$ is stable; otherwise, it is unstable.*

For the graphing procedure of the contour and illustrative examples, refer to [215].

As stated in the beginning, all the TFs under discussion in this section are restricted to pure fractional order. The problems for *non-commensurate* order, or more generally *irrational* order TFs could be much more complicated because they have infinite poles (and zeros) which cannot be simplified using a fundamental order. In [75], Sabatier *et. al* suggests the use of the recursive factorization given below to determine their stability. $G(s)$ is treated as a closed-loop TF formed by the open-loop TF:

$$\overline{G_n}(s) = \frac{G_n(s)}{G_n(s)+1}, \tag{2.74}$$

where

$$G_n(s) = \frac{1}{a_n s^{\alpha_n} + a_{n-1} s^{\alpha_{n-1}} + \cdots + 1}, \tag{2.75}$$

The term of the lowest order can be factorized:

$$\begin{aligned} G_n(s) &= \frac{1}{a_1 s^{\alpha_1}} \frac{1}{\frac{a_n}{a_1} s^{\alpha_n - \alpha_1} + \frac{a_{n-1}}{a_1} s^{\alpha_{n-1} - \alpha_1} + \cdots + 1} \\ &= \frac{1}{a_1 s^{\alpha_1}} \overline{G_{n-1}}(s). \end{aligned} \tag{2.76}$$

In the same manner, now, $\overline{G_{n-1}}(s)$ is treated as a closed-loop system:

$$\overline{G_{n-1}}(s) = \frac{G_{n-1}(s)}{G_{n-1}(s)+1}, \tag{2.77}$$

where

$$G_{n-1}(s) = \frac{1}{\frac{a_2}{a_1} s^{\alpha_2 - \alpha_1}} \frac{1}{\frac{a_n}{a_2} s^{\alpha_n - \alpha_2} + \frac{a_{n-1}}{a_2} s^{\alpha_{n-1} - \alpha_2} + \cdots + 1} \tag{2.78}$$

$$= \frac{1}{\frac{a_2}{a_1} s^{\alpha_2 - \alpha_1}} \overline{G_{n-2}}(s). \tag{2.79}$$

Repeat this procedure n times until $G_1(s)$ is obtained. Then the overall stability can be examined by applying the Nyquist criterion on each open-loop sub-system. There are other approaches, e.g. [75, 114, 124], but are not explored in more detail considering the practical usefulness. In this thesis, the truncation method will be used to handle the irrational order case.

2.3.4 Inverse response of fractional order transfer functions

Along with the vast spreading research on fractional calculus related subjects, the fractional calculus is being taken off its mysterious mask for more and more people. While it has been found application in many subjects, the lack of data support and physics foundation in some theoretical assumptions puts doubt on its practical value. For example, the topic of the geometric meaning of fractional derivatives has been discussed in the second international symposium on fractional calculus [216]; the characteristic ratio assignment (CRA) based control of *non-minimum phase* FO systems is presented in [217], yet, is based on pure assumption. This section addresses the inverse response behavior of FO systems with practical data support. The description of real-world phenomenon that generates such behavior is provided to support the argument of its existence, [218]. Along with this study, time domain characteristics of a class of linear FO TFs is documented.

In control theory, the inverse response refers to the phenomenon where the initial response of a linear system to a unit step signal has opposite sign with the steady state value [219]. For integer order systems, the transfer function of such a system contains at least one zero on the right half plane (RHP) in Laplace domain. Take the second order system as an example, the TF that gives inverse response has the following general form can be decomposed into two TFs with different time constants and gains:

$$G(s) = \frac{-bs+1}{a_2 s^2 + a_1 s + 1} = \frac{K_1}{\tau_1 s + 1} - \frac{K_2}{\tau_2 s + 1}. \tag{2.80}$$

The effect of a RHP zero on the Bode phase plot is a 90° phase drop. Hence, this type of systems are also called *non-minimum phase* systems. For fractional order systems, the inverse response become more complicated due to the non-integer orders.

In this research, two scenarios are observed to generate this behavior. One occurs in the temperature control during a semiconductor fabrication process introduced in section 1.2, which is resulted by the thermal contact issues between heaters and the reactor. The other one is observed in the temperature control of Peltier elements under insufficient heat dissipation power.

In the first scenario, the heaters are mounted on a ring shape metal texture (figure 5.26) surrounding a cylindrical reactor which has a different heat expansion rate with the ring. When heaters are turned up, the annuli expands faster than the cylindrical reactor. Thus, a small gap is formed in between, which consequently causes an temporary drop in the temperature. When the expansion of the reactor follows up the annuli, the contact is re-established and the temperature begins to rise. A mechanical sketch is shown in figure 2.12(a), and sample data is plotted in figure 2.12(b).

In the second scenario, an experimental platform is built for the purpose of emulating the above industrial temperature control, as described in a later section, 5.1. At the time when the emulator was built, this inverse response behavior was *not* expected to be reproduced because the hardware configuration of the platform is completely different from the actual industrial equipment. However, surprisingly similar response was observed by coincidence due to different causes. The emulator uses the Peltier elements to pump heat from one side to the other. When it is turned on, the cold side temperature initially drops. However, if the

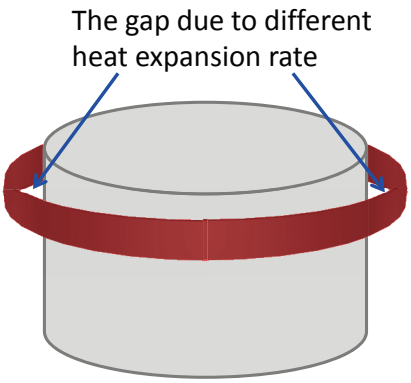

(a) Sketch of different heat expansion rate.

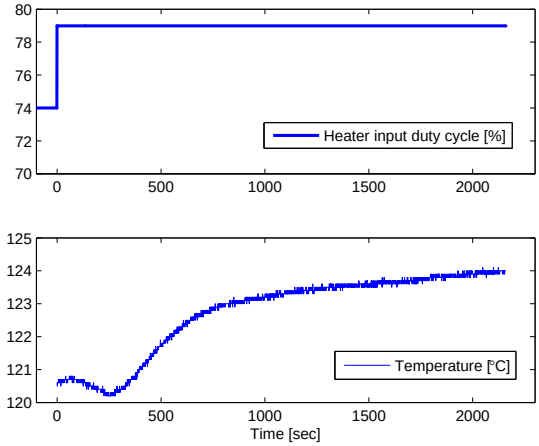

(b) Data showing the inverse response.

Figure 2.12: The data and sketch demonstrating the inverse response in the first scenario due to different heat expansion rates of cylinder and annuli.

cooling capability on the hot side is insufficient, the heat on the hot side will not be removed in time and will cumulate. Thus, the Peltier becomes powerless to continue the heat pumping and both sides warm up, which explains the inverse response in the temperature output. A sample data plot for this case is shown in figure 2.13. Note: it should be distinguished that in the actual process, the increase of the temperature is desired while for the emulator, the increase of the temperature is unwanted.

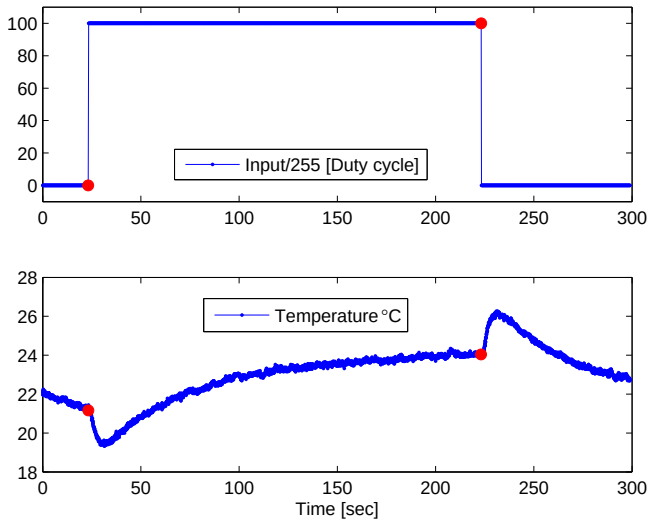

Figure 2.13: The raw data showing the inverse response

On the other hand, when the emulator is powered off, the Peltier element immediately stops the heat pumping. So, the temperature firstly increases due to the internal thermal

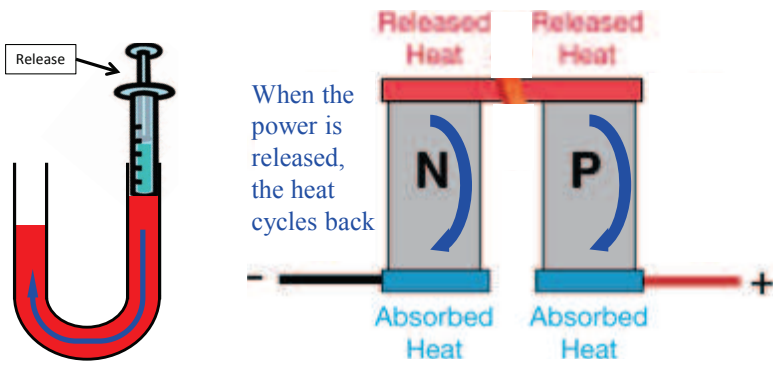

Figure 2.14: The sketch of a communicating vessel for illustrating the thermal cycling inside the Peltier element after power off.

cyclic, and then drops down to the ambient temperature due to natural dissipation. This can be observed from the 230∼300sec data segment in figure 2.13.

Since the Peltier effect is invertible whose inverse is the Seebeck effect [220], a back electromotive force (EMF) will be formed along with this inverse thermal cycling. This is like the phenomenon that a motor become a generator when the rotor is spinning due to inertia after the voltage is removed from the stator. As another analogy, the thermal cyclic is similar to the communicating vessel shown in the sketch 2.14, where when the pump stops, the liquid level in the right tube drops back, pushing the level in the left tube overshoots a bit because of the momentum. Finally, it pulls back again due to gravity.

Since the temperature process essentially contains fractional order dynamics [34, 221], the inverse response behavior can be better fitted by a fractional order non-minimum phase model compared with an integer order model,

$$\text{Second order}: \quad G(s) = \frac{K(-bs+)1}{a_2 s^2 + a_1 s + 1}, \tag{2.81}$$

$$\text{Fractional order}: \quad G(s) = \frac{K(-bs^\alpha + 1)}{a_2 s^{2\alpha} + a_1 s^\alpha + 1}, \ 0 < \alpha < 1. \tag{2.82}$$

The fitted parameters are $a_2 = 175.81$, $a_1 = 54.1$, $b = -39.7$, $K = 2.9$ for the second order model and $a_2 = 87.27$, $a_1 = 25.33$, $b = -21.41$, $K = 3.45$, $\alpha = 0.823$ for the FO model. The fitting result is plotted in figure 2.15, where the criteria is evaluated by the integral absolute error (IAE). By introducing the extra parameter α, the fitting error of the FO model is 15.4512, an improvement of 6.3% compared with the error of the second order model, 16.4217. Even better results can be achieved if a non-commensurate order model is used,

$$G(s) = \frac{K(-bs^\beta + 1)}{a_2 s^{2\alpha} + a_1 s^\alpha + 1}, \quad 0 < \beta < 2\alpha. \tag{2.83}$$

A difference between this model and the integer order model in equation (2.80) is that the number of polynomial terms on the numerator can be greater than the denominator,

$$G(s) = \frac{K(b_n s^{\beta_n} + b_{n-1} s^{\beta_{n-1}} + \cdots + b_1 s^{\beta_1} + 1)}{a_2 s^{2\alpha} + a_1 s^\alpha + 1}. \tag{2.84}$$

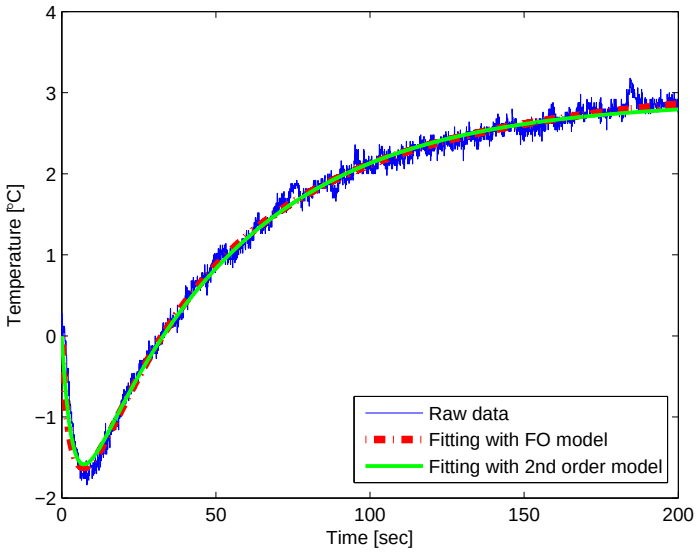

Figure 2.15: Fitting the FO inverse response data with different models.

which is able to provide more fitting freedom. However, the properness is still governed by the constraint $\beta_n < 2\alpha$. Dedicated definition and discussion about FO model properness is presented in the next section.

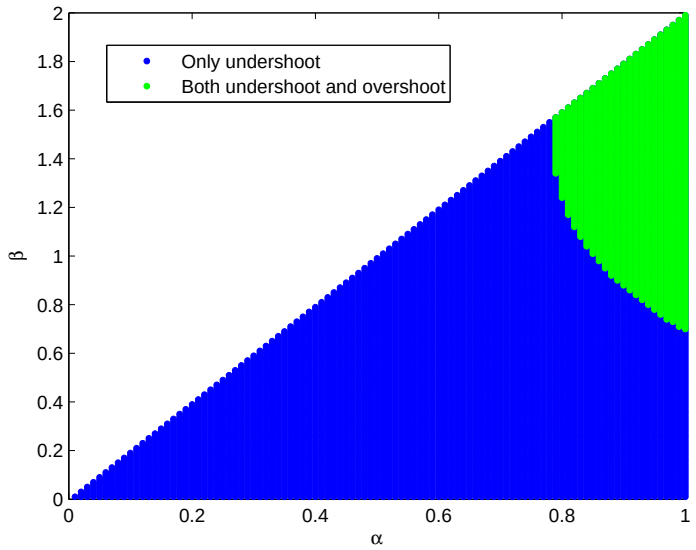

Figure 2.16: The map of overshoot and undershoot vs fractional orders.

In [73], Malti *et al.* explored the resonance conditions of elementary fractional transfer functions. In [222], Tavazoei *et al.* performed a survey on the time domain response of FO systems. In [83], Hartley *et al.* investigated the effect of the fractional-order damping term on the integral errors. To better understand the effect of the fractional orders on the inverse

response, a similar efforts is carried out on a normalized non-minimum phase model,

$$G(s) = \frac{-s^{\beta} + 1}{s^{2\alpha} + s^{\alpha} + 1}. \tag{2.85}$$

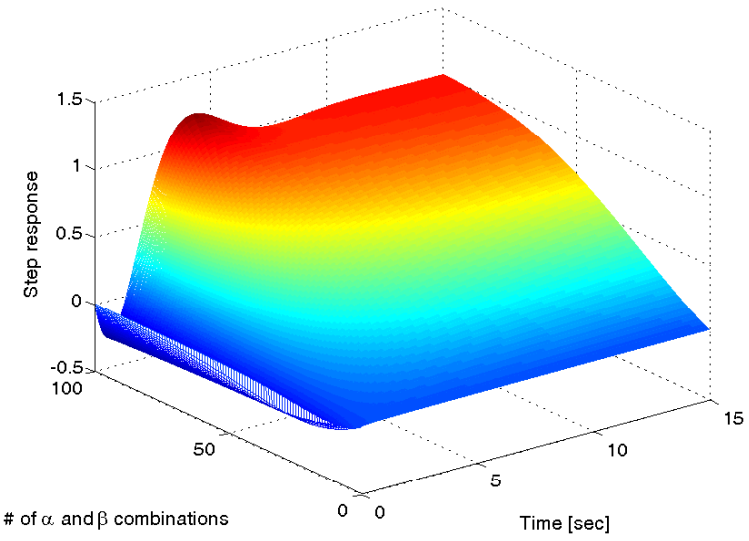

Figure 2.17: The 3D overview of the step response transition.

As shown in figures 2.16 and 2.17, an "order scanning" (will be described in section 3.3.1) is performed to reveal the relationship between the amplitude of the overshoot/undershoot and the orders. To guarantee the strict properness, the highest order on the numerator is limited to one step size lower than that of the denominator.

The envelop of the overshoot percentage versus the fractional orders is plotted in figure 2.18. The boundary of the model response with regard to a unit step input is shown in the green band in figure 2.19. These figures serve as a guidance of understanding the basic behavior of the system in equation (2.85) and furthermore in equation (2.83).

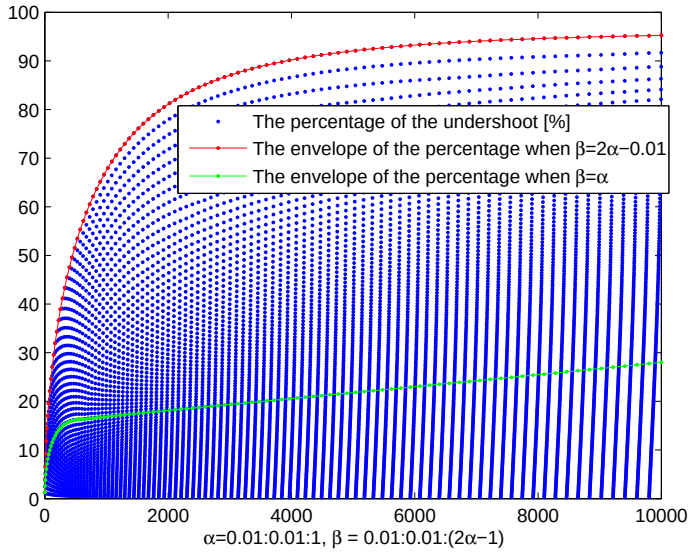

Figure 2.18: The percentage of the undershoot versus the fractional orders.

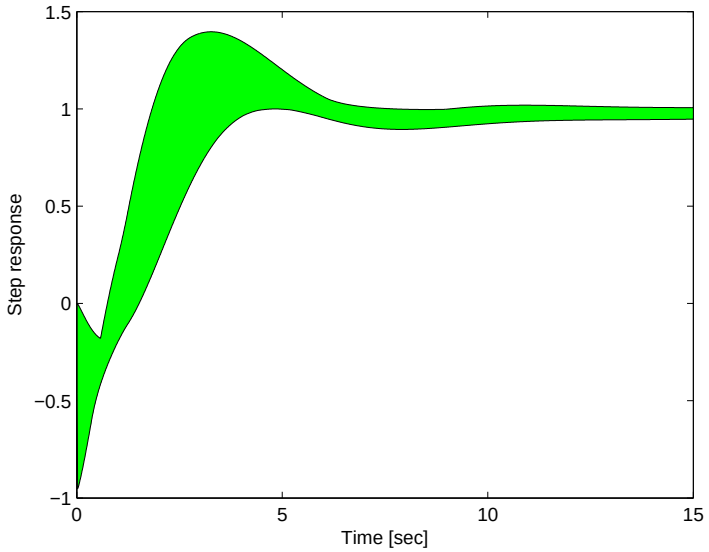

Figure 2.19: The bound of the overshoot and undershoot for different fractional orders on the numerator and denominator.

2.4 Numerical tools for fractional calculus and controls

In recent years, as fractional calculus becomes more and more broadly used across different academic disciplines, there are increasing demands for the numerical tools for the computation of fractional integration/differentiation, or the simulation of fractional order systems. Time to time, being asked about which tool is suitable for a specific application, the author decide to carry out this survey to present recapitulative information of the available tools in the literature, in hope of benefiting researchers with different academic backgrounds.

The fractional calculus got birth 300 years ago, and the research on fractional calculus experienced its boom in the past decades [155, 20, 19]. Besides the fundamental mathematical study, more and more researchers from different academic disciplines begin to utilize it in varieties of subject-associated research, such as in biology and biomedical [17, 223], sociology [224, 225], economics [226, 227], and control engineering [35, 50, 228], etc. Along with the rapid development of theoretical study, the numerical methods and practical implementation also made considerable progress as reviewed in section 1.4.

Sharp tools are prerequisite to a successful job. In this section, an extensive collection of Matlab based tools is presented for the numerical computation of fractional order integration/differentiation, as well as some toolboxes for engineering applications, with an emphasis on fractional order controls. A comprehensive table, table 2.3, is created to list the recapitulative information of these scattered tools in a dashboard view. Brief description and basic evaluation of these numerical algorithms are presented, in terms of usage, accuracy, unique features, advantages and drawbacks. Through such efforts, it is hoped that an informative guidance is provided to readers when facing to the problem of selecting a numerical tool for a specific application. While a text descriptive survey on some of the tools under discussion can be found in book [161], and 28 alternatives for the time-domain implementation of FO derivatives are documented in [229], this section addresses more quantitative comparison and practical usage. Thanks to the authors of these tools. It is these pioneers who bring great convenience for the practical use of FC and FO control.

2.4.1 Collection and description

@fotf

@fotf (fractional order transfer function) is a control toolbox for fractional order systems developed by Xue *et al.* Most of the functions inside are extended from the Matlab built-in functions. In [36], the code and usage of the @fotf toolbox are described in very detail. It uses the overload programming technique to enable the related methods of the Matlab built-in functions to deal with FO models. The transfer function objects generated from it can be interactive with those generated from the Matlab transfer function class. Yet, the overloading of associated functions such as `impulse()`, `step()`, etc, lost the plotting functionality. As a work around, users can simply define a time vector as the second input to these functions. fotf toolbox supports time delay in the TF, e.g. `fotf(a,na,b,nb,delay)`. It does not directly support transfer function matrix, hence, MIMO systems cannot be simulated directly. However, since it provides Simulink block encapsulation of the involved function `fotf()`, multiple input/output relationship can be established by manually adding loop interactions

in Simulink block diagrams. Therefore, the remark "could" is put in the "MIMO" column in table 2.3.

A small drawback with @fotf is that the sampling time has relatively big impact on the accuracy, which has been remarked in the validation comments in [36]. Encouragingly, an update is upcoming according to the author.

ninteger

Ninteger, non-integer control toolbox for Matlab, is a toolbox intended to help with developing fractional order controllers and assessing their performance, [79]. It uses integer order transfer functions to approximate the fractional order integrator/differentiator, $C(s) = ks^{\nu},\ \nu \in \mathbb{R}$. It offers three frequency domain approximation methods,

1. The CRONE method that uses a recursive discretization,

$$C(s) = k' \prod_{n=1}^{N} \frac{1 + s/\omega_{z,n}}{1 + s/\omega_{p,n}};$$

2. The Carlson's method that solves $C^{\alpha}(s)$ using Newton's iterative method,

$$C_n(s) = C_{n-1}(s) \frac{(\alpha - 1)C_{n-1}^{\alpha}(s) + (\alpha + 1)g(s)}{(\alpha + 1)C_{n-1}^{\alpha}(s) + (\alpha - 1)g(s)};$$

3. The Matsuda's methods, that approximates C with a gain known at several frequencies.

$$\begin{aligned} C(s) &= [d_0(\omega_0); \quad (s - \omega_{k-1})/d_k(\omega_k)]_{k-1}^{+\infty}, \\ d_0(\omega) &= |C(j\omega)|, \quad d_{k+1}(\omega) = \frac{\omega - \omega_k}{d_k(\omega) - d_k(\omega_k)}. \end{aligned}$$

It also provides Simulink block encapsulation of the involved functions, such as 'nid' and 'nipid' blocks. Moreover, it offers a user-friendly GUI for fractional order PID controller design.

There is a problem with ninteger toolbox in Matlab version 2013a or later. Without additional editing, it has conflicts with some built-in functions due to the overload editing of the Matlab built-in function "isinteger()". For example, calling the `mean()` function will prompt an error.

ooCroneToolbox

The CRONE Toolbox, developed since the nineties by the CRONE team, is a Matlab and Simulink toolbox dedicated to applications of non integer derivatives in engineering and science [60]. It evolved from the original script version to the current object-oriented version. A good feature of the CRONE toolbox is that some of the methods are implemented for MIMO fractional transfer functions. For example, executing `sysMIMO=[sys,sys;sys2,sys2]` generates a two-input-two-output TF matrix. Many simulation results in the literature are obtained using the CRONE toolbox such as the design of centralized CRONE controller with the combination of the MIMO-QFT approach in [230]. Several other toolboxes are inspired

by CRONE, e.g. ninteger and FOMCON. A drawback of the CRONE toolbox is that time delay cannot be incorporated into the generated FO TF. Manually multiplying the delay to the `frac_tf` object does not work either because the `exp()` operation is not overloaded by `frac_tf` class. CRONE is a toolbox much more powerful than merely simulating fractional order systems. In spite of this basic functionality, it is also capable of fractional order system identification and robust control analysis and design.

FOMCON

The FOMCON (Fractional-Order Modeling and Control) toolbox is developed by Tepljakov *et. al*, [231]. Its kernel utilizes the algorithms in fotf, ninteger and Crone. It encapsulates some of the major functionalities of those three toolboxes, and builds a GUI shell on top, aiming at extending classical control schemes for FO controller designs. The relation of FOMCON with the three toolboxes is shown in figure 2.20. Some notable changes/patches to the original fotf are:

- `newfotf()` uses the string parser to enable users to input TF as a string;
- `tf2ss()` is overloaded and `foss()` is added, which makes the conversion between an FO TF object and an FO state space object possible. The CRONE toolbox is also able to do the task, yet the script is encrypted in Matlab P code format.

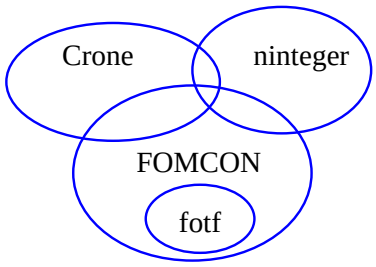

Figure 2.20: FOMCON's relation to other numerical tools, [2].

M-L functions

M-L functions, as the name implies, are Matlab functions developed for numerically computing the Mittag-Leffler function in equation (2.10). There are several versions of code by different authors available in the literature. Five of them are listed in table 2.3, where

1. `mlf(`α, β, x, p`)` is for the calculation of the 2-parameter M-L function in the form of $E_{\alpha,\beta}(x)$ with the precision of p for each element in x, and is a new version for `ml_func()`;

2. `ml_func([`α, β, γ, q`], `z, n, ε_0`)` is capable of computing the M-L function with either 1, 2, 3, or 4 parameters, and the script is available in the books [210] or [35]; It uses the fast truncation algorithm to improve the efficiency, and embeds the `mlf()` in the file such that when the fast truncation algorithm is not convergent, solution is guaranteed by trading off some efficiency;

3. `ml_fun`$(\alpha, \beta, x, n, \varepsilon_0)$ $(\alpha > 0, \beta > 0)$ is also for 2-parameter M-L function with error tolerance of ε_0, which is implemented using C-MEX .dll and can be used in Simulink through s-functions;
4. `gml_fun`$(\alpha, \beta, \gamma, x, \varepsilon_0)$ calculates the generalized M-L function with 3 parameters in the form of $E^{\gamma}_{\alpha,\beta}(x)$, [232];
5. `ml`$(x, \alpha, \beta, \gamma)$ can calculate the M-L function with either 1, 2, ro 3 parameters.

Alternatively, the generalized hypergeometric function `[pfq]=genHyper (a,b,z, lnpfq, ix, nsigfig)` in [233], or `[y,tt,nterms]=pfq (a,b,z,d)` in [234] can also achieve the numerical computation of the generalized M-L functions under certain conditions. For more details, refer to [157].

NILT

The inversion of Laplace transform is fundamentally important in the applications of Laplace transform method. It can be carried out with one of the following three approaches: 1). analytical solution using definition and basic properties; 2). Laplace transform tables; and 3). numerical computation. While analytical solutions are usually too hard to be obtained, and tables do not cover arbitrary cases, the numerical computation becomes an inevitable way. Among the numerous algorithms for numerical inversion of Laplace transform (NILT), `NILT` in [235, 236] and the "improved NILT" in [237, 238, 239] have relatively bigger literature exposure. Lubomir's NILT method applies the fast Fourier Transformation (FFT) and the ε-algorithm to speed up the convergence of infinite complex Fourier series. A very detailed description and performance evaluation of these methods is available in [240]. Hence, repetitive comparison among different NILTs are not presented here. Focus is mainly put on the comparison between NILT and other numerical methods.

A good feature of the two NILT code is that both support the direct input of time delay in the form of `exp(-Ls)`. Yet, `INVLAP()` gives some glitch at the end of the delay, for example, `[x,y]=INVLAP('1/(s* (s^0.5+1))*exp(-s)',0.01,10,1000)`. There is a tricky part need to be noted in evaluating the computational error of `NILT`. If the same initial, terminating and sampling time (t_0, t_f and $\mathrm{T_s}$) for other tools are used in the script, the `NILT` actually computes one point less than the other tools which use regularly spaced time vector. That is because: let $M = \frac{t_f - t_0}{T_s}$ represent the amount of points computed by `NILT`, then, the time interval is actually $T_s' = \frac{t_f - t_0}{M-1}$ due to the script `t=linspace(0,tm,M)`. Whereas the conventional assignment of time vector (`t=t0:Ts:tf`) generates `M+1` points. In order to compute the same amount of points aligned to the time stamps used for baseline analytical solution, the time vector for analytical computation needs to be adjusted so as to adapt to that used by `NILT`. This means to let analytical computation use the time vector generated by `NILT`, which can be achieved by either 1). `t=0:M*Ts/(M-1):M*Ts`, or 2). `t=linspace(0,tm,M)`. This cannot be done the other way around, i.e. replaced by `t = 0:Ts:M*Ts-Ts` nor `t=linspace(0,tm-Ts,M)`. Otherwise, cumulated computation error will cause inaccuracy of the final simulation result. Alternatively, if t_f is not a concern, user can assign one point less to `M` in the `NILT` script while keeping T_s unchanged. Thus, `NILT` generates the same time stamps except a t_f shortened by one sampling period. The difference

in dealing with time vectors can be easily visualized if longer sampling time is assigned. An example of the resulting computation error is demonstrated in figure 2.21. Similar time stamp assignment issue exists in `INVLAP()`. In addition, the initial time stamp is not allowed to be 0 due to the constraint in the `INVLAP()` script.

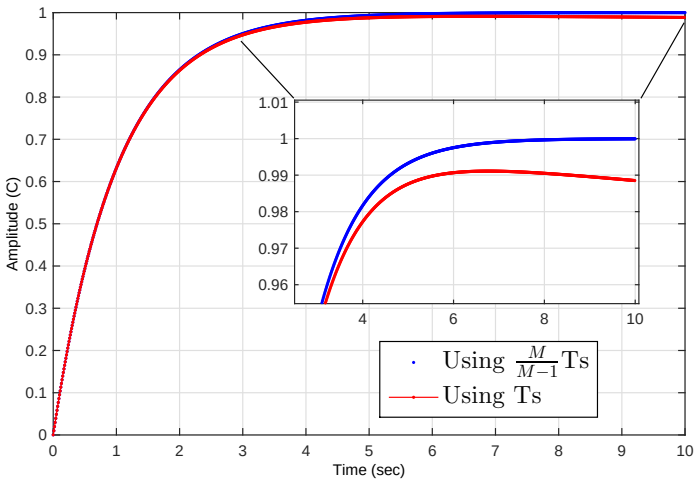

Figure 2.21: Computation error of NILT caused by mis-assignment of Ts.

dfod

DFOD (Digital Fractional Order Differentiator/Integrator) is a set of Maltab functions writhen by Petráš *et al.*, for the approximation of fractional order differentiators and integrators. There are three versions of dfod:

1. `dfod1()` is the IIR type based on continued fraction expansion (CEF), shown in equation (2.86), of weighted operator with the mixed scheme of the trapezoidal (Tustin) rule and the backward difference (Euler) rule, [241];

$$Z\{D^{\alpha}x(t)\} = CFE\{(\frac{1-z^{-1}}{T})^{\alpha}\}X(z) \approx (\frac{1}{T})^{\alpha}\frac{P_p(z^{-1})}{Q_q(z^{-1})}X(z). \tag{2.86}$$

2. `dfod2()` is the FIR type based on power series expansion (PSE), shown in equation (2.87), of the backward difference (Euler) rule, [242];

$$D^{\mp\alpha}(z) = \frac{1}{(1-z^{-1})^{\pm\alpha}} = \frac{T^{\mp\alpha}}{\sum_{j=0}^{\infty}(-1)^j\binom{\pm\alpha}{j}z^{-j}} \approx \frac{T^{\mp\alpha}}{Q_q(z^{-1})} \tag{2.87}$$

3. `dfod3()` is a new IIR type based on power series expansion of the trapezoidal (Tustin) rule, [243].

$$\text{Euler} : \mathrm{s}^{\alpha} \approx \left[\frac{1-\mathrm{z}^{-1}}{\mathrm{T}}\right]^{\alpha}, \quad \text{Tustin} : \mathrm{s}^{\alpha} \approx \left[\frac{2}{\mathrm{T}}\frac{1-\mathrm{z}^{-1}}{1+\mathrm{z}^{-1}}\right]^{\alpha}. \tag{2.88}$$

There are other FO algorithms based on IIR, such as `newfod()` by Chen [244].

Regarding discretization, besides the aforementioned methods used in the various tools, other methods exist such as the Prony's technique, direct discretization, the binomial expansion of the backward difference, etc., [137].

IRID

The impulse response invariant discretization (IRID) is a family of functions designed by Chen, Li, Sheng *et al.* [38, 245], for different approximation purposes based on the algorithm as its name implies. It includes the following members:

1. `irid_fod()` is designed to compute a discrete-time finite dimensional (z) transfer function to approximate a continuous irrational transfer function s^α where 's' is the Laplace transform variable and $-1 < \alpha < 1$. It has been tested that the algorithm still works for $\alpha > 1$ and $\alpha < -1$, by removing the input checking statement.
2. `irid_doi()` is for the approximation of distributed order integrator $\int_a^b \frac{1}{s^\alpha} d\alpha$, where '$a$' and '$b$' are arbitrary real numbers in the range of (0.5 ,1), and $a < b$.
3. `irid_dolp()` is for the approximation of a continuous-time fractional order low-pass filter in the form of $1/(\tau s + 1)^\alpha$
4. `irid_fsof()` is for the approximation of fractional second order filter in the form of $1/(s^2 + as + b)^\alpha$ where $0 < \alpha < 1$.
5. `BICO_irid()` is for the approximation of BICO (Bode's Ideal Cut-Off) transfer function in the form of $1/(s/w_0 + \sqrt{(s/w_0)^2 + 1})^\alpha$, where $\alpha > 0$.

ora_foc

`ora_foc()` is for the approximation of fractional order differentiators, $\frac{1}{s^\alpha}$, [246], using the Oustaloup-Recursive-Approximation method described in [247].

fderiv

`fderiv()` calculates the fractional derivative of order α for the given function $r(t)$ using the G-L definition, [248]. The input of the given function is represented by a vector of signal values. There is an improved implementation of this function, `fgl_deriv()`, by Jonathan, which uses vectorization for faster computation with Matlab, [249].

glfdiff

`glfdiff(y,t,`α`)` (G-L finite diff) is a Matlab function written by Xue *et al.* [250] for calculating the α^{th} derivative of a given function, whose inputs y, t are the signal and time vectors. It is based on the forward finite difference approximation of the G-L definition,

$$ {}_aD_t^\alpha f(t) \approx \frac{1}{h^\alpha} \sum_{j=0}^{(t-1)/h} \omega_j^{(\alpha)} f(t - jh), \tag{2.89} $$

where the binomial coefficients are recursively calculated, [250]:

$$ \omega_0^{(\alpha)} = 1, \quad \omega_j^{(\alpha)} = \left(1 - \frac{\alpha + 1}{j}\right) \omega_{(j-1)}^{(\alpha)}, \quad j = 1, 2, \ldots \tag{2.90} $$

Fractional differentiation and integration

Many of the above functions approximate the fractional order integral or derivative operator. This Matlab function calculates the α^{th} order derivative or integral of a function, defined in a given range through Fourier series expansion. The necessary integrations are performed with the Gauss-Legendre quadrature rule, [251]. Three examples are provided in this package, namely FO differ/integral of identity, cubic polynomial and tabular functions, respectively. The main call function is `fourier_diffint()`.

FIT

FIT is the Fractional Integration Toolbox developed by Santamaria Laboratory at the University of Texas at San Antonio, [252]. It is for the numerical computation of fractional integration and differentiation of the R-L type, and is designed for large data size, which allows parallel computing of multiple fractional integration/differentiation on GPUs (graphical processing units). The extrapolation and interpolation algorithms used by this toolbox are implemented in C++ and are integrated with Matlab via MEX mechanism. Detailed explanation can be found in [253].

DFOC

DFOC, written by Petráš *et al.*, is a digital version of the Fractional-Order PID Controller of the form:

$$C(s) = K + T_i \frac{1}{s^m} + T_d s^d. \tag{2.91}$$

It provides a transfer function of the FO PID controller for given parameters, [254].

FOPID

The fractional order PID (FOPID) controller toolbox, presented by Lachhab *et al.*, is for the design of robust fractional order $PI^{\alpha}D^{\beta}$ controllers, [255]. The tuning rules for the parameters follow those promoted in [41] and [58]. Thus, the fractional order PID tuning is converted to a 5-parameter optimization problem. This toolbox utilize the "non-smooth" H_{∞} synthesis in [256] to perform the minimization. For now, there is not a publicly available source for download.

Sysquake FO PID

In [257], Visioli and Pisoni *et al.* presented an interactive tool for fractional order PID controllers developed on the Sysquake software environment, which is a similar effort with that for integer order PIDs done by Åström *et al.* in [258]. Sysquake is a numerical computing environment based on a programming language mostly-compatible with Matlab. However, the interactive tool for FO PID runs in the Sysquake environment instead of Matlab. Hence, it is not reviewed in detail here.

Table 2.3: Matlab based numerical tools for computation of fractional operations and fractional order controls.

#	Name	Typical usage	Sample syntax	Author(s)	Source	Delay	MIMO
1	fotf	FO control toolbox	`s=fotf('s')`	Dingyü Xue	[250]	✓	Could
2	ninteger	FC and FOC toolbox	`nid(k,a,[w1 w2],5,'crone')`	D Valério	[79]	Could	Could
3	Crone	FO control toolbox	`frac_tf(1,frac_poly_exp(1,0.5)`	CRONE team	[59]	×	✓
4	FOMCON	FO modeling & control	`sys_foss = tf2ss(g)`	A Tepljakov	[231]	✓	✓
5a	mlf	2-param M-L func	`y=mlf(a,b,-t)`	I. Podlubny	[259]	N/A	N/A
5b	ml_func	$1 \sim 4$ param M-L func	`y=ml_func([a,b,r],-t)`	Dingyü Xue	[35]		
5c	ml_fun	2-param M-L func	`y=ml_fun(a,b,x,n,e)`	S. Mukhopadhyay	[260]		
5d	gml_fun	Generalized M-L func	`gml_fun(a,b,r,x,eps0)`	YQ Chen	[261]		
5e	ml	1,2,3-param M-L func	`e= ML(x,a,b,r)`	R Garrappa	[262]		
6a	NILT	Num Inverse of Laplace	Script based	L Brančík	[238]	✓	×
6b	INVLAP	Num Inverse of Laplace	`[t,y]=INVLAP('1/s',1,10,100)`	Code by Juraj	[263]	✓	×
7	dfod1,2,3	Digital FO diff/int	`sysdfod=dfod3(n,T,r)`	I Petráš	[241]	N/A	N/A
8	irid_fod ...	Impulse Resp Invariant	`df=irid_fod(-.5,.1,5)`	YQ Chen	[245]	N/A	N/A
9	ora_foc	Oustaloup-Rec-Approx	`ora_foc(0.5,2,0.1,100)`	YQ Chen	[264]	N/A	N/A
10	fderiv	FO diff of r(t)	`y=fderiv(0.5,r,Ts)`	F. M. bayat	[248]	N/A	N/A
11	glfdiff	Finite Diff of G-L	`y1=glfdiff(y,t,r)`	Dingyü Xue	[250]	N/A	N/A
12	fourier_diffint	FO diff of f(x)	`fourier_diffint(f,x,..)`	G Papazafeiropoulos	[251]	N/A	N/A
13	FIT	FO integration toolbox	`fracIntegrationSIM(...)`	Marinov *et al.*	[252]	N/A	N/A
14	DFOC	Discrete FO PID	`DFOC(K,Ti,Td,m,d,Ts,n)`	I Petráš	[254]	N/A	×
15	FOPID	FO PID	—	Lachhab *et al.*	[255]	—	×
16	FOCP	Fractional optimal control	Calling RIOTS	C Tricaud *et al.*	[265]	×	✓
17	FSST	FO S-S Toolkit	Simulink blocks	D. Sierociuk	[266]	✓	✓
18	FVO	Fractional variable order	`ban(alpha,N,h)`	Podlubny *et al.*	[267]	N/A	N/A
19	forlocus	RL plot of FO TFs	`forlocus(num,den,l)`	Zhuo Li *et al.*	[212]	N/A	N/A

The 'Delay' column denotes if the script/toolbox is able to handle time delay in the FO model.
The 'MIMO' column denotes if the script/toolbox is able to handle MIMO FO models.

FOCP

In [268], Tricaud and Chen *et al.* formulated the Fractional Optimal Control Problems (FOCP) into the integer order format by using a rational approximation of the fractional derivative obtained from the singular value decomposition (SVD) of the Hankel matrix of the impulse response. Then, RIOTS_95, described in section 4.3.1.2, is called to perform the optimization. The scheme is potentially able to solve any type of FOCPs and is implemented in Matlab for public accessibility, [265]. It supports MIMO FO optimal control, but does not handle time delay due to the limitation of RIOTS.

FSST

FSST is a simulation toolkit in Matlab/Simulink for the fractional order discrete state-space system education. The toolkit consists of a set of C-MEX s-functions which are encapsulated in Simulink blocks. Several typical fractional order system simulation examples are provided as shown in figure 2.22, such as the fractional order state-space model and the fractional Kalman filter (FKF), [269]. The version 1.7 is available for free download at [266]. Two of the superior strengths of FSST are: 1.) it can directly simulate MIMO systems since it is a Simulink block kit handling state space representations; 2.) it is able to incorporate the initial conditions into the dynamic equations to be simulated, which is a unique feature among all the aforementioned tools. The drawback of FSST is that the step size has large impact on the simulation results, even larger than the impact by "cilcular" buffer size. A sample illustration is plotted in figure 2.23.

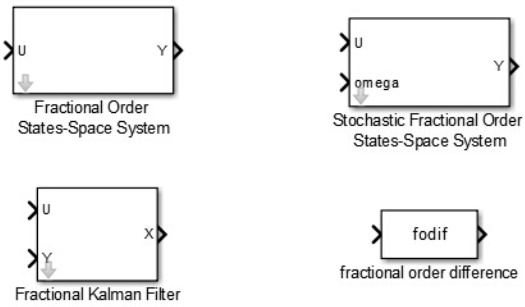

Figure 2.22: The Simulink block set provided in FSST.

Fractional variable orders

All the above tools/toolboxes (except `irid_doi()`) deal with constant fractional orders. Yet, there exists a type of differentiations that have fractional variable orders (FVO). The definitions in the G-L format are given as follows, [270]:

Definition 6 (The 1^{st} type FVO)**.**

$$ {}_0D_t^{\alpha(t)} f(t) = \lim_{h \to 0} \frac{1}{h^{\alpha(t)}} \sum_{r=0}^{n} (-1)^r \binom{\alpha(t)}{r} f(t - rh). \tag{2.92} $$

The 2^{nd} and 3^{rd} types can be found in the same reference.

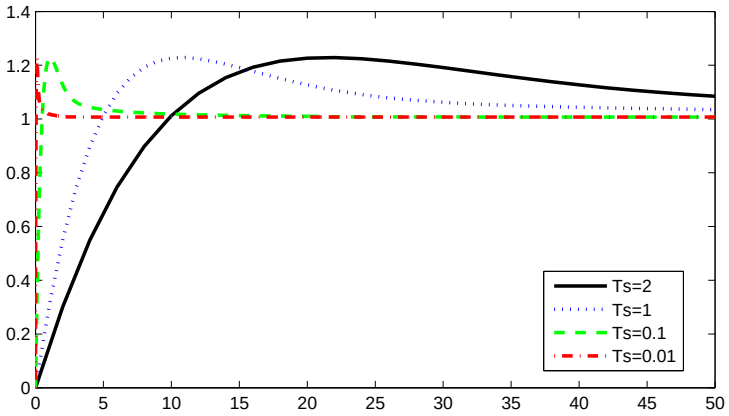

Figure 2.23: The impact of simulation step size on the FSST toolbox.

Regarding the fractional variable order differentiation, there are dedicated tools. Podlubny *et al.* offers a matrix approach that unifies the numerical differentiation of integer order and the n-fold integration, using the so-called triangular strip matrices, [267]. It is available for download at [271] and can be applied on the solution to FODEs and FPDEs.

Sierociuk *et al.* provides a C-MEX s-function based Simulink toolkit, "fvoderiv", for this purpose, [272]. It supports Matlab real-time-workshop (RTW).

The toolbox "vod" created by Valério *et al.* calculates variable fractional or complex order derivatives. R-L, Caputo and G-L definitions are provided; the three types of definitions in [270] are all considered. Fuzzy supervised implementations in Simulink are also provided, [273].

FO RL

Three Matlab based scripts for plotting root locus of fractional order TFs are available. Two early works are `frlocus()` in [213], and the code attached in the paper [129] by Machado *et al.*. The other is `forlocus()` developed by the author and used to generate the figures in section 2.3, which is listed in the last row in table 2.3. Besides, the newest version of @fotf toolbox also features the root locus plot of FO systems.

Other tools

Text description of a few tools listed above can also be found in [274]. There are other fractional calculus related tools or Matlab scripts available for specific applications, such as the fractional Fourier transform (FrFT) [162, 163], closed-form solutions to linear fractional order differential equations, `fode_sol()` [35], the M-L random number generator `mlrnd()` [275], digital fractional order Savitzky-Golay differentiator [276], and the functions for simulating fractional-order chaotic systems [33], etc. Considering the scope of research, they are not enumerated here and only fundamental FC and FO control related tools are reviewed.

2.4.2 Evaluation and comparison

2.4.2.1 Comparison I

To evaluate the collected tools, several groups of benchmark problems and inputs are designed. For the FO control toolboxes, the following problems are used,

1. Baseline model: first order transfer function,

$$g_b(s) = \frac{1}{s+1},$$

whose time domain analytical solution of its step response is: $y(t) = 1 - e^{-t}$;

2. Impulse response of half order integrator:

$$g_{hint}(s) = \frac{1}{\sqrt{s}},$$

whose time domain analytical solution is: $\frac{1}{\sqrt{\pi t}}$;

3. TF with a half order pole:

$$g_{hp}(s) = \frac{1}{\sqrt{s}+1},$$

whose time domain analytical solution is:

$$\frac{1}{\sqrt{t}} E_{\frac{1}{2},\frac{1}{2}}(-\sqrt{t}), \text{ or equivalently, } \frac{1}{\sqrt{\pi}\mathrm{t}} - \mathrm{e^t erfc}[\sqrt{\mathrm{t}}];$$

4. The commensurate order TF:

$$g_{com}(s) = \frac{6s^{1.2} + s^{0.8} + 2s^{0.4} + 3}{5s^{1.6} + s^{0.8} + 2};$$

5. Step response of the irrational order TF:

$$g_{ir}(s) = \frac{2s^{\sqrt{3}} + 1}{s^{\sqrt{5}} + 3s^{\sqrt{2}} + 1}.$$

The accuracy is quantified by the conventional integral absolute error (IAE) criteria, $S = \int_0^T |e(t)|dt$. All comparison have been kept as fair as possible. The numerical values of the time domain analytical solution using Matlab built-in functions are assumed to be accurate and is adopted as the baseline. The computational errors when $T_s = 0.05$ are summarized in table 2.4, where the row indices represent the methods numbered in table 2.3, and the column indices represent the test problems respectively. Besides, 'M' denotes the Matlab built-in TF and '-' means the underlying method is not applicable for the test problem. Two sample plots of the step responses of problems 1 and 5 are shown in figures 2.24 and 2.25. For problems 4 and 5, since analytical solution is hard to obtain, all methods are compared to the values computed by fotf.

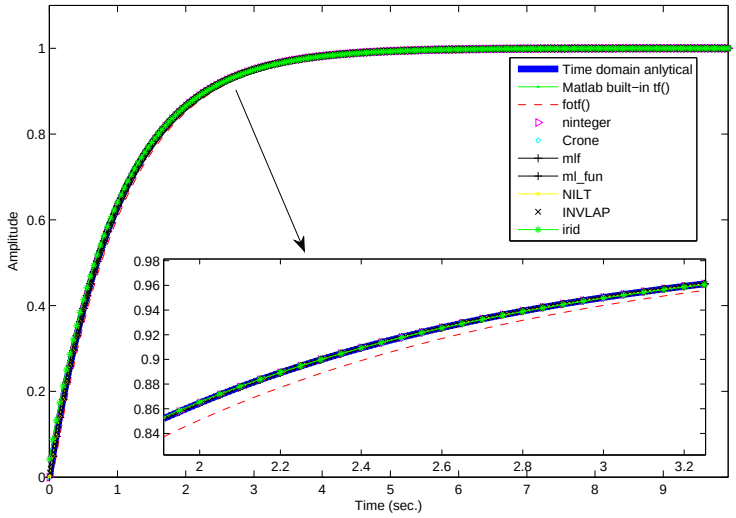

Figure 2.24: Comparison of the step responses of problems 1.

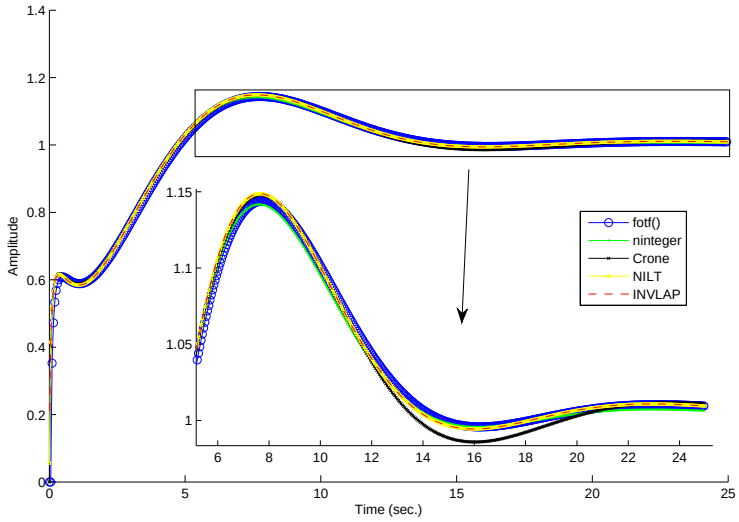

Figure 2.25: Comparison of the step responses of problem 5.

For the impulse response of the half-order integrator, the first point is ignored for error calculating because it is infinity. Two graphic views of the comparison are shown in figures 2.26(a) and 2.26(b), with `Ts=0.01` and `Ts=0.1` respectively.

As stated in [245], `irid_fod()` uses finite dimensional (z) TF as the approximation method. Hence, the order of the (z) TF has impact on the approximation accuracy. The error listed in table 2.4 is based on the 10^{th} order approximation. An illustrative plot is shown in figure 2.27. The sampling time also has impact on its accuracy. The anti-intuitive fact is that relatively greater `Ts` gives higher accuracy. A heat map of the error on the field

Table 2.4: Evaluation results on the test problems 1∼5.

Error / Method	1	2	3	4	5
M	0	-	-	-	-
1	1.4955	8.4176	6.6813	"0"	"0"
2	3.18×10^{-13}	2.5287	0.3831	9.8434	2.5519
3	0.4956	2.9627	1.4254	10.454	3.1857
5a	0	-	4.69×10^{-4}	-	-
5c	8.62×10^{-12}	-	1.08×10^{-10}	-	-
6a	0.0016	0.0236	0.0206	6.1528	2.4477
6b	0.0059	0.0012	2.49×10^{-5}	3.4722	1.5042
8	0.5327	0.0071	0.2189	-	-

of `Ts=0.01:0.001:0.1` and `order=3:30` is plotted in figure 2.28. At some particular high orders, "rank deficient" would occur during the call of `prony()` inside `irid_fod()`. Users can choose appropriate orders according to their specific accuracy requirement.

The analytical expression of M-L function is a summation of infinite terms. Hence, it is not surprising to see the numerical computation induced error in the results.

2.4.2.2 Comparison II

Table 2.5: Quantitative comparison of function int/diff tools.

Methods / Criteria	Analytical	`fderiv()`	`glfdiff()`	`fourier_diffint()`	FIT
Error 1	-	140.5000	1.8232	792.4660	0.0000
Elapsed T1	0.0001	1.4028	0.0029	0.0874	0.0209
Error 2	-	339.7973	2.1208	250.5433	0.0743
Elapsed T2	0.0001	1.4105	0.0029	0.0893	0.0201

`fderiv()`, `glfdiff()`, `fourier_diffint()` and FIT are integration /differentiation tools for functions. For this group of tools, the following two problems are designed to compare the performance.

1. Half order derivative of the function $y(t) = 3t$ on the interval of $[0, 5]$, whose analytical solution is,

$$ {}_0D_t^{0.5} y = \frac{3\Gamma(2)}{\Gamma(1.5)}\sqrt{t}. \tag{2.93} $$

2. 0.75 order integration of the function $y(t) = \sqrt{t}$, whose analytical solution is,

$$ {}_0D_t^{-0.75} y = \frac{\Gamma(1.5)}{\Gamma(2.25)} t^{1.25}. \tag{2.94} $$

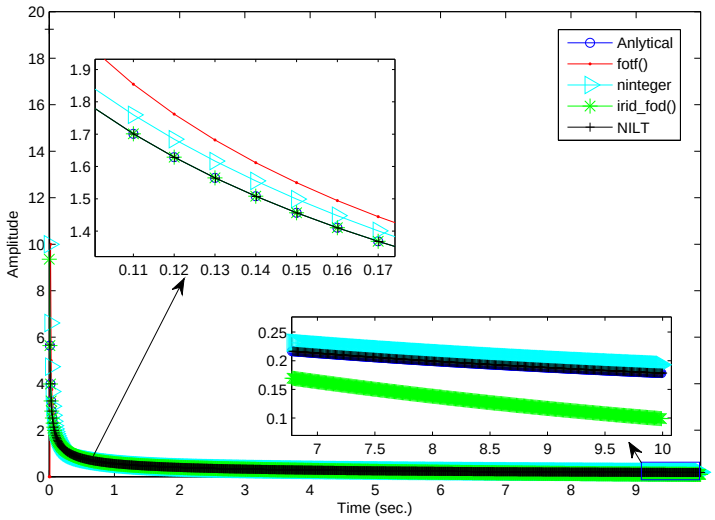

(a) `Ts=0.01`

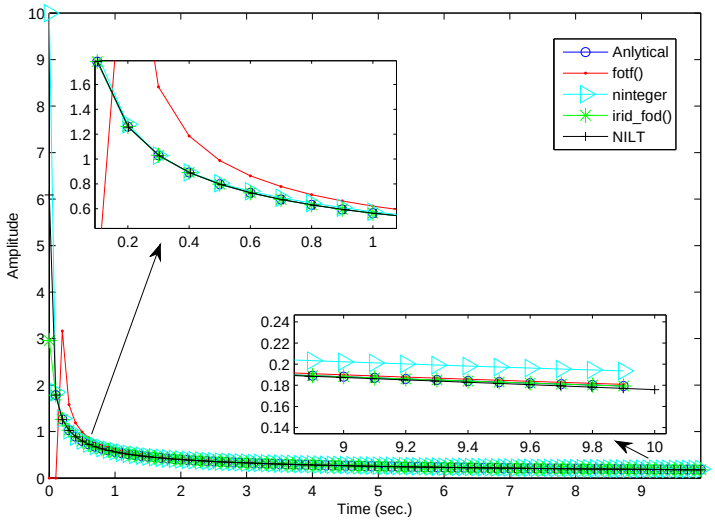

(b) `Ts=0.1`

Figure 2.26: Comparison of the impulse responses of the half order integrator.

The time steps are all set to 0.01 sec. It can be seen that `fourier_diffint()` performs not as well as other methods although a big number of Fourier and Gaussian coefficients have been assigned (default values are 260 and 520 for identity polynomial). Its performance on a 3^{rd} order polynomial is better. The results are plotted in figures 2.29 and 2.30. Quantitative comparison including computational error and averaged elapsed time (for 20 runs each) are listed in table 2.5, for the above two problems respectively.

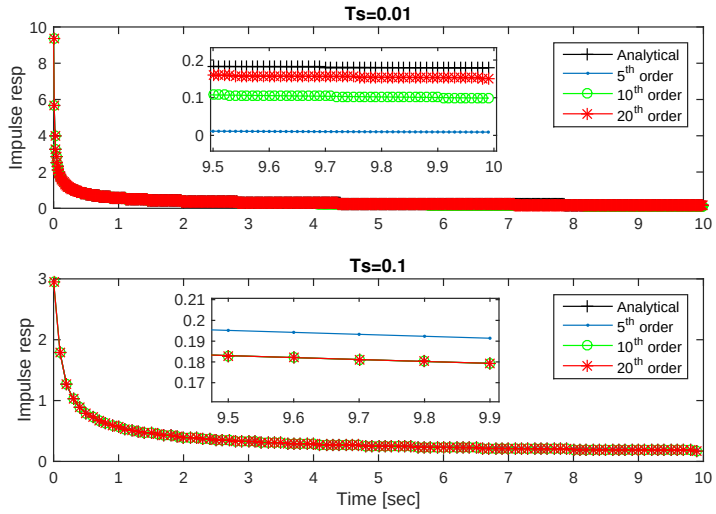

Figure 2.27: The T_s and order impact on `irid_fod()`.

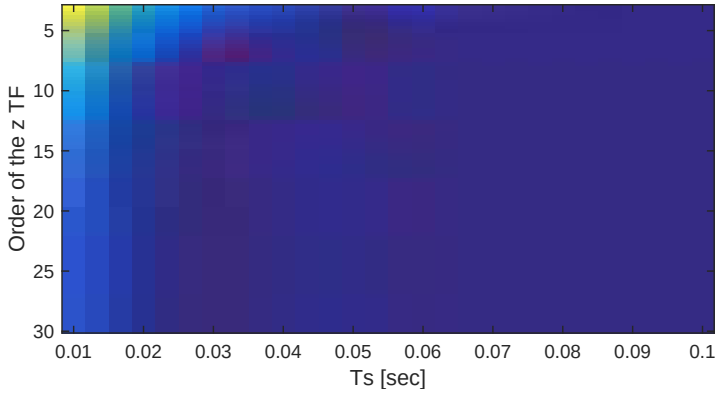

Figure 2.28: The heat map of approximation error of `irid_fod()` versus the order and sampling time.

2.4.2.3 Comparison III

Although the simulation of fractional order pseudo state space models can be achieved indirectly, some toolboxes do provide the direct simulation capability, such as the CRONE toolbox and FSST. Since the function `frac_ss` in CRONE toolbox only adopts the input of commensurate order systems, for comparison purposes, the following commensurate order pseudo state space model is selected,

$$\begin{aligned} \begin{bmatrix} x_1 \\ x_2 \end{bmatrix}^{(0.7)} &= \begin{bmatrix} 0 & 1 \\ -0.1 & -0.2 \end{bmatrix} \begin{bmatrix} x_1 \\ x_2 \end{bmatrix} + \begin{bmatrix} 0 \\ 1 \end{bmatrix} u \\ y &= \begin{bmatrix} 0.1 & 0.3 \end{bmatrix} \begin{bmatrix} x_1 \\ x_2 \end{bmatrix} \end{aligned} \tag{2.95}$$

To involve more tools into comparison, the FO integrator blocks in the FOTF and Ninteger toolboxes are used to represent the above fractional differential equations in Simulink, as

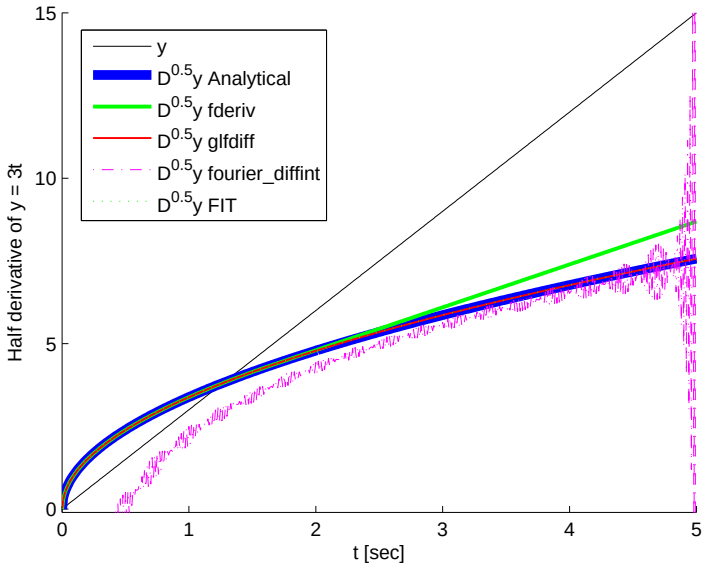

Figure 2.29: Comparison of half derivative of function $y(t) = 3t$, using `fderiv()`, `glfdiff()`, `fourier_diffint()` and FIT respectively.

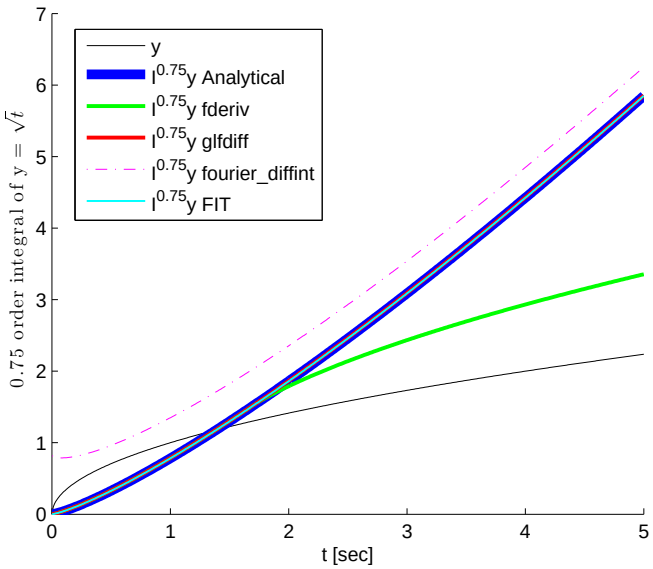

Figure 2.30: Comparison of 0.75^{th} order integration of function $y(t) = \sqrt{t}$, using analytical solution, `fderiv()`, `glfdiff()`, `fourier_diffint()` and FIT respectively.

shown in figure 2.31. The comparison of the unit step responses computed by the four toolboxes are plotted in figure 2.32, from which it can be seen that the result obtained using FSST (1 sec for step size) has bigger difference from the others. However, since analytical solution is not easy to obtain, it is insufficient to claim which method gives highest accuracy. Hence, quantitative comparison is not provided. As an alternative, users can transform the

above FO S-S model to an FO transfer function model, assuming zero initial conditions,

$$G(s) = C(s^{\alpha}I - A)^{-1}B = \frac{3s^{0.7} + 1}{10s^{1.4} + 2s^{0.7} + 1}. \tag{2.96}$$

Thus, the NILT scripts can be used to compute the numerical solution, which has relatively higher reliability according to the authors observation.

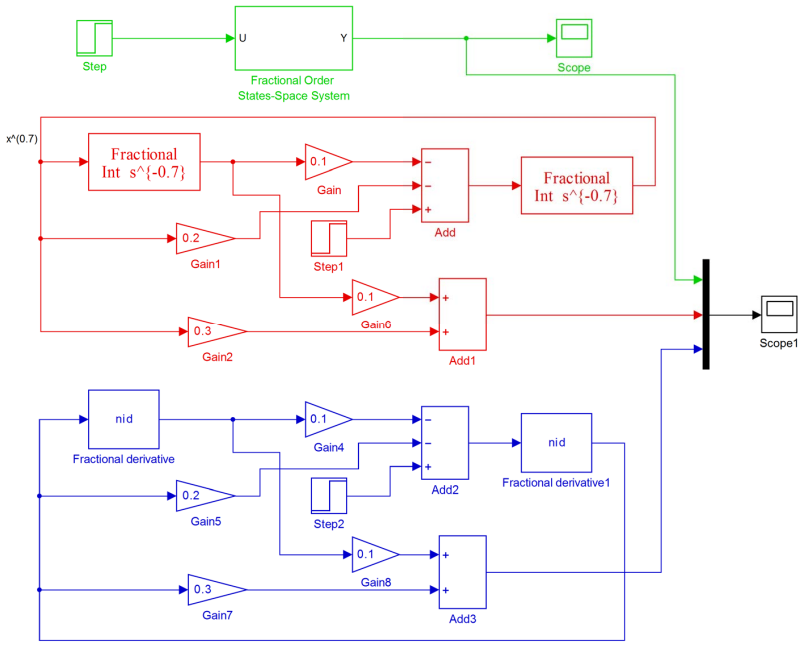

Figure 2.31: The Simulink block diagrams for the FO pseudo S-S model in equation (2.95).

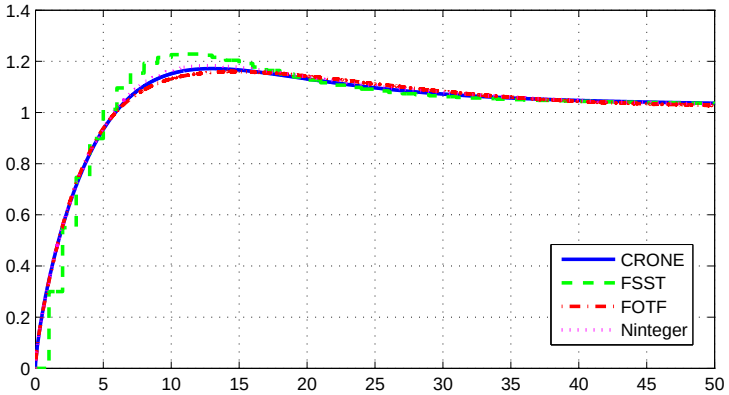

Figure 2.32: Comparison of the simulation results of the FO pseudo S-S model obtained with different toolboxes.

2.4.2.4 Summary

A tricky part for the simulation of fractional order systems is that even if the system is broken down to the bottom layer, i.e. the analytical solution, it usually still involves the computation of M-L functions, which still needs to rely on the numerical tools or scripts. From the comparison, it can be seen that in the category of integrating/differentiating a function, glfdiff and FIT outperform other tools in terms of accuracy; in the category of control system simulation, NILT always provides higher accuracy. However, other toolboxes has advantages, for example, ninteger and CRONE toolbox provide integrator blocks in Simulink, which makes the simulation of nonlinear systems possible.

Chapter 3

Fractional Order Process Modeling and Identification

> You make your own chances.
>
> — O. Henry, *Mammon and the Archer*

If we don't have a model, make one.

3.1 Fractional order processes

Fractional order models can be commonly found in biology, chemistry and physics. To name a few, the membrane charging model in [17], the fractional impedance in botanic elements [277], the ion channel gating model in [278], and the heat transfer process in [65]. In spite of the slow dynamics, FO models can be found presence in electrical engineering and motion controls as well. For example, the analog FO control element which is called "fractor" in [11], the FO velocity model in [58], and the FO circuits in [33]. More real-world instances can be referred to the literature review in section 1.4.

As FO models being adopted to depict more and more phenomena, industrial processes begin to use them as well. The most brilliant way of modeling a process is to build through physics or chemistry principles and math deduction. Such kind of models contain the most compound and profound practical insights. However, due to the complexity and hybridity of realistic engineering problems, this is usually infeasible. In general, the commonly used modeling approach in engineering contains two steps: model structure selection and parameter identification. In this chapter, several selected modeling and identification techniques are briefly reviewed. Two new frequency domain based methods, employing the relay feedback approach, are developed and presented in subsections 3.3.3 and 3.3.2. Nonlinear FO system identification is addressed in section 3.4, where the feedback linearization of fractional order systems are proposed and investigated.

3.2 Model structure selection for fractional order systems

The first physical system to be widely recognized that demonstrating "fractional" behavior is probably the semi-infinite lossy (RC) transmission line, [139, 17]. Heaviside considered its impedance using the operational calculus which is later on recognized as: $V(s) = \frac{1}{\sqrt{s}} I(s)$. As the time goes, more and more physical phenomenon are discovered to exhibit "fractional" behavior, [279, 161].

3.2.1 Physics based model selection

Two fractional calculus related physical scenarios that are most commonly encountered in the industrial processes are stated in the following subsections. Fractional order model selection for similar engineering applications are recommended to refer to these model structures.

3.2.1.1 Thermal models

Thermal processes are most commonly seen in the conventional industries. In [280, 72], Oustaloup and Malti *et. al* investigated the developing of a new device for heat flux estimation in machining tools during severe machining or in high enthalpy plasma flow. In [139], Das *et. al* explored the modeling problem of furnace wall encountered during the development of a fuel-efficient nuclear plant control system. In [281, 34], Petras *et. al* studied the heat transfer process on a PCT40 experimental platform, and in heterogeneous media on a Peltier module based platform. All of these applications use the thermal model of the ideal heating process on a semi-infinite beam described by the heat transfer equation with no energy loss:

$$\frac{\partial^2}{\partial \lambda^2} T(t, \lambda) = a \frac{\partial}{\partial t} T(t, \lambda), \tag{3.1}$$

with the initial condition: $T(0, \lambda) = T_0$ and boundary condition: $T(t, 0) = T(t)$, where $T(t, \lambda)$ is the temperature of the beam at time $t > 0$ and 1-D spatial coordinate $\lambda > 0$; a is the thermal diffusivity determined by the heat conduction coefficient k, the heat capacity c and density ρ of the material. Let $u(t, x) = T(t, \lambda) - T_0$ Applying the Laplace transform gives,

$$\frac{\partial^2}{\partial \lambda^2} U(s, \lambda) = asU(s, \lambda). \tag{3.2}$$

Since the heat flux is defined as $H(t, \lambda) = \partial T(t, \lambda)/\partial \lambda$, then, the above equation leads to a fractional order transfer function relation between temperature and the heat flux at λ,

$$G(s) = \frac{U(s, \lambda)}{H(s, \lambda)} = \frac{1}{\sqrt{as}}, \quad [281] \quad \text{or} \tag{3.3}$$

$$G(s) = \frac{U(s, \lambda)}{H(s, \lambda)} = \frac{1}{\sqrt{as}} exp(-\lambda\sqrt{as}), \quad [72]. \tag{3.4}$$

The relation between temperature and the heat flux at λ with energy loss is derived in [72] as:

$$G(s) = \frac{T(s, \lambda)}{H(s, \lambda)} = \frac{k}{\sqrt{as} + 1}. \tag{3.5}$$

An recent application of fractional order thermal models in the bituminous froth heater control in the oil sands extraction industry can be found in [135].

3.2.1.2 Rheological models

Damping is the usually used artifice in the vibration control of mechanical systems. The integer order Kelvin-Voigt model is used to depict the stress-strain relationship of Maxwell materials composed of a purely viscous damper and purely elastic spring in parallel,

$$\sigma(t) = [E + \eta\frac{d}{dt}]\varepsilon(t), \tag{3.6}$$

where σ is the stress, ε denotes the strain, and η is the viscosity. The strain response to a suddenly applied stress, σ_0, is,

$$\varepsilon(t) = \frac{\sigma_0}{E}(1 - e^{-\frac{E}{\eta}t}), \tag{3.7}$$

which is exactly the time domain solution to the step response of a first order transfer function. There are variations of this model, such as the 3-parameter Zener model [282]. More references can be found in [191].

When the Newtonian elements (dashpot) is replaced by a Scott-Blair element that reveals viscoelastic behavior, the fractional Kelvin-Voigt model is proposed to describe the stress relaxation and creep behavior, [283, 161],

$$\sigma(t) = [E + \eta\frac{d^\alpha}{dt^\alpha}]\varepsilon(t), \tag{3.8}$$

where the order of the derivative depicts the material's characteristic, $\alpha = 1$ depicts viscous liquid while $\alpha = 0$ depicts elastic solid. Values in between depict materials that are instantaneously elastic and long-term viscous [284, 285]. Variations of this model include the fractional Zener model. This equation naturally leads to a fractional order TF model in the following form,

$$G(s) = \frac{k}{\tau s^\alpha + 1}. \tag{3.9}$$

When a mass is connected to such a fractional order damping structure, the displacement, $X(s)$, with regard to a driving force, $F(s)$, can be derived. After normalization, it is expressed as,

$$G(s) = \frac{X(s)}{F(s)} = \frac{1}{s^2 + as^\alpha + 1}, \tag{3.10}$$

which is called the *spring-mass-viscodamped* dynamics in [83]. Taking a step further, this model is extended to the form that possesses a distributed order by Sheng, Chen *et. al*, [286, 287],

$$G(s) = \frac{X(s)}{F(s)} = \frac{1}{s^2 + \int_a^b c(\alpha)s^\alpha d\alpha + 1}. \tag{3.11}$$

This type of FO models are not only used in mechanical engineering, but also in other industries. For example, a recent application of using fractional derivatives to simulate viscoelastic fluids in the computer animation industry can be found in [288] and [289]. With this technique, computer animation is expected to deliver better user experiences.

3.2.1.3 Fractional order plasma models

Plasma, sometimes called glow discharge, is often referred to as the fourth fundamental state of matters. It is used in many emerging industries, such as surface treatment, aerospace metallurgy, and bio-pharmaceuticals, [290, 291, 292]. As mentioned in section 1.2, this research is originated from problems posed in the plasma etching industry, such as the plasma DC bias modeling. Therefore, two plasma physics related models that utilize fractional calculus are reviewed for later reference in section 5.7.

Ion energy distribution (IED) is one of the many crucial measures of plasma status. Lieberman *et al.* proposed a computation method for ion energy distribution of multi-frequency capacitive discharges [293], in which the following Fourier transfer function,

$$g(f) = \frac{1}{((cf\tau_i)^p + 1)^{1/p}}, \quad p > 0 \tag{3.12}$$

is chosen to determine the ion response $V_i(t)$ to the sheath voltage $V_s(t)$. This model is in the form of Gravrilyak-Negami function [294]. It fits a lot of experimental data well, and is derived from the following relaxation equation,

$$\frac{\partial V_i(x,t)}{\partial t} = -\frac{V_i(x,t) - V_s(x,t)}{\tau_i}. \tag{3.13}$$

In [295], the electron heating in a capacitive radio frequency with non-Maxwellian distributions is studied. Usually, the electron velocity distribution (EVD) in a bulk plasma is given by $f_0(u,t) = g_0(u - u_0(t))$, where $g_0(u)$ takes a single temperature Maxwellian distribution,

$$g_0(u) = n_0 \left(\frac{m_e}{2\pi e T_e}\right)^{\frac{1}{2}} exp(\frac{-m_e u^2}{2eT_e}) \tag{3.14}$$

where m_e, T_e and u are the mass, temperature and velocity of electrons, respectively. However, if the temperature is not uniform, the EVD needs to be approximated by a bi-Maxwellian or even generalized Maxwellian distribution, in which the distribution function has a *warmer tail*, i.e. it decreases as a power law of the velocity u rather than exponentially, [296].

$$g_0(u) = \frac{n_0}{(\sqrt{\pi}\theta)^3} \frac{\Gamma(\kappa+1)}{\sqrt{\kappa^3}\Gamma(\kappa - \frac{1}{2})} (1 + \frac{u^2}{\kappa\theta^2})^{-(\kappa+1)}, \tag{3.15}$$

where $\theta = \sqrt{(2\kappa - 3)T_e/\kappa m_e}$ and κ is the spectral index. This inverse power law distribution has been confirmed by practical observation in many circumstances.

The modeling of plasma impedance is briefly described in section 5.7.

3.2.1.4 Relaxation models

The *Cole-Cole model* is used to describe dielectric relaxation in polymers [297], and has a similar form to the above IED model in equation (3.12),

$$\varepsilon^*(\omega) - \varepsilon_\infty = \frac{\varepsilon_s - \varepsilon_\infty}{1 + (j\omega\tau)^{1-\alpha}}, \quad 0 < \alpha < 1, \tag{3.16}$$

where ε^* is the complex dielectric constant, ε_s and ε_∞ are the static and infinite frequency dielectric constant. This is actually the equation (3.10) in the complex frequency domain. When $\alpha = 0$, the Cole-Cole model reduces to the *Debye model*,

$$\varepsilon^*(\omega) - \varepsilon_\infty = \frac{\varepsilon_s - \varepsilon_\infty}{1 + j\omega\tau}. \tag{3.17}$$

As another relaxation modeling example, Nigmatullin *et al.* proposed a *Cole-Davidson* model for the dielectric relaxation in [298]. More relaxation models have been discussed in subsection 2.2.1.3 and can be found in the references therein, e.g. [284].

From these examples, it can be seen that fractional order dynamic model structures indeed benefit industrial productions and hence, have their value of existence.

3.2.1.5 Time series models

The AR, ARX, ARMA, etc., models are often used in time series analysis. Control engineers use them for system identification, [299]. For fractional order systems, the output has totally different characteristics from that of the integer models in terms of correlation. Thus, these models can no longer depict the time series generated by FO systems, and FARIMA is created.

Definition 7 (AR model)**.**

A process is auto-regressive of order p, AR(p), if there exist constant $a_1, \dots a_p$ such that,

$$X_t = \sum_{k=1}^{p} a_k X_{t-k} + \varepsilon_t \tag{3.18}$$

ε_t is a Gaussian white noise, [40]. The AR(p) process is weakly stationary if and only if all the roots of the polynomial $P(z) = 1 - a_1 z - \cdots - a_p z^p$ lie outside the unit circle in the complex plane.

The above process $\{X_t\}$ is a moving average of order q, MA(q) if there exist constants $b_1, \dots b_q$ such that,

$$X_t = \sum_{k=0}^{q} b_k \varepsilon_{t-k}. \tag{3.19}$$

Definition 8 (ARX model)**.**

The auto-regressive with external input (ARX) model has the following format,

$$a(d)y(t) = b(d)u(t) + e(t), \quad or \quad y(t) = \frac{b(d)}{a(d)}u(t) + \frac{1}{a(d)}e(t), \tag{3.20}$$

where a and b are polynomials with regard to d. Linear regression can be used for model parameter estimation. The development of ARX models using fractional order and orthonormal basis filter parametrization can be found in [300, 301].

Definition 9 (ARMAX model)**.**

The auto-regressive moving average with external input (ARMAX) model can be expressed as,

$$a(d)y(t) = b(d)u(t) + e(t), \quad or \quad y(t) = \frac{b(d)}{a(d)}u(t) + \frac{c(d)}{a(d)}e(t). \tag{3.21}$$

Model parameters *cannot* be estimated using linear regression.

Definition 10 (OE model)**.**

The Output Error (OE) model has the form below:

$$a(d)y(t) = b(d)u(t) + a(d)e(t), \quad or \quad y(t) = \frac{b(d)}{a(d)}u(t) + e(t). \tag{3.22}$$

In [302], Poinot and Trigeassou *et al.* identified a diffusion process using the OE model.

Definition 11 (ARMA model)**.**

The autoregressive-moving average (ARMA) process X_t is defined as

$$\Phi(d)X_t = \Theta(d)\varepsilon_t, \tag{3.23}$$

where d is the back-shift operator; or following the above format,

$$X_t = \sum_{i=1}^{p} a_i X_{t-i} + \sum_{j=1}^{q} b_j \varepsilon_{t-j} + \varepsilon_t. \tag{3.24}$$

It is known that an integer order LTI systems can be characterized by a linear difference equation known as the ARMA model in the discrete case, [40]. However, the ARMA model only characterizes short-range-dependant property of the time series. For fractional order LTI systems, the outputs in fact possesses LRD characteristic. Thus, the fractional ARMA and FARIMA models are proposed.

Definition 12 (BJ model)**.**

The Box-Jenkins (BJ) model is a combination of the AR and MA models [303]. It assumes that the time series is stationary. Otherwise, Box and Jenkins recommend differencing non-stationary series one or more times to achieve stationarity, which produces an ARIMA model.

The block diagrams of the AR, ARX, BJ and OE models can be found in Ljung's book [299], chapter 4.

Definition 13 (ARIMA model)**.**

The auto-regressive integrated moving average (ARIMA) model is a generalization of the ARMA model, which can be viewed as a "cascade" of a non-stationary and a wide-sense stationary model.

Definition 14 (FARIMA model)**.**

The fractional ARIMA (FARIMA) processes (sometimes called ARFIMA) are widely used in modeling LRD time series. It is defined in [304] as,

$$\Phi_p(d)X_t = \Theta_q(d)(1-d)^{-\alpha}\varepsilon_t, \tag{3.25}$$

where $(1-d)^{-\alpha}$ is the fractional differencing operator. When $d = 0$ the FARIMA(p, d, q) process reduces to the usual ARMA(p, q) process.

Definition 15 (CARIMA model)**.**

The controlled ARIMA model can be expressed using the z parameter in the following form [305]:

$$A(z^{-1})y(k) = B(z^{-1})u(k-1) + \frac{C(z^{-1})}{\Delta u(k)}e(k) \tag{3.26}$$

One of the main use of the CARIMA model is in the generalized predictive control [306].

There are other generalized forms of the ARIMA model, such as the vector ARIMA (VARIMA) for multiple time series [307], and the nonlinear ARIMA (NARIMA) for the nonlinear dependent time series on the past values.

Definition 16 (Fractional ARMA model)**.**

The fractional ARMA process $X = (X_t)_{t\in R}$ based on the Brownian motion $W = (W_s)_{s\in R}$ is defined in [308] as,

$$X_t = \int_{-\infty}^{t} f(t-s)dW(s). \tag{3.27}$$

Its Laplace transform in the roots format is [308],

$$F(s) = \prod_{k}^{K}(s-a_k)^{\alpha_k}. \tag{3.28}$$

These models belong to the whole family time series models, and they can be selected accordingly for specific fractional order modeling scenarios.

3.2.2 Data based model selection

In the industry, physics modeling may not always be the primary preference considering the cost-reward ratio in terms of time and labor. Moreover, it usually turns out that physics models may not fit the data well due to un-modeled dynamics, assumptions and simplifications based upon which they are built. Therefore, model structures are selected according to empirical observation in many cases. For example, to the author's experience, if a system's reaction curve has fast initial response but approaches the steady state very slowly (usually called to have the Mittag-Leffler shape), then, a fractional order transfer function will probably fit the data well regardless of its physical meaning.

In [71], Malti *et. al* selected the following model structure to fit the data from resistor heated aluminum rod experimental platform and was proven to be effective,

$$G(s) = \frac{b_0}{a_2 s^{\alpha_2} + a_1 s^{\alpha_1} + 1} e^{-Ls}. \tag{3.29}$$

For the cases where fractional order non-minimum phase behavior occurs, the model structure discussed in section 2.3.4 should be considered.

The most commonly used integer order model in the industry should count the first order plus time delay (1OPTD). Without surprise, its fractional form sibling, fractional order plus time delay (FOPTD) model, is frequently used in FO controls,

$$G(s) = \frac{K}{Ts^{\alpha} + 1} e^{-Ls}, \quad (0 < \alpha < 2), \tag{3.30}$$

where K, T, L are constants. This model is good enough to depict many linear dynamic system responses including the aforementioned examples, and is also acceptable to approximate relatively higher order models.

The above discussed model selection mainly focuses on single loop scenarios. For MIMO cases where individual input-output can be measured, the overall model can be obtained by choosing suitable structure for each individual loop and then, combine them into a transfer function matrix or pseudo state equation expression. Model selection and identification of nonlinear fractional order systems are discussed in section 3.4.

3.3 Parameter identification for fractional order models

Following the model structure selection discussed in the previous section, the next concern nails down to the parameter identification, which is a big subject in the system identification theory. Numerous methods for integer order models have been developed, see the books, [299, 309, 310]. Some of them have been attempted to identify fractional order systems, as reviewed in section 1.4, others are briefly reviewed as follows. For example, Oukacine, Djamah *et al.* identified fractional order models using pseudo-random binary sequence (PRBS). They also extended the multi-model identification to fractional order nonlinear models, [311]. Victor *et al.* developed a two-step algorithm for model order identification, [66]. Djouambi *et al.* identified FO systems using a digital adjustable fractional order integrator [312]. Tavakoli *et al.* presented methods to identify the order and parameters of fractional systems from noisy step response data [313]. Liu *et al.* applied the modulating function method on FO systems [314]. In [315] and [316], fractional order models are identified by curve fitting using the time domain analytical solution given by the Mittag-Leffler function. Heuristic search algorithms have also been employed to identify FO models, [317, 318].

There are still many methods not generalized for FO cases. This section reviews some of the existing methods, and introduces two new methods in the frequency domain.

3.3.1 Order scanning by time domain data fitting

For model parameter estimation, the first method arising in minds of many control engineers might be the least squares method. This method has been incorporated into algorithms and

been used for fractional order system identification. For example, the *srivcf*-algorithm gives the *srivcf*-based solution at each iteration by,

$$\rho^{iter+1} = (\Phi^{iter}\Phi^T)^{-1}\Phi^{iter}Y^* \tag{3.31}$$

where y^* is the noisy output and Φ is the regressor. For fractional order models, *srivcf*-algorithm follows the same scheme, [71].

$$\mathbf{P}_\rho = \hat{\sigma}^2(\Phi\Phi^T)^{-1} \tag{3.32}$$

where $\hat{\sigma}^2$ is the empirical estimation of the noise variance.

As a variant of the least squares fitting, the IAE, ITAE, etc, are also used to estimate the parameters of an over-determined system, i.e. the data points are more than needed (usually contradictory) for determining the unknown parameters. This gives rise of the question: to what extent the model complexity impact the fitting results. For example, the model order selection is discussed in [303]. The Akaike information criterion (AIC) answers this problem quantitatively. AIC is a measure of the relative quality of a statistical model for a given set of data, [319, 320]. It is usually used to judge if a data set is under-fitted or over-fitted by a model.

Definition 17 (Akaike information criterion)**.** *For a supposed statistical model, let L be the maximized value of the likelihood function; k be the number of estimated parameters in the model. Then the AIC value of the model is*

$$AIC = 2k - 2ln(L). \tag{3.33}$$

Similar to this idea, when fitting a data set using a fractional order model, the number of fractional orders and the value of each order need to be determined. One of the techniques is to estimate the orders along with the other model parameters all together, [316, 315]; another is to scan the orders with designed change of step size, during which other model parameters are estimated while the fractional order is fixed at each step, [83]. There are other techniques such as [321]. Among these techniques, the order scanning is a simple and straightforward methods. Hence, a handy tool for performing this task is developed for repetitive use and is available in [322]. The use of this technique for some quick order estimation is presented in section 5.3.

3.3.2 Using the relay with an FO integrator for system identification

As the name implies, the relay feedback approach utilizes a relay shape nonlinearity in the feedback loop of a system, which has generally two uses. One is for auto tuning the PID controller parameters and the other is for model identification. This section and the next section mainly address its use in identification.

The relay feedback approach is one of the most commonly used techniques in the industrial automation because of its simple-to-implement feature and practical value. Two detailed surveys on its development can be found in [323, 324]. More recent advances are available in [325]. As this method receives so much research attention, more than ten types of its variants

have been created in the past two decades. In this section, inspired by fractional calculus, a new variant is proposed with unique advantages over other types of relay feedback experiment schemes. In [326, 327], Lee and Sung *et al.* presented a seemingly similar approach in terms of the title. The difference from the current work lies in the block diagram connection and the profile of control signals. The FO integrator in their setup is connected behind the relay, which consequently, generates control signals in the "power law" shape instead of the square waveforms directly generated by relays. From this point of view, the proposed setup is more loyal to the original relay feedback idea.

Before presenting the proposed relay feedback variant, five types of traditional relay feedback identification methods are reviewed with comments given on some practical details. The review uses the generalized pseudo frequency response (PFR) concept to obtain a unified derivation scheme.

3.3.2.1 The pseudo frequency response concept

The notion of pseudo frequency response is introduced in this context for generalizing the operation between describing functions (DF) and the actual frequency responses of a linear element. This is feasible because after the approximation with regard to a particular input, the nonlinearity has lost. Hence, the DF is essentially a complex number acting as a gain and phase shift effect on the linear part remained in the system. The origin of this idea is inspired by the pseudo transfer function concepts for some special scenarios in model identification, [328, 329], and the illustration starts from the describing function method.

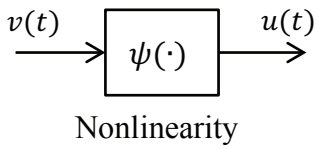

Figure 3.1: The block diagram representation of the static nonlinearity.

The DF method is the dominant approach for approximating a linear equivalence of relay type nonlinearities. The DF of a memoryless static nonlinearity, ψ as shown in figure 3.1, is defined to be the ratio of the first harmonic of its output to that of its input, [330].

Definition 18 (Describing function)**.**

Let $v_n(t)$ and $u_n(t)$ denote the Fourier series of the periodic input $v(t)$, and output $u(t)$, respectively,

$$v_n(t) = a_{0_v} + \sum_{k=1}^{\infty}[a_{k_v}\cos(k\omega t) + b_{k_v}\sin(k\omega t)], \tag{3.34}$$

$$u_n(t) = a_{0_u} + \sum_{k=1}^{\infty}[a_{k_u}\cos(k\omega t) + b_{k_u}\sin(k\omega t)], \tag{3.35}$$

where a_k and b_k are the triangular form Fourier coefficients, with the footnote u and v for output and input respectively. Then, the describing function of ψ is:

$$\Psi = \frac{c_{1_u}}{c_{1_v}}, \tag{3.36}$$

where c_{1_u} and c_{1_v} are the exponential form Fourier coefficients of the fundamental frequency terms,

$$c_{1_u} = \frac{a_{1_u} - jb_{1_u}}{2}, \quad c_{1_v} = \frac{a_{1_v} - jb_{1_v}}{2}.$$

Conventionally, the DF by default takes the assumption of a sine wave input. If $v(t)$ has significant difference from a sine wave, a re-derivation of the DF is usually required, [331]. In this work, the notion of pseudo frequency response $\mathbb{G}(u(t))$ is used to replace the input dependant DF in approximating the frequency characteristic of the nonlinear elements, regardless of whether or not the input is a sine wave.

As an example, for the typical relay nonlinearity depicted by the sign function,

$$u = \psi(v) = sgn(v)H = \begin{cases} H, & v \geq 0, \\ -H, & v < 0, \end{cases} \tag{3.37}$$

the PFR to a cosine wave input is:

$$\mathbb{G}(A\cos(\omega t)) = \frac{\frac{4H}{2\pi} - 0j}{\frac{A}{2} - 0j} = \frac{4H}{\pi A}, \tag{3.38}$$

which is the same with its PFR to a sine wave input. However, this equality is a coincidence which doesn't always hold true for complex nonlinearities such as non-symmetric ones.

From this generalization, the frequency response of a linear element can be treated as an *input independent* PFR.

3.3.2.2 A brief review of the relay feedback identification and its variants

A. The ideal relay feedback

In 1984, Åström and Hägglund introduced the relay feedback technique for automatic tuning PID controllers by bringing the system to a self-sustained oscillation [332]. This method was then extended by Luyben to identify a transfer function of a distillation process [333].

Assume the process to be identified is approximated by an LTI model $G(s)$, as shown in the block diagram in figure 3.2. Then, the ideal relay with an amplitude of H has a PFR of $\mathbb{G}_{ideal}(A\sin(\omega t)) = \frac{4H}{\pi A}$ as derived in the previous section. Considering the negative unit feedback, it pushes the process to the so-called critical oscillation, i.e. the $(-1, 0)$ point on the Nyquist curve shown in figure 3.3,

$$|\mathbb{G}_{ideal}(A\sin(\omega_u t))G(j\omega_u)| = 1, \tag{3.39}$$

where ω_u is the so-called ultimate frequency which is reached at the critical oscillation point. Thus, the process gain at the phase $\varphi_p = -\pi$ is,

$$|G(j\omega_u)| = \frac{\pi A}{4H}. \tag{3.40}$$

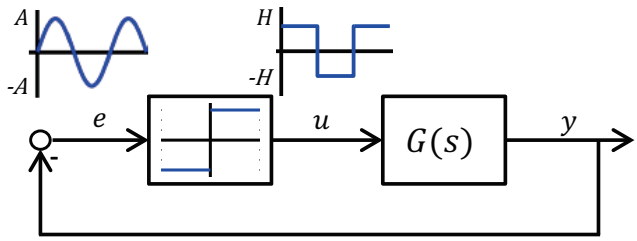

Figure 3.2: The block diagram of the ideal relay feedback.

Depending on the LTI model structures, corresponding parameters can be calculated based on this frequency information. For the first order plus time delay model,

$$G(s) = \frac{K}{Ts+1}e^{-Ls}, \tag{3.41}$$

the parameters K, L, T can be calculated by the following formulae,

$$K = G(0), \tag{3.42}$$

$$T = \frac{\sqrt{(KK_u)^2 - 1}}{\omega_u}, \tag{3.43}$$

$$L = \frac{1}{\omega_u}(-\varphi_p - \arctan\sqrt{(KK_u)^2 - 1}), \tag{3.44}$$

where $K_u = \frac{1}{|G(j\omega_u)|}$ is the ultimate gain, and K is the steady state gain that can be obtained through varieties of methods, such as reading off from a step test or the ratio of the integration of output to input, [334]. The equations for computing other model structures can be referred to [335, 336].

B. The relay with hysteresis

The ideal relay setup is straightforward and simple to implement, but a concern lies in the practical response of the processes with small delay or no delay. In this case, the frequency response has hardly or even no intersection with the negative real axis on the Nyquist plot until reaching very high frequency. Thus, the relay with hysteresis shown in figure 3.4(a) is used to assure the appearance of the sustained oscillation within reasonable frequency ranges of the industrial processes. The effect of the hysteresis on the input signal is like a delay, as shown in figure 3.4(b). Hence, by evaluating the input and output, the PFR of the relay with hysteresis can be obtained,

$$\mathbb{G}_{hyst}(A\sin(\omega t)) = \frac{4H}{\pi A}e^{-j\phi}, \tag{3.45}$$

where $\phi = \arcsin(\frac{\varepsilon}{A})$. Again, considering the negative unit feedback, it can be seen in figure 3.3 that the frequency response point identified by the relay with hysteresis is $\frac{4H}{\pi A}\angle(-\pi+\phi)$, at which the gain and phase of the process are,

$$|G(j\omega_\phi)| = \frac{\pi A}{4H} \quad \text{and} \quad \varphi_p = -\pi + \phi, \tag{3.46}$$

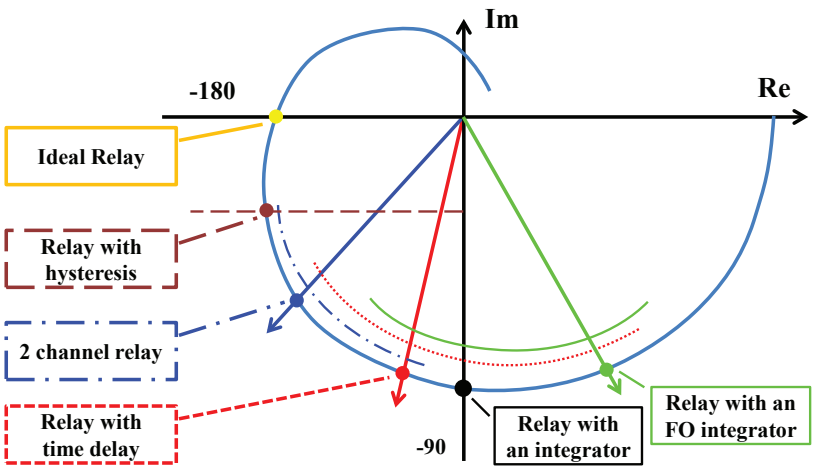

Figure 3.3: The frequency response points on the Nyquist curve identified by different types of relay feedback experiment schemes.

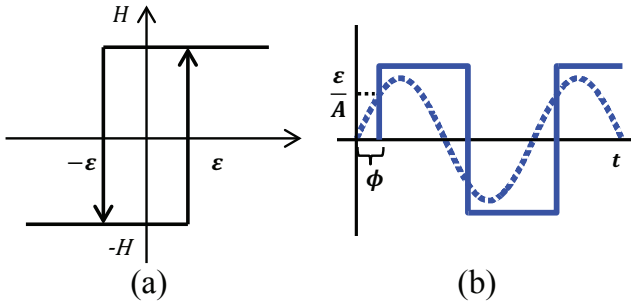

Figure 3.4: The schematic of the relay with hysteresis. (a) The nonlinear characteristic; (b) the input and output waveform.

respectively. Note that the hysteresis must satisfy $0<\varepsilon<A$ because otherwise, the relay will output a constant zero. This condition limits the identifiable process phase within the range of $(-\frac{\pi}{2}, -\pi)$.

Again, for first order with time delay models, the same set of equations (3.42∼3.44) can be used to compute the parameters by substituting the phase and oscillation frequency.

C. The relay with time delay

Similar to the relay with hysteresis, the relay with time delay presented in [337] has the same effect of inserting a certain phase shift between the input and output, and it makes no difference whether the delay is placed in front of or behind the relay. The PFR for this type of relay when input is a sine wave is,

$$\mathbb{G}_{delay}(A\sin(\omega t)) = \frac{4H}{\pi A}e^{-jl}, \tag{3.47}$$

where $l > 0$ is the artificially inserted time delay as shown in figure 3.5. This PFR is the same with equation (3.45) except that the delayed time is *irrelevant* to the amplitude of the

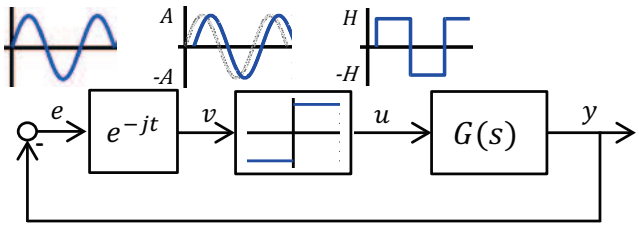

Figure 3.5: The block diagram of the relay feedback setup with time delay.

input. Without this limitation, the time delay can provide a wider range of phase shift than the hysteresis. The gain and phase of the process at the identified frequency point are,

$$|G(j\omega_l)| = \frac{\pi A}{4H} \quad \text{and} \quad \varphi_p = -\pi + l. \tag{3.48}$$

D. The relay with an integrator

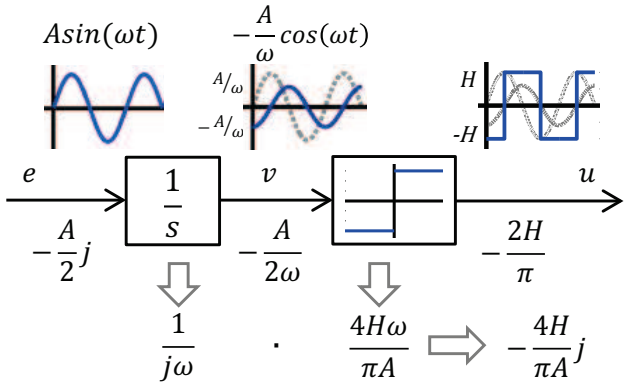

Figure 3.6: The block diagram and the signal transform of the relay with an integrator in the front.

The relay feedback with an integrator is another way to identify a process at a frequency response point other than the critical oscillation point [338]. When the integrator is connected in front of the relay, the PFR can be obtained by multiplying the frequency response of the integrator with the PFR of the ideal relay, as shown in figure 3.6,

$$\begin{aligned} \mathbb{G}_{int}(A\sin(\omega t)) &= \frac{1}{j\omega}\mathbb{G}_{ideal}(-\frac{A}{\omega}\cos(\omega t)) \\ &= -\frac{4H}{\pi A}j. \end{aligned} \tag{3.49}$$

Graphically, it appends an additional $\frac{\pi}{2}$ phase lag to the process output. Hence, the phase of the process at the identified frequency response point is $\varphi_p = -\frac{\pi}{2}$, which is also illustrated in figure 3.3.

As another variant to this method, the integrator connected behind the relay can be found in [339]. Theoretically, by connecting a differentiator, a point on the positive imaginary axis in figure 3.3 can be identified, mentioned in [340]. However, this is not widely used in practice.

E. The two channel relay feedback method

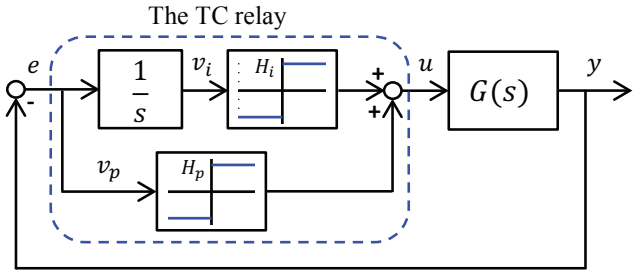

Figure 3.7: The block diagram of the TC relay controlled process.

The two channel (TC) relay feedback introduced by Waller *et al.* in 1997 suggests a parallel connection of the ideal relay and the relay with an integrator, [340]. In the similar manner of manipulating transfer functions, the PFR of the TC relay can be obtained by adding up the PFR of the ideal relay in equation (3.38) and that of the relay with integrator in equation (3.49),

$$\begin{aligned} \mathbb{G}_{TC}(A\sin(\omega t)) &= \mathbb{G}_{ideal}(A\sin(\omega t)) + \mathbb{G}_{int}(A\sin(\omega t)) \\ &= \frac{4H_p}{\pi A} - \frac{4H_i}{\pi A}j, \end{aligned} \tag{3.50}$$

where H_p and H_i are the amplitudes of the ideal relay and the integral relay, respectively, as shown in figure 3.7. This can be verified by evaluating the Fourier series of the input and output of the overall setup in the dashed lined box.

Following equation (3.50), the gain and phase of the process identified by the TC relay feedback are,

$$|G(j\omega_{TC})| = \frac{\pi A}{4\sqrt{H_p^2 + H_i^2}}, \tag{3.51}$$

$$\varphi_p = -\pi + \arctan(\frac{H_i}{H_p}). \tag{3.52}$$

It is easy to see that by varying H_p and H_i, the frequency response point to be identified can be arbitrarily selected within the third quadrant, yet, only in the third quadrant because $\arctan(\frac{H_i}{H_p}) \in (0, \frac{\pi}{2})$.

A drawback of the TC relay is that when $H_p = H_i$, it cannot be used to identify processes with little time delay, because the output of the two channels will cancel each other instead of bringing the system to oscillation, as demonstrated in figure 3.8. That means it cannot identify lots of processes at the phase of $-\frac{3}{4}\pi$ in practice.

Besides the aforementioned setups, there are other variant relay feedback experiment schemes, such as the biased relay [341] and the parasitic relay [342] which identifies multiple frequency response points in a single relay test. Since they either use the time domain transient information or the fast Fourier transforms, the derivation of their PFRs are not enumerated here.

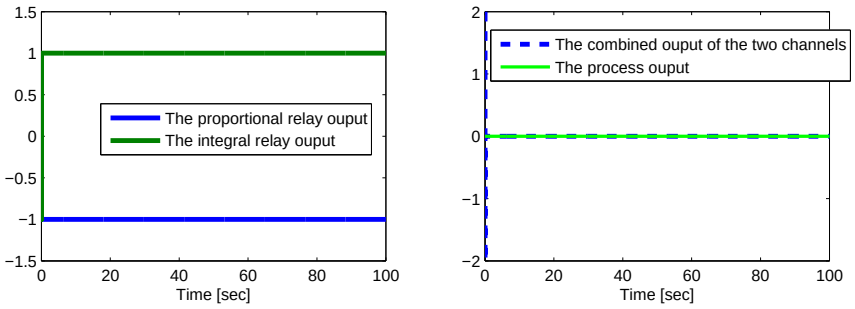

(a) The two channels (b) The outputs

Figure 3.8: A demonstration of the TC relay output cancelation.

3.3.2.3 The proposed relay feedback method

In the proposed relay feedback setup, a fractional order integrator is connected in front of the relay to provide a competitive adjustable phase shift range to the processes, as shown in figure 3.9.

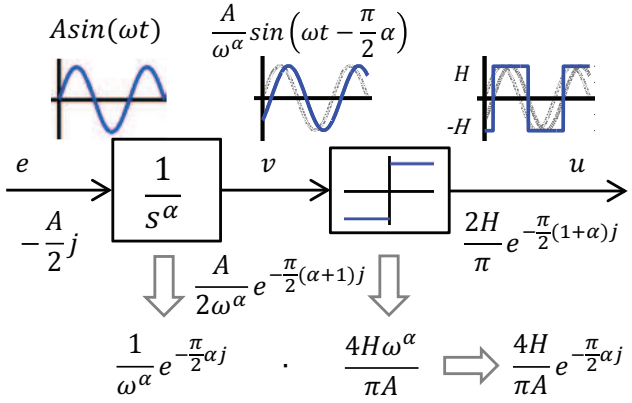

Figure 3.9: The block diagram and signal transform of the relay with an FO integrator.

In this context, the R-L definition for fractional order integral in equation (2.3) is used, and the first block in figure 3.9 denotes the Laplace transform of the FO integral operator in equation (2.18), For practical reasons such as stability concerns [343], α is set in $(0, 2)$.

The PFR of the relay with an FO integrator

The FO integrator is a linear element, its PFR is just its frequency response,

$$\frac{1}{(j\omega)^\alpha} = \frac{1}{\omega^\alpha} e^{-\frac{\pi}{2}\alpha j}. \tag{3.53}$$

Following the previously elaborated PFR concept, the PFR of the entire setup including the

relay is,

$$\begin{aligned}\mathbb{G}_{FOint}(A\sin(j\omega)) &= \frac{1}{(j\omega)^{\alpha}}\mathbb{G}_{ideal}\left(\frac{A}{\omega^{\alpha}}\sin\left(\omega t-\frac{\pi}{2}\alpha\right)\right)\\ &= \frac{1}{(j\omega)^{\alpha}}\frac{4H\omega^{\alpha}}{\pi A}=\frac{4H}{\pi A}\frac{1}{(j)^{\alpha}}.\end{aligned} \tag{3.54}$$

Alternatively, this can be derived in the following procedure, as illustrated in figure 3.9. Assume the input $e(t)$ to this relay setup has a sinusoidal first harmonic. After the FO integrator, the output is shifted in a phase angle corresponding to the fractional order α,

$$v(t)=\frac{A}{\omega^{\alpha}}\sin\left(\omega t-\frac{\pi}{2}\alpha\right), \tag{3.55}$$

According to the properties of the Fourier series of FO operators, the Fourier series of an FO integrated function equals to the FO integration of the Fourier series of the function, [35],

$$F\left\{I^{\alpha}x\left(t\right)\right\}=I^{\alpha}F\left\{x\left(t\right)\right\}. \tag{3.56}$$

Thus, the Fourier coefficient of the first harmonic of the signal after the FO integrator, $v(t)$, is

$$c_{1_v}=\frac{1}{(j\omega)^{\alpha}}\frac{A}{2j}=\frac{A}{2\omega^{\alpha}}e^{-\frac{\pi}{2}(1+\alpha)j}. \tag{3.57}$$

When $v(t)$ passes through the ideal relay, it becomes a shifted square wave expressed as,

$$u(t)=\begin{cases}-H & , \quad 0<t<\frac{T}{4}\alpha \text{ and } -\frac{T}{4}\alpha+kT<t<\frac{T}{4}\alpha+kT,\\ H & , \quad \frac{T}{4}\alpha+kT<t<\frac{3T}{4}\alpha+kT,\end{cases} \tag{3.58}$$

where T is the oscillation period and $k=0,1,2,\ldots$. The Fourier coefficient of its first harmonic is,

$$\begin{aligned}c_{1_u} &= \frac{-\frac{4H}{\pi}\sin\left(\frac{\pi}{2}\alpha\right)-j\frac{4H}{\pi}\cos\left(\frac{\pi}{2}\alpha\right)}{2}\\ &= \frac{2H}{\pi}e^{-\frac{\pi}{2}(1+\alpha)j}.\end{aligned} \tag{3.59}$$

To obtain the PFR of the overall setup, c_{1_u} is divided by c_{1_e},

$$\begin{aligned}\mathbb{G}_{FOint}(A\sin(j\omega)) &= \frac{c_{1_u}}{c_{1_e}}=\frac{\frac{2H}{\pi}e^{-\frac{\pi}{2}(1+\alpha)j}}{\frac{A}{2j}}\\ &= \frac{4H}{\pi A}e^{-\frac{\pi}{2}\alpha j}=\frac{4H}{\pi A}\frac{1}{(j)^{\alpha}},\end{aligned} \tag{3.60}$$

which matches the result in equation (3.54) perfectly. Thus, the gain and phase of the process identified by the relay with an FO integrator are,

$$|G(j\omega_{FO})|=\frac{\pi A}{4H} \quad \text{and} \quad \varphi_p=-\pi+\frac{\pi}{2}\alpha. \tag{3.61}$$

Identifying LTI model parameters

When such a relay setup is connected to a process in a negative unit feedback loop, the frequency response of the process at the investigated point can be obtained. Then, the first order plus time delay model parameters T and L can be, again, calculated from the equations (3.43 $\sim$ 3.44), with the corresponding ω and φ_p substituted.

The advantages and limitations of the proposed method

The major advantages of the proposed relay feedback setup over other variants are listed below:

1. The relay with an FO integrator provides a wider selectable phase range for the process to be identified. So, for processes of slow dynamics such as the temperature control in chemical or bio engineering, it is more meaningful and realistic to approximate a model based on the frequency response that is close to a nominal operational point.
2. Although the relay with time delay provides a even larger range of the identifiable process phase, it worths a notice that the pure delay results in a zero output at the beginning. By contrast, the FO integrator behaves rather a phase shift effect instead of a pure delay, as illustrated in figure 3.10. Hence, a quarter of the oscillation period can be saved for identifying ultra-slow processes.
3. The shifted phase of the FO integrator can be pre-determined. This is unlike using the relay with hysteresis, where there is no way to do so without priori knowledge of the process output. The reason lies in the dependency of the shifted phase on the amplitude of the process output, as shown by equation (3.45).

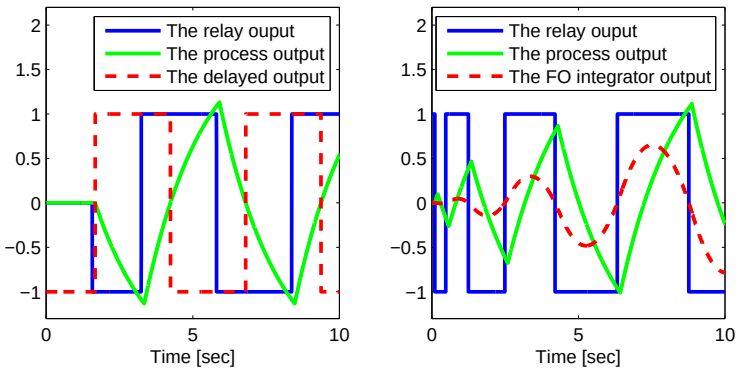

Figure 3.10: Comparison between the initial response of delay and FO integrator. Left: with delay; Right: with FO integrator in the front.

On the other hand, the relay with an FO integrator cannot get rid of some of the common limitations suffered by other relay feedback variants in that it is essentially an approach based on the following assumptions:

1. The output of the process has a first harmonic close to the sine wave;
2. The higher order harmonics of the process output need to be small enough to be neglected.

Failure to satisfy either of the above conditions will result in big identification error. For example, a first order process usually outputs a triangle shape waveform under the relay test, and an identification error ranging from $-18\% \sim 27\%$ can be expected [344, 345]. Large measurement noise will also affect the identification.

Dedicated simulation examples for the demonstration of the proposed method are available in section 5.2.

3.3.3 Using the relay feedback approach for linear FO system identification

Although the relay feedback approach has been widely used to identify integer order processes, fractional order model identification using relay has not been reported. Hence, the research in this part extends the discussion in the previous section and fills this blank.

3.3.3.1 The frequency response of an FOPDT model

The system under investigation can be modeled by an LTI fractional order transfer function with time delay, as expressed in equation (3.30) in section 3.2.2. To identify the model parameters, i.e. $K,\ T,\ L, \alpha$ using the relay feedback method, the frequency response of the model needs to be derived. By substituting the Laplace parameter s with $j\omega$, the transfer function is converted to:

$$G\left(j\omega\right) = \frac{K}{T(j\omega)^{\alpha}+1}e^{-Lj\omega}. \tag{3.62}$$

Applying Euler's formula, $j^{\alpha} = e^{j\frac{\pi}{2}\alpha}$, equation (3.62) becomes:

$$\begin{aligned} G\left(j\omega\right) &= \frac{K}{T\omega^{\alpha}e^{j\frac{\pi}{2}\alpha}+1}e^{-Lj\omega} \\ &= \frac{K}{T\omega^{\alpha}\left[\cos\left(\frac{\pi}{2}\alpha\right)+j\sin(\frac{\pi}{2}\alpha)\right]+1}e^{-Lj\omega}. \end{aligned} \tag{3.63}$$

Thus, the gain of the system frequency response is:

$$\begin{aligned} \left|G\left(j\omega\right)\right| &= \frac{|K|}{\left|T\omega^{\alpha}\left[\cos\left(\frac{\pi}{2}\alpha\right)+j\sin(\frac{\pi}{2}\alpha)\right]+1\right|} \\ &= \frac{|K|}{\sqrt{\left[T\omega^{\alpha}\cos\left(\frac{\pi}{2}\alpha\right)+1\right]^2+(T\omega^{\alpha})^2\sin^2(\frac{\pi}{2}\alpha)}} \\ &= \frac{|K|}{\sqrt{\left(T\omega^{\alpha}\right)^2+2T\omega^{\alpha}\cos\left(\frac{\pi}{2}\alpha\right)+1}}. \end{aligned} \tag{3.64}$$

Accordingly, from equation (3.63) we have,

$$G\left(j\omega\right) = \frac{K\left[T\omega^{\alpha}\cos\left(\frac{\pi}{2}\alpha\right)+1-jT\omega^{\alpha}\sin\left(\frac{\pi}{2}\alpha\right)\right]}{\left[T\omega^{\alpha}\cos\left(\frac{\pi}{2}\alpha\right)+1\right]^2+T^2\omega^{2\alpha}\sin^2\left(\frac{\pi}{2}\alpha\right)}e^{-Lj\omega}.$$

Then, the phase of the system is:

$$\angle G = -\arctan\left(\frac{T\omega^{\alpha}\sin\left(\frac{\pi}{2}\alpha\right)}{T\omega^{\alpha}\cos\left(\frac{\pi}{2}\alpha\right)+1}\right)-L\omega. \tag{3.65}$$

From equations (3.64) and (3.65) it can be observed that the modulus and phase of the frequency response of an FO TF not only depend on the steady state gain K, the time constant T, and the time delay L, but also depend on the fractional order, α.

3.3.3.2 The equations for computing FOPDT model parameters

By reorganizing equation (3.64), a quadratic equation with respect to T can be derived,

$$\omega^{2\alpha}T^2 + 2\omega^{\alpha}cos\left(\frac{\pi}{2}\alpha\right)T + 1 - \frac{K^2}{|G(j\omega)|^2} = 0. \tag{3.66}$$

Vieta's formula can be used to obtain the solution,

$$T = \frac{-\cos\left(\frac{\pi}{2}\alpha\right) + \sqrt{\cos^2\left(\frac{\pi}{2}\alpha\right) + \left|\frac{K}{G(j\omega)}\right|^2 - 1}}{\omega^{\alpha}}, \tag{3.67}$$

where the other solution is abandoned. To assure the physical meaning of the resulting time constant, i.e. not negative or complex, the existence of a positive real solution to the above equation needs to be evaluated. Let

$$\Delta = \cos^2\left(\frac{\pi}{2}\alpha\right) + \left|\frac{K}{G(j\omega)}\right|^2 - 1.$$

Since K is the DC gain, that is $K = G(0)$, it must be greater than the system gain at any other frequencies, which can be seen from equation (3.64). Thus, $\left|\frac{K}{G(j\omega)}\right|^2 > 1$ gives $\Delta > 0$, and the existence of a real solution is guaranteed. Meanwhile, $\left|\frac{K}{G(j\omega)}\right|^2 > 1$ derives $\sqrt{\Delta} > |\cos^2\left(\frac{\pi}{2}\alpha\right)|$. Hence, $T = [\sqrt{\Delta} - \cos(\frac{\pi}{2}\alpha)]/\omega^{\alpha} > 0$ and there always exists a physically meaningful solution as the time constant.

Similarly, the time delay is computed in the following way through equation (3.65)

$$L = -\frac{1}{\omega}\left[\angle G + \arctan\left(\frac{T\omega^{\alpha}\sin\left(\frac{\pi}{2}\alpha\right)}{T\omega^{\alpha}\cos\left(\frac{\pi}{2}\alpha\right) + 1}\right)\right]. \tag{3.68}$$

For comparison, recall the equations for computing the time constant and time delay for integer order systems via relay feedback tests in [333], as listed in equations (3.42∼3.44). It can be seen that the equations for the first order with time delay model are special cases of that for FOPDT models by setting $\alpha = 1$ in equations (3.67) and (3.68). This verifies the correctness of the proposed method.

3.3.3.3 Obtaining system information from the relay feedback test

The model in equation (3.30) has four unknown parameters which need at least four equations to solve. While equations (3.67) and (3.68) serve as two, the other two equations can be established in the following manner: 1) determine the system DC gain separately; 2) identify two different frequency response points using different types of relays.

Multiple approaches for the purpose of determining K have been proposed in the literature [323]. Shen *et. al* suggested the use of the ratio between the integral of the output y and

input u of the system via a biased relay test, [334],

$$K = G(0) = \frac{\int_0^{P_u} y(t)dt}{\int_0^{P_u} u(t)dt}, \tag{3.69}$$

where P_u is the period of the self-sustained oscillation during the relay test. Shen's method is adopted in this paper because it has been verified to be valid for fractional order models through experiments. Mathematical proof follows the same format of that for integer orders.

The most critical part of the relay feedback approach is to determine the system gain $|G(j\omega)|$ at the ultimate frequency ω_u via the describing function analysis [330]. Denote the oscillation period, amplitude of the relay and the system output by P_u, H and A, respectively, so, the system gain at such a point is,

$$|G(j\omega_u)| = \frac{1}{K_u}, \quad \text{where } K_u = \frac{4H}{\pi A},\ \omega_u = \frac{2\pi}{P_u}. \tag{3.70}$$

The system phase is $\angle G(j\omega_u) = -\pi$.

With variants of relays, frequency response points other than the critical oscillation point can be identified. For instance, the aforementioned relay variants reviewed in the previous section are able to identify either a point on the negative imaginary axis or multiple points in the third and forth quadrant, as shown in the sketch in figure 3.3. A selection of two different relays from the reviewed variants can provide the oscillation information of two points on the system frequency response curve. In this way, a duplicate of equation (3.67) with different ω and $|G(j\omega)|$ is produced,

$${\omega_1}^{2\alpha}T^2 + 2{\omega_1}^{\alpha}cos\left(\frac{\pi}{2}\alpha\right)T + 1 - \frac{K^2}{|G(j\omega_1)|^2} = 0, \tag{3.71}$$

$${\omega_2}^{2\alpha}T^2 + 2{\omega_2}^{\alpha}cos\left(\frac{\pi}{2}\alpha\right)T + 1 - \frac{K^2}{|G(j\omega_2)|^2} = 0, \tag{3.72}$$

from which T and α can be solved. Consequently, L can be solved using equation (3.68). Thus, four equations are established sufficiently to solve the four model parameters.

3.3.3.4 Summary of the proposed method

The above proposed methods can be briefly summarized in the following three steps to handle practical problems.

1. The system steady state gain K is determined through equation (3.69) using a biased relay test;
2. Two frequency response points are identified from one or two relay tests, and equations (3.71) and (3.72) are used to compute the time constant T and the fractional order α;
3. Equation (3.68) is used to compute the time delay.

Simulation and practical implementation of this proposed method are available in the simulation and experiment sections 5.3.

3.4 Nonlinear fractional order system identification

The commonly used methods for nonlinear system analysis includes: 1.) the phase plane analysis, 2.) the describing function method, and 3.) the Lyapunov's second method, etc. Some of them has been extended to analyzing fractional order dynamics with nonlinearities, for example, the phase portrait in section 2.2 and the DF method in the previous section. However, these analysis are based on the prerequisite of a model. So, a model needs to be built prior to this. While some early efforts can be found in [346] and [347], a deep dig into the literature will reveal the scarce in the related research. Thus, this section picks up the thread and continues the investigation in nonlinear fractional order system identification.

Historically, nonlinear system identification can be roughly categorized into the following four basic approaches, each defined by a model class, [348, 349, 350],

1. Volterra series models,
2. Block structured models,
3. Neural network models,
4. Nonlinear ARMAX models.

Let such categorization be kept for fractional order systems for now. For instance, nonlinearity is added into the model obtained in section 3.2 by using Volterra series, [72], in order to capture the nonlinear behavior of the system; the fractional order ARMAX model is mentioned in [351]. The following discussion starts with basic model structures and stretches to more practical consideration for system identification. Two dedicated case studies of identifying practical thermal processes are stated in sections 5.1 and 5.5 to better illustrate the proposed concept.

3.4.1 Identification of fractional order Hammerstein and Wiener models

As a member in the block structured model category, the Hammerstein model refers to a model with a static nonlinearity at the input, and the Wiener model refers to that with an output nonlinearity. The combination of the two forms a Wiener-Hammerstein (W-H) model which is also called the "sandwich" model. These model types, consisting of nonlinearity in connection with integer order dynamics, are well studied in the literature, and are used in many industrial fields due to their generality. However, those consisting of fractional order dynamics are rarely addressed. Reviews of some relevant discussion are covered in this section. A practical application scenario will be presented in section 5.5.

The block diagram of the integer order Hammerstein model is shown in figure 3.11, where $\varphi(\cdot)$ denotes the nonlinearity and $d(t)$ denotes the measurement noise. The internal signal $v(t)$ are usually assumed to be not measurable. In [352], Malti, Oustaloop *et al.*, for the first time, considered the linear fractional order dynamics for H as expressed in equation (2.26).

They also provided two error-optimization based algorithms for the parameter identification of such models. One is the equation error algorithm using standard least squares reviewed in section 3.3. The difference from integer order case is that the optimum, $\theta = [a_1, \cdots, a_L, \alpha_1, \alpha_1 b_2, \cdots, \alpha_1 b_J, \cdots, \alpha_M, \alpha_M b_2, \cdots, \alpha_M b_J]^T$, is estimated by:

$$\hat{\theta} = (\Phi^T \Phi)^{-1} \Phi Y(t),$$

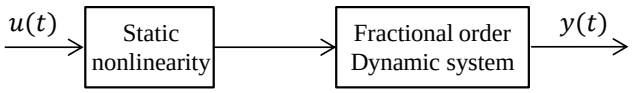

Figure 3.11: The block diagram of a Hammerstein model.

where $\Phi = [\Phi_0\ \Phi_1\ \cdots\ \Phi_M]$;

$$\Phi_0 = \begin{bmatrix} -D^{n_{a1}}y(t) & \cdots & -D^{n_{aL}}y(t) \\ \vdots & \ddots & \vdots \\ -D^{n_{a1}}y(0) & \cdots & -D^{n_{a1}}y(0) \end{bmatrix};$$

$$\Phi_k = \begin{bmatrix} -D^{n_{b1}}u^k(t) & \cdots & -D^{n_{bL}}u^k(t) \\ \vdots & \ddots & \vdots \\ -D^{n_{a1}}u^k(0) & \cdots & -D^{n_{a1}}u(0) \end{bmatrix}; k = 1, \ldots, M,$$

and the minimization criterion is based on the quadratic predictive error,

$$J(\theta) = \int_0^K (y(t) - \hat{y}(t|\theta))^2 dt. \tag{3.73}$$

The other algorithm is based on output error minimization, in which the criterion is,

$$J(\theta) = \int_0^K (e(t))^2 dt = \int_0^K (y(t) - \hat{y}(t))^2 dt, \tag{3.74}$$

where $\hat{y}(t|\theta)$ in equation (3.73) is replaced by,

$$\hat{y}(t) = \mathcal{L}^{-1}[\frac{s^{n_{b1}} + b_2 s^{n_{b2}} + \cdots + b_J s^{n_{bJ}}}{1 + a_1 s^{n_{a1}} + \cdots + a_L s^{n_{aL}}}] * \sum_{k=1}^{M} \alpha_k u^k(t), \tag{3.75}$$

In [353, 354] Li, Chen *et al.* discusses the complete parametric identification of FO Hammerstein systems. The nonlinearity under consideration has the polynomial form $\varphi(u) = \Sigma_{i=0}^{n} \beta_i u^i$, and the linear part of the model is in the form of commensurate fractional order ARX or OE, as described in section 3.2.1.5,

$$G(p) = \frac{B(p)}{A(p)} = \frac{\sum_{i=0}^{m} b_i p^{i\alpha}}{1 + \sum_{j=0}^{n} a_j p^{j\alpha}}. \tag{3.76}$$

They proposed an identification algorithm that consists of three steps, i.e. to identify the parameters of the nonlinear term, the fractional order linear term, and the fractional order, respectively. For the order estimation, the iterative learning technique is employed.

In [355], Vanbeylen focused on the generation of initial estimations for the integer order W-H models using a fractional approach. The initialization is one of the major difficulties

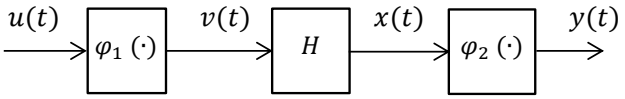

(a) Setup I.

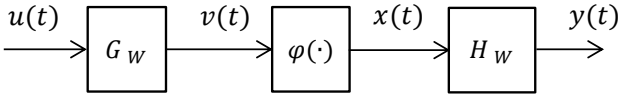

(b) Setup II.

Figure 3.12: The block diagram of the Wiener-Hammerstein model.

resides in the identification procedure, and is crucial to the avoidance of suboptimal local minima in an iterative optimization procedure. There are two types of setup for the W-H models, as shown in figure 3.12, and the latter is studied in the reference. The key part of the approach is to represent the W-H dynamics by fractional order zero-pole models,

$$\hat{G}_W(z,\alpha,\beta) = \frac{\prod_{i=0}^{m_W}(1 - z_k^{BLA} z^{-1})^{\beta_k}}{\prod_{i=0}^{n_W}(1 - p_k^{BLA} z^{-1})^{\alpha_k}}, \quad \hat{G}_H(z,\alpha,\beta) = \frac{\prod_{i=0}^{m_H}(1 - z_k^{BLA} z^{-1})^{1-\beta_k}}{\prod_{i=0}^{n_H}(1 - p_k^{BLA} z^{-1})^{1-\alpha_k}}. \tag{3.77}$$

where BLA refers to the term "best linear approximation", and α, β are the introduced fractional order powers. Again, the parameters are estimated using the least squares with optimization criteria as the following:

$$J(\theta) = ||K(\alpha,\beta,u)\theta_{NL} - y||_2^2,$$

where $K(\alpha,\beta,u) = \hat{G}_H(q,\alpha,\beta) f_m(\hat{G}_W(q,\alpha,\beta)u(t))$, and f_m is the nonlinearity expressed by a weighted sum of basis functions.

In [93], Liao, Wang *et al.* investigated the subspace identification of nonlinear fractional order MIMO systems using the Hammerstein model, and this method is reviewed in section 3.5 through another publication of these authors. For more identification approaches related to fractional order Hammerstein/Wiener models, refer to [351].

3.4.2 Selection of excitation

The selection of excitation is an art in system identification, which is like designing a quiz. For ARMA models, it is well known that to obtain the system behavior on the full spectrum, the persistent excitation (PE) condition needs to be met. The commonly used input that meets the PE condition is the pseudo-random binary sequence (PRBS). In spite of the traditional discussion in the spectrum sense, the following research concerns about the amplitude, which is called the input shape design in this context.

In sections 3.3.2 and 3.3.3, the responses of linear FO process models under the relay shape excitation have been discussed. This subsection investigates the impacts of input shapes on nonlinear systems.

The idea is originated from the scenario that deals with an nonlinear industrial process with operational points across a wide range. In this case, local linearization fails and the above Hammerstein model for input/output nonlinearity does not work either because the nonlinearity not only relies on the input, but also relies on the initial condition of the states. For this purpose, different shapes of inputs are designed. For example, figure 3.13 shows the inputs for identifying the so-called absolute gain K_a, the relative gain K_r and the potential gain K_p. This leads to the difficulty in linearization, though, because a single linearization scheme is not able to handle the whole range. For example, the Jacobian type (tangential) linearization does not cover the wide operational range; and the gain scheduling using lumped parameter ignores the transient even if it models the steady state correctly. This prblem is further studied in detail in the next section.

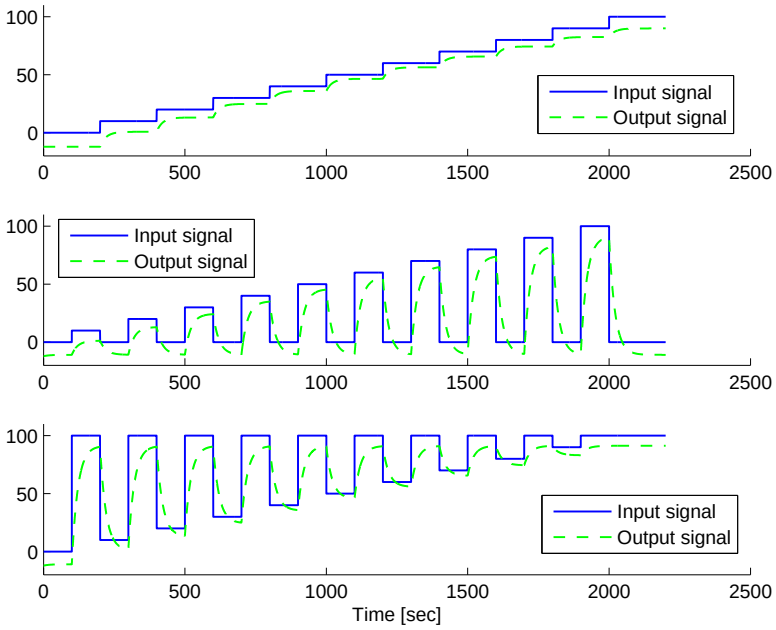

Figure 3.13: The design of three different input types.

3.4.3 Linearization of nonlinear fractional order systems

In nonlinear system analysis, linearization is a frequently used means to obtain a linear approximation of a nonlinear system that is *usually* valid in a small region around the operating point. For nonlinear fractional order systems, it is also useful. Hence, the purpose of this section is to provide theoretical foundation for the application discussed in the later part of this thesis, where a very detailed study of the identification and linearization of a practical industrial process using nonlinear fractional order models is provided, section 5.5.

3.4.3.1 Extending existing linearization theorems to fractional order systems

In [356], Li *et al.* extended the linearization theorems for fractional dynamics. Consider the following autonomous fractional differential equation in the Caputo sense,

$$ {}_0^C D_t^\alpha x(t) = f(x(t)), \tag{3.78} $$

its linearization at a working point x_w is $Df(x)|_{x=x_w}$.

Definition 19 (Equilibrium point)**.** *The point x_e is an equilibrium point of system in equation (3.78) if and only if $f(x_e) = 0$.*

Definition 20 (Hyperbolic equilibrium point)**.** *Suppose point x_e is an equilibrium point of system (3.78) and all the eigenvalues of the linearized matrix $Df(x_e)$ at the equilibrium point x_e satisfy: $|\lambda| \neq 0$ and $|arg(\lambda)| \neq \frac{\pi}{2}\alpha$, then, it is a hyperbolic equilibrium point.*

Theorem 3. *If the origin O is a hyperbolic equilibrium point of equation (3.78), then, vector field $f(x)$ is topologically equivalent with its linearization vector field. $Df(0)x$ in the neighborhood $\delta(0)$ of the origin, O.*

This theorem can be regarded as the fractional version of the Hartman theorem in [357].

3.4.4 Fractional order feedback linearization

This section addresses the feedback linearization of nonlinear fractional order (FO) systems. We start from a practical problem posed from the temperature control of an industrial process, in which the traditional Jacobian type local linearization is not applicable. This consequently motivates the use of feedback linearization that could potentially linearize a process over a larger scale. Then, the analysis is generalized to a class of nonlinear FO systems. However, since feedback linearization has not been established for nonlinear FO systems, we propose the basic definitions as well as necessary and sufficient conditions.

3.4.4.1 Problem description

This research is originated from the temperature control of the manufacturing equipment in the silicon wafer processing industry introduced in chapter 1. The given task requires high precision control of the reaction chamber temperature during both transient and steady-state. Initially, conventional modeling and linearization techniques are attempted. A fractional order transfer function with time delay is selected as the basic model structure to depict the dynamics. An output dependent look-up table is created to characterize the static nonlinearity.

As an illustrative example, in the particular scenario under investigation, the control authority has a range between the lower and higher bound $[u_l, u_h]$ due to the saturation protection of the hardware. This control signal range actuates the temperature in a total operational range of $[T_l, T_h]$. Identification of the nonlinearity is performed under open-loop control by sequentially increasing the control signal with a fixes step size, $\Delta u = (u_h - u_l)/N$ where $N \in \mathbb{N}$, as shown by the blue curve in figure 3.14. Then, the steady-state temperature

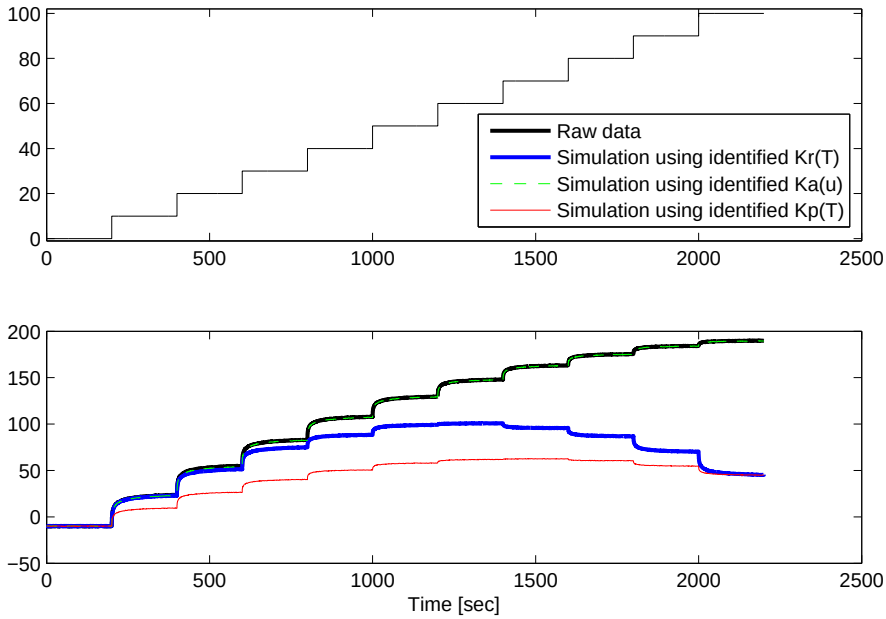

Figure 3.14: The nonlinear gain versus input and output.

data T_n $(n = 1, 2, \ldots, N{+}1)$ is recorded to construct the nonlinearity look-up table,

$$K_r(T_i) = \frac{\Delta T_i}{\Delta u_i} = \frac{T_{i+1} - T_i}{u_{i+1} - u_i} = \tan(\gamma), \quad i = 1, 2, \ldots, N, \tag{3.79}$$

which is referred to as the "relative" gain in the context, and the angle γ is illustrated in figure 3.16. If Δu is sufficiently small, K_r is just the derivative of the nonlinear curve,

$$K_r = \lim_{\Delta u_i \to 0} \frac{\Delta T_i}{\Delta u_i} = \left.\frac{dy}{du}\right|_{u=u_i}, \tag{3.80}$$

This model fits the raw data segments well at each local operational point, as shown by the green curves in figure 3.15. However, the overall response cross the entire operational range has big mis-match with the actual process, which is resulted by the non-zero initial conditions cross the overall temperature range. To guarantee the model accuracy at steady-state, the characterization of the nonlinearity is changed to be input dependent. Therefore, the look-up table is re-built to reflect the absolute nonlinear relationship between the input and output,

$$K_a(u_i) = \frac{T_i - T_l}{u_i - u_l} = \tan(\theta), \quad i = 2, \ldots, N{+}1. \tag{3.81}$$

Combining this static nonlinearity with a dynamic linear FO model forms a fractional order Hammerstein model shown in figure 3.11.

The model parameters can be identified through data fitting. This model is able to match the overall dynamic of the process under open-loop control, especially at steady state, which is shown by the in figure 3.14. Nevertheless, obvious mis-match can be observed if it is

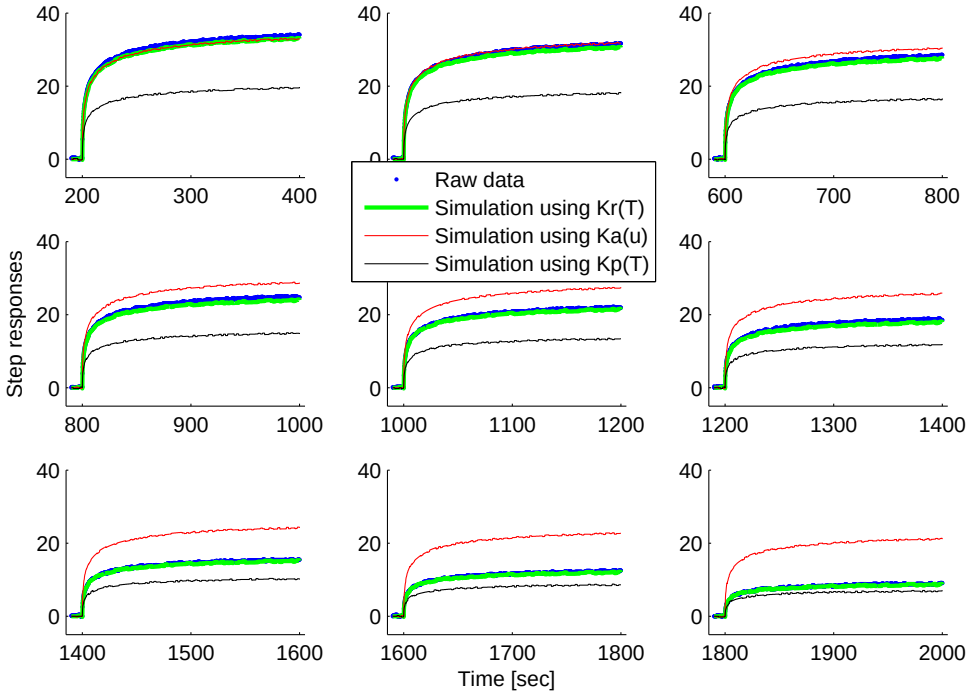

Figure 3.15: Fitting the data segments of the responses to the stair inputs using different gains.

used to fit the raw data piecewise, as shown by the red curves in figure 3.15. Moreover, when it is used to develop a model based feed-forward controller, even bigger mis-match occurs compared with the actual process under closed-loop control. The model output under closed-loop control with a PID controller is much different from the actual process output under the same closed-loop control signal. It has been examined that the process outputs are within acceptably small neighborhoods around the operational points T_i where the local linearization is performed, i.e. $(T_i - \varepsilon, T_i + \varepsilon)$, which does not violate the prerequisite of local linearization. However, although the output stays within range, the control input reaches saturation during transient. Hence, during the initial part of the transient, the process is equivalent to running under open-loop, but with different operational condition, i.e. the saturated control signal. This is shown by the green lines during 4.5 to 5.5 sec in figure 3.18. The difference in the operational condition between the stair input and the saturated input is the fundamental cause of the mismatch. To depict the nonlinear gain under saturated control signal at different temperature levels, the "potential" gain is defined as the following,

$$K_p(T_i) = \frac{T_h - T_i}{u_h - u_i} = \tan(\phi), \quad i = 1, 2, \ldots, N, \tag{3.82}$$

which characterize the potential amount that the process could rise if the saturated control signal is not removed. The three gains has the following relationship,

$$K_a(u_l) = K_r(T_l), \quad K_r(u_h) = K_p(T_h), \quad K_a(u_h) = K_p(T_l), \tag{3.83}$$

as illustrated in figure 3.17.

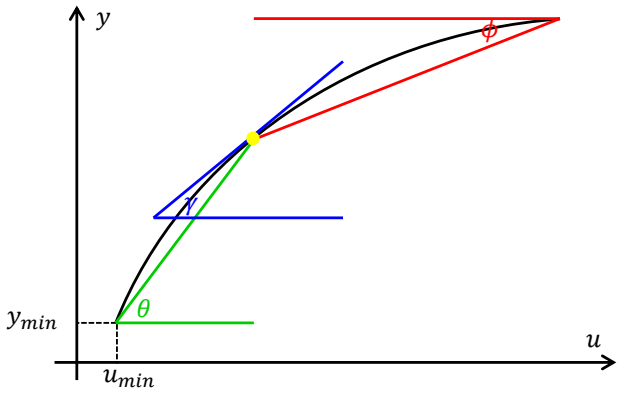

Figure 3.16: The three calculation methods for the nonlinear gain at a particular point.

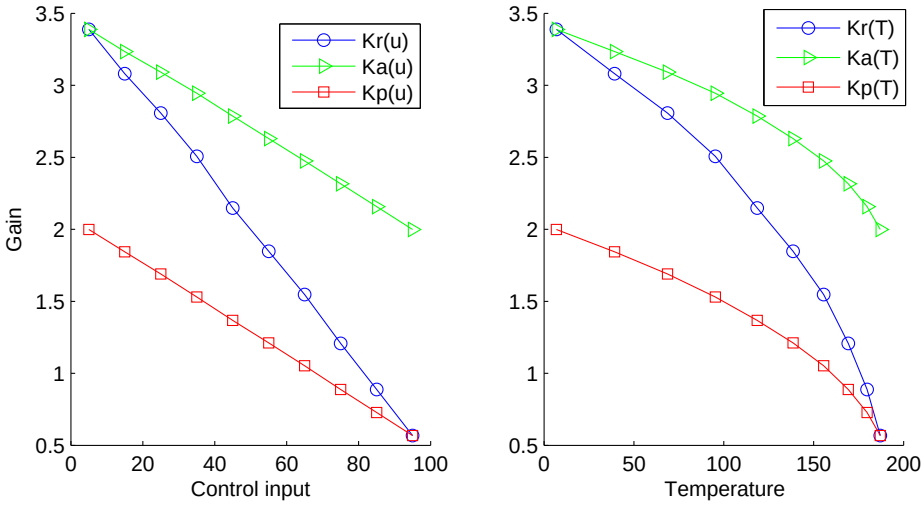

Figure 3.17: The nonlinear gain versus input and output.

From the above reasoning, it can be seen that non of the three nonlinear gain relationship can completely characterize the nonlinearity as a whole, considering the big operational range and both transient and steady-state. Hence, it raises the need for feedback linearization of fractional order systems.

3.4.4.2 Problem formulation

Let $\Omega \subseteq \mathbb{R}^n$ be a neighborhood region of the origin. The nonlinear fractional order system under consideration takes the following form,

$$\begin{aligned} {}_0^C D_t^\alpha x(t) &= f(x) + G(x,u), \\ y(t) &= h(x) \end{aligned} \tag{3.84}$$

where $x, y \in \mathbb{R}^n$, $u \in \mathbb{R}^p$, f and h are sufficiently smooth real analytic functions on $\Omega \subseteq \mathbb{R}^n$. To avoid the of infinite terms induced by the fractional differentiation and for the convenience

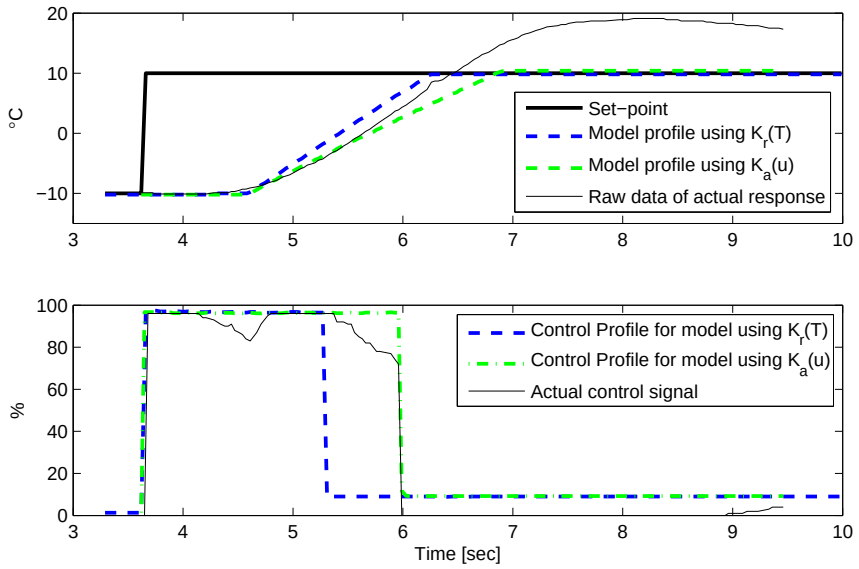

Figure 3.18: The transient under saturated closed-loop control is equivalent to that under open-loop step control signal.

of proceeding the derivation, it is assumed that the nonlinearity $G(x,u)$ can be sufficiently approximated by the product of p terms of a polynomial expansion and the input u,

$$G(x,u) = \sum_{i=1}^{p} g_i(x)u. \tag{3.85}$$

The research aim in this paper is to find a state feedback control

$$u = s(x) + \sigma(x)v$$

and a diffeomorphism

$$z = T(x)$$

such that the nonlinear model in equation (3.84) can be transformed into a equivalent linear model,

$$\begin{aligned} {}_0^C D_t^\alpha z(t) &= Az(t) + Bv, \\ y(t) &= h(T^{-1}z). \end{aligned} \tag{3.86}$$

Then, traditional techniques for linear systems, such as pole placement, can be used to design the control law v for the linearized process. The new state z is called the linearizing state and the control law u is called the linearizing control law. In addition, in order to avoid complications associated with the global problems induced by the fractional derivation, only local feedback linearization is focused, where the coordinate transformation and control law are only defined locally.

3.4.4.3 Feedback linearization of fractional order systems

The feedback linearization can linearly represent the original nonlinear model over a larger operating range. For integer order systems, the feedback linearization consists of two operations: 1.) nonlinear mapping of coordinates; and 2.) nonlinear feedback. Generally, the input-output linearization and the input-state linearization are the commonly used approaches for these two steps, [358]. Respectively, the input-output linearization linearizes the mapping between the transformed inputs (v) and the actual outputs (y); and the input-state linearization linearizes the mapping between the transformed inputs and the entire vector of transformed state variables. This subsection investigates whether the same procedure can be used for fractional order systems. In [359], Valérie and Oustaloup *et al.* considered the fractional rubout control of a specific nonlinearity and used the input-output linearization. However, the control object with nonlinearity under discussion is of integer order. The feedback linearization of fractional order systems has not been proposed. Even definitions are not given. Hence, some definitions and lemmas are introduced in this section under the same paradigm for integer order cases. This will consequently raise the problem of Lie derivative of fractional orders, which is called the *fractional Lie derivative* in this context,

$$\begin{aligned} \frac{d^\alpha y(t)}{dt^\alpha} &= \frac{\partial^\alpha h}{\partial x^\alpha}[f(x)+g(x)u] \\ &\neq L_f^\alpha h(x) + L_g^\alpha h(x) u; \end{aligned} \tag{3.87}$$

but since the chain rule generally does not hold for fractional derivatives, same derivation used for integer order cases can not be established. Relevant reference is hardly available in the literature, [360]. Hence, to avoid this problem, the nonlinearity under investigation is approximated by polynomials, and constraints are put during the derivation. For the definitions that cannot be extended parallely, revision are made according to the conventional FO techniques in [150, 361].

3.4.4.4 Feedback Linearization vs Jacobian Linearization

Before showing the main results, it is worth mentioning the advantage of feedback linearization of the nonlinear FO system over the Jacobian Linearization approximation.

Consider the Jacobian linearization of the nonlinear fractional order system (3.84) at the equilibrium point (x_0, y_0) with u_0,

$$\begin{aligned} {}_0^C D_t^\alpha x(t) &= \left[\frac{df(x_0)}{dx} + \frac{dg(x_0)}{dx}u_0\right](x-x_0) + G(x_0)(u-u_0), \\ y(t) &= y_0 + \frac{dh(x_0)}{dx}(x-x_0) \end{aligned} \tag{3.88}$$

Then the Jacobian model can be rewritten as the following linear state-space system

$$\begin{aligned} {}_0^C D_t^\alpha x(t) &= Ax + Bu, \\ y(t) &= Cx. \end{aligned} \tag{3.89}$$

It should be point out that the Jacobian model is an exact representation of the nonlinear model (3.84) only at (x_0, u_0) and at other operating points, however, the linearized model may yield unwelcome performance and robustness.

Next, a class of nonlinear fractional order control techniques is presented which transforms the original nonlinear model into a linear model. This differs from Jacobian linearization in that feedback linearization is achieved by exact state transformations and feedback, rather than by linear approximations of the dynamics.

3.4.4.5 Input-state Linearization

To introduce the idea of input-state linearisation, let us start with the problem of stabilizing the origin of the following problem

$$\begin{cases} {}_0^C D_t^\alpha x_1 = -x_2, \\ {}_0^C D_t^\alpha x_2 = x_1 - 2\sin(x_1 + x_2 + 0.5) + x_2^2 + u. \end{cases} \tag{3.90}$$

Choosing $u = 2\sin(x_1 + x_2 + 0.5) - x_2^2 + v$ to cancel the nonlinear term $2\sin(x_1 + x_2 + 0.5)$, and consider the new set of state variables $z_1 = x_1, z_2 = x_2$, the following corresponding linear system can be obtained,

$$\begin{cases} {}_0^C D_t^\alpha z_1 = -z_2, \\ {}_0^C D_t^\alpha z_2 = z_1 + v. \end{cases} \tag{3.91}$$

Then, a stabilizing state feedback control $v = -k_1 z_1 - k_2 z_2$ need to be designed to place the eigenvalue of the closed-loop system,

$$\begin{cases} {}_0^C D_t^\alpha z_1 = -z_2, \\ {}_0^C D_t^\alpha z_2 = -(k_1 - 1)z_1 - k_2 z_2. \end{cases} \tag{3.92}$$

For example, let $v = 3z_1 - 4z_2$. Then, the closed-loop dynamics become,

$$\begin{cases} {}_0^C D_t^\alpha z_1 = -z_2, \\ {}_0^C D_t^\alpha z_2 = 4z_1 - 4z_2 \end{cases} \tag{3.93}$$

is stable, whose poles are both placed at -2. In terms of the original state x_1 and x_2, one has the original input,

$$u = 2\sin(x_1 + x_2 + 0.5) - x_2^2 + 3x_1 - 4x_2$$

and since both z_i $(i = 1, 2)$ converge to zero, we see that the original state x_i $(i = 1, 2)$ converges to zero.

Theorem 4 (Input-state Linearization)**.**

The nonlinear fractional order control system in equation (3.84) is said to be input-state feedback linearizable, if it can be transformed into the following equivalent linear system

$${}_0^C D_t^\alpha z(t) = Az(t) + Bv(t) \tag{3.94}$$

via a state feedback control $u = s(x) + \sigma(x)v$ and a change of variables $z = T(x)$.

3.4.4.6 Input-output linearization

By using a nonlinear transformation and introducing a new input variable v, the objective of input-output linearisation is to establish a linear relationship between the output y and the input v. This can be achieved without addition conditions on the internal dynamics of the system apart from their stability.

To extend the input-output linearisation to fractional order systems, the stabilization of the following problem at the origin can be used as a starting point,

$$\begin{cases} {}_0^C D_t^\alpha x_1 = x_1 - 4x_2, \\ {}_0^C D_t^\alpha x_2 = x_1 - 3x_2 - 2\sin(x_1 + x_2 + 1) + u/(1 + x_1^2 + x_2^2), \\ y = x_1 + x_2. \end{cases} \tag{3.95}$$

Then,

$$\begin{aligned} {}_0^C D_t^\alpha y(t) &= {}_0^C D_t^\alpha \left[x_1(t) + x_2(t)\right] \\ &= 2x_1(t) - 7x_2(t) - 2\sin(x_1 + x_2 + 1) + \frac{u}{1 + x_1^2 + x_2^2}. \end{aligned} \tag{3.96}$$

Let $(z_1, z_2) = (x_1, x_2)^T \in \mathbb{R}^2$, $\sigma(x) = 1 + x_1^2 + x_2^2$,
$s(x) = \sigma(x)\left[2x_1(t) - 7x_2(t) - 2\sin(x_1 + x_2 + 1)\right]$ and the control law be $u = s(x) + \sigma(x)v$. Then, the full system in equation (3.95) can also be described by

$$\begin{cases} {}_0^C D_t^\alpha z_1 = z_1 - 4z_2, \\ {}_0^C D_t^\alpha z_2 = -z_1 + 4z_2 + v, \\ y = z_1 + z_2. \end{cases} \tag{3.97}$$

Moreover, since the new dynamics is linear and controllable, a stabilizing state feedback control $v = -k_1 z_1 - k_2 z_2$ can be designed to place the eigenvalue of the closed-loop system,

$$\begin{cases} {}_0^C D_t^\alpha z_1 = z_1 - 4z_2, \\ {}_0^C D_t^\alpha z_2 = -(k_1 + 1)z_1 - (k_2 - 4)z_2, \\ y = z_1 + z_2. \end{cases} \tag{3.98}$$

For example, let $v = 2.5z_1 - 8z_2$. Then, the closed-loop dynamics becoming

$$\begin{cases} {}_0^C D_t^\alpha z_1 = z_1 - 4z_2, \\ {}_0^C D_t^\alpha z_2 = 1.5z_1 - 4z_2, \\ y = z_1 + z_2. \end{cases} \tag{3.99}$$

is stable, whose poles are placed at $-1, -2$. In terms of the original state x_1 and x_2, one has

$$u = \left(1 + x_1^2 + x_2^2\right)\left[2x_1(t) - 7x_2(t) - 2\sin(x_1 + x_2 + 1) + 2.5x_1 - 8x_2\right].$$

Since both z_1 and z_2 converge to zero, the original states x_1 and x_2 converges to zero.

Now, the pavement is sufficient for introducing the following definition:

Definition 21 (Input-output Linearization)**.**

The nonlinear fractional order control system in equation (3.84) is said to be input-output feedback linearizable, if it can be transformed into the following equivalent linear system

$$\begin{aligned} {}_0^C D_t^\alpha z(t) &= Az(t) + Bv(t), \\ y(t) &= Cz(t) \end{aligned} \tag{3.100}$$

via a state feedback control $u = s(x) + \sigma(x)v$ and a change of variables $z = T(x)$.

Thus, the stabilization problem for the nonlinear system has been reduced to a stabilization problem for a controllable linear system. Feedback linearization cancels the nonlinearities in a nonlinear system so that the closed-loop dynamic is linear.

A general nonlinear fractional order control system,

$${}_0^C D_t^\alpha x = F(x, u) \tag{3.101}$$

is (locally at (x_0, u_0)) feedback linearizable if it is (locally at (x_0, u_0)) feedback equivalent to a control linear system of the form,

$${}_0^C D_t^\alpha x = Ax(t) + B\gamma(x)(u - s(x)). \tag{3.102}$$

Theorem 5 (Static state feedback linearizable)**.**

An affine nonlinear fractional order control system

$${}_0^C D_t^\alpha x(t) = f(x) + G(x)u \approx f(x) + \sum_{i=1}^{p} g_i(x)u, \quad x \in \mathbb{R}^n \tag{3.103}$$

$$y(t) = h(x) \tag{3.104}$$

with $f(0) = 0$ and $rankG(0) = p$ is said to be static state feedback linearizable, if it can be transformed into an asymptotic Mittag-Leffler stability linear system

$$\begin{aligned} {}_0^C D_t^\alpha z(t) &= Az(t) + Bv(t), \\ y(t) &= h(T^{-1}z) \end{aligned} \tag{3.105}$$

via a state feedback control $u = h(x) + l(x)v$ and a change of variables $y = T(x)$.

3.4.4.7 State feedback control: M-L stabilization

Whether a system is controllable is a useful information, because it determines if a given initial state x_0 can be steered to the origin in finite time using the input $u(t)$. Moreover, if a system is not completely controllable, it can be decomposed into a controllable and a uncontrollable subsystem. On the other hand, if the subspace of the system is stable, it is said to be stabilizable, i.e., the uncontrollable states decays to origin by themselves. By utilizing the definition of Mittag-Leffler stability in [54], a general framework of the state feedback control for M-L stabilization of the fractional order system is given.

Theorem 6 (Asymptotically Mittag-Leffler stable)**.**

Let $x(t) = 0$ be the equilibrium point of the following fractional order system,

$$ {}_0^C D_t^\alpha x = F(t, x),\ (t, x) \in [0, \infty) \times \Omega. \tag{3.106} $$

Assume that there exists a Lyapunov function $V(t, x(t)) : [0, \infty) \times \Omega \to \mathbb{R}$ and three class-κ functions $k_i,\ i = 1, 2, 3$ such that,

$$ (i) \quad k_1(\|x\|) \leq V(t, x(t)) \leq k_2(\|x\|), \tag{3.107} $$

$$ (ii) \quad {}_0^C D_t^\alpha V(t, x(t)) \leq -k_3(\|x\|). \tag{3.108} $$

Then the equilibrium point of system (3.106) is asymptotically Mittag-Leffler stable, [54].

By utilizing Theorem 6, we then obtain that state feedback M-L stabilization of nonlinear fractional order system is generalized to test whether the system with a state feedback control u is M-L stabilizable.

Criterion 1 (Static state feedback linearizable)**.**

The fractional order system

$$ {}_0^C D_t^\alpha x(t) = f(x) + G(x)u,\ (t, x) \in [0, \infty) \times \Omega \tag{3.109} $$

with the state feedback control $u = s(x) + \sigma(x)v$ is said to be static state feedback linearizable, if there exists a smooth function $V(t, x(t)) : [0, \infty) \times \Omega \to \mathbb{R}$ and three κ-class functions $k_i,\ i = 1, 2, 3$ such that,

$$ (i) \quad k_1(\|x\|) \leq V(t, x(t)) \leq k_2(\|x\|), \tag{3.110} $$

$$ (ii) \quad {}_0^C D_t^\alpha V(t, x(t)) \leq -k_3(\|x\|). \tag{3.111} $$

Through the above proposed definitions and preliminary theorems, it is revealed that the related derivation used for integer order systems, such as the Lie derivative, cannot be used for FO systems due to the failure of chain rule and semi-group property on fractional derivatives. Hence, a general solution is not easy to obtain. Nevertheless, particular solutions is presented in chapter 5 through simulation and experiment for a case study.

3.4.4.8 Summary

The nonlinear system identification is indeed an interesting practical topic. More work has been done on this direction during this research, such as the floating ball app for the MESABox in section 6.2. However, since mathematically rigorous result was not obtained for some of the efforts, they are arranged into the miscellaneous research results in chapter 6, and the future research opportunities on these topics are stated in chapter 7.

3.5 Fractional order multi-input-multi-output processes

Due to the existence of single-input-single-output (SISO) FO systems, multi-input-multi-output (MIMO) fractional order systems naturally exist [40, 362]. Compared to SISO cases, MIMO processes consisting of fractional order dynamics are relatively less addressed in the FO control research field. Although there is theoretical study in the literature, exploration

does not go beyond simulation. This section briefly reviews some of the existing work on MIMO FO modeling. Decoupling and control of MIMO FO systems will be discussed in chapter 4. Furthermore, a realistic MIMO FO control problem will be presented in chapter 5. Note that the differences between a MIMO process and a multi-variable system lies in the input and output. A multi-variable system is not necessarily MIMO.

In [95], Liao, Wang *et al.* extended the traditional subspace method in frequency domain to identify MIMO FO systems with time delay in states. The m-input-l-output model under consideration is of the following form:

$$\begin{cases} D^{\alpha}x(t) &= Ax(t-\tau)+Bu(t) \\ y(t) &= Cx(t)+Du(t) \end{cases} \tag{3.112}$$

where $A \in \mathbb{R}^{n\times n}$, $B \in \mathbb{R}^{n\times m}$, $C \in \mathbb{R}^{l\times n}$, $C \in \mathbb{R}^{l\times m}$, τ is the time delay, and $0 < \alpha < 2$ is the order of the FO derivative. Perform Laplace transform to equation (3.112), and define:

$$X_{\alpha}(s) \triangleq (s^{\alpha}e^{\tau s}I_{n\times n} - A)^{-1}Be^{\tau s}, \qquad \tilde{B} \triangleq [B \;\; 0_{n\times m}],$$
$$\tilde{D} \triangleq [0_{l\times m} \;\; D], \quad \tilde{U}(s) \triangleq [e^{\tau s}I_{m\times n} \;\; I_{m\times m}]^T.$$

Then, it is rewritten as:

$$\begin{cases} s^{\alpha}e^{\tau s}X_{\alpha}(s) &= AX_{\alpha}(s)+\tilde{B}\tilde{U}(s) \\ H(s) &= CX_{\alpha}(s)+\tilde{D}\tilde{U}(s) \end{cases} \tag{3.113}$$

When the input and output data matrices, $\mathbb{H}$ and $\mathbb{U}$, are acquired, the coefficient matrices can be identified by using a generic algorithm to iterate the following procedure,

$$\mathbb{H} = Q_q\mathbb{X} + \Gamma_q\mathbb{U}, \tag{3.114}$$

where O_q is the extended observability matrix and Γ_q is as follows:

$$O_q = \begin{bmatrix} C \\ CA \\ \vdots \\ CA^{q-1} \end{bmatrix}, \qquad \Gamma_q = \begin{bmatrix} \tilde{D} & 0 & \cdots & 0 \\ C\tilde{B} & \tilde{D} & \cdots & 0 \\ \vdots & \vdots & \ddots & 0 \\ CA^{q-2}\tilde{B} & CA^{q-2}\tilde{B} & \cdots & \tilde{D} \end{bmatrix}$$

Using singular value decomposition (SVD), a weighting function can be obtained,

$${W_1}^{-1}\mathbb{H}/\mathbb{U} = \begin{bmatrix} U_1 & U_2 \end{bmatrix} \begin{bmatrix} S_1 & 0 \\ 0 & 0 \end{bmatrix} \begin{bmatrix} V_1^T \\ V_2^T \end{bmatrix}. \tag{3.115}$$

Then, $O_q = W_1U_1S_1^{1/2}$ can be calculated, and A and C can be estimated,

$$A = \underline{O}_q\overline{O}_q, \quad C = \overline{\overline{O}}_q \tag{3.116}$$

where $\underline{O}_q$ denotes Q_q without the last l rows, $\overline{O}_q$ denotes Q_q without the first l rows, and $\overline{\overline{O}}_q$ denotes the first l rows of O_q. Finally, B and D can be calculated with the least squares method.

In [363], Victor, Oustaloup *et al.* extended the flatness principle to linear fractional order MIMO systems with an application in thermal processes, as shown in the following definition.

Definition 22 (Differentially flat)**.** *Let $x^{(\nu)}$ denote $D_t^\nu x$ in this context. A fractional order system $x^{(\nu)} = f(x,u)$, with m inputs and n outputs, is differentially flat if one can find a set of independent variables z (co-called fractional flat output), such that each system variable, including the inputs, is a function of the flat output and a finite number of its time derivatives,*

$$z = h(x, u, u^{(\nu)}, u^{(2\nu)}, \ldots, z^{(\beta\nu)}), \quad z \in \mathbb{R}^m \tag{3.117}$$

where β is a finite m-tuple of integers, and ν is the commensurable order, such that

$$\begin{aligned} x &= \mathcal{A}(z, z^{(\nu)}, \ldots, z^{(\alpha\nu)}) \\ u &= \mathcal{B}(z, z^{(\nu)}, \ldots, z^{((\alpha+1)\nu)}) \end{aligned} \tag{3.118}$$

make the following equivalent system equation:

$$\mathcal{A}^{(\nu)}(z, z^{(\nu)}, \ldots, z^{(\alpha\nu)}) = f\left(\mathcal{A}(z, z^{(\nu)}, \ldots, z^{(\alpha\nu)}) + \mathcal{B}(z, z^{(\nu)}, \ldots, z^{((\alpha+1)\nu)})\right). \tag{3.119}$$

After all, any method or combined methods for traditional integer order processes can be used for modeling the fractional order MIMO processes, but with the formulas re-derived for FODE, FO TF or FO S-S models. Some of the derivation are straightforward while some are difficult, and some derivations are easy in theory but hard for practical implementation.

Chapter 4

Fractional Order Process Control

Don't loaf and invite inspiration; light out after it with a club.

—Jack London

"Go West, young man." – Horace Greeley. "Go fractional. There, you will find inspiration." –Prof. Yangquan Chen.

This chapter prepares a wide variety of flavors on fractional order process controls. While some are gathered from the literature, the methods described in sections 4.2 and 4.4 are newly developed. Then, in chapter 5, examples are given with regard to their simulation and practical application.

4.1 Fractional order controllability and observability

This section briefly reviews the controllability and observability of fractional order systems since they are the fundamental issues that need to be considered before performing controls. The evaluation of controllability and observability of linear FO systems in the pseudo state-space representation is straightforward, whereas for FO systems in other forms and nonlinear FO systems, it is relatively harder.

Definition 23 (FO observability Gramian)**.** *The observability Gramian of a system with fractional order α is the positive symmetric matrix in $\mathcal{M}_{n\times n}(\mathbb{R})$, [364]:*

$$\mathcal{O}_\alpha(t_0,t_1) \triangleq \int_{t_0}^{t_1} E_\alpha(A^T\tau^\alpha)C^TCE_\alpha(A\tau^\alpha)d\tau, \tag{4.1}$$

where $E_\alpha(A^T\tau^\alpha)$ is the fractional order state transition matrix introduced in equation (2.56).

Similar to the the theorem for integer order models, we have the following.

Theorem 7 (FO observability)**.** *The system in equation (2.55) is observable on $[t_0,t_1]$ if*

and only if $\mathcal{O}_\alpha(t_0, t_1)$ is positive definite, which is equivalent to,

$$\mathcal{O} \triangleq \begin{bmatrix} C \\ CA \\ \vdots \\ CA^{n-1} \end{bmatrix} \text{ has rank n.} \tag{4.2}$$

For the fractional differential equations in the polynomial form:

$$\begin{aligned} P(\sigma)\xi &= Q(\sigma)u, \\ y &= R(\sigma)\xi, \end{aligned} \tag{4.3}$$

where $u \in \mathbb{R}^m$ is the control, ξ is the partial state, and $\sigma = s^\alpha$; it is observable iff P and R are *right* coprime.

Definition 24 (FO controllability Gramian)**.** *The controllability Gramian of a system with fractional order α is the positive symmetric matrix in $\mathcal{M}_{n\times n}(\mathbb{R})$:*

$$\mathcal{C}_\alpha(t_0, t_1) \triangleq \int_{t_0}^{t_1} (t_1 - \tau)^{(1-\alpha)} E_\alpha(A, t_1 - \tau) B B^T E_\alpha(A^T, t_1 - \tau) d\tau. \tag{4.4}$$

Note that, the term $(t_1 - \tau)^{(1-\alpha)} E_\alpha(A, t_1 - \tau)$ is not the state transition matrix, which is different from that for integer order systems.

In duality, the theorem for FO controllability is as the following:

Theorem 8 (FO controllability)**.** *The system in equation (2.55) is controllable on $[t_0, t_1]$ if and only if $\mathcal{C}_\alpha(t_0, t_1)$ is positive definite, which is equivalent to,*

$$\mathcal{C} \triangleq [B \; AB \; \cdots \; A^{n-1}B] \text{ has rank n.} \tag{4.5}$$

For fractional differential equations in the polynomial form in equation (4.3), it is controllable iff P and Q are *left* coprime.

Other controllability and observability related discussion on FO systems can be found in [365] and the paper collection in [23], such as the constrained controllability of h-difference linear systems with two fractional orders, and the observability of positive fractional-order discrete-time systems.

4.2 Decoupling linear fractional order MIMO processes

Decoupling the interactions among the inputs and outputs is a frequently encountered problem in industrial process control. For integer order MIMO processes, one of the methods is to extend the input-output linearization approach to the so-called input-output decoupling, [358]; other methods may involve the derivation of the inverse of interactions as a decoupling intermedium among primary loops through singular value decomposition (SVD). An example can be found in [366]. Yet, there has not been such studies for fractional order processes. This section investigates the decoupling of linear fractional order MIMO processes. Without

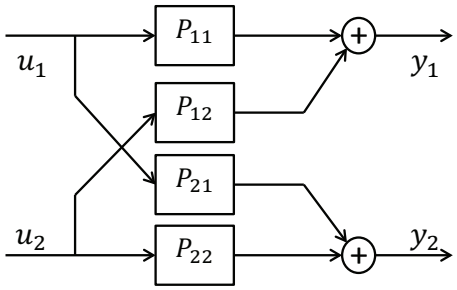

Figure 4.1: The block diagram of a TITO process.

loss of generality, TITO processes are investigated with emphasis. Some of the results were published in [367].

The system under investigation is a process model abstracted from a temperature control loop in the semiconductor manufacturing industry, as shown in figure 4.1. It is an LTI system that can be depicted by the pseudo state equation (2.55) in chapter 2, where ${}_0D_t^{\alpha}x(t)$ denotes the fractional differentiation with respect to time in the Caputo sense as in equation (2.6), and the fractional orders are $\alpha = [\alpha_{11}, ..., \alpha_{22}] \in (0, 2)$. The state matrix A, input matrix B and output matrix C are of the following forms respectively,

$$A = \begin{bmatrix} -\frac{1}{T_{11}} & 0 & 0 & 0 \\ 0 & -\frac{1}{T_{12}} & 0 & 0 \\ 0 & 0 & -\frac{1}{T_{21}} & 0 \\ 0 & 0 & 0 & -\frac{1}{T_{22}} \end{bmatrix}, B = \begin{bmatrix} \frac{K_{11}}{T_{11}} & 0 \\ 0 & \frac{K_{12}}{T_{12}} \\ \frac{K_{21}}{T_{21}} & 0 \\ 0 & \frac{K_{22}}{T_{22}} \end{bmatrix}$$
$$C = \begin{bmatrix} 1 & 1 & 0 & 0 \\ 0 & 0 & 1 & 1 \end{bmatrix}.$$

Similar to the way of manipulating integer order differential equations, by taking Laplace transforms, the pseudo-state-space representation of the above FO differential equations can be derived, with zero initial condition assumed. Furthermore, the state-space representation can be converted to a transfer function matrix in the same manner as is done for integer order models [35],

$$Y(s) = P(s)\,U(s), \tag{4.6}$$

where

$$P(s) = C(s^{\alpha}I - A)^{-1}B = \begin{bmatrix} P_{11}(s) & P_{12}(s) \\ P_{21}(s) & P_{22}(s) \end{bmatrix}, \tag{4.7}$$

and each element P_{ij} is an FO transfer function,

$$P_{ij}(s) = \frac{K_{ij}}{T_{ij}s^{\alpha_{ij}} + 1},\ i, j = 1, 2. \tag{4.8}$$

The off-diagonal elements P_{12} and P_{21} are the causes of the interaction between two primary loops. For integer order processes, multiple approaches exist to decouple the interaction as

mentioned earlier. No matter which method is used, the goal is to eliminate or minimize the interaction. The same goal is pursued for fractional order processes. In the following subsections, the decoupling of FO processes will be presented. The cases of zero time delay will be discussed first. Then, the cases with time delay will be dealt with separately.

4.2.1 The ideal decoupling

With the ideal decoupling, the decoupled process is expected to have a diagonal transfer function matrix in the form below:

$$G(s) = P(s)\,D(s) = \begin{bmatrix} P_{11}(s) & 0 \\ 0 & P_{22}(s) \end{bmatrix}, \tag{4.9}$$

where $D(s)$ is the transfer function matrix of the decoupler,

$$D(s) = \begin{bmatrix} D_{11}(s) & D_{12}(s) \\ D_{21}(s) & D_{22}(s) \end{bmatrix}. \tag{4.10}$$

An illustration of the system connection with an ideal decoupler is shown in figure 4.2. Based on the decoupling requirement in equation (4.9), four equations can be established:

$$\begin{aligned} P_{11}(s)\,D_{11}(s) + P_{12}(s)\,D_{21}(s) &= P_{11}(s) \\ P_{11}(s)\,D_{12}(s) + P_{12}(s)\,D_{22}(s) &= 0 \\ P_{21}(s)\,D_{11}(s) + P_{22}(s)\,D_{21}(s) &= P_{22}(s) \\ P_{21}(s)\,D_{12}(s) + P_{22}(s)\,D_{22}(s) &= 0. \end{aligned}$$

The decoupler elements are then given by the solution:

$$\begin{aligned} D_{11}(s) &= \frac{P_{11}(s)\,P_{22}(s)}{P_{11}(s)\,P_{22}(s) - P_{12}(s)\,P_{21}(s)} \\ D_{12}(s) &= \frac{-P_{12}(s)\,P_{22}(s)}{P_{11}(s)\,P_{22}(s) - P_{12}(s)\,P_{21}(s)} \\ D_{21}(s) &= \frac{-P_{11}(s)\,P_{21}(s)}{P_{11}(s)\,P_{22}(s) - P_{12}(s)\,P_{21}(s)} \\ D_{22}(s) &= \frac{P_{11}(s)\,P_{22}(s)}{P_{11}(s)\,P_{22}(s) - P_{12}(s)\,P_{21}(s)}. \end{aligned} \tag{4.11}$$

Plugging equation (4.8) into the solutions will give the fractional order ideal decoupler.

At this stage, the properness of such decoupling elements needs to be examined. When the four channels have the same fractional order, the decoupler is obviously proper (i.e. strictly proper or bi-proper), with the same highest order 2α on both the numerator and the denominator. When the fractional orders are different, it can be seen that the resulting decoupler is still proper. Taking the first element as an example:

$$D_{11}(s) = \frac{A}{A - B}, \tag{4.12}$$

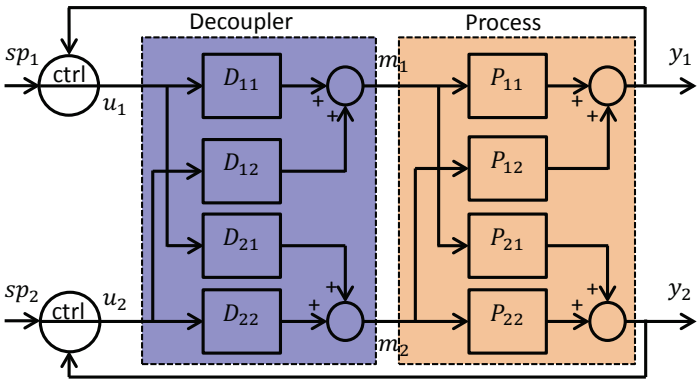

Figure 4.2: The block diagram of the ideal decoupling.

where

$$\begin{aligned} A &= K_{11}K_{22}\left(T_{12}s^{\alpha_{12}}+1\right)\left(T_{21}s^{\alpha_{21}}+1\right) \\ B &= K_{12}K_{21}\left(T_{11}s^{\alpha_{11}}+1\right)\left(T_{22}s^{\alpha_{22}}+1\right), \end{aligned}$$

the highest order of the denominator is $\max(\alpha_{12}\alpha_{21}, \alpha_{11}\alpha_{22})$ while that of the numerator is $\alpha_{12}\alpha_{21}$, and the relationship among the fractional orders does not affect the properness.

4.2.2 The simplified decoupling

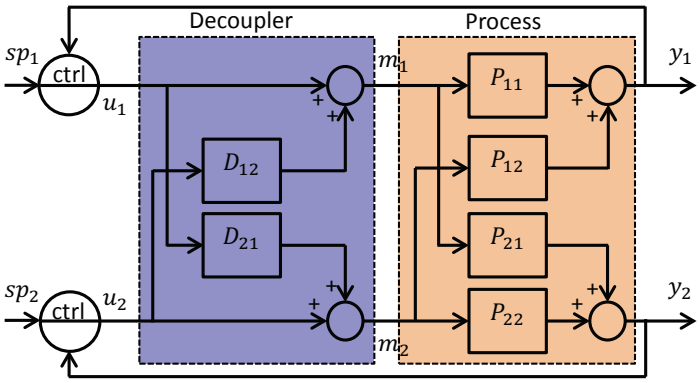

Figure 4.3: The block diagram of the simplified decoupling.

Compared with the ideal decoupling, the simplified decoupling has less stringent requirements on the diagonal elements of the process. In other words, it does not emphasize much on what the primary loops become after decoupling. Instead, it assigns less task to the decoupler by setting the diagonal elements to be 1, as shown in figure 4.3,

$$D(s) = \begin{bmatrix} 1 & D_{12}(s) \\ D_{21}(s) & 1 \end{bmatrix}. \tag{4.13}$$

Thus, the following two equations are used to satisfy the decoupling condition, i.e. to make the process diagonal,

$$\begin{aligned} P_{11}(s) D_{12}(s) + P_{12}(s) D_{22}(s) &= 0, \\ P_{21}(s) D_{12}(s) + P_{22}(s) D_{22}(s) &= 0, \end{aligned}$$

with the solution being:

$$D_{12}(s) = -\frac{P_{12}(s)}{P_{11}(s)}, \quad \text{and} \quad D_{21}(s) = -\frac{P_{21}(s)}{P_{22}(s)}. \tag{4.14}$$

This leads to a simpler decoupler transfer function but a relatively more complicated decoupled process,

$$G(s) = \begin{bmatrix} P_{11} - \frac{P_{12}P_{21}}{P_{22}} & 0 \\ 0 & P_{22} - \frac{P_{12}P_{21}}{P_{11}} \end{bmatrix}. \tag{4.15}$$

To evaluate the properness in this circumstance, different cases need to be considered. When the fractional orders are same, i.e. $\alpha_{11} = \alpha_{12} = \alpha_{21} = \alpha_{22}$, the decoupler will be in a fractional order filter form [40]. If the fractional orders are different, it may result in an improper decoupler that may not be realizable. Specifically, for example, when $\alpha_{11} > \alpha_{12}$, the second decoupler element is improper,

$$D_{12}(s) = -\frac{K_{12}(T_{11}s^{\alpha_{11}} + 1)}{K_{11}(T_{12}s^{\alpha_{12}} + 1)}.$$

Although the resulting process is proper,

$$G_{11}(s) = \frac{A - B}{C},$$

where A and B are the same as in equation (4.12), and

$$C = K_{22}(T_{11}s^{\alpha_{11}} + 1)(T_{12}s^{\alpha_{12}} + 1)(T_{21}s^{\alpha_{21}} + 1),$$

it cannot be achieved in practice because a fractional order differentiator $s^{\alpha_{11}-\alpha_{12}}$ will be factorized from $D_{12}(s)$ by the means we use for integer order systems, such as long division or partial fraction expansion. Similar to a pure differentiator in integer order control systems, such a fractional order differentiator will also amplify noise and result in divergent or singular solutions of system responses, which is not acceptable in practice. Some research on the existence of decouplers for integer order singular systems can be referred to in [368, 369]. Thus, to guarantee the existence of a proper simplified decoupler, the FO TITO process model needs to satisfy the following condition,

$$\alpha_{11} \leq \alpha_{12} \text{ and } \alpha_{22} \leq \alpha_{21}. \tag{4.16}$$

Otherwise, the conventional decoupling techniques do not apply. In order to still utilize them, a different model structure can be selected to approximate the process, such as FO transfer functions with two poles, either commensurate or not. This is a topic for future exploration.

4.2.3 The inverted decoupling

Briefly, the inverted decoupling method is to achieve the ideal-decoupled performance in equation (4.9), using simplified decoupling elements in equation (4.13). This is accomplished by subtly re-routing the decoupling block connections [370], as shown in figure 4.4. As an extension to the FO case, the FO TITO processes can be treated in the same manner.

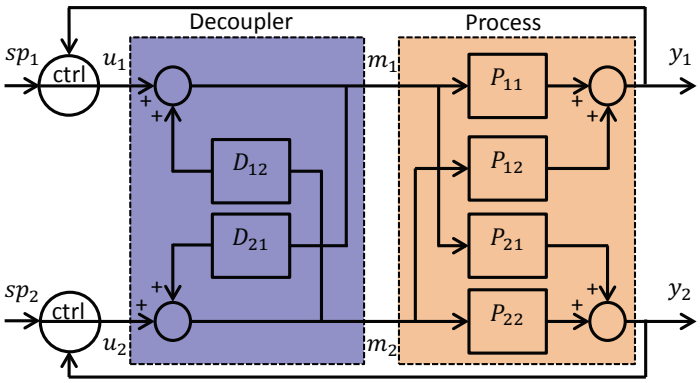

Figure 4.4: The block diagram of the inverted decoupling.

Since the inverted decoupler uses the same decoupling elements as the simplified decoupler, the condition for the existence of a proper inverted decoupler is the same as equation (4.16).

4.2.4 Decoupling fractional order processes with time delay

The aforementioned discussion considers the process models with no time delay, which is too ideal to be true in practice. Nevertheless, it is not a problem when the models have dead time because the techniques for dealing with time-delayed integer order models can also be used for FO processes. Specifically, denoting the dead time by L_{ij}, the model in equation (4.8) becomes the following:

$$\tilde{P}_{ij}(s) = \frac{K_{ij}}{T_{ij}s^{\alpha_{ij}} + 1} e^{-sL_{ij}}. \tag{4.17}$$

Consequently, the decoupler elements for the simplified, as well as the inverted decoupling in equations (4.14) become the forms below,

$$\tilde{D}_{12}(s) = -\frac{K_{12}\left(T_{11}s^{\alpha_{11}} + 1\right)}{K_{11}\left(T_{12}s^{\alpha_{12}} + 1\right)} e^{-(L_{12}-L_{11})s}, \tag{4.18}$$

$$\tilde{D}_{21}(s) = -\frac{K_{21}\left(T_{22}s^{\alpha_{22}} + 1\right)}{K_{22}\left(T_{21}s^{\alpha_{21}} + 1\right)} e^{-(L_{21}-L_{22})s}. \tag{4.19}$$

When $L_{12} < L_{11}$ and/or $L_{21} < L_{22}$, the decoupler is non-causal, which is to be avoided during the realization of transfer functions. This problem can be fixed by artificially adding a time delay to the decoupler as described in the work of Wang *et al.* [371]. Thus, the refined

decoupler $\tilde{D}(s)$ becomes the following form:

$$\tilde{D}\left(s\right)=\left[\begin{array}{cc} e^{-v(L_{22}-L_{21})s} & D_{12}\left(s\right)e^{-v(L_{12}-L_{11})s} \\ D_{21}(s)e^{-v(L_{21}-L_{22})s} & e^{-v(L_{11}-L_{12})s} \end{array}\right], \tag{4.20}$$

where the function $v(L)$ is defined as:

$$v\left(L\right)=\left\{\begin{array}{lll} L, & \text{if} & L > 0, \\ 0, & \text{if} & L \leq 0. \end{array}\right. \tag{4.21}$$

Remark: the definition of $v(L)$ is inaccurate in the original proposed form. The value should be L when $L > 0$. The inaccurate usage of this method in [372, 366] should be corrected.

4.2.5 The relative gain array for MIMO fractional order processes

The relative gain array (RGA) is a useful tool to characterize the loop interactions in MIMO processes, from which the advise for suitable input-output pairing can be drawn [373]. While the static RGA only evaluates the steady-state gains, the frequency dependent RGA evaluates the process gains at the corresponding operational frequencies of interest. For the LTI model with one FO pole, as in equation (4.8), the gain depends not only on the traditional model parameters K, T and L, but also on the FO order α,

$$\begin{aligned} \left|G\left(j\omega\right)\right| &= \left|\frac{K}{T(j\omega)^{\alpha}+1}e^{-Lj\omega}\right| \\ &= \left|\frac{K}{T\omega^{\alpha}e^{j\frac{\pi}{2}\alpha}+1}\right| \\ &= \frac{|K|}{\left|T\omega^{\alpha}\left[\cos\left(\frac{\pi}{2}\alpha\right)+j\sin(\frac{\pi}{2}\alpha)\right]+1\right|} \\ &= \frac{|K|}{\sqrt{\left(T\omega^{\alpha}\right)^{2}+2T\omega^{\alpha}\cos\left(\frac{\pi}{2}\alpha\right)+1}}. \end{aligned} \tag{4.22}$$

Hence, the frequency dependant RGA is:

$$RGA = G(j\omega)\cdot(G(j\omega)^{-1})^{T}, \tag{4.23}$$

where $G(j\omega)$ takes the form in equation (4.22). This will be illustrated through simulation example 3 in Sec. 5.4.

Three examples on TITO decoupling and an industrial application of 4×4 decoupling will be provided in chapter 5.

4.3 Model predictive control of fractional order MIMO processes using RIOTS

A rough statistic approximates that more than 80% of the feedback control devices in the industry use PID controllers [374]. For the rest percentage, model predictive control (MPC) takes the dominant part [375]. As the second most popular industrial control algorithm, MPC

has drawn lots of research attention ever since its emerging [376, 377, 378, 379]. However, extending the MPC to FO processes is not yet mature in spite of some exploration efforts, e.g. the application of MPC to fractional thermal systems [380, 381, 382] and two others [300, 383]. For a survey on this topic, refer to [384]. Thus, extending MPC to FO processes is investigated in this section, along with the implementation using RIOTS. Some preliminary results is published in [385].

4.3.1 Fractional order model predictive control

MPC is a multivariable control algorithm developed by engineers in Shell Oil Cooperation in the 1970s and found wide application in the industrial process control thereafter. In general, it is a control concept of combining the optimal control with the use of digital control. It computes a cost criteria for a finite-time horizon in the future based on a plant model sampled at the current time. This strategy is performed on the fly repetitively by looking ahead of a receding time horizon [386]. Therefore, the MPC is also called the receding horizon control (RHC). One of the advantages of MPC is that the decoupling of loop interactions is already taken into consideration [387], and there is no additional effort needed for the decoupling. The disadvantage is the high reliance on model. If a process is hard to model or the model contains too much uncertainty, it loses the precision of predicting.

In fact, the MPC can be broken down to an optimal control problem during each time interval because its key step is the optimization. Thus, the main strategy in this section is to utilize the foundation of fractional optimal control (FOC) for extending the use of MPC to FO processes.

4.3.1.1 Fractional order optimal control

The optimal control of fractional order systems is studied relatively more than the MPC, therefor, there are more resources for moving onto FO MPC from FOC. For example, a general formulation and solution scheme for fractional optimal control problems (FOCP) is presented by Agrawal *et al* [388]. In this formulation, the definition of FO derivatives uses the left and right R-L form expressed in equations (2.4) and (2.5). Then, the FOCP under consideration is to find the optimal control $u(t)$ for an FO system that minimizes the performance index,

$$J(u) = \int_0^T F(x, u, t)dt, \tag{4.24}$$

subject to the system dynamic constraints:

$${}_0D_t^\alpha x = G(x, u, t) \quad (0 < \alpha < 1), \tag{4.25}$$

and the initial condition:

$$x(0) = x_0, \tag{4.26}$$

where $x(t)$ is the state variable. Sometimes, additional terms containing x can be included in equation (4.24) at the end point. As an example, the optimization of a linear FODE given

the cost criteria of an integral of quadratic form can be stated as the following,

$$J(u) = \frac{1}{2}\int_0^1 [q(t)x^2(t) + r(t)u^2]dt, \tag{4.27}$$

subject to:

$${}_0D_t^\alpha x = a(t)x + b(t)u. \tag{4.28}$$

Following the derivation in [388], the Euler-Lagrange equations for the above FOCP is obtained,

$$\begin{aligned} {}_0D_t^\alpha x &= G(x,u,t), & (4.29)\\ {}_tD_1^\alpha \lambda &= \frac{\partial F}{\partial x} + \lambda\frac{G}{\partial x}, & (4.30)\\ 0 &= \frac{\partial F}{\partial u} + \lambda\frac{G}{\partial u}, & (4.31) \end{aligned}$$

and $x(0) = x_0$, $\lambda(1) = 0$. Regarding the solution to the fractional E-L equations and furthermore FOCPs, numerous methodologies and results are available in the literature. In [389], Tricaud and Chen *et al* formulated the fractional time-optimal control problem (TOCP) and provided the solution to the TOCP of a fractional double integrator . In [268], the solution of FOCP using SVD-based rational approximations is investigated. [390] presented an approximation method for numerically solving FOCPs of the general form, and Sweilam *et al* provided numerical solution for some types of FOCPs [391]. In [392, 393], Dzieliński *et al* studied the FOCPs in the linear quadratic discrete-time case under the constraints of fixed final time and free final state. A similar effort is also available in [394]. In [167], Vinagre and Feliu *et al* did a case study using the Wiener-Hopf method on the optimal fractional controllers for commensurate order systems.

In this context, following the paradigm in [268, 390] and [389], the FOCPs can be solved using the Matlab toolbox RIOTS, which is an outstanding optimal control problem solver over other similar softwares, such as SOCS [395], DIRCOL [396] and MISER3 [397], according to the surveys [398, 399, 400, 401].

4.3.1.2 Introduction to RIOTS

The RIOTS (Recursive Integration Optimal Trajectory Solver) is a Matlab toolbox designed to solve a broad class of optimal control problems, including trajectory and endpoint constraints, control bounds, variable initial conditions with integral and/or endpoint cost functions [402]. It utilizes multiple ingenious techniques to realize the critical routines in the algorithm. For example, it uses LSODA [403] to perform the variable-step integration, NPSOL [404] for the constrained optimization, and automatic differentiation (ADOL-C) [405] for derivative and gradient checking. RIOTS is sufficiently capable of solving classic optimal control problems of integer order systems [406, 407, 408], and has been extended to solve the FOCPs by Tricaud and Chen *et al* [409, 268].

The optimal control problems to be solved by RIOTS can be formulated in the form below :

$$\min_{(u,\xi)\in L_\infty^m \times R^n} f(u,\xi) = g_o(\xi, x(b)) + \int_a^b l_o(t,x,u)dt \tag{4.32}$$

subject to:

$$\begin{aligned} \dot{x} = h(t,x,u), x(a) = \xi, t \in [a\ b] \\ u^j_{min}(t) < u^j(t) < u^j_{max}(t) \\ \xi^j_{min}(t) < \xi^j(t) < \xi^j_{max}(t) \\ l^v_{ti}(t,x(t),u(t)) \leq 0, v \in Q_{ti} \\ g^v_{ei}(\xi,x(b)) \leq 0, v \in Q_{ei} \\ g^v_{ee}(\xi,x(b)) = 0, v \in Q_{ee} \end{aligned} \tag{4.33}$$

where $x(t) \in R^{n_x}$, $u(t) \in R^{n_u}$, $g : R^{n_x} \times R^{n_x} \to R$, $l : R \times R^{n_x} \times R^{n_u} \to R$, $h : R \times R^{n_x} \times R^{n_u} \to R^{n_x}$, $Q = \{1, ..., q\}$; and $L^m_\infty[a,b]$ is the space of the Lebesgue measurable, essentially bounded functions $L^m_\infty[a,b] \to R^{n_u}$. The subscripts o, ti, ei, ee on the function $g(\cdot,\cdot)$ and $l(\cdot,\cdot,\cdot)$ are objective function, trajectory constraint, endpoint inequality constraint and endpoint equality constraint, respectively. u is the control variable and ξ is the initial state.

RIOTS uses the Matlab C MEX mechanism to integrate the functionality into the Matlab environment. The detailed instructional manual and function explanation are well documented in [410]. Up to now, RIOTS has experienced four generations of evolution as listed in table 4.1.

Table 4.1: The version history of RIOTS

Year	Contributor	OS	Compiler	Matlab Ver	MEX Ver	Ref
1995	A Schwartz	SunOS 4.1.4	Sun C compiler	4	v4	[402]
2002	Y Chen	DOS & Windows	Watcom C	4, 5.0	v4	[406]
2005	J Liang	Windows & Linux	VC++ & GNU gcc	6.5	v6	[236]
2014	T Zhao	Windows 64bit	MS Visual C++	7.14∼8.2	winmex64	[385]

4.3.2 Using RIOTS for MPC in general settings

MPC can take different types of models for prediction [306], such as step response models, discrete transfer functions, ARIMA models, state-space models, etc. To make it convenient for multi-variable process control, the state-space model is used here. Thus, the general settings of the predictive control problem using RIOTS are stated as the following.

Consider the system described by the S-S model below,

$$\begin{cases} x(i+1) = Ax(i) + Bu(i) + w(i) \\ y(i) = Cx(i) + Du(i) + v(i) \end{cases} \tag{4.34}$$

where the state is $x(i) \in R^{n_x}$, the input is $u(i) \in R^{n_u}$ and the output is $y(i) \in R^{n_y}$. The state noise is $w(i)$ and the measurement noise is $v(i)$.

With equation (4.34) giving one-step estimate $\hat{x}(i+1)$, the estimated system outputs from time $t+2$ to $t+N_p$ can be derived as:

$$\begin{cases} \hat{x}(i+k+1|i) = A\hat{x}(i+k|i) + Bu(i+k|i) \\ \hat{y}(i+k|i) = C\hat{x}(i+k|i) + Du(i+k|i) \end{cases} \tag{4.35}$$

where $\hat{x}(i+k+1|i)$ stands for the estimation of states at time $i+k+1$, and $\hat{y}(i+k|i)$ is the estimation of system output at time $i+k$.

The cost function to be minimized is:

$$J = \sum_{k=1}^{N_p} [\hat{y}(i+k|i) - r(i+k)]^T W_y [\hat{y}(i+k|i) - r(i+k)] \tag{4.36}$$

where $r(i+k)$ is reference input at instant $i+k$, and W_y is a positive definite matrix with dimension $n_y \times n_y$. Generally, index J can be used for both SISO and MIMO systems. In MIMO systems, MPC can overcome coupling interactions implicitly.

An advantage of MPC over traditional control is the allowance of boundary constraints on control input and output:

$$\begin{aligned} u_{min} < u(i) < u_{max} \\ y_{min} < y(i) < y_{max}. \end{aligned} \tag{4.37}$$

At each interval, a control output sequence within control horizon N_u is calculated by minimizing the cost function in equation (4.36) with constraints in equation (4.37), but only the first control adjustment in the calculated sequence is implemented. Then the optimization is repeated after new measurement gets updated.

4.3.3 Using RIOTS for fractional order MPC

Now, continued with the initial intention, the realization of FO MPC though piece-wise FOCP can be performed. According to the principles behind MPC, RIOTS can be used to fulfill the repeated online optimization through a single call during each optimization horizon. Since RIOTS can deal with MIMO, nonlinear and time-varying problems with constraints, RIOTS based MPC also has the ability to control these systems. RIOTS-based MPC was first proposed in [408], but it was for linear or nonlinear integer order systems. A straightforward application of RIOTS-based MPC on FO systems can be achieved by reformulating the equation (4.32) to the discrete cost function in equation (4.36), and replacing the integer order system dynamic constraints in equation (4.35) with the FO process model in equation (4.25), through the Oustaloup recursive approximation method,

$$s^\alpha = C \prod_{n=1}^{N} \frac{1 + s/\omega_{z,n}}{1 + s/\omega_{p,n}}, \tag{4.38}$$

which is valid within a certain frequency range of the approximation interval.

To demonstrate this procedure in detail, an experiment will be presented in chapter 5.

4.4 Fractional order sliding-model based extremum seeking control

4.4.1 Fractional order sliding mode control

Sliding mode control (SMC) is a nonlinear control law that alters the dynamics of a system by application of a discontinuous control signal that forces the system to "slide" along a cross-section of the systems normal behavior. It is well known that SMC is a particular type of Variable structure control system. The main feature of SMC is switching the control law to force the states of the system from the initial states onto some predefined sliding surface. SMC, as an effective robust control method, has been applied to a wide variety of complex systems and engineering problems. On the other hand, fractional calculus introduced in the early 17th century deals with integration and derivatives of arbitrary orders. Increasing applications of FO calculus in almost all fields of science and engineering were witnessed recently. In fact, FO controllers are obviously important to the practical world. The SMC methodology has been designed for FO chaotic systems in many published results [411, 412]. Some applications of FO SMC has been investigated in [50, 49].

4.4.2 Fractional order extremum seeking control

The extremum seeking control (ESC) is a model-free online optimization control scheme that addresses unknown performance functions with measurable input and output [413, 414]. It is rated as the third popular controller in the industry, ranking after PID and MPC. It has been extended to fractional order and found application in many areas such as the fractional horse power dynamometer control in [415], the cognitive lighting control in [49], and the photovoltaic max power point tracking [416], etc.

While being an effective control strategy, this technique has drawbacks such as the sensitivity to parameter selection which makes it fragile. Failure to track the power extremum has been observed in some particular cases. With the motivation of reducing the human involvement in parameter tuning and improving the control performance, research is carried out to explore the enhancement of the regular ESCs. For example, in [417], Yin *et al.* developed a sliding-mode ESC law by replacing the conventionally used sign function with its fractional order derivative, based on a new variable structure control involving the hyperbolic tangential function, so as to reduce the chattering vicinity around the optimal point.

4.4.3 Combining the fractional order SM with ESC

In this section a fractional order SM-ESC is proposed to further improve both the performance and robustness of the integer order SM-ESCs. The benefits of making such extra efforts are demonstrated through a case study in section 5.7.

Denoting the adjustable capacitor as the control input u, and the load power as the system output y, the plasma impedance matching using the ESC can be formulated to a single-input-single-output (SISO) nonlinear model,

$$\begin{aligned} \dot{x} &= f(x,t) + g(x,t)u, \\ y &= h(x), \end{aligned} \tag{4.39}$$

A schematic of FO SM-ESC approach is shown in Fig. 4.5.

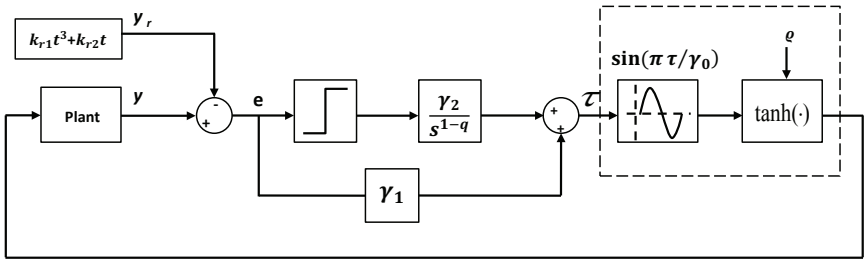

Figure 4.5: The block diagram of the proposed FO SM-ESC scheme.

Without loss of generality, the maximum seeking problem is addressed, with the inverse case, minimum seeking, omitted. The knowledge of the performance function in equations (5.27) or (4.39) is not assumed. All parameters of the uncertain system belong to a compact set Ω.

Assumption 1.

There exists a positive constant $\underline{g}$ such that $0 < \underline{g} \leq ||g(x,t)||, \forall t \in [0, t_M)$. Thus, the system (4.39) has relative degree of one due to $g(x,t) \neq 0$, for all x.

Assumption 2.

There exists a unique point x^* such that $h'(x^*) = 0$ and $h''(x^*) < 0$. For any given $\varepsilon > 0$, there exists $\rho = \rho(\varepsilon)$ such that $|h'(x)| > \varepsilon, \forall x \notin D_\rho$, where $D_\rho = \{x : ||x - x^*|| < \rho/2\}$ is called ρ-vicinity of x^*.

According to (4.39), we have $\dot{y} = h'f + k_p u$, where $k_p = h'g$. Therefore, one has $|k_p| \geq \underline{k}_p$, where $0 < \underline{k}_p \leq \underline{g}\varepsilon$ when $x \notin D_\rho$.

Assumption 3.

There exist known functions $\bar{h}$, and $\eta_1 \in K_\infty$, with η_1 locally Lipschitz, a known non-negative function $\psi_1(x,t)$ continuous in x, piecewise continuous and upper-bounded in t such that $||f(x,t)|| \leq \eta_1(||x||) + \psi_1(x,t)$ and $|h'| \leq \bar{h}(||x||)$.

As shown in figure 4.5, the FO SM-ESC is proposed as

$$u = \varrho(t)\tanh\left(\mathrm{sgn}\left(\frac{\pi}{\gamma_0}\tau\right)\right), \tag{4.40}$$

$$\tau(t) = \gamma_1 e(t) + \gamma_2 D^{q-1}\mathrm{sgn}(e(t)), \tag{4.41}$$

where $0 < q < 1$, D is a Riemann-Liouville fractional operator, ϱ is a designed modulation function (continuous in t) to be specified later on, $\gamma_i, (i = 0, 1, 2)$ are appropriate constants and the error signal $e(t)$ is defined as

$$e(t) = y(t) - y_r(t), \tag{4.42}$$

where

$$y_r(t) = k_{r1}t^3 + k_{r2}t, \quad y_r(0) = y_{r0}, \tag{4.43}$$

with $k_{r1} \geq 0, k_{r2} \geq 0$, and y_{r0} is the initial condition which will be chosen later on.

Remark 1. The purpose of utilizing $y_r(t)$ is to force y close to the neighborhood of the maximum point y^*. If y_{r0} is greater than the optimal point, y can have a faster tracking performance. y^* may be constantly changing along with time, since the plasma temperature, the electron-neutral collision frequency, the gas flow and the gap space are often changing. However, an upper bound for y^* exists and can be estimated. In order to have faster speed, y_{r0} could be selected greater than the estimated upper bound. Thus, y_r will guarantee that y increases to the maximum point.

Remark 2. According to *Remark 1*, the error signal is negative. Hence,

$$\begin{aligned} D^q \mathrm{sgn}(e) &= -\frac{1}{\Gamma(1-q)} \frac{d}{dt} \int_0^t \frac{1}{(t-s)^q} ds \\ &= -\frac{t^{-q}}{\Gamma(1-q)}, \quad t > 0. \end{aligned} \tag{4.44}$$

Now, $\varrho(t)$ should be proposed such that $y(t)$ tracks $y_r(t)$ as long as possible. $y(t)$ is forced to reach the vicinity of y^* and stays close to y^*. To this end, the function is designed such that $\dot{\tau}(t) = 0$. According to equation (4.41), one has

$$\dot{e} = -(\gamma_2/\gamma_1) D^q \mathrm{sgn}(e). \tag{4.45}$$

Hence, y tries to track y_r when y stays away from a small vicinity of y^*, as long as k_p is away from zero. In contrast, once y reaches the vicinity of y^*, the controllability is lost since k_p tends to zero. Thus, y_r will not be able to drag y. However, y reaches the neighborhood of y^* as expected. It will be shown that y remains close to y^* in the proof of Theorem 2.

Remark 3. From the comparison between FO and IO SM-ESC for Plasma impedance matching, the main difference lies in the use of $D^{q-1}\mathrm{sgn}(e)$ in the controller (4.44). Hence, $D^q \mathrm{sgn}(e)$ instead of $\mathrm{sgn}(e)$ can affect the tracking performance of y. Actually, from equation (4.44), $|D^q \mathrm{sgn}(e)| \gg 1 = |\mathrm{sgn}(e)|$) during the initial period. Thus, one can conclude that FO SM-ESC with $0 < q < 1$ achieves a faster tracking performance than IO SM-ESC does, even when $|D^q \mathrm{sgn}(e)|$ is less than 1 during the next time interval.

On the other hand, the time derivative of $\tau(t)$ is obtained as

$$\dot{\tau}(t) = \gamma_1 k_p u - \gamma_1 k_{r1} t^2 + \xi_s, \tag{4.46}$$

where $\xi_s := \gamma_1 h' f - \gamma_1 k_{r2} + \gamma_2 D^q \mathrm{sgn}(e)$. Denoting $k = \gamma_1 k_p$, one has

$$\dot{\tau} = k(u + \omega),$$

in which $\omega := \gamma_1 k_{r1} t^2/k + \mu$ with $\mu = \xi_s/k$. According to Assumption 3, one has $|\mu| \leq \hat{\mu}$ in which $\hat{\mu} \leq (\gamma_1 \bar{h} \tilde{f} + \gamma_1 \bar{h}^2 + \gamma_1 k_{r2} + \gamma_2 \varpi)/\underline{k}$ with $\tilde{f} = \eta_1(2||x||) + \psi_1(x,t), \underline{k} = \gamma_1 \underline{k}_p$.

In the following theorem, one possible ϱ implementation is proposed such that finite-time escape is avoided and realization of the τ-sliding modes is guaranteed.

Theorem 9.

Consider the system in equation (4.39) with the control law in equation (4.40). Outside the δ-vicinity, if ϱ satisfies

$$\varrho \tanh^2[\sin(\pi\tau/\gamma_0)] \coloneqq [(\gamma_1 \bar{h}\tilde{f} + \gamma_1 \bar{h}^2 + \gamma_1 k_{r2} + \gamma_2 \varpi) + ||y_t|| e^{-\alpha_1 t}]/\underline{k} + \alpha, \tag{4.47}$$

with $\alpha_1 > 0, \alpha > 0$, then, while $x \notin D_\rho$, one has: (i) no finite-time escape occurs in the system signals ($t_M \to +\infty$) and (ii) a sliding mode on switching manifold $\tau(t) = l\gamma_0$ is reached in finite time for some integer l.

Proof. Consider the following non-negative functions

$$W_1(\tau) = \int_0^\tau \tanh\left(\sin\left(\frac{\pi}{\gamma_0}\epsilon\right)\right) d\epsilon,\ W_2(\tau) = \gamma_m - W_1, \tag{4.48}$$

where γ_m denotes the maximum value of $W_1(\tau)$.

The time derivative of W_1 and W_2 are obtained

$$\begin{aligned} \dot{W}_1 &= k\left\{\phi \tanh^2\left(\sin\left(\frac{\pi}{\gamma_0}\tau\right)\right) + \mu \tanh\left(\sin\left(\frac{\pi}{\gamma_0}\tau\right)\right)\right\} \\ &\quad -\gamma_1 k_{r1} t^2 \tanh\left(\sin\left(\frac{\pi}{\gamma_0}\tau\right)\right) \\ \dot{W}_2 &= -\dot{W}_1. \end{aligned} \tag{4.49}$$

Since $|\tanh(\sin[(\pi/\gamma_0)\tau]| \leq 1$, one has

$$\begin{aligned} \dot{W}_1 &\leq k\{\phi \tanh^2[\sin[(\pi/\gamma_0)\tau]\} + |k||\mu| + \gamma_1 k_{r1} t^2, \\ \dot{W}_2 &\leq -k\{\phi \tanh^2[\sin[(\pi/\gamma_0)\tau]\} + |k||\mu| + \gamma_1 k_{r1} t^2. \end{aligned} \tag{4.50}$$

Due to $|k||\mu| \leq |k|\hat{\mu}$, one can derive

$$\begin{aligned} \dot{W}_1 &\leq -|k|\{\phi \tanh^2[\sin[(\pi/\gamma_0)\tau] - \hat{\mu}\} + \gamma_1 k_{r1} t^2, \quad \text{if } \operatorname{sgn}(k) < 0, \\ \dot{W}_2 &\leq -|k|\{\phi \tanh^2[\sin[(\pi/\gamma_0)\tau] - \hat{\mu}\} + \gamma_1 k_{r1} t^2, \quad \text{if } \operatorname{sgn}(k) > 0. \end{aligned} \tag{4.51}$$

On the other hand, one has $-|k| \leq -\underline{k}$. Thus, it can be concluded that

$$\dot{W}_1 \leq -||y_t|| e^{-\alpha_1 t} - \underline{k}\alpha + \gamma_1 k_{r1} t^2, \quad \text{if } \operatorname{sgn}(k) < 0, \tag{4.52}$$

$$\dot{W}_2 \leq -||y_t|| e^{-\alpha_1 t} - \underline{k}\alpha + \gamma_1 k_{r1} t^2, \quad \text{if } \operatorname{sgn}(k) > 0, \tag{4.53}$$

holds everywhere, with $\alpha \geq 0, \alpha_1 > 0$. Then, it avoids finite-time escape in the system signals.

Proposition 3.

First, assume that $|\tau(t)|$ escapes in some finite time $t_1 \in [0, t_M)$. From equation (4.41), it can be known that $e(t)$ and $y(t)$ can also escape at $t = t_1$. Hence, there exists $t_2 \in [0, t_1)$ such that

$$||y_t|| \geq e^{\alpha_1 t}[\alpha_2 - \underline{k}\alpha + \gamma_1 k_{r1} t_1^2],$$

in which $\alpha_2 \geq 0$. Moreover, from equations (4.52) and (4.53), one has

$$\begin{aligned} \dot{W}_1 &\leq -\alpha_2 - \gamma_1 k_{r1} t_1^2 + \gamma_1 k_{r1} t^2 \leq -\alpha_2, \ \ \forall t \in [t_2, t_1), \quad \text{or} \\ \dot{W}_2 &\leq -\alpha_2 - \gamma_1 k_{r1} t_1^2 + \gamma_1 k_{r1} t^2 \leq -\alpha_2, \ \ \forall t \in [t_2, t_1), \end{aligned} \tag{4.54}$$

independently of $\text{sgn}(k)$. Since $\tau(t)$ is absolute continuous and escapes in $t = t_1$, there exists $t_e \in [t_2, t_1)$ and an integer l_τ such that $\tau(t_e) = l_\tau \gamma_0$. Therefore, $W_1(t_e) = 0$ (if l_τ is an even number) or $W_2(t_e) = 0$ (if l_τ is an odd number). It is clear that $W_1(t) = 0, \forall t \in [t_e, t_1)$ or $W_2(t) = 0, \forall t \in [t_e, t_1)$ from equation (4.54) in this interval. To avoid the abuse of notation, $W_i(\tau(t))$ is replaced by $W_i(t)$, for $i = 1, 2$. Consequently, $\tau(t) = l_\tau \gamma_0$ is uniformly bounded $\forall t \in [t_e, t_1)$, i.e., a contradiction. Thus, τ, e and y cannot escape in finite time. In addition, one has that $x, \hat{x}$ and all closed loop signals cannot escape in finite time ($t_M \to +\infty$).

Proposition 4.

According to Property (i), there exists a finite time $\bar{t} \geq 0$ such that $\dot{W}_i \leq -\alpha_{\bar{t}}, \forall t \geq \bar{t}$ and $0 < \alpha_{\bar{t}} < \underline{k}\alpha$, for $i = 1$ or $i = 2$. Hence, $W_i(t) \leq -\alpha_{\bar{t}}(t - \bar{t}) + W_i(\bar{t}), \forall t \geq \bar{t}$. Consequently, there exists a finite time $t^* \geq \bar{t}$ such that $W_i(t) = 0, \forall t \geq t^*$. Moreover, the corresponding points $\tau = l\gamma_0$ for which $W_1(\tau) = 0 (W_2(\tau) = 0)$ occur only for even(odd) value of l. In the neighborhood of the points $\tau = l\gamma_0$,

$$\text{sgn}(\tanh(\sin(\pi\tau/\gamma_0))) = \text{sgn}(\tanh(\tau - l\gamma_0))$$

for l being an even number or

$$\text{sgn}(\tanh(\sin(\pi\tau/\gamma_0))) = \text{sgn}(-\tanh(\tau - l\gamma_0))$$

for l being an odd number. Now, one can derive the following inequality for l being either an even number ($\text{sgn}(k) < 0$) or an odd number ($\text{sgn}(k) > 0$). Selecting a Lyapunov candidate $V = 0.5(\tau - l\gamma_0)^2$ and taking its derivative with respect to time, one has

$$\dot{V} = (\tau - l\gamma_0)\dot{\overbrace{(\tau - l\gamma_0)}} \leq 0.$$

Hence, a sliding mode occurs in finite time on one of the manifolds $\tau = l\gamma_0$, independently of $\text{sgn}(k)$. The proof is completed.

Next, it is shown that the FO SM-ESC in equation (4.40) and the modulation function in equation (4.45) guarantee that x reaches D_ρ of the unknown x^*. The oscillations around y^* can be made to high-order infinitesimal, $O(\gamma_0)$.

Theorem 10 (Global extremum-seeking control)**.**

Consider the system in equation (4.39) under the control law in equations (4.40) and (4.41) and the modulation function in equation (4.46). If assumptions (1-3) hold, then: (i) D_ρ is globally attractive and is obtained in finite time and (ii) for sufficiently small γ_0, the oscillations around y^* can be made of order $O(\gamma_0)$.

Proof. The proof of the properties (i) and (ii) of Theorem 2 are given as follows:

(i)Attractiveness of D_ρ: It is assumed $x \notin D_\rho, \forall t \in [0, t_M)$. Since $\tau = l\gamma_0$ can occur in finite time, there exists a finite time t_f such that $\dot{\tau} = 0$. Therefore, one has that $\dot{e} = -(\gamma_2/\gamma_1)D^q\text{sgn}(e), \forall t \geq t_f$. According to the analysis of Remarks 1 and 2, the error $e = y - y_r$ tends to zero. Moreover, one has $y_r > y^* \geq y$ and $e < 0$. Then, one assures that y increases with

$$\dot{y} = k_{r1}t^2 + k_{r2} - (\gamma_2/\gamma_1)D^q\text{sgn}(e) > 0.$$

Hence, x goes to ρ-vicinity of y^*, which is a contradiction. Thus, D_ρ is attained in some finite time. Consequently, x remains or oscillates around D_ρ and similarly y stays in some small vicinity of $y^*, \forall t$ large enough. During these oscillations, τ can go from one sliding manifold to another manifold $\tau = l\gamma_0$ for l being an odd number. Next, it will be shown that these oscillations can be made ultimately of order $O(\gamma_0)$, with γ_0 from (4.40).

(ii) Oscillations of order around $O(\gamma_0)$: According to Assumption 5, ρ can be made arbitrarily small such that $|y - y^*| = O(\gamma_0)$ when $x \in D_\rho$. Thus, if x remains in D_ρ for all t, the corresponding neighborhood of y^* can be made of order $O(\gamma_0)$. Otherwise, if x oscillates around D_ρ, $|y - y^*| = O(\gamma_0)$ also holds when x leaves the set D_ρ.

In fact, one has $e(t) < 0, \forall t > 0$. One has $D^q\text{sgn}(e) < 0, \forall t > 0$. Assume that x reaches D_ρ from inside at some time $\tilde{t}_1 > 0$ and $\tau(t)$ is not in sliding mode when $t = \tilde{t}_1$. Note that D_ρ is invariant when $\tau(t)$ is in sliding mode. Define $\tilde{\tau}(t) := \tau(t) - \tau(\tilde{t}_1), \tilde{y}(t) := y(t) - y(\tilde{t}_1)$, one has

$$\begin{aligned}\tilde{\tau}(t) = \gamma_1\tilde{y}(t) - \gamma_1 k_{r1}(t^3 - \tilde{t}_1^3) - \gamma_1 k_{r2}(t - \tilde{t}_1) \\ +\gamma_2({}_{\tilde{t}_1}D_t^{q-1}\text{sgn}(e)), \quad t \geq \tilde{t}_1,\end{aligned} \tag{4.55}$$

where $k_{s1} = 0, k_{s2} = 0$ if y_r is saturated, and $k_{s1} = k_{r1}, k_{s2} = k_{r2}$ otherwise. From the above equation, one can conclude that

$$\begin{aligned}|\tilde{y}(t)| \leq \gamma_1|\tilde{\tau}(t)| + \gamma_1 k_{s1}(t^3 - \tilde{t}_1^3) + \gamma_1 k_{s2}(t - \tilde{t}_1) \\ +\frac{\gamma_2}{\Gamma(2-q)}(t - \tilde{t}_1)^{1-q}.\end{aligned} \tag{4.56}$$

Let $\tilde{t}_2$ be the first time when $\tau(t)$ reaches the next sliding manifold $\tau(t) = \tau(\tilde{t}_2)$ (independent to x being inside or outside D_ρ) and $\tilde{t}_3$ is the first time when x reaches the frontier of D_ρ again (from outside). It is obvious that $\tilde{t}_2 \geq \tilde{t}_1 > \tilde{t}, \tilde{t}_3 \geq \tilde{t}_1 > \tilde{t}$. Then, there are two cases: (i) $\tilde{t}_3 > \tilde{t}_2$ and (ii) $\tilde{t}_3 \leq \tilde{t}_2$.

For case (i), let $t \in [\tilde{t}_1, \tilde{t}_2]$ and first consider $t \in [\tilde{t}_1, \tilde{t}_2)$. $\tau(t)$ is not in sliding motion during this time interval $[\tilde{t}_1, \tilde{t}_2)$. Hence, there exists some integer l such that $l\gamma_0 < \tau(t) < (l+1)\gamma_0$. Moreover, $1 \geq |\tanh(\text{sgn}(\pi\tau(t)/\gamma_0))| > 0, \forall t \in [\tilde{t}_1, \tilde{t}_2)$. Since $l\gamma_0 < \tau(t) < (l+1)\gamma_0$ and $\tanh(\text{sgn}(\pi\tau(t)/\gamma_0)) \neq 0$ for all $t \in [\tilde{t}_1, \tilde{t}_2)$, they guarantee an appropriate positive constant α so that $|\dot{\tau}(t)| \geq \underline{k}|u + \omega| \geq \underline{k}(\alpha) \geq \tilde{\alpha}$ in which $\tilde{\alpha} = \underline{k}\alpha$ is a positive constant. Thus, $(t - \tilde{t}_1) \leq |\tilde{\tau}|/\tilde{\alpha}, \forall t \in [\tilde{t}_1, \tilde{t}_2)$ and it can be concluded that $(t - \tilde{t}_1)$ is of order $O(\gamma_0), \forall t \in [\tilde{t}_1, \tilde{t}_2)$. Since $t^3 - \tilde{t}_1^3 = (t - t_1)(t^2 + t_1^2 + tt_1)$ and $t \in [\tilde{t}_1, \tilde{t}_2)$, one has $(t^2 + t_1^2 + tt_1) < \zeta$ in which $\zeta = t_2^2 + t_1^2 + t_2t_1$. Therefore, one can conclude that $t^3 - \tilde{t}_1^3 \leq |\tilde{\tau}|\zeta/\tilde{\alpha}, \forall t \in [\tilde{t}_1, \tilde{t}_2)$. Thus, $(t^3 - \tilde{t}_1^3)$ is of order $O(\gamma_0), \forall t \in [\tilde{t}_1, \tilde{t}_2)$. According to equation (4.56), one can also assure

that $y(t) - y(\tilde{t}_1)$ is of order $O(\gamma_0), \forall t \in [\tilde{t}_1, \tilde{t}_2)$. Moreover, by continuity, $y(t) - y(\tilde{t}_1)$ is also of order $O(\gamma_0), \forall t \in [\tilde{t}_1, \tilde{t}_2]$.

For case (ii), let $t \in [\tilde{t}_1, \tilde{t}_3]$. Then, following the first part of the proof of case (i), it can be directly obtained that $y(t) - y(\tilde{t}_1)$ is of order $O(\gamma_0), \forall t \in [\tilde{t}_1, \tilde{t}_2]$. Then, consider $t \in [\tilde{t}_2, \tilde{t}_3]$. $\tau(t)$ is in sliding motion during this interval. Therefore, one has $\dot{\tau}(t) = 0$. From equation (4.44), one has that $\dot{y} = k_{r1}t^2 + k_{r2} - (\gamma_2/\gamma_1)D^q \text{sgn}(e) > 0$ which is strictly increasing, $\forall t \in [\tilde{t}_2, \tilde{t}_3]$. Hence, one can obtain that $y(t) - y(\tilde{t}_1)$ is also of order $O(\gamma_0), \forall t \in [\tilde{t}_2, \tilde{t}_3]$. Since this is also valid for the interval, the proof is complete that the oscillation outside D_ρ is of order $O(\gamma_0)$ in case (i), $\forall t \in [\tilde{t}_1, \tilde{t}_3]$.

4.5 Other control schemes for fractional order MIMO processes

Besides the newly developed control schemes for FO MIMO processes in preceding sections, other methods exist as alternatives for various scenarios. Some of them are reviewed briefly in this section.

4.5.1 Fractional order PI$^\lambda$D$^\mu$ controllers

To be a comprehensive study on process controls, the discussion on PID controllers can not be omitted. In fractional order controls, the FO PID controller enjoys the same level of popularity as in integer order controls. Due to the introduction of two extra tuning parameters, more diversified combinations are generated, namely PI$^\lambda$, [PI]$^\lambda$, PD$^\lambda$, [PD]$^\lambda$, and PI$^\lambda$D$^\mu$ controllers. The transfer function of the the FO PI$^\lambda$D$^\mu$ controller can be generally expressed as the following:

$$C(s) = K_p + K_d s^\mu + K_p \frac{1}{s^\lambda}. \tag{4.57}$$

The parameter tuning of these controllers have been well discussed in the literature, to name a few, tuning the FO PID using the Ziegler-Nichols (Z-N) type rules [418], an easy tuning method of FO PI controllers for position servo systems using loop-shaping [419], etc. Besides the conventionally used tuning criteria for classic integer order PIDs, novel tuning rules are developed. For example, the "flat phase" tuning rules [420] get widely adopted, which is based on the iso-damping property originated from Bode's ideal cutoff characteristic.

$$G_{Bode}(s) = \frac{k}{[(s^2+1)^{0.5} + s]^q}. \tag{4.58}$$

One of the reasons for this set of tuning rules not being used for integer order PIDs as common as for FO PIDs is that the three equations usually result in no solution for integer PIDs due to the lack of two tuning nobs. The study on the "flat phase" tuning rules is quite mature, for example, the feasible regions for certain classes of LTI FO transfer functions are investigated in [58]. Hence it is not addressed here. For more information, refer to [27, 421, 422, 423] and [316].

4.5.2 Fractional order robust control

In the industry, it is impossible to expect a perfect model due to the complexity of real world problems. Therefore, robust control has much practical value because of the consideration of uncertainties and the tolerance of model inaccuracy. For fractional order systems, robust control also receives considerable research attention. For example, a dedicated monograph on advances in robust fractional control can be found in [424], in which the H_∞ control of FO systems, dynamic inversion, and the robust tuning of fractional order PID controllers are presented. In fact, the "flat phase" tuning rule mentioned in section 4.5.1 also contains the robust thinking, because the phase margin of the compensated process has very slight variance against process parameter variation.

In [425], Tavazoei *et al.* designed the robust control with invariant phase margin for FO systems,

$$C(s) = (hs^\alpha + L)\hat{G}^{-1}(s), \tag{4.59}$$

for the following FO system under unit feedback configuration,

$$G(s) = \frac{1}{Ts^\beta + 1}\hat{G}(s), \tag{4.60}$$

where $\beta \in (0, 2)$ and $T > 0$. They summarize the relation between phase margins and gain crossover frequencies in the designed control system for different values of parameter.

As mentioned in the literature review, section 1.4, and the tool evaluation, section 2.4, the CRONE toolbox is dedicated for non-integer order robust control. Some solid results on the FO robust control are obtained based on it, e.g. the centralized CRONE controller for non-square multi-variable systems [230]. In [426], the robust fractional-order temperature control of a steel slab reheating furnace with large time delay uncertainty is discussed, where the model of the process is integer order while the design specifications of the FO controller take the robustness into consideration.

4.5.3 Fractional order iterative learning control

The iterative learning control (ILC) is a batch procedure that operates on a given objective system repeatedly on a fixed time interval so that the reference signal can be better and better tracked as the operation repeats [427]. It was first published in 1978 by Uchiyama *et al.* For fractional order processes, the ILC needs to deal with the fractional order dynamic equations,

$$\begin{cases} x^{(\alpha)}(t) &= f(t, x, u), \\ y(t) &= g(t, x, u) \end{cases} \tag{4.61}$$

Briefly, the objective of FO ILC is to search the desired control input $u_d(t)$ using the recursive algorithm,

$$u_{k+1}(t) = \mathcal{R}(u_k(t), e_i(t)) \quad (k = 0, 1, 2, ...), \tag{4.62}$$

where $e_i(t) = y_d(t) - y_i(t)$ is the difference between the current system output and the desired system output. For fractional order processes that have online metrology difficulty, the FO ILC is a good choice.

Chapter 5

Software and Hardware in-the-Loop Simulation and Implementation

> Practice is the sole criterion for testing truth.
>
> — Mao Zedong, the founding father of P. R. China

Make it work, and work better (under constraints). That is all about engineering.

As mentioned in previous chapters, fractional order modeling and control have found application in many areas, such as the motion control of a horse power dynamometer in [58] and the cruise control of unmanned arial vehicles in [428, 429] and [46]. Beyond the applications reported in the literature, this chapter provides intensive simulation and experimental results of the applications in process controls, with regard to the corresponding topics discussed in the previous chapters. To supplement the forgoing theoretical study, this chapter is data heavy.

5.1 Description of the experimental platform

Part of the research work in this dissertation is sponsored by Lam Research Corporation, and some experiments are performed on the associated industrial equipment. However, since the equipment is not always accessible, and due to confidential agreements, a hardware-in-the-loop experimental platform is developed as an alternative.

5.1.1 Hardware configuration

As shown in figure 5.1, the platform consists of two Peltier modules mounted on a metal plate. The working principle of the heat pumping of the internal transistors inside a Peltier element is shown in the schematic diagram in figure 5.2. A similar setup can be referred to in [430]. A fan is attached to the other side of each Peltier element, respectively, and the fans are maintained at a constant blowing speed during operation. Two H-bridge circuits are used as the power management units to actuate the Peltiers. Four non-contact infra-red thermalmeters, MLX90614, are installed and aligned in parallel on a board facing to the metal plate for real-time temperature gradient measurement, as shown in figure 5.3. Thus,

the overall hardware setup is in a two-input-four-output configuration which can be further extended to multi-input-multi-output if the fans are included into the control. An Arduino Uno board, built upon the Atmega328p-pu microchip, is used as the bottom layer control unit, and the upper layer control algorithms are programmed in Matlab/Simulink. The Matlab Support Package For Arduino (MSPA) (also known as Arduino IO Package [431]), is used as the communication interface between the PC and the Arduino.

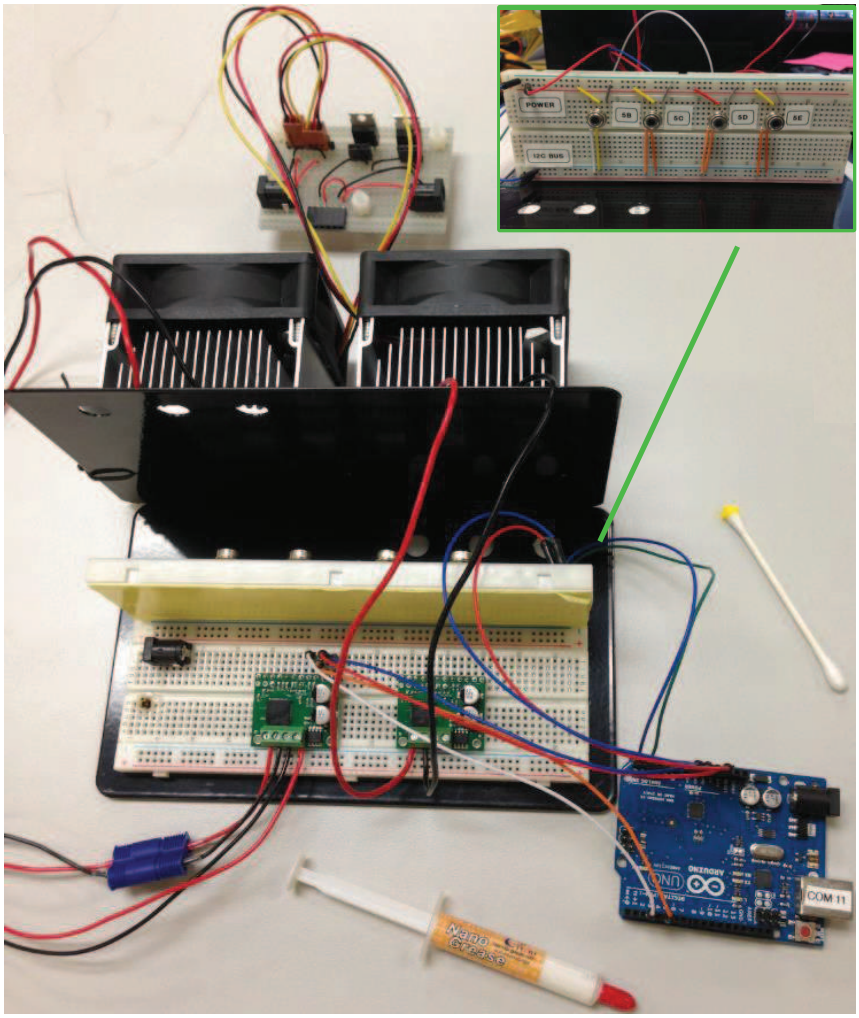

Figure 5.1: The hardware configuration of the Peltier cold plate platform.

A simultaneous goal of building this platform is for low-cost laboratory education of controls. This platform is built upon the foundation of the MESABox [432] and costs less than $150. Additional description of the detailed "virtual machine type" firmware configuration can be found in [210] and [432]. Through numerous experiments, the behavior of the platform is abstracted, and measurable evidence for using fractional order models is summarized.

As a parallel review of this type of platforms, similar platforms for fractional order modeling and control emulation can be found in the literature. Malti *et al.* developed an aluminum heat transfer platform, [67], to investigate the parameter and order estimation

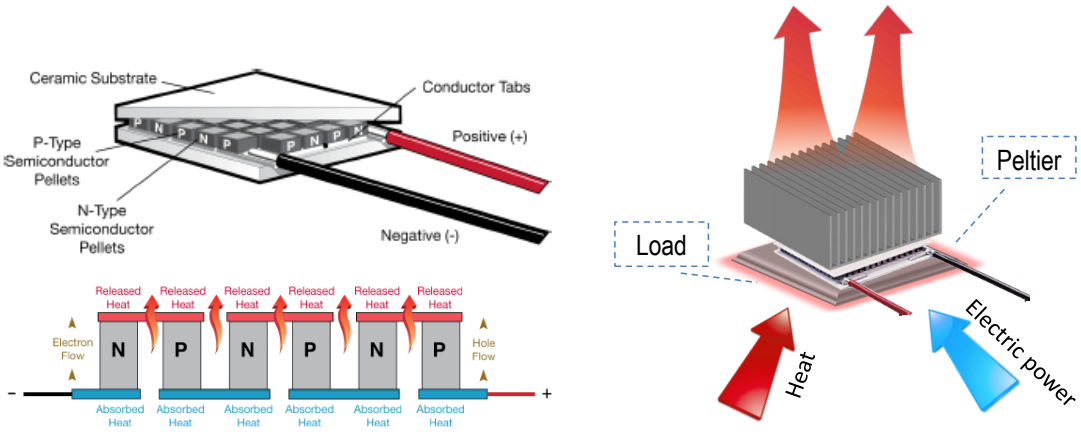

(a) The schematic, figure from [433].

(b) The working principle.

Figure 5.2: The schematic and principle of Peltier heat pumping.

of FO models. Petras *et al.* developed a metal beam with Peltier elements [34], and a heating-cooling experimental platform [281], to study the heat transfer in heterogeneous media. Macias *et al.* studied the FO PID control on the same platform in [434]. Malek *et al.* used the Quanser based heat flow experimental (HFE) platform to explore the modeling and control of FO heat processes [316]. While each experimental platform has its unique characteristics, the platform in this dissertation has some properties that are different from any of the enumerated platform, such as the previously mentioned FO inverse response. Hence, the discussion on this direction involves novel interests.

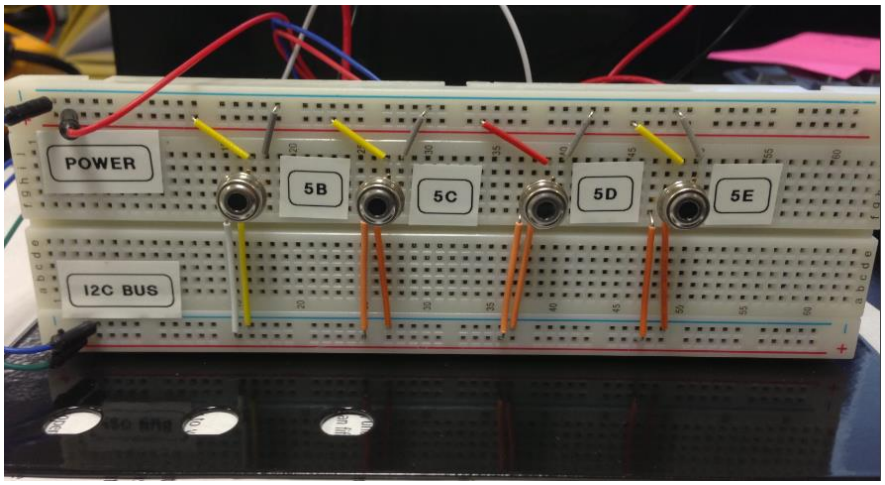

Figure 5.3: The thermal sensor array of the MIMO experimental platform.

5.1.2 Software support

The implementation of the Peltier element is not trivial because of the difference between physical theory of the thermal-electrical characteristics and the engineering perspective of the Peltier element. There are even contradictory operational instructions in the literature,

e.g. [435, 433].

During the creation of this platform, technical contributions on implementation issues were made to the society of Matlab/Simulink on Arduino. An I^2C augmenting block for MSPA is developed. The driving force of this effort is the fact that the Arduino Uno board has limited analog and digital inputs/outputs (I/Os) that is insufficient for MIMO setups requiring more than ten I/Os. Moreover, the sequential reading of the I/Os is very inefficient. For these reasons, a Simulink block is developed for the I^2C bus communication between the Arduino and the thermometers, under the same paradigm as that of the MSPA. In fact, the Arduino community provides the I^2C bus communication library, but it is not compatible with Simulink; on the other hand, the MSPA is Matlab/Simulink friendly but does not feature the I^2C capability. Hence, this side work provides users with the I^2C function block within the Simulink environment so that the sophisticated control algorithms involving more I/Os in Matlab/Simulink can be utilized and implemented on the Arduino hardware. The developed supplemental block is available for download in [436].

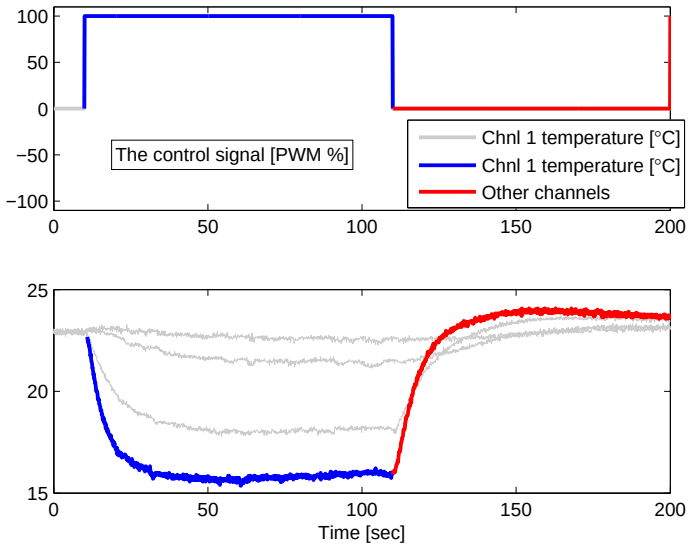

Figure 5.4: Open loop power-on cooling and power-off heating.

5.1.3 Characterization of the basic dynamic behavior

Any good control starts from a well understanding of the controlled object. To grasp the basic characteristic of the platform, four actuation modes are categorized, namely,

1. power on cooling;
2. power off cooling (natural dissipation);
3. power on heating (reverse powered);
4. power off heating (thermal cyclic).

The data acquired from the four thermalmeters for the four modes are plotted in figure 5.4 and 5.5, respectively, with the first channel marked in color. It can be observed that mode

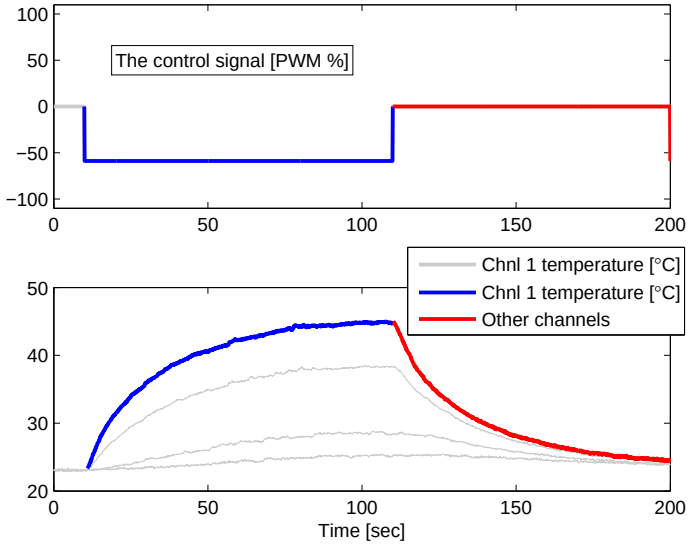

Figure 5.5: Open loop power-on heating and power-off cooling.

1 and 4 have similar dynamics which can be approximated by an FO transfer function model with two poles, while the pair of 2 and 3 have similar dynamics that can be approximated by an FO model with one pole.

The temperature reading of the thermal sensors are roughly calibrated at the normal operational range, $-10 \sim 40°\text{C}$. A photo of the calibration is shown in figure 5.6;

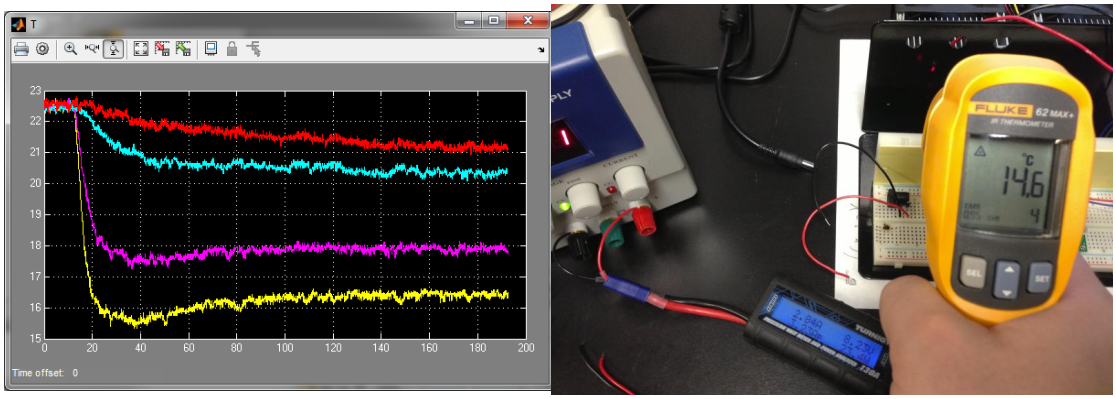

Figure 5.6: A photo of calibrating the thermal sensors.

Example: computing the heat pumping capability of a Peltier element

Assume the ambient temperature is $T_a = 20°\text{C}$. To bring the load temperature to $T_l = 3°\text{C}$, the Peltier cold side is required to stay at $T_c = 0°\text{C}$. In order to maintain this temperature difference, 25W of power needs to be pumped from the load. Given a Peltier element with the ratings of: DC 12V, 3.6A, its hot side needs to dissipate heat at the power of $P = 25 + 12 \times 3.6 = 68.2\text{W}$. If a heat sink with thermal resistance $R \approx 0.15°\text{C/W}$ is mounted to the hot side

of the Peltier, then the hot side will stay at temperature $T_h = 68.2 \times 0.15 + T_a \approx 30°\text{C}$. Hence, the temperature difference generated by this Peltier in this circumstance is $\Delta T_h - T_c = 33°\text{C}$.

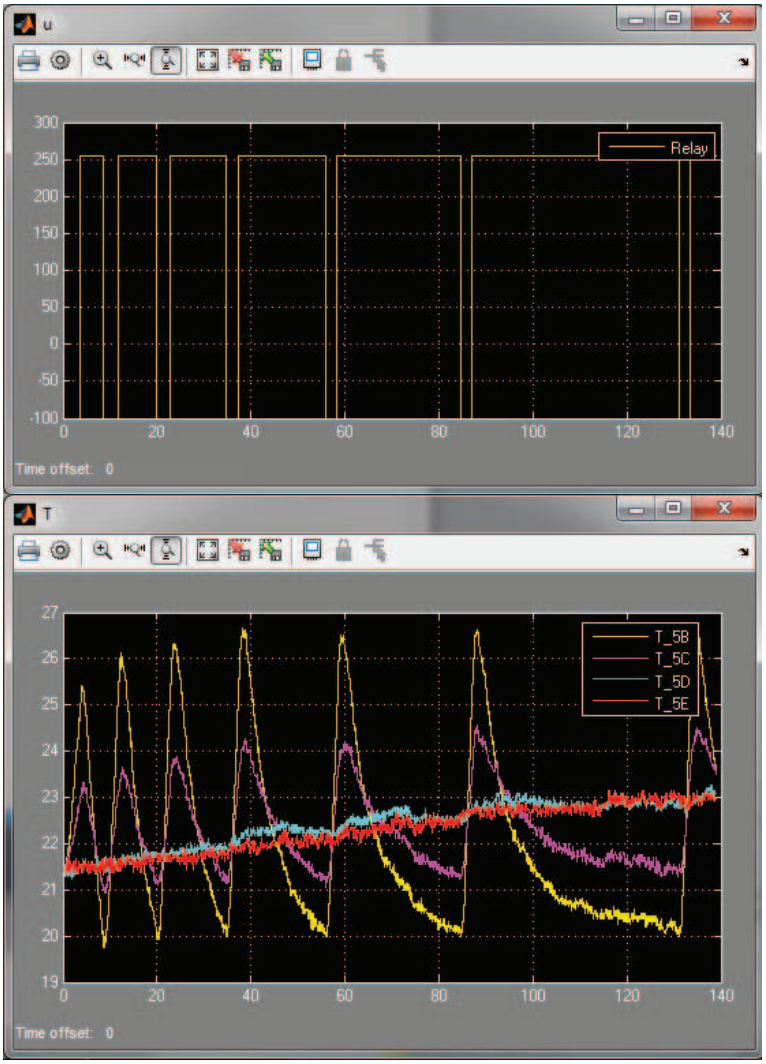

Figure 5.7: The nonlinear behavior of the experimental platform under relay feedback test. Top: relay signal; Bottom: the temperature.

5.1.4 The fractional order nonlinear behavior

The experiment purpose is to cool down the cold side of the metal plate to ambient temperature from a higher temperature; notice the data trace after 150 seconds. If no control is added, the plate naturally cools down following an inverse power law as shown by the blue curve in the lower sub-figure in figure 5.8. When it is under PI control, the plate temperature can decrease faster to the ambient temperature, as shown by the green curve in the lower sub-figure in figure 5.8. However, contradictory to one's intuition, the control signal is not able to drop back to 0 after the temperature equals the ambient temperature, which is shown by the green curve in the middle sub-figure in figure 5.8. The additionally cumulated heat

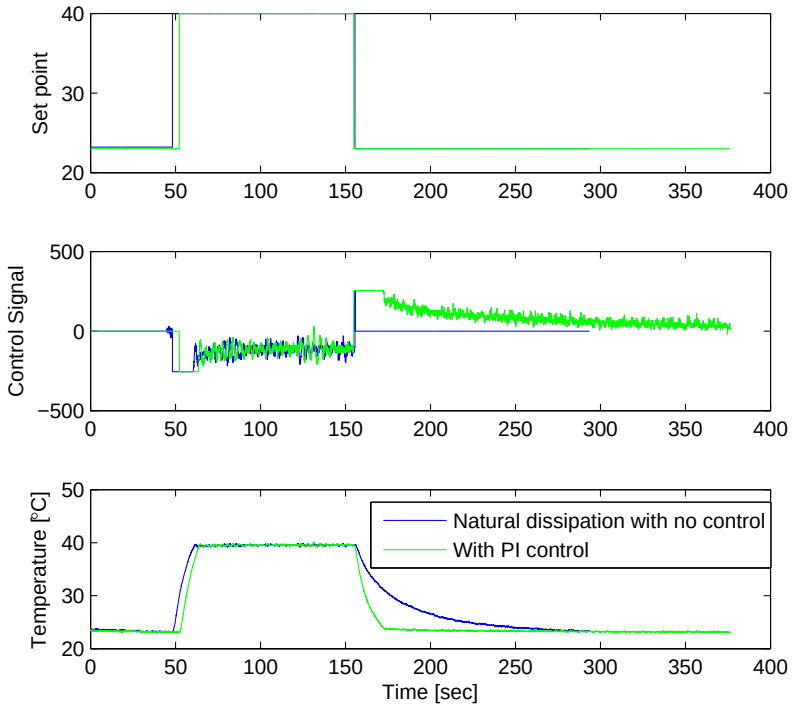

Figure 5.8: The closed loop response under a PI control

caused by the pumping effort will maintain the control signal at a non-zero value, which makes the plant very energy inefficient. Assume the control signal could drop to zero, but recall mode IV (power off heating mode) in section 5.1, then, the temperature would bounce back as soon as the cooling effort is removed, which prevents the removal of the control signal.

Explicitly, the dissipated power on the hot side needs to satisfy the following equation to balance the plate temperature at a constant value,

$$Q_d = Q_p + Q_e + Q_0. \tag{5.1}$$

That means the heat to be dissipated on the hot side of the Peltier equals the sum of the initial heat Q_0, the pumped heat Q_p and the heat transferred from external electricity Q_e. The transient follows the Fourier's law,

$$q = \frac{dQ}{dt} = -k\nabla T. \tag{5.2}$$

When no control is added, $Q_p = 0$ and $Q_e = 0$, then the time needed for the plate temperature to drop to ambient temperature can be solved from the above equation (5.2). Although this takes relatively longer time, there is no energy consumption throughout this process. When control is added, the cold side temperature drops faster because $Q_p \neq 0$. However, if the control is retrieved at this time, the temperature will rise again due to the thermal cyclic

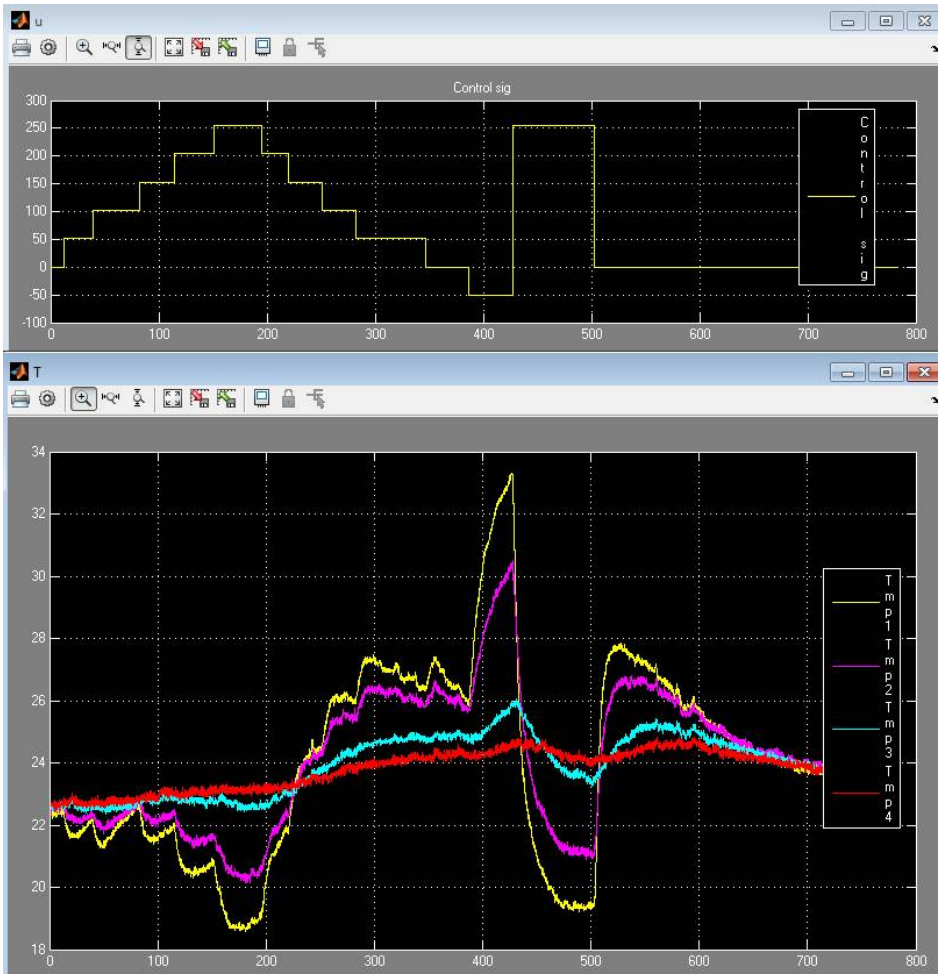

Figure 5.9: The severe nonlinear behavior of the peltier experimental platform under particular operational condition.

shown in figure 2.14, which results in a non-zero Q_e and thus, the system enters a dead loop. The relay feedback data in figure 5.12 is another proof for the existence of such nonlinear behavior. The yellow trace for channel 1 in the figure shows that the Peltier is becoming more and more powerless to cool down the plate when the cumulated heat is not dissipated in time, which eventually results in an "always on" control signal.

The severe nonlinear behavior under insufficient cooling capacity is shown in figure 5.9. A nonlinear FO model with a limit cycle can be used to characterize this behavior. Smarter control algorithms need to be employed to accomplish the control task. For example, a nonlinear quadratic optimal control problem can be solved to generate a controller which takes into consideration of both error and fuel in finite time,

$$J = \frac{1}{2}e^T S e + \frac{1}{2}\int_{t_0}^{t_f}(e^T Q e + u^T R u)dt, \tag{5.3}$$

where e denotes the control error, u denotes the control efforts, and S, Q, R denote the weighting matrices. By adjusting the weight of the error and energy requirements, different

performance can be achieved. The explicitly experimental results will be presented in future research documentations.

5.2 Simulation results for the relay feedback with an FO integrator

Consider the first element in the transfer function matrix of the Wood-Berry process [437],

$$G(s) = \frac{12.8}{16.7s + 1} e^{-s}. \tag{5.4}$$

Six types of relay feedbacks are simulated to obtain the frequency response information of the process individually. A sample plot of a test run is shown in figure 5.10. The identified model parameters are listed in table 5.1, where A and T_o are the amplitude and period of the oscillation, respectively, and the $\text{err}(\%) = 1 - \tilde{T}/T$ is the identification error for T. (Note: Since A usually can be determined accurately and L is computed based on T, error is only listed for T.) It can be seen that with the specified relay parameters, the TC relay gives the least identification error while the relay with an integrator gives the most error.

Table 5.1: The frequency response information of the relay feedback test.

	φ_p	A	T_o	$\tilde{T}$	err(%)	L
Ideal	$-180°$	0.743	3.900	13.604	18.54	1.00
Hyst	$-104.4°$	1.121	6.360	13.561	18.80	1.23
Delay	$-122.7°$	1.444	7.580	13.561	18.79	0.79
Int	$-90°$	4.909	26.51	13.358	20.01	1.29
TC	$-116.5°$	3.995	11.40	16.451	1.49	1.04
FO int	$-108°$	2.929	15.55	13.548	18.88	1.22

By adjusting the fractional order α from 0.1 to 1.9 with a set size of 0.2, a comprehensive sweep of the process frequency response in the third and fourth quadrant can be performed. The detailed values are listed in table 5.2. An undesired outcome is that due to computational numerical errors, the parameter estimation when $\alpha > 1.3$ fails to work, because the FO integrator is realized by Oustaloup discretization in the bandwidth of 0.01 and 100. In this case, a better numerical tool for FO integration is to be used.

5.3 Simulation and experiment of relay feedback identification of fractional order models

This section describes the step-by-step usage of the proposed method in section 3.3.3.

5.3.1 Simulation

Consider the model below which is modified from the first element in the transfer function matrix of the Wood-Berry distillation process [437],

$$G(s) = \frac{12.8}{16.7s^{0.5} + 1} e^{-s}.$$

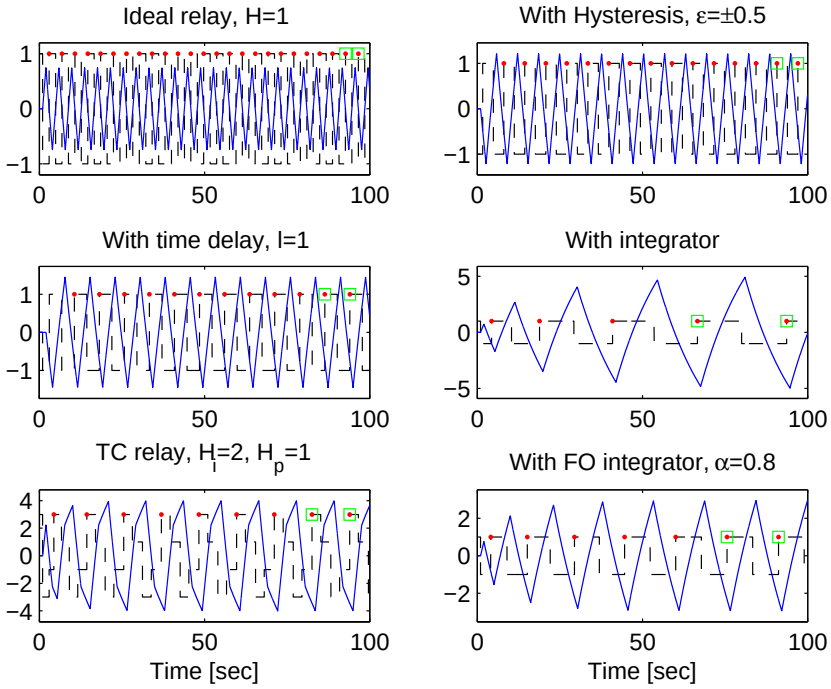

Figure 5.10: A sample plot of the test run with 6 types of relay variants.

Table 5.2: The frequency response information with α changing.

α	φ_p	A	T_o	$\tilde{T}$	err(%)	L
0.1	$-171°$	0.857	4.440	13.42	19.66	1.04
0.3	$-153°$	1.120	5.860	13.54	18.92	1.09
0.5	$-135°$	1.541	8.080	13.54	18.91	1.13
0.7	$-117°$	2.245	11.84	13.55	18.87	1.15
0.9	$-99°$	3.735	20.08	13.57	18.73	1.24
1.1	$-81°$	6.726	39.00	14.70	17.96	1.67
1.3	$-63°$	10.22	73.04	14.44	13.48	2.39
1.5	$-45°$	12.16	122.2	17.36	3.98	1.09
1.7	$-27°$	12.77	228.9	28.87	-72.85	-7.24
1.9	$-18°$	12.80	530.4	66.53	-298.4	-43.08

The unit step response of this model is plotted in figure 5.11. It can be seen that by changing the order from 1 to 0.5, the rising time of the step response is increased significantly from about 50 seconds to 500 seconds. This makes the identification procedure extremely time consuming if the reaction curve method or data fitting method is used. In contrast, the relay feedback test can settle down to sustaining oscillation after a few cycles within 50 seconds, with any type of relay variant, as shown in figure 5.12. This reveals one of the advantages of

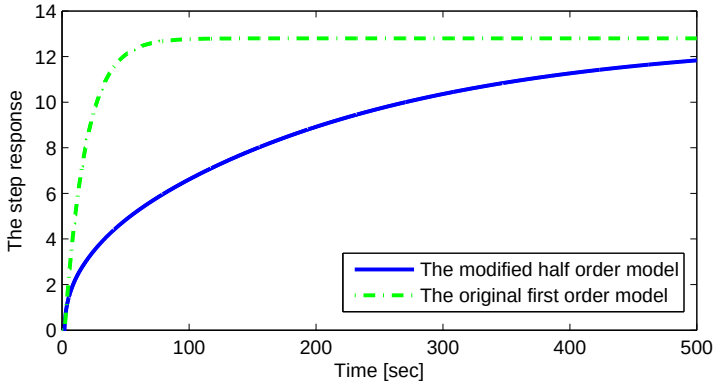

Figure 5.11: The step responses of the original and modified first element in the Wood-Berry model.

the proposed method.

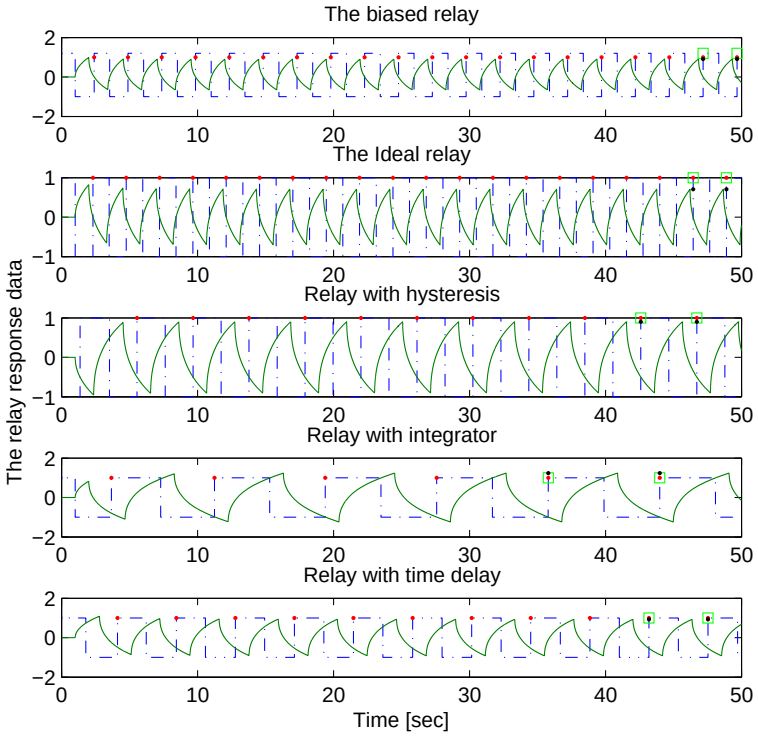

Figure 5.12: The data acquired from different types of relay test.

The oscillation information including the system gain, phase, the oscillating period and amplitude are listed in table 5.3, where $|G(j\omega_u)|$ and ω_u are computed from A and P_u through equation (3.70).

Following the procedure in section 3.3.3.4, the steady state gain is computed from the biased relay test data, $K = 12.3$. The time constant and the fractional order are calculated

Table 5.3: The oscillation information for the relay test in figure 5.12.

	Ideal	Hyst $\varepsilon = 0.1$	Int	Delay $d = \frac{\pi}{4}$
$\angle G$	$-\pi$	$\arcsin(\frac{\varepsilon}{A}) - \pi$	$-\frac{\pi}{2}$	$d - \pi$
H	1	1	1	1
A	0.6849	0.8802	1.2669	0.9277
$\lvert G(j\omega_u)\rvert$	0.5536	0.7070	1.1246	0.9332
P_u	2.4520	4.1150	8.2500	4.6010
ω_u	2.5625	1.5269	0.7616	1.4277

by plugging the information of the ideal relay and the relay with hysteresis into equations (3.71) and (3.72), which gives:

$$T = 14.1, \text{ and } \alpha = 0.5.$$

Since the analytical solution to equations (3.71) and (3.72) is difficult to determine, the numerical computation is performed with a step size of 0.1 for α, as shown in figure 5.13. Finally, the dead time $L = 0.9323$ is obtained from equation (3.68). So, the identification is

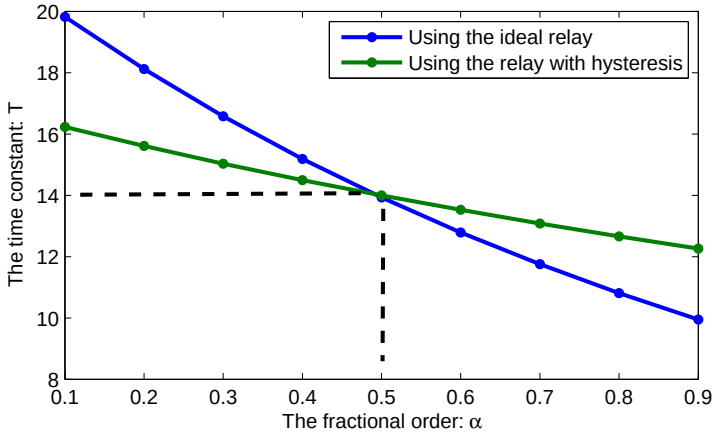

Figure 5.13: Numerically solving equations (3.71) and (3.72) using simulation data.

completed.

Alternatively, using the combination of the test information from relay with an integrator and a time delay, i.e. the latter two columns in table 5.3, yields similar results,

$$T = 13.89, \text{ and } \alpha = 0.5.$$

The identification error compared to the true values of the model parameters are listed in table 5.4. The error for T is as high as 16.2%. However, this is expected because the describing function analysis is based on the assumption of a sinusoidal input to the relay [335]. Since the system output shown in figure 5.12 is more triangle shape than a pure sinusoidal, using the first harmonic to approximate it will reasonably introduce big error. Similar amount of identification error ranging from $5\% \sim 27\%$ has been reported for integer

Table 5.4: The identification error.

	K	T	L	α
True value	12.8	16.7	1	0.5
Identification 1	12.3	14.1	0.93	0.5
Error (%)	3.9	15.57	7	0
Identification 2	12.3	13.89	0.93	0.5
Error (%)	3.9	16.83	7	0

order systems in the literature, see [327, 438, 344, 345]. Smaller identification error can be achieved by implementing more complex relay setups, but it is not addressed here because the main purpose is to show the capability. For systems with higher fractional order dynamics, the output can be more close to sinusoidal. In such case, the identification error will be smaller and a good FOPDT model approximation can be obtained. This is demonstrated via an experiment in the next section.

5.3.2 Experiments

To investigate the practical feasibility of the proposed method, experiments are performed on the Peltier based temperature control platform as shown in figure 5.1.

The first input-output channel is selected to do the experiments. The control signal is the voltage applied to the Peltier unit through a MOSFET H-bridge. The value is the bi-directional PWM signal having a resolution of 2^8 for $9V$, representing $0 \sim 100\%$ duty cycle. Two tests are performed respectively.

5.3.2.1 The step tests

A step test of heating is done under the ambient temperature of $21°C$. This is to identify a model for the purpose of comparing with the later on identified model from relay tests. In the step test, the actuator is set to run at a duty cycle of 25% in order to avoid the nonlinear behavior of the Peltier unit. The data is plotted in figure 5.14, and an FOPDT model is obtained by curve fitting as shown in figure 5.15,

$$G(s) = \frac{0.1584}{15.79s^{0.8} + 1} e^{-0.86s},$$

where the fractional order α is determined by order scanning with a step size of 0.05. The fitting is based on the time domain analytical solution given by the Mittag-Leffler function in equation (2.10). The tool for numerical computation is available in [259]. The integral of time multiply by absolute error (ITAE) versus the fractional order is plotted in figure 5.16, from which the optimal order of 0.8 can be read off. Since the temperature change is a heat transfer process, it is reasonably enough to exhibit fractional order behavior, [439].

5.3.2.2 The relay feedback test

Firstly, a biased relay feedback test is performed. The block diagram is shown in figure 5.17. Considering the nonlinear behavior of the Peltier, the bias H_0 is selected to be 40% and the amplitude H is selected to be 60%, so as to achieve a roughly symmetric performance in

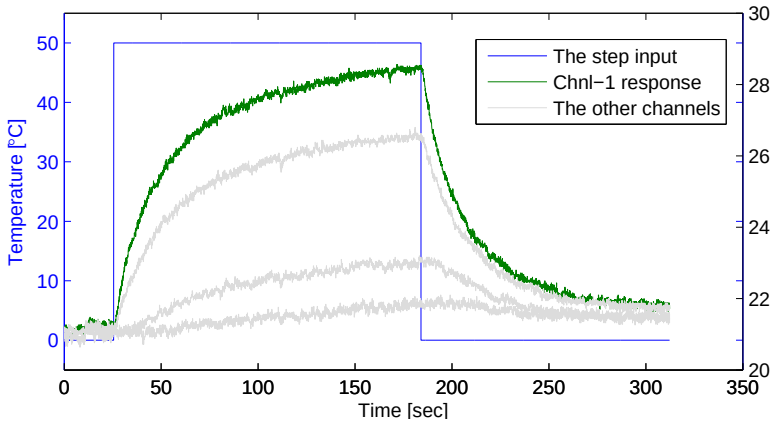

Figure 5.14: The step responses of the temperature control test platform.

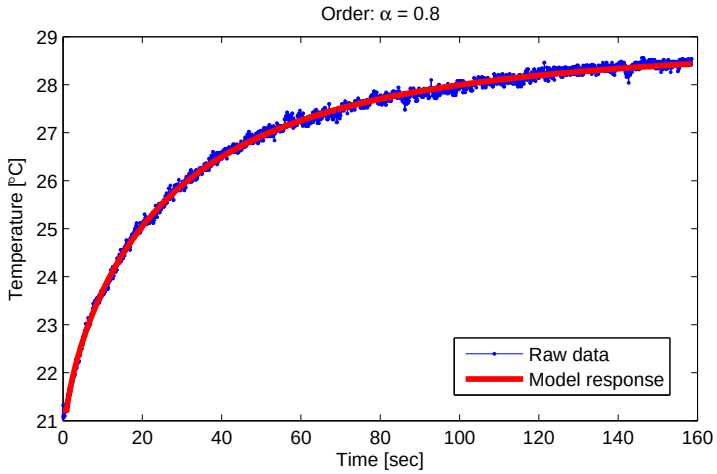

Figure 5.15: Fitting the step response data using Mittag-Leffler function.

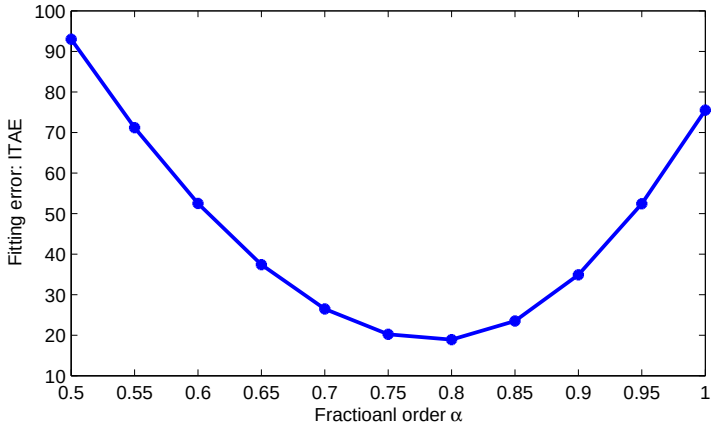

Figure 5.16: Scanning the best fitting fractional order.

heating and cooling. The hysteresis is set to be $\varepsilon = \pm 3^{\circ}$C around the ambient temperature.

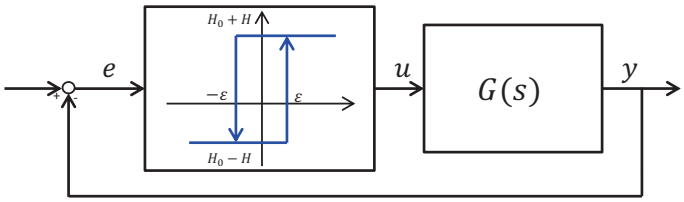

Figure 5.17: The block diagram of the biased relay feedback with hysteresis.

The data is plotted in the upper plot in figure 5.18, from which the steady state gain can be calculated, i.e. $K = 0.16$, and the oscillation amplitude and period can be read off:

$$A_1 = 3, \text{ and } P_{u1} = 11.9.$$

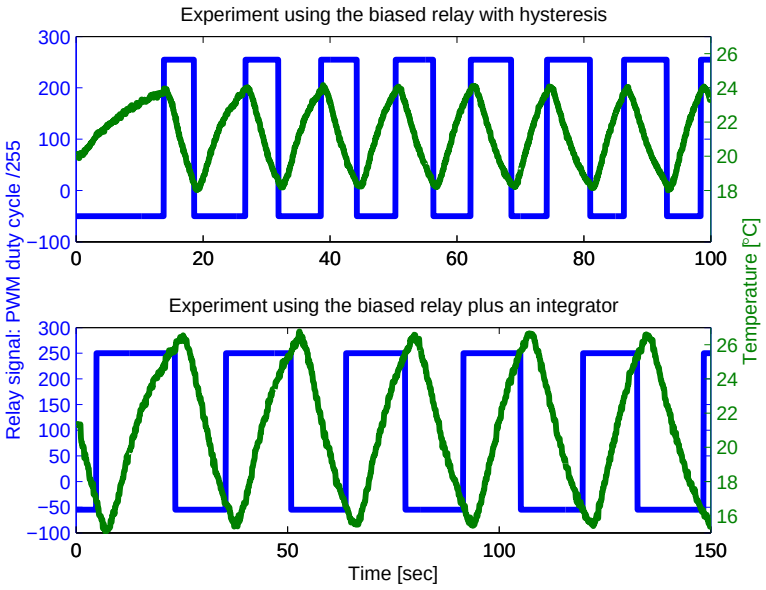

Figure 5.18: The raw data of the relay experiment.

To obtain the information for another oscillation point, the relay with an integrator is used to perform the second relay test, data of which is plotted in the bottom plot in figure 5.18. The oscillation amplitude and period are:

$$A_2 = 5.67, \text{ and } P_{u2} = 27.48.$$

The time constant and the fractional order can be numerically calculated via equations (3.71) and (3.72):

$$T = 16.19, \text{ and } \alpha = 0.8,$$

which is shown in figure 5.19. The dead time can be either estimated form the raw data or calculated from the equation (3.68), $L = 0.77$. This result closely matches the model

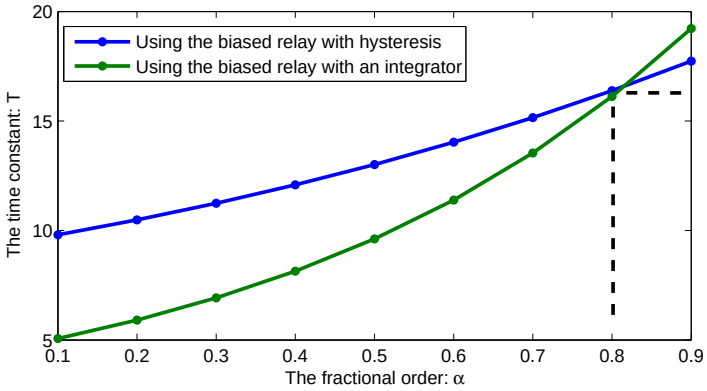

Figure 5.19: Numerically solving equations (3.71) and (3.72) using the experimental data.

obtained through curve fitting of the step test data, which takes about three times longer. So, system identification of the test platform using the proposed method is successful and efficient in terms of time and energy consumption.

5.4 Simulation and implementation of the fractional order auto-decoupling

5.4.1 Simulation examples

Example 1:

Consider the process below with FO transfer function elements, which is modified from the model of the thermo-electric temperature control experimental platform described in section 5.1,

$$P(s) = \begin{bmatrix} \frac{1.2}{2s^{0.5}+1} & \frac{0.6}{3s^{0.7}+1} \\ \frac{0.5}{s^{0.8}+1} & \frac{1.5}{3s^{0.6}+1} \end{bmatrix}.$$

An output noise is added to emulate the measurement noise with the signal-to-noise ratio (SNR) of about 31dB. The step responses of the individual channels before and after decoupling are plotted in figure 5.20, from which it can be observed that the three decoupling methods still apply to different fractional orders as long as the condition in equation (4.16) is satisfied. The output signals from the inverted decoupler are plotted in figure 5.21 for reference.

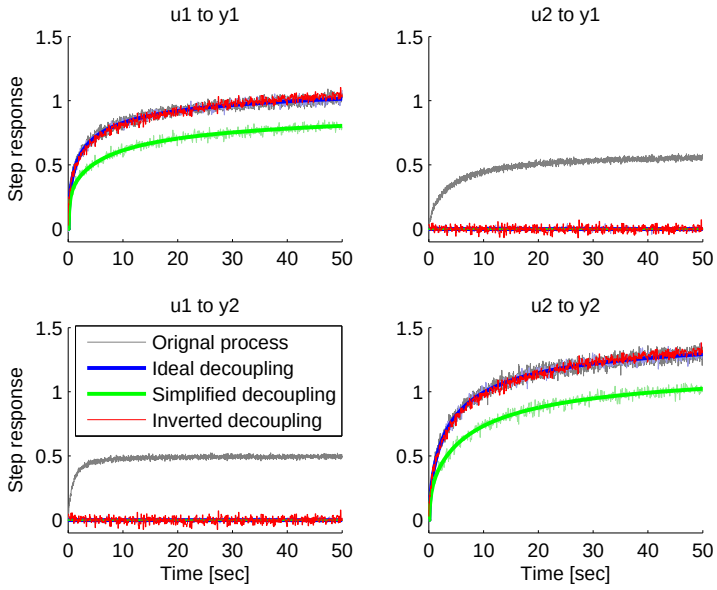

Figure 5.20: The open-loop step responses of the system in Example 1, before and after decoupling.

Example 2:

To illustrate the concept in section 4.2.4, consider the following FO process with dead time, which is modified from the Wood-Berry distillation process in [437] by changing the integer

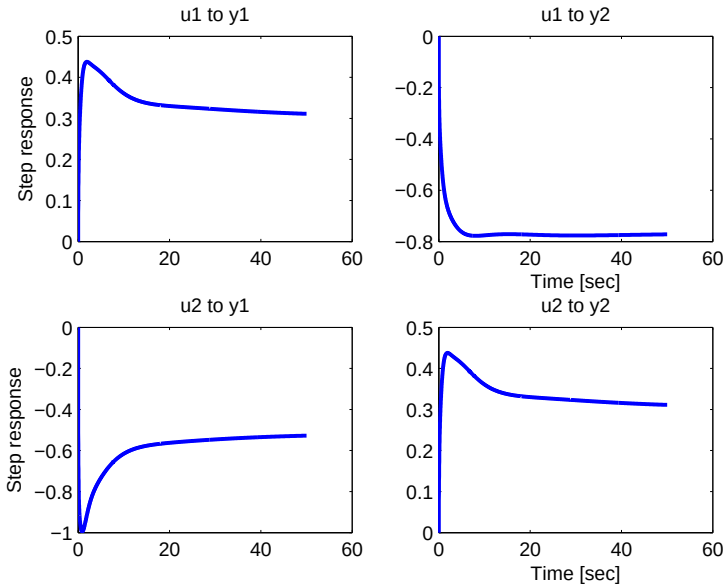

Figure 5.21: The output signals of the inverted decoupler. Left: u_1 step, u_2 zero; right: u_1 zero, u_2 step. Top plots are from D_{12} and bottom are from D_{21}.

order to half order and swapping the dead time of the primary and the interactive loops,

$$P(s) = \begin{bmatrix} \frac{12.8e^{-3s}}{16.7s^{0.5}+1} & \frac{-18.9e^{-s}}{21.0s^{0.5}+1} \\ \frac{6.60e^{-s}}{10.9s^{0.5}+1} & \frac{-19.4e^{-7s}}{14.4s^{0.5}+1} \end{bmatrix}.$$

Since $L_{12} < L_{11}$ and $L_{21} < L_{22}$ in this example, the manipulation of dead time needs to be included into the decoupler design. Following equation (4.20), the simulation result is shown in figure 5.22. While the artificial time delays ensure the causality of the decoupler, the advantage of being able to derive the input to decoupling element from the secondary-loop actuator is lost, [370]. It can be seen that although both decouplers achieve "perfect control" [373] at steady state, there are differences in the transients. The simplified decoupling with the artificial time delay can completely eliminate the interaction, although it changes the primary loop (this change can be compensated by controllers). By contrast, the inverted decoupling keeps the primary loop unchanged, but the decoupling effect at the initial part is a little off from expectation. In practical implementation, the selection of which decoupling to be used can be determined by control performance specifications.

Example 3:

Consider again the process model in example 2, but change the input u_2 to a periodic signal,

$$u(t) = \begin{bmatrix} u1 \\ u2 \end{bmatrix} = \begin{bmatrix} unitstep \\ 0.5\sin(10t) \end{bmatrix}.$$

Such input signal combinations are usually used in chemical reaction processes where one reaction species is kept at a constant supply rate while the other is injected periodically. In

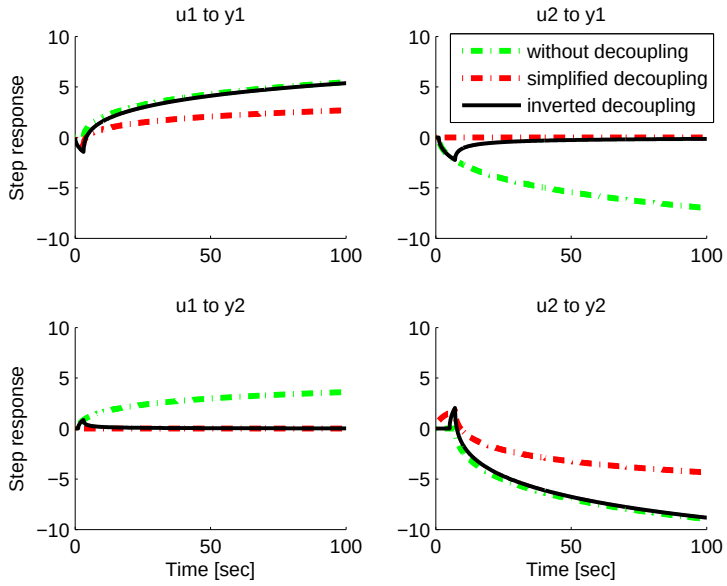

Figure 5.22: The open-loop step responses of the system in Example 2, using different decoupling methods.

this case, the frequency dependant RGA will play a more important role than the static RGA. For comparison, the RGAs of the original and the modified Wood-Berry process are plotted in figure 5.23 as an illustration of section 4.2.5. In this example, although the frequency

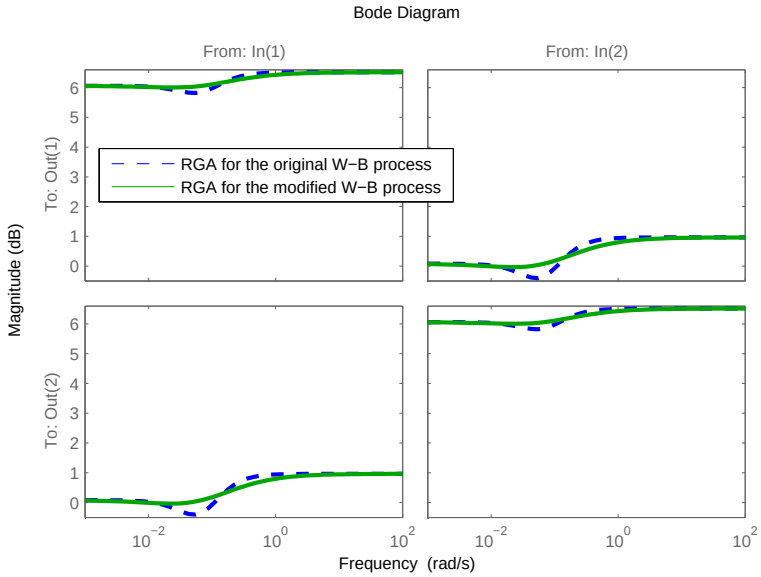

Figure 5.23: The RGA of the original and modified Wood-Berry processes.

dependant RGA differs from the integer order model, the paring does not change. For some

practical processes, the paring may even change across broad band.

The simulation result using unit feedback proportional control with inverted decoupling is plotted in figure 5.24. The green line shows that the two primary loops interfere each other significantly before decoupling, which appears in the form of fluctuations for channel 1 and a bias for channel 2. The blue line shows that the interaction is well decoupled by the fractional order inverted decoupler.

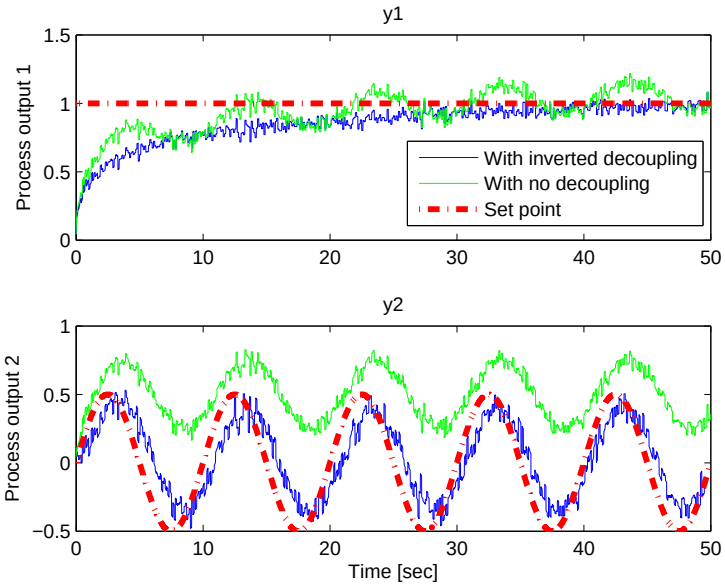

Figure 5.24: The closed-loop step response for Example 3, with both inputs on.

The simulation is performed in Matlab with the help of "Ninteger" toolbox [80] for solving the fractional integration and differentiation. A sample Simulink block diagram implementing the inverted decoupler is drawn in figure 5.25.

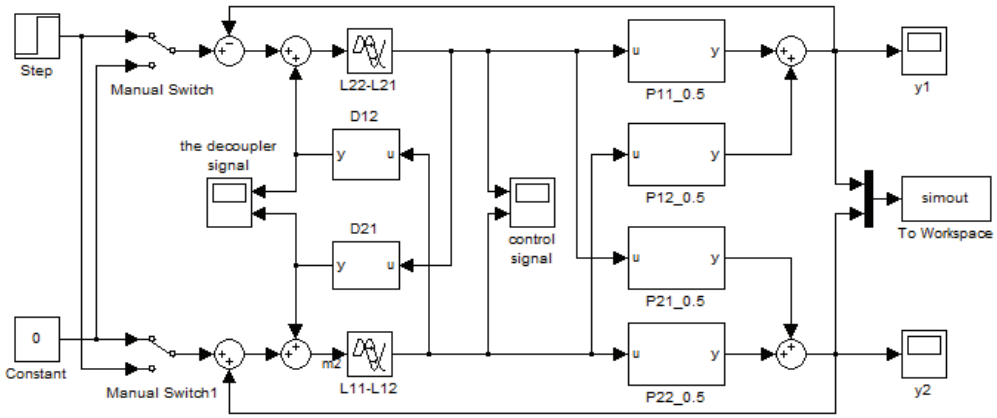

Figure 5.25: A sample Simulink block diagram of inverted decoupling.

5.4.2 Implementing the fractional order auto-decoupling on a 4×4 MIMO thermal process

The decoupling procedure is applied on a temperature control problem in an industrial process. (Note: due to confidential agreements, technical details are omitted and data are scaled to dimensionless.)

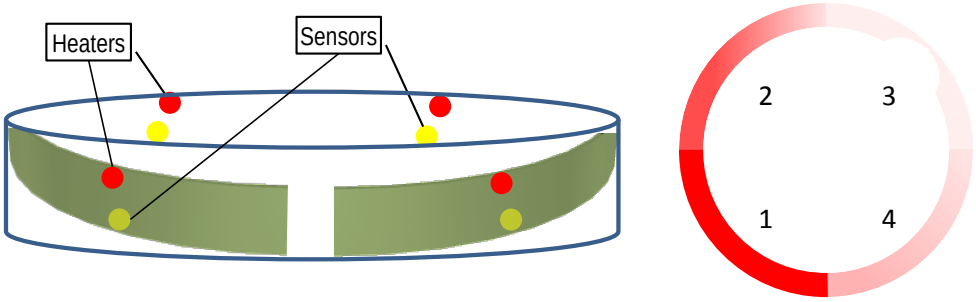

(a) Side view. (b) Top view.

Figure 5.26: The schematic of the annulus heater divided into four sectors.

Different from the scenario described in section 5.5, the control object under investigation is a ring shape device divided into 4 sectors with a coil evenly attached to each sector as the heat source, as shown in figure 5.26(a). To characterize the loop interactions, open-loop step response data is acquired by sequentially turning on one heat source while keeping the other three off. The steady state gain matrix computed from the data reveals asymmetric interaction among the zones, i.e. each zone has higher influence on the next zone clockwise, lower influence on the next zone counter-clockwise, and negligible influence on the diagonal zone. The physical reason might be the sensor-heater misalignment during the mechanical installation, which is assumed to be an uncorrectable fact.

Since this is a thermal process, a fractional order transfer function matrix is chosen as the model structure,

$$G(s) = \begin{bmatrix} g_{11} & g_{12} & 0 & g_{14} \\ g_{21} & g_{22} & g_{23} & 0 \\ 0 & g_{32} & g_{33} & g_{34} \\ g_{41} & 0 & g_{43} & g_{44} \end{bmatrix}. \tag{5.5}$$

In that the interaction between diagonal zones is negligible, the secondary off-diagonal elements in the above matrix are set to zeros for simplicity. Model parameters are identified using the relay feedback method described in section 3.3.3, because the relay feedback method takes much shorter time than the step test for an FO model whose order is much smaller than 1. Figure 5.27 shows a cluster simulation of the model with parameter uncertainties added in. The simplified decoupling is employed. The fractional orders of the transfer function elements are examined to guarantee the properness of the resulting FO decoupler. The parameter identification and the inversion of the TF matrix are programmed and executed automatically to perform the task. Figure 5.28 shows the implementation diagram. Before

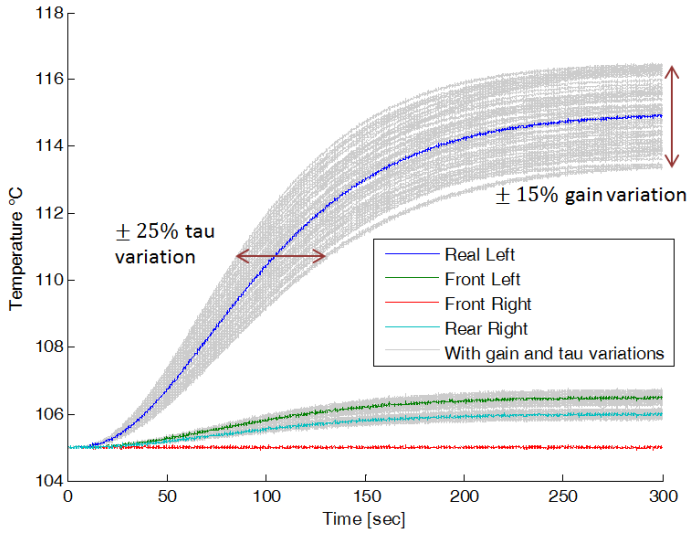

Figure 5.27: The sample responses of the four loops with respect to one heater actuation.

the decoupling, the input signals to the heaters are $[u_1,\ u_2,\ u_3,\ u_4]^T$ from the PID controllers. Now, these signals are fed to a computation unit and the control signals for decoupling, $[m_1,\ m_2,\ m_3,\ m_4]^T$, are generated,

$$\begin{bmatrix} m_1 \\ m_2 \\ m_3 \\ m_4 \end{bmatrix} = \begin{bmatrix} \hat{D}_{11} & \hat{D}_{12} & \hat{D}_{13} & \hat{D}_{14} \\ \hat{D}_{21} & \hat{D}_{22} & \hat{D}_{23} & \hat{D}_{24} \\ \hat{D}_{31} & \hat{D}_{32} & \hat{D}_{33} & \hat{D}_{34} \\ \hat{D}_{41} & \hat{D}_{42} & \hat{D}_{43} & \hat{D}_{44} \end{bmatrix} \begin{bmatrix} u_1 \\ u_2 \\ u_3 \\ u_4 \end{bmatrix} \tag{5.6}$$

where $\hat{D}_{ij}$ are the discredited approximation of the resulting FO filters.

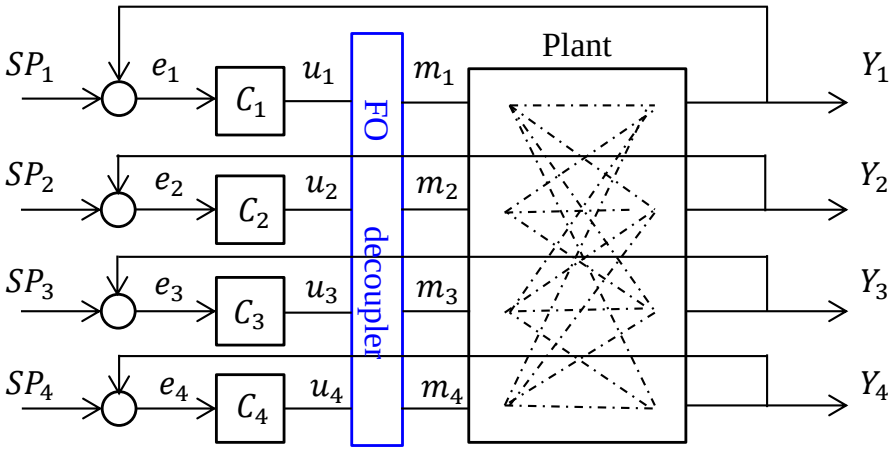

Figure 5.28: The block diagram for implementation.

The data log of the "auto-decoupling" procedure, including the parameter identification and the computation of the decoupling control signal, is shown in figure 5.29, in which

the data during $0 \sim 3500$ sec shows the loop interaction before decoupling, the data during $3500 \sim 7000$ shows the auto-identification and the data during $7000 \sim 10000$ sec shows the loop performance after decoupling. Through comparison, it can be seen that the loop interaction after the auto-decoupling is significantly suppressed.

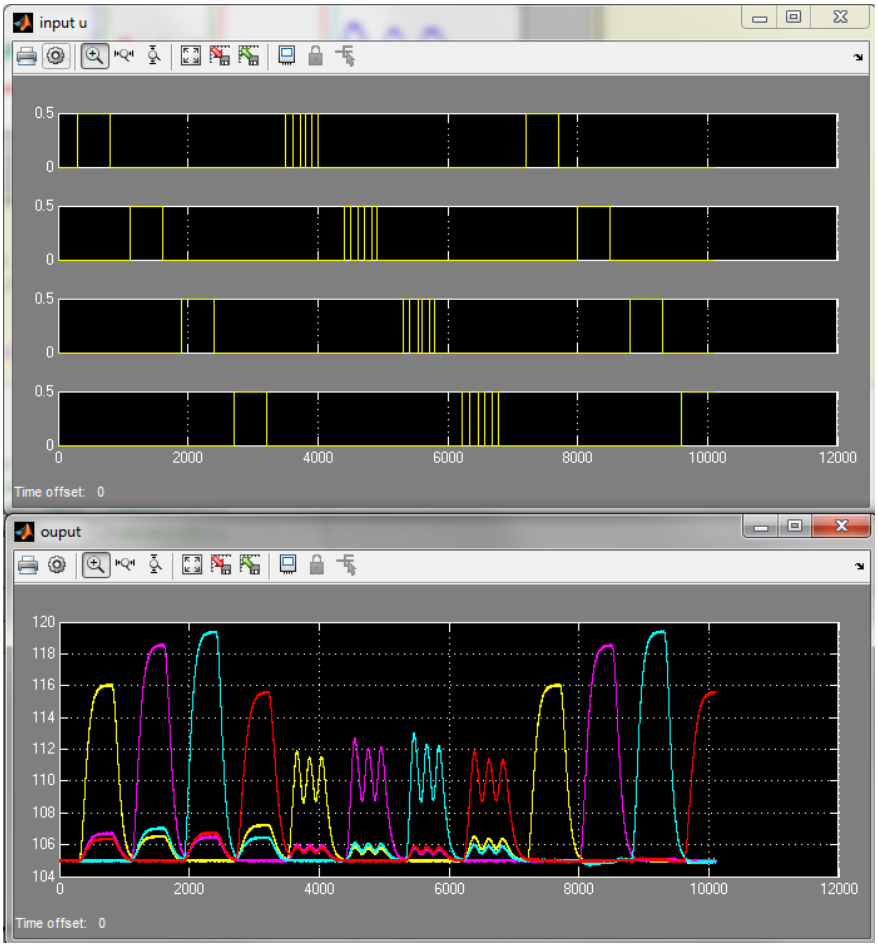

Figure 5.29: The data log of the auto-decoupling procedure.

As a quantitative evaluation of the decoupling performance with uncertainties, the normalized loop interaction gain matrix before and after decoupling are listed below in equations (5.7) and (5.7), respectively. By comparison, it can be seen that the original loop interaction gets much attenuated, and a negligibly slight symmetric interaction is achieved.

$$K_{cpb} = \begin{bmatrix} 1.000 & 0.112 & 0.001 & 0.210 \\ 0.153 & 1.000 & 0.101 & 0.003 \\ 0.000 & 0.149 & 1.000 & 0.136 \\ 0.123 & 0.003 & 0.120 & 1.000 \end{bmatrix}, \tag{5.7}$$

$$K_{cpa} = \begin{bmatrix} 1.000 & 0.027 & 0.001 & 0.005 \\ 0.003 & 1.000 & 0.032 & 0.007 \\ 0.004 & 0.017 & 1.000 & 0.067 \\ 0.003 & 0.007 & 0.004 & 1.000 \end{bmatrix}. \tag{5.8}$$

5.5 A practical case study of the identification and the feedback linearization of a nonlinear fractional order MIMO process

The simulation presented in this section is to support the fractional order feedback linearization discussed in section 3.4.4. The control object is a chucking substrate with heating capability, and a schematic sketch is shown in figure 5.30. Note: due to confidential agreements, raw data are substituted by simulation data or re-scaled to dimensionless.

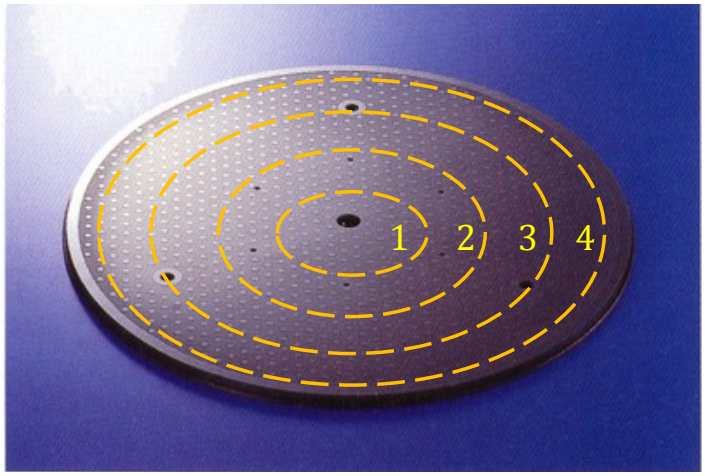

Figure 5.30: The schematic of heating substrate divided into 4 annuli zones.

The following nonlinear fractional order dynamic equation is abstracted to depict the heating of the device,

$$\begin{aligned} {}_0^C D_t^{0.5} x(t) &= -\frac{1}{21}x(t) + \frac{1}{21}\varphi\left[(-0.016u(t) + 3.6)u(t)\right] && (5.9) \\ y &= x - 10, && (5.10) \end{aligned}$$

where $\varphi(\cdot)$ denotes the saturation protection nonlinearity used in the practical process.

The nonlinearity of the process gain is captured by exciting it with a stair input, as shown by the blue curve in figure 3.14, and the nonlinear gain defined by three different calculation types are plotted in figure 5.31.

For this particular case, since the output is linear to the state, the input-output linearization is equivalent to the input-state linearization. According to criterion 1, the transformed input can be expressed as the following:

$$v = C\sum_{i=1}^{\infty} E_{\alpha,1}(\lambda_i t^\alpha)x(0) + t^{\alpha-1}E_{\alpha,\alpha}(\lambda_i t^\alpha) * G(u,x), \tag{5.11}$$

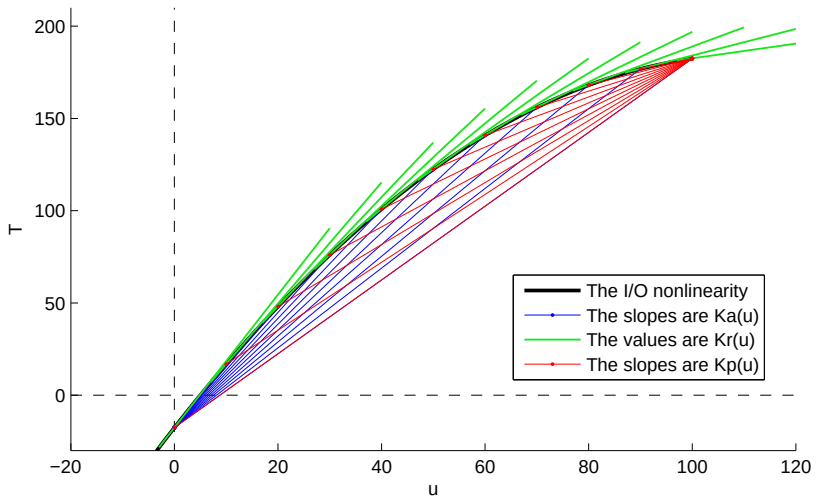

Figure 5.31: The nonlinear gain versus input and output.

Where $E_{\alpha,\beta}(x)$ is the Mittag-Leffler function,

$$E_{\alpha,\beta}(x) \quad = \quad \sum_{k=0}^{\infty} \frac{x^k}{\Gamma(\alpha k + \beta)} \quad (\alpha > 0, \beta > 0). \tag{5.12}$$

The linearized system response is shown in figure 5.32, from which it can be seen that the $y - v$ relationship is linear, in contrast to the black curve in figure 5.33.

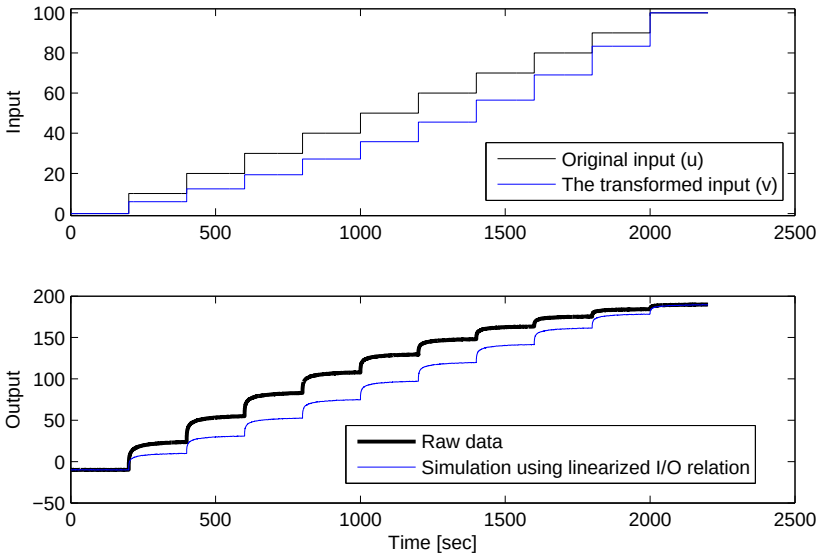

Figure 5.32: The simulated overall response of the linearized system to the transformed input.

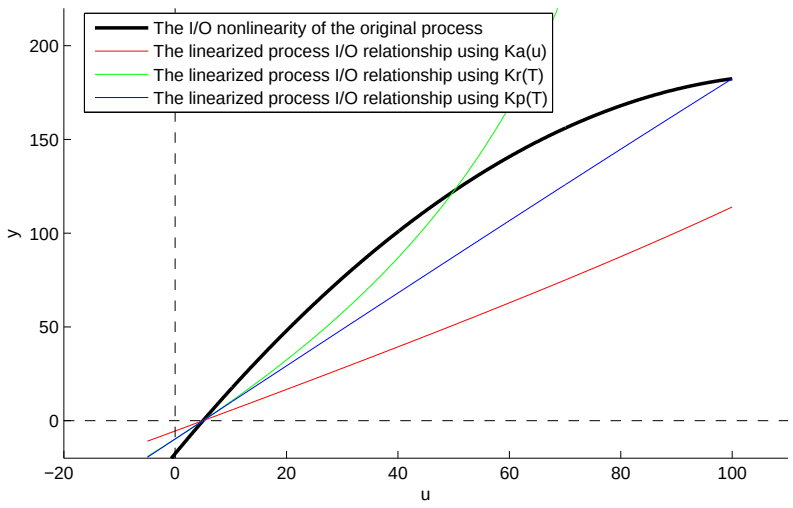

Figure 5.33: The linearized input/output relation using different compensation methods.

Eventually, a *model based time-optimal feed-forward controller* is developed based on this nonlinear modeling and linearization.

5.6 Experiment of the fractional order MPC using RIOTS on the Peltier platform

In this section, the FO MPC using RIOTS proposed in section 4.3 is implemented on the 2-input-2-output HIL experimental platform. As introduced in section 5.1, the experimental platform is highly nonlinear. The dynamics of cooling and heating are asymmetric. Therefore, two models are abstracted from raw data to represent the cooling and heating:

$$\begin{bmatrix} y_1 \\ y_2 \end{bmatrix} = \begin{bmatrix} \frac{-0.018}{6.73s^{0.9}+1} & \frac{-0.008}{6.91s^{0.9}+1} \\ \frac{-0.008}{6.86s^{0.9}+1} & \frac{-0.019}{6.68s^{0.9}+1} \end{bmatrix} \begin{bmatrix} u_1 \\ u_2 \end{bmatrix}. \tag{5.13}$$

$$\begin{bmatrix} y_1 \\ y_2 \end{bmatrix} = \begin{bmatrix} \frac{-0.158}{15.7s^{0.8}+1} & \frac{-0.035}{15.9s^{0.8}+1} \\ \frac{-0.037}{15.8s^{0.8}+1} & \frac{-0.16}{16.0s^{0.8}+1} \end{bmatrix} \begin{bmatrix} u_1 \\ u_2 \end{bmatrix}. \tag{5.14}$$

As a baseline visualization, figure 5.8 shows the system response to a step set-point reference under no control and under a basic PI control. In order to use the RIOTS based FO MPC (RMPC) to deal with the obtained FO MIMO system, a reformulation is performed to convert the FO transfer function matrix into the pseudo state-space representation,

$$\begin{bmatrix} \dot{x}_{11} \\ \dot{x}_{12} \\ \dot{x}_{21} \\ \dot{x}_{22} \end{bmatrix} = \begin{bmatrix} a_{11} & 1 & 0 & 0 \\ 0 & a_{12} & 0 & 0 \\ 0 & 0 & a_{21} & 0 \\ 0 & 0 & 0 & a_{22} \end{bmatrix} \begin{bmatrix} x_{11} \\ x_{12} \\ x_{21} \\ x_{22} \end{bmatrix} + \begin{bmatrix} b_{11} & 0 \\ 0 & b_{12} \\ b_{21} & 0 \\ 0 & b_{22} \end{bmatrix} \begin{bmatrix} u_1 \\ u_2 \end{bmatrix} \tag{5.15}$$

$$\begin{bmatrix} y_1 \\ y_2 \end{bmatrix} = \begin{bmatrix} c_{11} & c_{12} & 0 & 0 \\ 0 & 0 & c_{21} & c_{22} \end{bmatrix} \begin{bmatrix} x_{11} \\ x_{12} \\ x_{21} \\ x_{22} \end{bmatrix} \tag{5.16}$$

where $\{a_{ij}, b_{ij}, c_{ij}\}, (i, j = 1, 2)$ are the parameters in the system matrix, input matrix and output matrix, respectively.

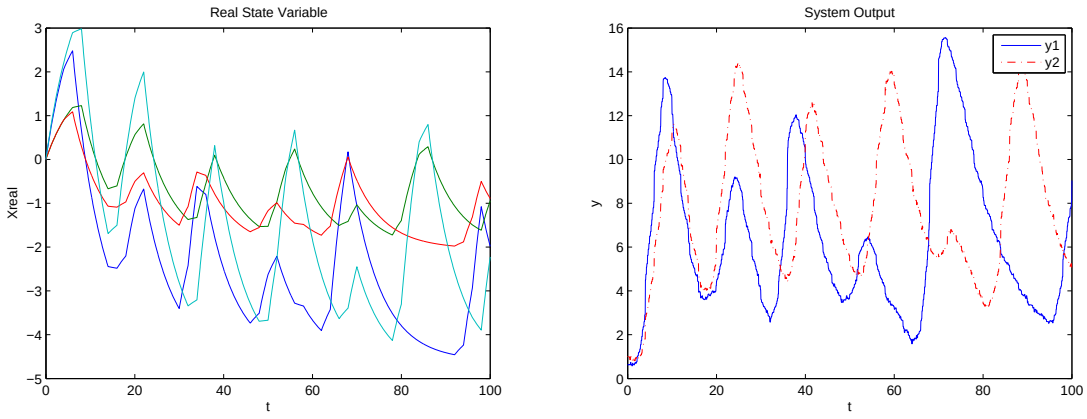

(a) The real states. (b) The system output.

Figure 5.34: The state and output of the system under MPC using RIOTS.

The experiment is carried out within a small temperature set-point range to avoid the significant nonlinear behavior. The ambient temperature is at $24°C$. The RIOTS based FO MPC is compared with the MPC in Matlab Toolbox (MMPC) to control the system. For both control systems, the sample time is $T_s = 0.2s$. For the follwoing sample demonstration, the reference inputs are $\begin{bmatrix} r_1 \\ r_2 \end{bmatrix} = \begin{bmatrix} 26 \\ 29 \end{bmatrix}$, for the left and right Peltiers, respectively. The maximum control input is mapped within the limit range of $u_1 \in [-255\ 255], u_2 \in [-255\ 255]$. For MMPC, the predictive horizon is $N_p = 30$ and the control horizon is $N_m = 20$. Whereas in RMPC, considering the computation speed, the predictive horizon and the control horizon are $N_p = 40$ and $N_u = 10$, and the weighting matrix is tuned as $W_y = \begin{bmatrix} 1 & 0 \\ 0 & 0.5 \end{bmatrix}$. The Simulink block diagrams of the experiment using MMPC and RMPC are shown in figures 5.35 and 5.36, respectively. The experimental results are shown in figures 5.39, 5.40, 5.37, and 5.38, from which it can be seen that the RMPC outperforms the MMPC under this severe nonlinear circumstance. (Note: the ambient temperature bias in the MMPC result is removed during the running of Simulink due to some technical issues.)

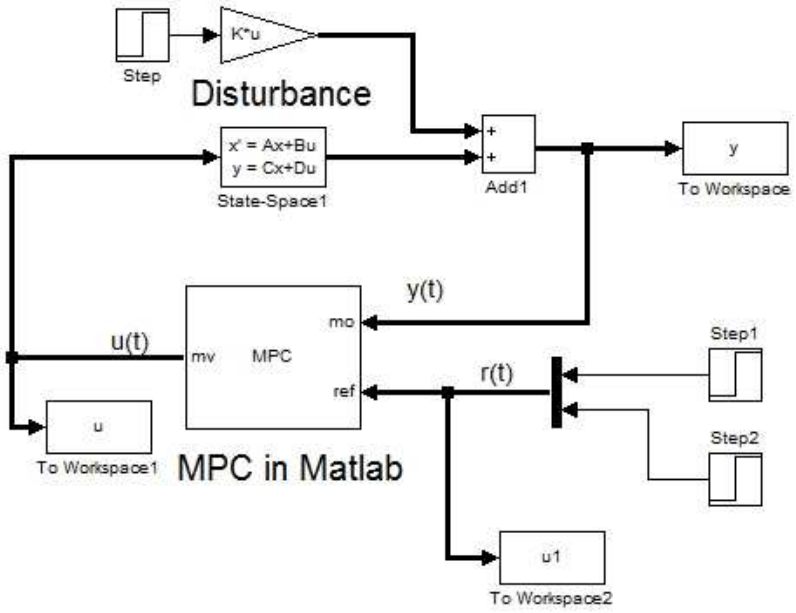

Figure 5.35: Simulink block diagram of the MIMO system using Maltab built-in MPC

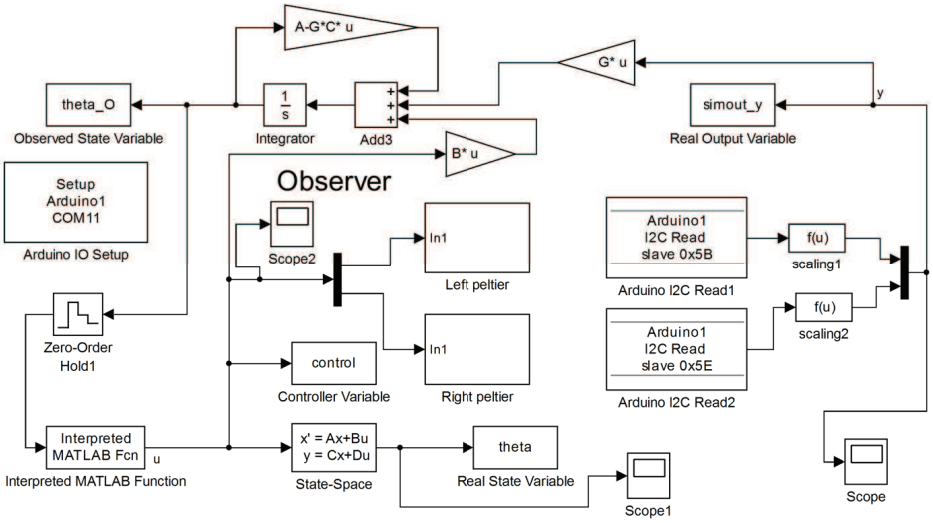

Figure 5.36: Simulink block diagram of the MIMO system using RIOTS based MPC

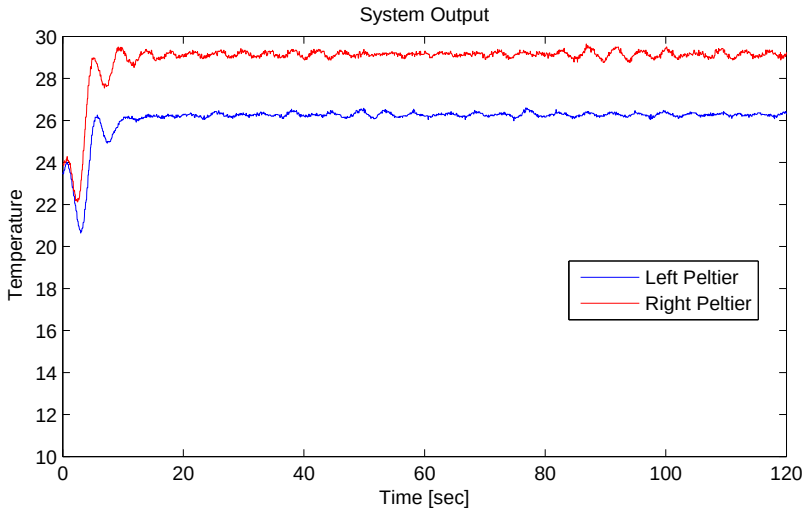

Figure 5.37: System outputs of the MIMO system using RIOTS based MPC

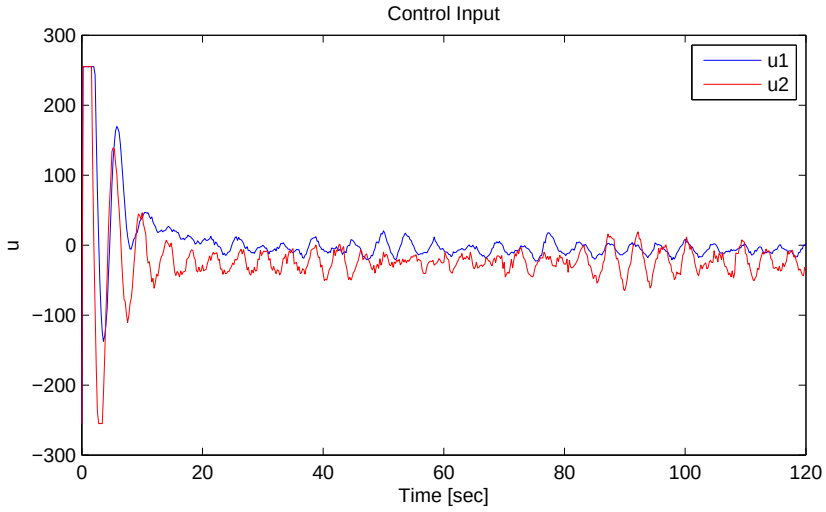

Figure 5.38: Control inputs of the MIMO system using RIOTS based MPC

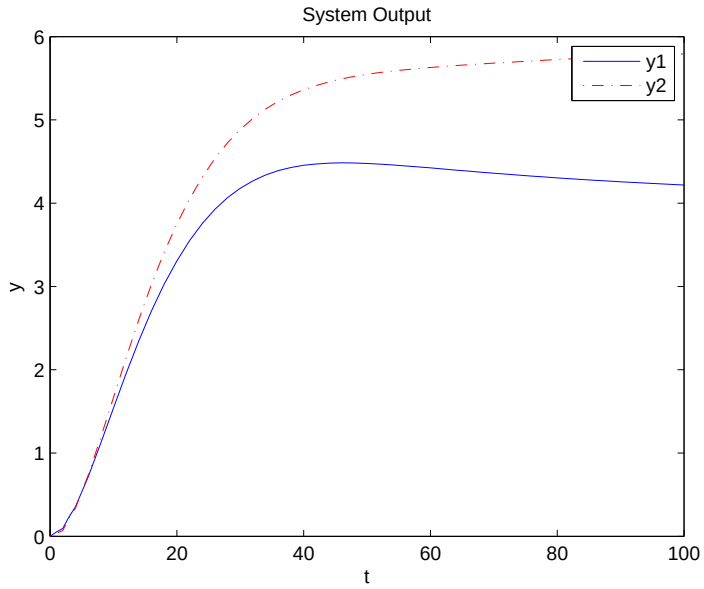

Figure 5.39: System outputs of the MIMO system using Maltab built-in MPC

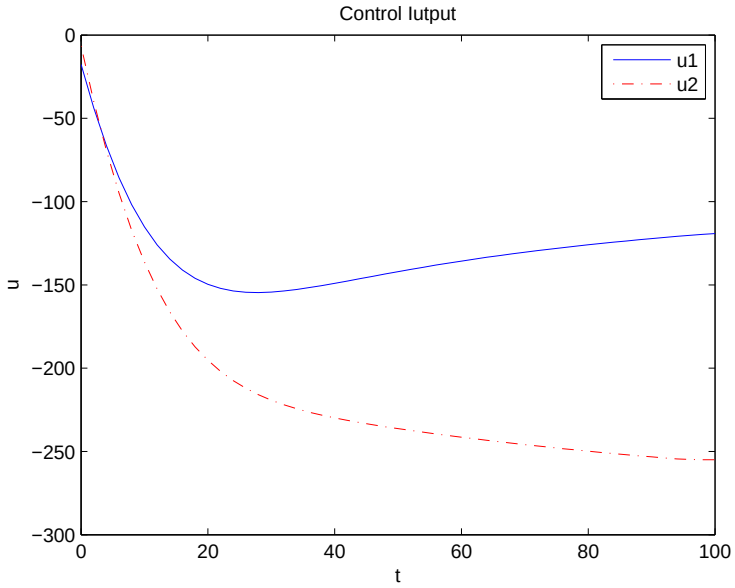

Figure 5.40: Control inputs of the MIMO system using Maltab built-in MPC

5.7 Simulation of FO ESC for plasma impedance matching

The radio frequency (RF) power is the common power source for plasma ignition in the industry. It is a common sense that wherever RF is used, the impedance matching needs to be considered. Although the matching technology for static loads is mature, new challenges emerge when loads with dynamic nonlinear impedance are dealt with, among which the plasma impedance matching is a typical case.

The plasma is complex and its impedance is hard to model [440]. To briefly state the complexity, some classic formulations are listed to explain why traditional controllers such as the PID and MPC are not well applicable, which naturally leads to the use ESCs. Then, simplified circuit models of the plasma impedance are reviewed for matching network design and simulation.

5.7.1 Formulation of the plasma impedance

Using the ESC to match the RF powered plasma impedance in real time is a relatively novel idea. Some work and results using the regular sinusoidal ESC were presented in [441] and [442].

The plasma impedance matching concerns about determining the adjustable component values in the matching network to steer the RF power delivery to the maximum point and remain at such point thereafter. This perfectly fits in the logic flow of the ESC.

The impedance is a critical electric characteristic of plasma. One of the reasons that makes it hard to model is the measurement. Although many approaches have been invented, such as the VI or impedance probe [443, 444] and the Langmuir probe [445], the accurate measurement of the industrial plasma during operation is still hard if not impossible. This is because any contact sensing inside or around the plasma is so invasive that it affects the plasma status. In other words, the values measured by the probes are no longer those when the probes are not there. Hence, virtual metrology has been proposed and widely adopted, [446, 447, 448].

The plasma impedance is closely related to the plasma status which is affected by numerous factors. Therefore, it is essentially a nonlinear function of many parameters including the plasma temperature T, density n_0, the electron-neutral collision frequency ν_m, the gas flow rate G, the gap space between electrodes d, the RF power P_{rf}, frequency ω, etc. It is usually expressed in a "black-box" form in control system design [441],

$$Z_p = f_p(T, \nu_m, n_0, P, \omega, d, M) \tag{5.17}$$

where f_p is an unknown nonlinear function.

In plasma physics, different equations are deduced to calculate the impedance of different types of plasma. Depending on the scale of the plasma and the demand of estimation accuracy, corresponding approximations can be selected. For example, the space plasma impedance can be derived from the Maxwell's equations and the generalized Ohm's Law [449, 450],

$$\mathbf{E} + \mathrm{v} \times \mathbf{B} = \eta \mathbf{J} + \frac{1}{\mathrm{n}_e} (\mathbf{J} \times \mathbf{B} - \nabla \mathbf{P}) + \frac{\mathrm{m}_2}{{\mathrm{n}_e}^2} \frac{\partial \mathbf{J}}{\partial \mathbf{t}} \tag{5.18}$$

with **E** the electrical field, **B** the magnetic flux density, **J** the current density, $\nabla \mathbf{P}$ the pressure gradient and η the conductivity coefficient. On the other hand, for the small-scale low-pressure industrial plasma, some variables play more dominant roles than others. Thus, the calculation can be simplified. For instance, the reactance of the capacitive reactor plasma can be approximately determined by the RF current I and the bulk plasma thickness d, [451, 452],

$$X_p = \frac{4\omega}{|I|^2} \int (\omega_m - \omega_e) d^3x, \tag{5.19}$$

where ω_m and ω_e are the harmonic electric and magnetic energy densities, respectively. The bulk plasma admittance is presented in [290] as follows,

$$Y_p = j\omega\epsilon_p \frac{A}{d} \tag{5.20}$$

where A is the electrode area, and ϵ_p is the plasma dielectric constant determined by ω, ν_m and the electron plasma frequency ω_{pe},

$$\epsilon_p = \epsilon_0 \left[1 - \frac{\omega_{pe}^2}{\omega(\omega - j\nu_m)} \right]. \tag{5.21}$$

Plugging ϵ_p into equation (5.20) will give us the plasma admittance in the form of a combination of inductance (L), resistance (R) and capacitance (C):

$$Y_p = j\omega C_0 + \frac{1}{j\omega L_P + R_p} \tag{5.22}$$

where $C_0 = \epsilon_0 A/d$ is the vacuum capacitance determined by the electrodes' gap distance d and area A; $L_P = 1/(\omega_{pe}^2 C_0)$ is the plasma inductance, and $R_p = \nu_m L_P$ is the plasma resistance.

These equations are insightful from physics point of view, but their practical value for control engineers is limited. Real-time estimation or analytical solution of the plasma impedance cannot be expected from these equations. Therefore, many control engineers choose to bypass the tedious physics modeling and directly use simplified electrical models consisting of LRC components instead. In [290, 3, 453], the plasma impedance is modeled as an LRC circuit illustrated in figure 5.41. In [454], it is modeled with additional diodes to capture the nonlinear behaviors under varying or multi-frequency RF sources, as shown in figure 5.42. In the simulation section of this paper, an LRC model is employed as the nominal plasma impedance. Fluctuations are added based on process data, empirical observation, and the implication of equations (5.19)$\sim$(5.22). For example, higher pressure results in higher collision rate and consequently higher resistance, etc. Thus, the programmed plasma impedance become a dynamic model that evolves with the environmental changes.

5.7.2 The RF impedance matching

Similar to the propagation of light and wave, the RF power will also be reflected when transmitted from one dielectric to another. Thus, appropriate matching networks are needed to minimize the power reflection from the load, or equivalently, to maximize the power

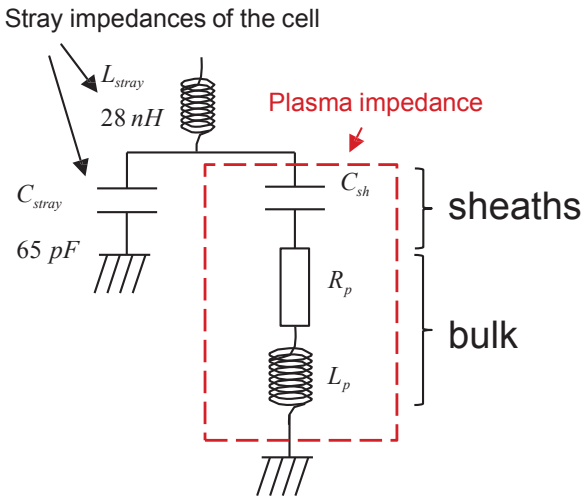

Figure 5.41: The LRC circuit representation of the plasma impedance, [3].

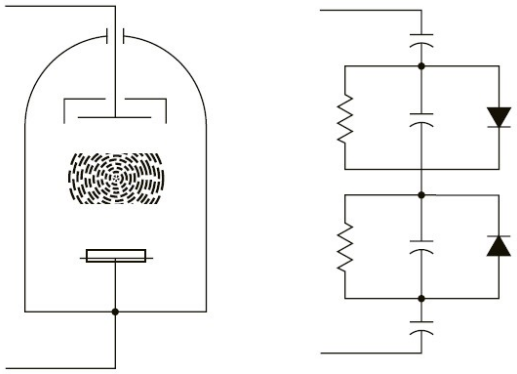

Figure 5.42: Modeling the nonlinearity of the plasma impedance using LRC circuit with diodes, [454].

transfer to the load. The load power is the remaining part of the forward power excluding the reflected power, $P_l = P_f - P_r$. It can be calculated as:

$$P_l = \frac{1}{2} V_l I_l^* = \frac{1}{2} V_s \frac{R_l}{Z_s + Z_l} \frac{V_s}{(Z_s + Z_l)^*}, \tag{5.23}$$

where V_s and V_l are the source and load voltages, respectively; $Z_s = R_s + jX_s$, and $Z_l = R_l + jX_l$ are source and load impedance as shown in figure 5.43. According to the Maximum Power Transfer theorem, the maximum power can be achieved when the impedance is matched, i.e. when the load impedance is equal to the complex conjugate of the source impedance [455],

$$Z_s = Z_l^*. \tag{5.24}$$

In such case, $P_r = 0$ and

$$P_l = P_f = \frac{1}{2} V_s \frac{R_l}{2R_l} \frac{V_s}{2R_l} = \frac{V_s^2}{8R_l}. \tag{5.25}$$

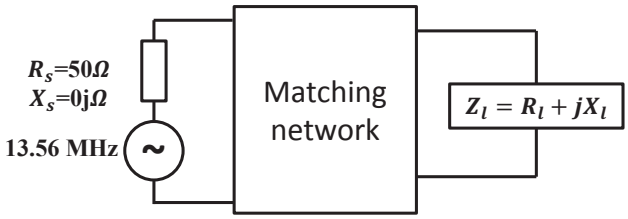

Figure 5.43: The schematic of the matching network between an RF source and a load.

As a quantification of the matching outcome, the reflection coefficient from the source to the load is defined as follows, [455],

$$\Gamma = \frac{Z_l - Z_s}{Z_l + Z_s}, \tag{5.26}$$

with $\Gamma = 0$ representing that the impedance is matched.

Taking into consideration the matching network, the load impedance Z_l in equations (5.24)∼(5.26) are substituted by $Z_{ml} = f_z(Z_m, Z_l)$ where $Z_m = f_m(C)$ is an abstract representation of the tunable matching network impedance via the capacitor C, and f_z is a function of Z_l and Z_m. The exact expressions of f_z and f_m are determined by the type of the matching network in use, and they can be calculated according to the Kirchhoff′s law and Thévenin′s theorem. However, this is not addressed in this paper because: 1) the FO SM-ESC is a model independent controller which does not require the complete knowledge of the relationship between the input and output; 2) even if f_z is determined, f_p in equation (5.17) is still unknown by all means. Thus, the overall relationship between the input and output is still not able to be determined:

$$P_l = h(C), \tag{5.27}$$

where h is unknown and is usually called the performance function in ESCs. To illustrate this concept, a control block diagram is drawn in figure 5.44.

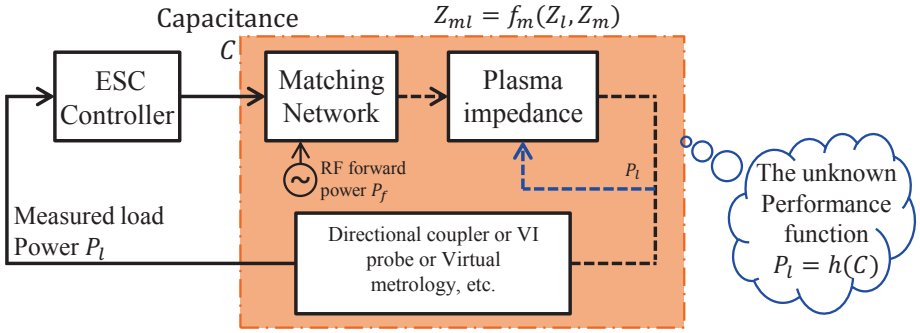

Figure 5.44: The control block diagram for the plasma impedance matching.

5.7.3 Simulation

The impedance matching of a capacitively coupled plasma (CCP) using an "L" network is simulated here as a case study. As the name implies, the industrial CCP has a capacitive impedance affected by the reaction recipes including the applied RF power, reactor pressure, temperature, and so on. The RF power source has a frequency of 13.56 MHz and a 50Ω inner resistance which is an industrial convention. Let the RF forward power be $1000W$. (Remark: most RF generator equipment can provide forward power with a range larger than the rated value so as to give the matching network some margin for possible performance degradation. For simulation purposes, the forward power is set fixed in this context.) Assume that the plasma impedance has a nominal value of $Z_{p0} = 5 - 30j\ \Omega$ when the reactor recipe is $T = 110°\text{C}$, $P = 300$ mTorr and $G = 45$ sccm. A basic "L" shape matching network with an adjustable motor-driven capacitor is used to perform the task. A schematic is shown in figure 5.45.

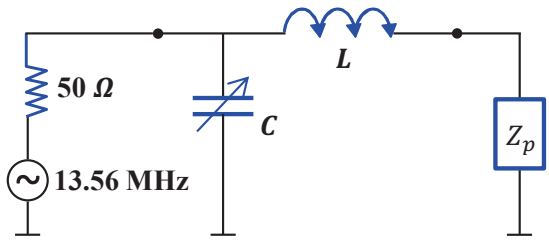

Figure 5.45: The connection of the "L" shape matching network.

For the nominal plasma impedance, the inductance and capacitance of such a network can be predetermined via some Smith Chart manipulation [456],

$$L = 528 \text{ nL}, \quad C = 778.5 \text{ pF}.$$

This will make the nominal impedance "side-look" like 50Ω so that the power delivered to the plasma is maximized.

A periodic fluctuation, a step change and white noise are added to the temperature, pressure and gas flow, respectively, as shown in figure 5.46. These perturbations in the recipe species produce a varying plasma impedance around Z_{p0}, which furthermore results in a drifting power peak. However, as long as it lies in the tuning space of the matching network, the maximum power transfer can be achieved by adjusting the capacitor. A sweep of the capacitor values is performed for several sets of recipes, as plotted in figure 5.47. This is just to give a visual illustration of the peak power drifting. A sweep is not available in real-time practice because the big power reflection and time consumption during the sweep are impermissible. Moreover, the recipe hardly stays fixed for sweep.

To model the actuation time of the motor driven capacitor, a transfer function is identified from real data, as shown in figure 5.48,

$$G(z) = \frac{0.04(z + 0.72)}{(z - 0.74)^{-2}}, \ f_{PWM} = 10Hz. \tag{5.28}$$

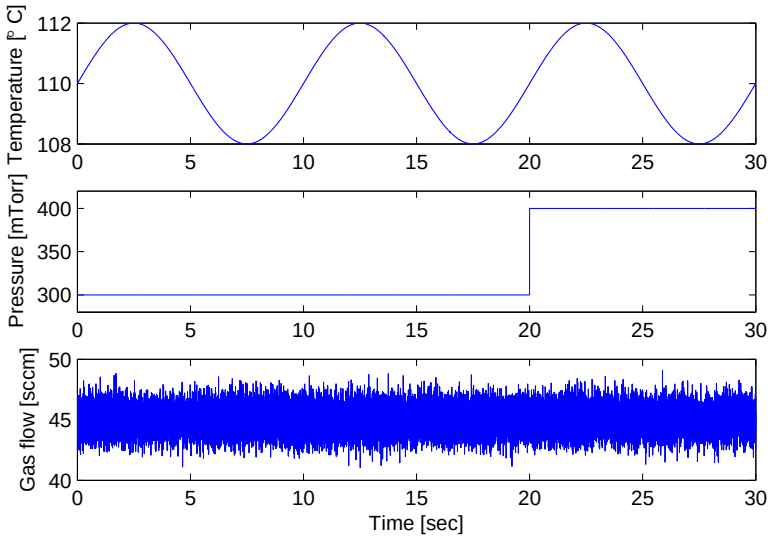

Figure 5.46: The simulated perturbations of the recipe species.

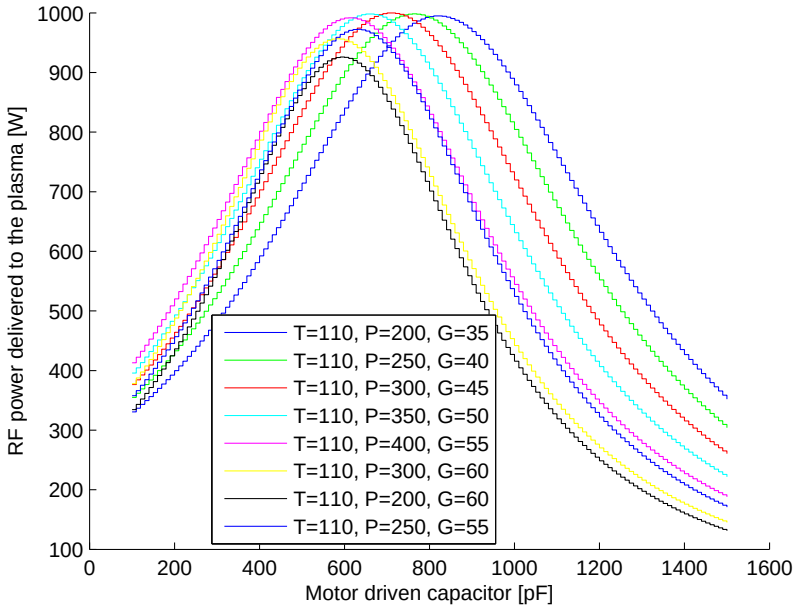

Figure 5.47: The sweep of the capacitor values under different CCP reactor recipes, with a step size of 10 pF.

The Simulink block diagram of this setup is shown in figure 5.49, and the implementation of the fractional order integrator utilizes the Matlab toolbox introduced in [79]. Using the proposed FO SM-ESC, the maximum load power is quickly detected and is tracked in real time regardless of the power peak drifting. The control performance is plotted in figure 5.50 including the power output P_l and the capacitance input C. It can be seen that the proposed

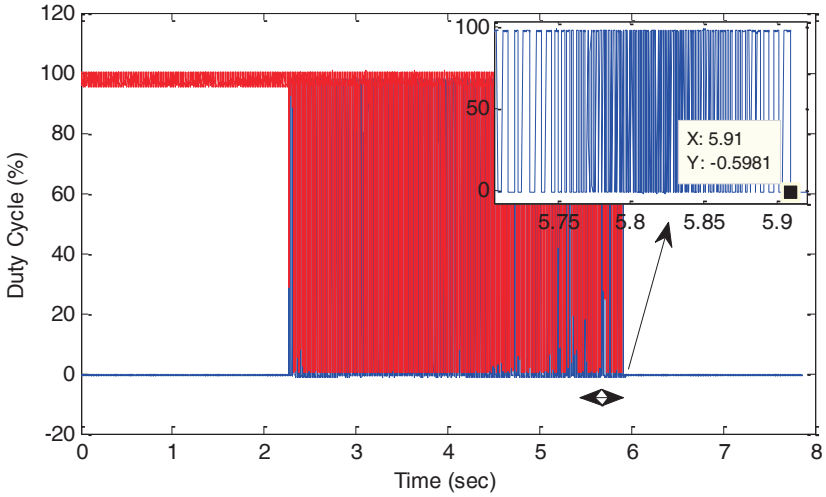

Figure 5.48: The PWM signal of the driving motor.

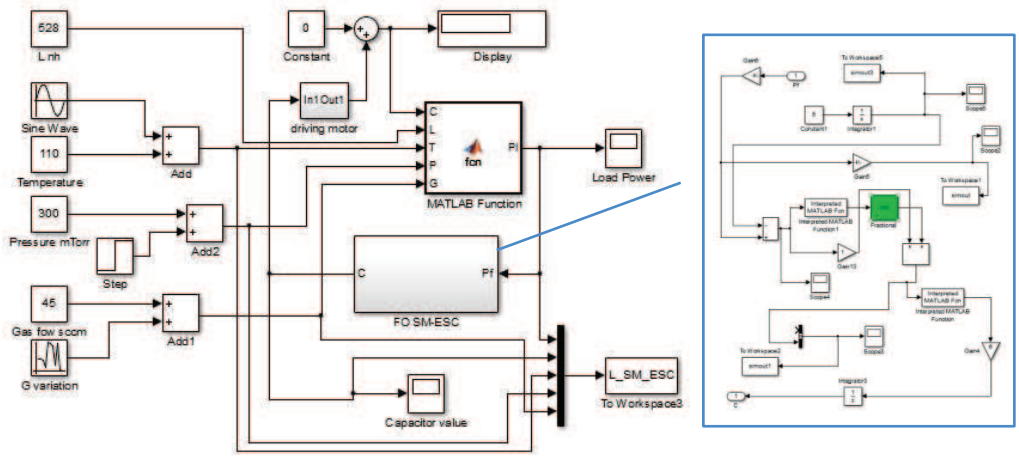

Figure 5.49: The Simulink block diagram for the CCP impedance matching using FO SM-ESC.

method successfully detects the optimal capacitance that matches the plasma impedance within 2 seconds including the motor driving time. In addition, the maximum power is maintained within 2% error range against the severe recipe changes. In comparison, the IO SM-ESC with the same set of controller parameters needs much longer time to detect the optimal capacitance, which is also shown in figure 5.50.

For more comparison, the matching performance using the sinusoidal ESC under the same recipe condition is plotted in figure 5.51, from which it can be seen that the performance is not as good as that achieved by the proposed enhancement, in terms of both reaching time and tracking error. Specifically, if the amplitude of the sine signal in the ESC is set big, reaching time can become shorter, but a larger tracking error is resulted; on the other hand, if it is set small, the tracking error is decreased, but the reaching time become longer. When the parameters are selected improperly, this ESC may fail to lock the power peak even if

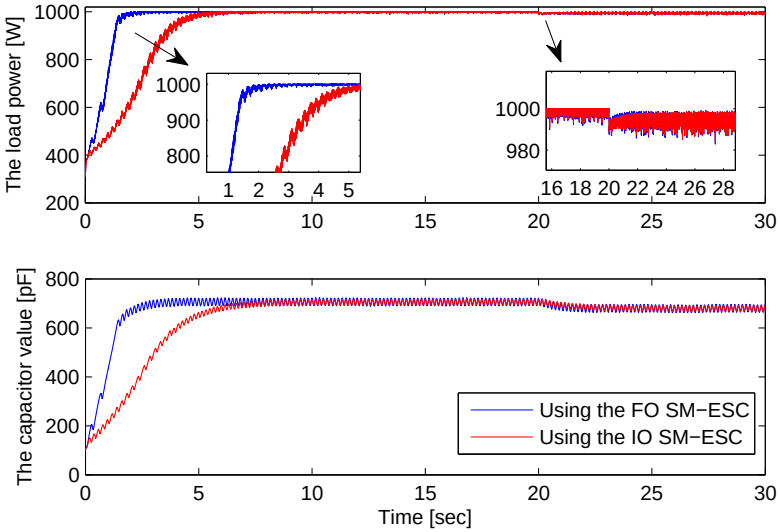

Figure 5.50: Comparison of the matching outcome between fractional and integer order SM-ESCs.

detects it, as shown in figure 5.52.

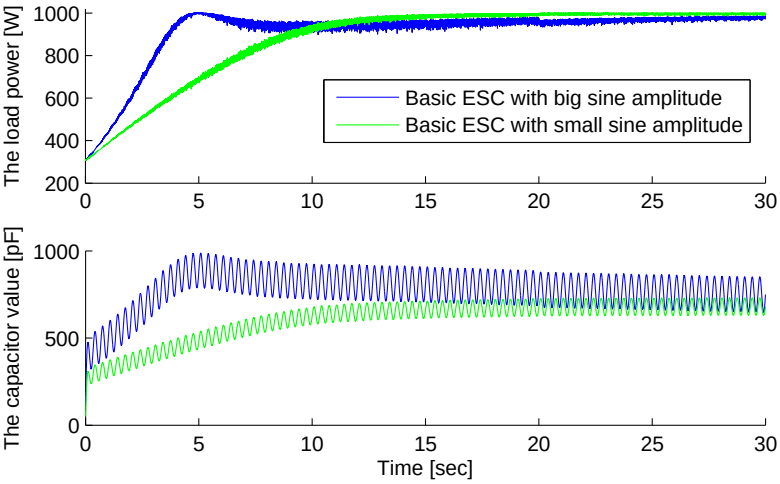

Figure 5.51: Matching the CCP impedance with an "L" shape network using the sinusoidal ESC.

The proposed control strategy has also been verified on other scenarios such as matching the inductively coupled plasma (ICP) using "T" shape matching network. Other case studies are available but are not enumerated here due to limited space.

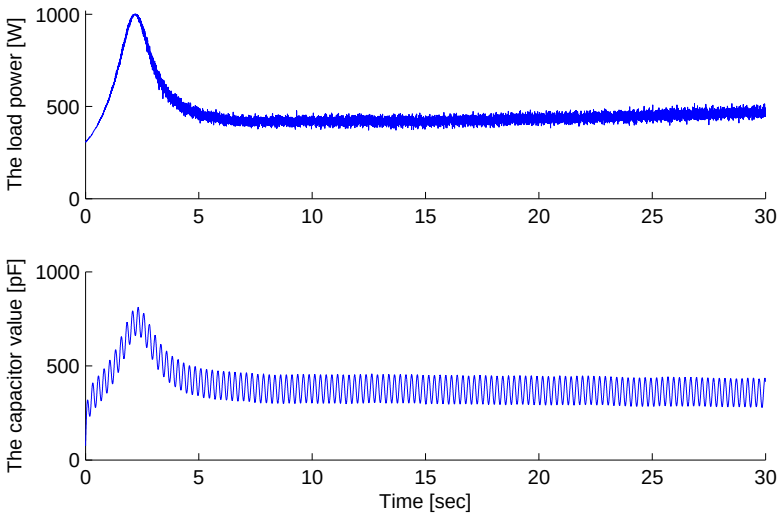

Figure 5.52: The failure of extremum tracking using sinusoidal ESC due to improper parameter selection.

Chapter 6

Beyond Fractional Order Process Control

> History doesn't repeat itself, but it does rhyme.
>
> — Mark Twain

Murphy's law states: anything that can go wrong, will go wrong. Psychological implications usually drive people to do unwilling things subconsciously, and hence, results in the occurrence of rare events at a higher probability than they were expected. Eventual, It appears to fulfill the common saying: the more you worry about one thing, the worse it gets.

This chapter serves as a cadenza part of this dissertation, so as to present some miscellaneous research efforts on fractional calculus related topics.

6.1 Lévy flight based random search

There are numerous approaches to perform the function minimization task, for example, the gradient descending methods [457], meta-heuristic algorithms [458], dynamic programming [459], linear programming (LP), etc [460]. As a particular example, the order scanning procedure discussed in section 3.3.1 uses the Matlab built-in functions 'fminsearch' or 'fminunc' based on the simplex method which belongs to the gradient descending category. In this dissertation, a practically useful search method is developed to further fulfill the data fitting task during the order scanning procedure, and it turns out to be effective. The Matlab script is available for download in [461]. This search method implants the Lévy flight based randomization into the particle swarm optimization (PSO) algorithm [462] in the meta-heuristic category.

Definition 25 (Lévy flight)**.** *A Lévy flight is a random walk in which the step-lengths have a probability distribution that is heavy-tailed [463], such as the Lévy distribution whose probability density function (pdf) is,*

$$f(x;\mu,c)=\sqrt{\frac{c}{2\pi}}\frac{e^{-c/[2(x-\mu)]}}{(x-\mu)^{3/2}}, \tag{6.1}$$

where μ is the location parameter and c is the scale parameter. For example, when defined as a walk in a 2-dimension plane, the steps are in isotropic random directions.

The connection between Lévy flight and the fractional calculus can be found in the fractional order partial differential equation (2.51) which is used to depict the random walks. An important property of the Lévy flight is that its mean squared displacement (MSD) does not converge because its θ moment is:

$$\left\langle |x|^{\theta} \right\rangle \sim t^{\theta/\alpha}. \tag{6.2}$$

Thus, when $\theta = 2$ and $\alpha < 2$, it diverges. Having this feature, "long jumps" appears occasionally in the walk, which is an obvious characteristic that distinguishes the Lévy flight from the Brownian motion. Incorporating this feature in the PSO algorithm for the particle velocity update is likely to provide better performance in terms of global randomization, because the long jumps help particles with escaping the local minimum [464]. The Matlab script is created based on such technique and is briefly described below.

`[gbest, xb] = levyPSO(func, vars)` is a function that searches for the global minimum of an n-Dimensional function defined in 'func' using the PSO algorithm based on Levy distribution randomization. It returns the global (not guaranteed) minimal value and the coordinate at which the function takes that value. The input to this function is designed in the similar manner to the Matlab built-in function "fminsearch()". Sample syntax: `[gbest, xb] = levyPSO(func_test, [0 0], [100 100], 100, 200)` for 2-D optimization, and `[gbest, xb] = levyPSO(func_test_3d, [0 0 0], [100 100 100], 100, 200)` for 3-D function optimization.

The performance of this function is tested on the attached test functions within the download file. It is competitive with fminsearch() and GOAT() in terms of the target hitting rate (locating global minimum successfully), and it is better than the built-in particleswarm() in Matlab 2014b. When adequate swam size (not too large) is used, it completes the search faster than GOAT() and fminsearch(). Although fminsearch() is not in the same algorithm category as the PSO, the comparison is made because the input and output of the levyPSO() are designed in the same paradigm as fminsearch(). Moreover, both of them are used for the aforementioned order scanning problems.

As a visual illustration, the minimum search on a 2-D function using the Lévy based PSO is shown in figure 6.1, in which the left sub-figure shows the sample random walk trace of a single particle.

More information on this research topic can be found in [465] and [466]. The PSO algorithm is also used to approximate a fractional order system by an integer order model [467].

6.2 The MESABox Apps for control tutorial

To fulfil the need of personalized portable lab modules for the mechatronics course teaching, a Matlab Application (App) framework named MESABox is developed (MESA stands for Mechatronics, Embedded Systems and Automation, and is the name of a laboratory in UC Merced). A snapshot of the existing App gallery is shown in figure 6.2. Several typical Apps are developed for the demonstration of feedback control concepts, such as the "Floating ball App" in figure 6.3 and the "fan-plate App" in figure 6.4. They are used to illustrate the height control of an floating ball inside a tube and the displacement control of a plate in the

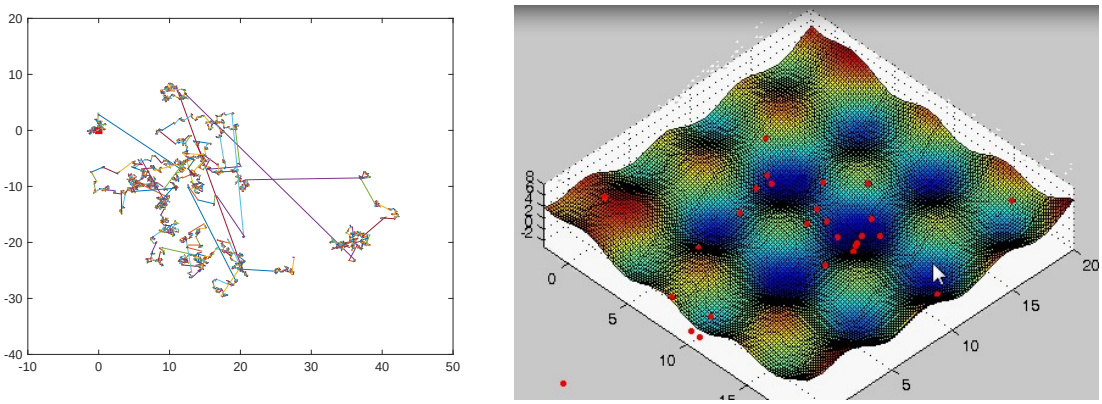

(a) A particle doing Levy flight. (b) Particles on the 2-D function surface.

Figure 6.1: The demonstration of Lévy flight based PSO for a single objective function minimum search problem.

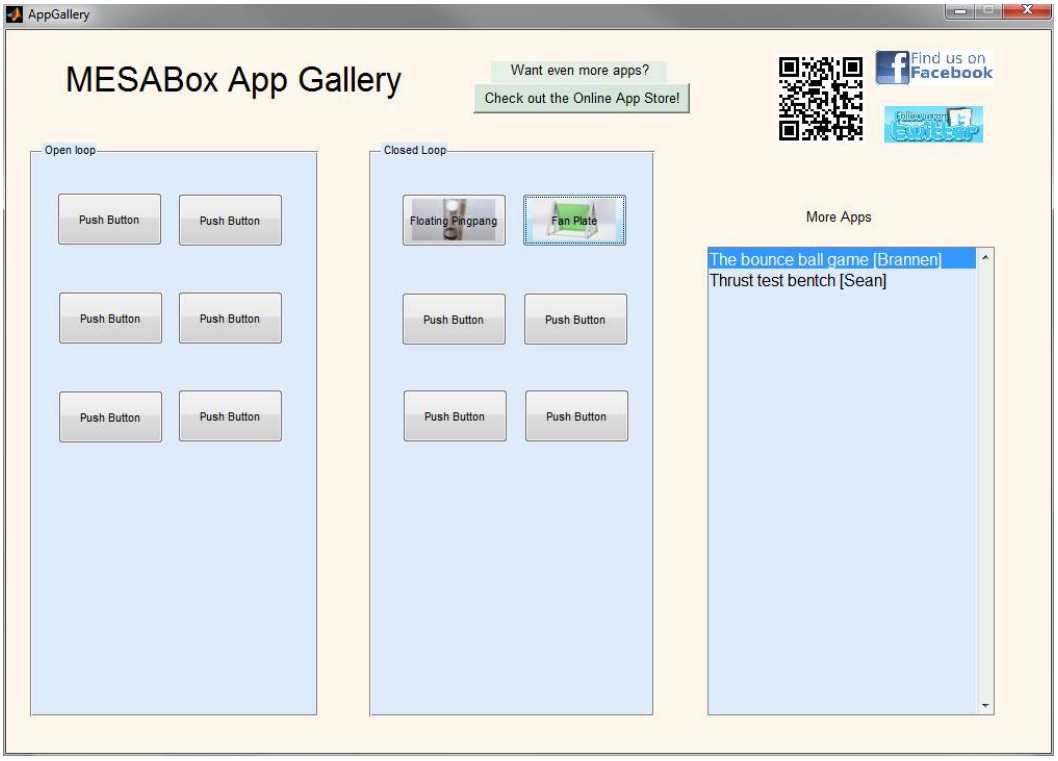

Figure 6.2: The snapshot of the MESABox Apps gallery.

gas flow, respectively. With the help of 3D printing technology, varieties of components are fabricated for fast-prototyping of control systems. A detailed description can be found in [432] and the associated workshop.

In order to demonstrate the use of typical sensors and actuators, dedicated Apps are developed. For example, the "Stagger Chassis App" uses infra-red sensors and motors driven by the Arduino motor shield board. The XBee bluetooth module is used for the

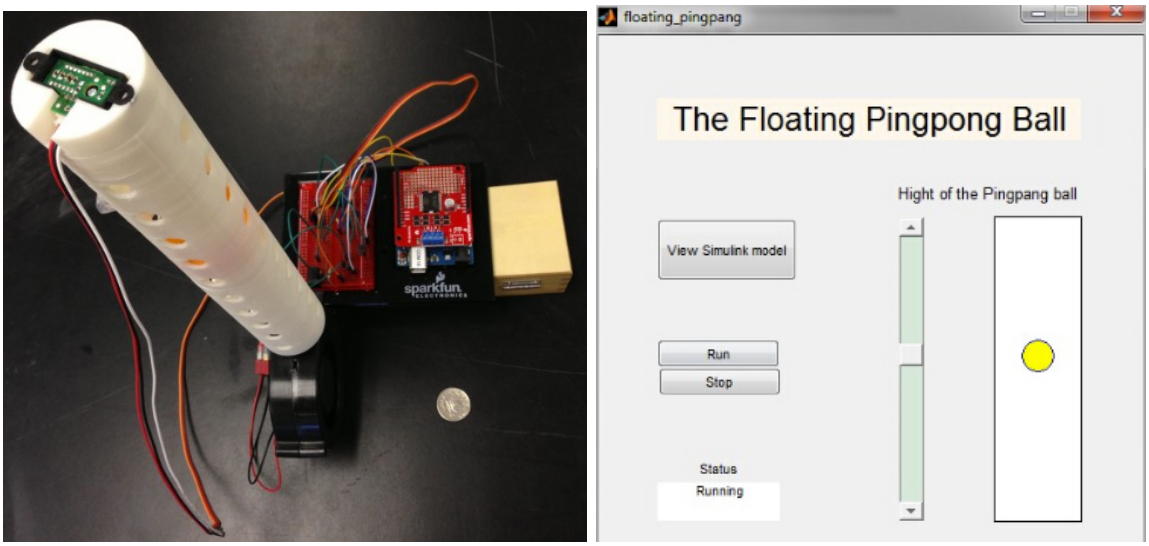

(a) Hardware of the Floating Ball App. (b) GUI of the Floating Ball App.

Figure 6.3: The Floating Ball App in the MESABox.

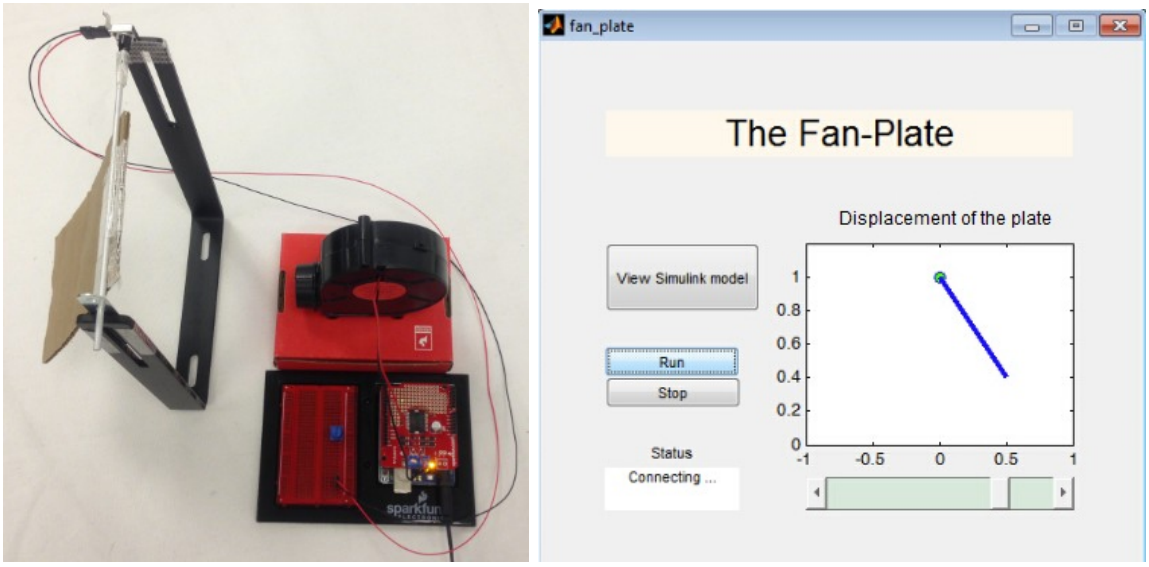

(a) Hardware of the Fan-Plate App. (b) GUI of the Fan-Plate App.

Figure 6.4: The Fan-Plate App in the MESABox.

communication with PC so that wireless control can be performed through Matlab/Simulink in real-time. This implementation has not been reported in the community. The hardware configuration and the supporting software GUI is shown in figure 6.5. As another example, the "Heating Box App" shown in figure 6.6 uses the resistance heating pads and thermal couples for temperature controls.

(a) Hardware. (b) GUI of the Stagger Chassis App.

Figure 6.5: The Stagger Chassis App in the MESABox.

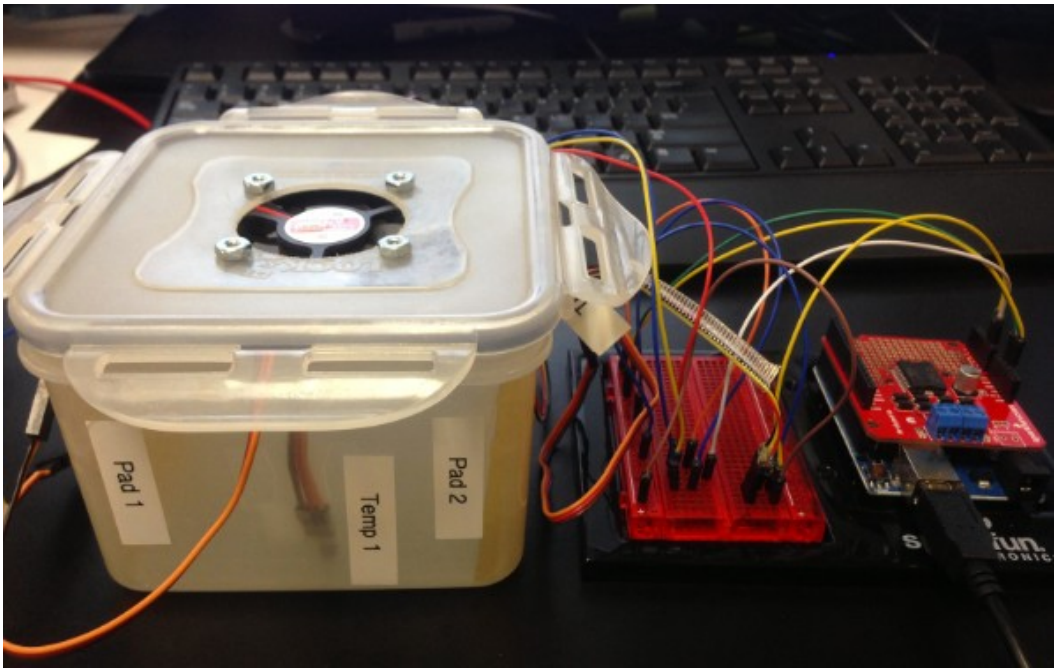

Figure 6.6: The Heating Box App in the MESABox.

6.3 EtherCAT timing jitter characterization

EtherCAT, (Ethernet for Control Automation Technology) is an Ethernet-based field-bus system invented by the German company Beckhoff Automation, [468]. It is later on developed into an international standard for the device communication in industrial controls. As a network based protocol, the timing of the packet cyclic among the networked devices is supposed to have jitter.

Jitter is the deviation from true periodicity of a presumed periodic signal in electronics and telecommunications, often in relation to a reference clock source, [469]. There are numerous types of jitter in electrical engineering, such as the sampling jitter in AD/DA (analog-digital/digital-analog) conversion, the packet jitter in computer networks, and the seek jitter in the audio disc extraction.

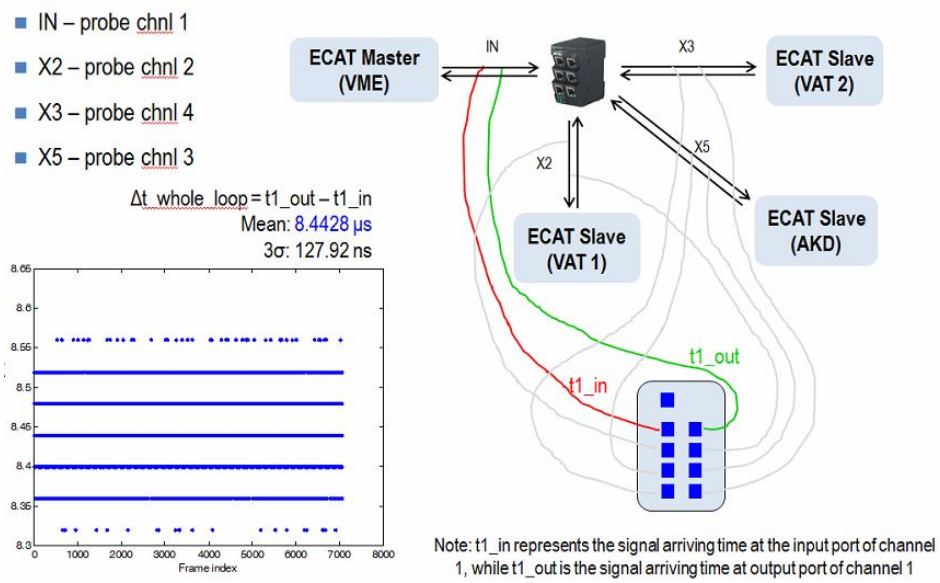

Figure 6.7: Hardware setup for the packets sniffing.

Jitter can be quantified in the same terms as all time-varying signals, e.g. root mean square (RMS) or peak-to-peak displacement. It is known that jitter distribution of the network communication is usually significantly *non-Gaussian* [470]. This can occur if the jitter is caused by external sources such as power supply noise. In these cases, peak-to-peak measurements might be more useful. Many efforts have been made to meaningfully quantify distributions that are neither Gaussian nor have meaningful peaks. In the monograph [469], the self-similar processes (defined below) in telecommunications are investigated. In [471], contributions to networked control systems using FC is discussed. Inspired by this research, the timing jitter analysis of an EtherCAT network in an industrial control system is performed.

Description 1 (Self-similarity)**.** *If* (X_{at}) *and* $a^H(X_t)$ *have identical finite-dimensional distributions for all* $a > 0$*, then* X *is self-similar with parameter* H *[472].*

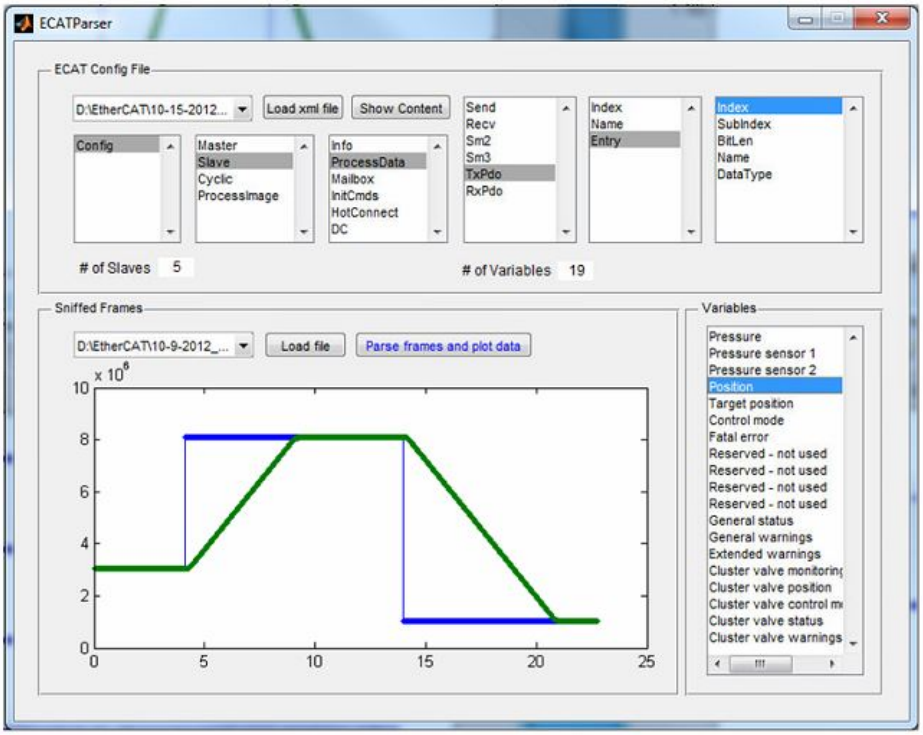

Figure 6.8: The Matlab based GUI for packets data parsing and analysis.

To capture the packets, an EtherCAT probe, ET2000 [473], is inserted into the network through the EtherCAT junction slave, Omron GX-JC06-H. The schematic of the hardware setup is shown in figure 6.7. The open-source network-sniffing software, Wireshark [474], is used to capture and log the packets into a PC. EtherCAT packets are extracted by applying some filters in Wireshark, such as "`eth.type ==0x88a4`" for specifying the Ethernet type, and "`esl.port==0 or esl.port ==2 and frame.len == 196`" for specifying the port and frame length.

A Matlab based GUI, as shown in figure 6.8, is developed to simplify the data parsing and the jitter analysis. Time stamps parsed by this GUI are shown in figure 6.9. Since the investigated network environment only contains 6 devices, which is relatively idle and pure, the timing jitter fits a Gaussian distribution in this circumstance.

6.4 Fractional calculus and finance - a cadenza section

Most academic researches have the potential to be converted into productive forces or economic benefits, and so does fractional calculus. The previous five chapters have shown the benefits of applying FC on industrial process control. In this section, some novel attempts of applying FC on financial market data analysis are discussed with theoretical hypotheses. While there are innumerable research work in this field, e.g. [475, 476], the author would just like to reveal some interesting attempts and discoveries, as some side work related to fractional calculus along the main thread of the dissertation research. This section does not serve as professional financial analysis or market prediction. It can be treated as either

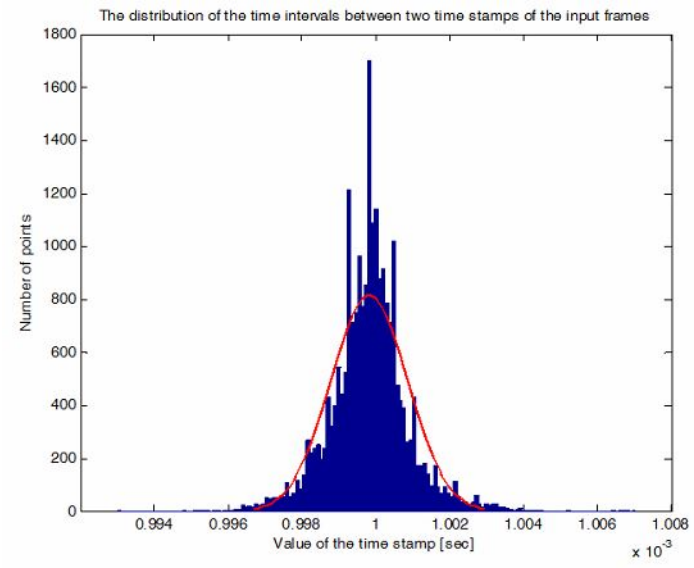

Figure 6.9: The distribution of the timing jitter.

hypothetical coincidence, or rhapsodic mindstorm. One of the original motivations of this research lies in the long time debated propositions: whether or not the financial market has long memory; whether or not it is predictable, etc. During the exploration, some tests with uncertain conclusion are attempted and bold conjecture are promoted.

6.4.1 Price has memory

Whether the financial market has long memory is a hot debated topic. Various propositions have been proposed in the literature. Some economists claim it has, while others are against this opinion. For example, [477] illustrates the existence of long-term memory in stock market prices; [226] proposes a new model for the long memory property of stock market returns; and [478] discusses the long range dependence (LRD) and self-similarity in the financial markets. Moreover, before investigating the long memory issue, in the first place, whether or not the price movement in the financial market is a stochastic process is even questioned. The following two sections express some of the author's reasoning. The long memory and LRD are closely related to the heavy-tailed distributions, which have been observed in many natural phenomena including physical and sociological phenomena, etc. Mandelbrot established the use of heavy-tailed distributions to model real-world fractal phenomena, e.g. Stock markets, earthquakes, climate, etc. To proceed, basic definitions of these terms are briefly given as the following.

Description 2 (Long range dependence)**.** *Long range dependence, also called long memory or long-range persistence, is a phenomenon that arises in the analysis of spatial or time series data. It relates to the rate of decay of statistical dependence, with the implication that this decays more slowly than an exponential decay, typically a power-low decay.*

The LRD phenomenon was first observed and documented by the British hydrologist Harold Edwin Hurst in 1951, during his study of reservoirs along the Nile river [479]. LRD is

often related to self-similar processes and has been used in various fields such as internet traffic modeling, econometrics, hydrology, linguistics and the earth sciences. Different mathematical definitions of LRD are used in different contexts and purposes. Some references can be found in [480]. Generally, a time series is said to have long range dependence if its covariance tends to zero as time goes, but so slowly that the sum of the covariance diverges,

$$\lim_{n\to\infty} Cov(x_0, x_n) = 0 \tag{6.3}$$

$$\sum_{n=0}^{\infty} |Cov(x_0, x_n)| = \infty. \tag{6.4}$$

Heavy-tailed distribution can be characterized by its pdf,

$$\lim_{x\to\infty} e^{\lambda x} P[X > x] = \infty \text{ for all } \lambda > 0. \tag{6.5}$$

The trend lines in technical analysis are the best application examples of price having memory. In addition, due to the fractal property of the price charts, the trend line analysis can be applied on any time scaled chart, indicating that prices have memory of both short and long term. Due to participant's psychological projection and their reaction, thereby, technical analysis works well quite often [481]. This is also why skeptics say it is a self-fulfilling prophecy.

6.4.2 Price has memory?

History can be extremely similar, but on the other hand, it doesn't repeat. Imagine, if history repeats, then the correlation, the trend of price charts and so on become so obviously informative that all players become winners in a game, which is not true from statistics. The fact is, although the financial market is not a zero-sum game, most participants lose [482], even investment banks. One of the recent examples account the application of bankruptcy protection by FXCM Inc. in January 2015 [483].

In the famous book "*A Random walk down wall street*" [227], the Princeton Economist Dr. Malkiel believes that stock prices are largely random. However, the randomness *does not* have long memory as he states, "*The stock market has little, if any, memory*". In the counter book, "*A Non-Random Walk Down Wall Street*" [484] by the MIT Finance professor Lo and the Wharton Finance professor MacKinla, a number of essays are collected offering empirical evidence that valuable information can be extracted from security prices. Therefore, they argue that the price movements are not completely random and predictable components do exist. However, on the LRD issues, they draw the same conclusion with Malkiel as they *do not* find long-term memory in stock market return data. Related research can also be found in [485].

While this argument is still controversial, one may choose to adopt a bit from each faction of the debate and agree that there are both random and non-random aspects in the financial markets. The following discussion views the "memoryless" issue from another perspective based on simple arithmetic. Leveraged exchange traded funds (ETFs) are a type of financial products invented a decade ago for tracking the daily performance of an index or commodity futures.

Example 6.1: Consider the scenario shown in figure 6.10(a). Assume A is a 3x leveraged ETF tracking the commodity B, and both of them worth \$10 a share/contract initially on day 1. On Day 2, B rises by 10% to \$11. So, A surges 30% to \$13 accordingly. On the next day, B plunges to \$9, which is a $1 - 9/11 = 18.18\%$ decrease. Hence, A follows B by 3x leverage, and drops by 54.54% to \$5.91. On day 4, B goes back to \$10, which is a $10/9 = 11.11\%$ increase. A increases by 33.33% to \$7.88.

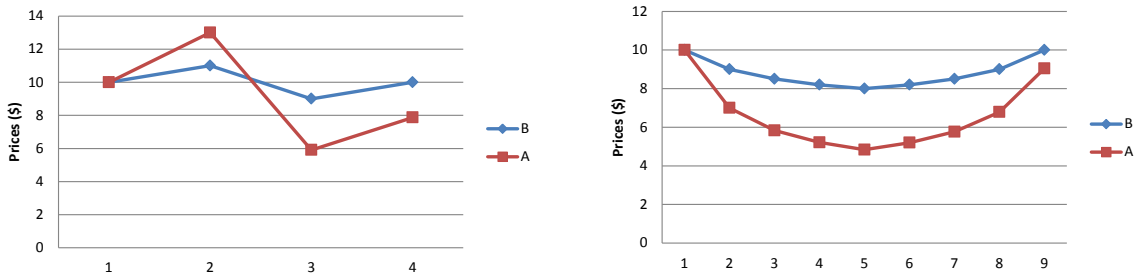

(a) Path 1. (b) Path 2.

Figure 6.10: The chart demonstration of path dependence in example 6.1.

After all, B recovers to the original value as if there is no movement, but A ends up at a price 21% lower than its origin. In spite of this property, the movement of A is path dependent, as demonstrated in figure 6.10(b). These are the common characteristics of leveraged ETFs. Moreover, the underlying futures/indices tracked by them suffer from contango. By the same token, their counterparts perform poorly as well, which is resulted by the beta-slippage [486] on top of the aforementioned reason. All these factors make these type of financial products doom to have a bearish bias. Their prices decline perennially in the big trend and have an *extremely* low possibility to return to the initial levels. There are only few circumstances where an leveraged ETF outperforms the underlying index. For instance, B increases gradually and smoothly. The above example can be formulated to a conditionally convergence problem of the following series,

$$A_k(x, B_k) = A_{k-1}(x, B_{k-1})[1 + x(\frac{B_k}{B_{k-1}} - 1)], \quad (B_k \geq \frac{2}{3}B_{k-1}), \tag{6.6}$$

where $k = 2, 3, \ldots$ denotes the number of day under investigation and x is the leveraged multiple. For this kind of financial products, the long term trends are so obvious that they *cannot* be characterized by random walk with Gaussian distributed step sizes. An initial short position would generate 99% profit in three-year time scope. From this sense, prices of this type of financial products has no memory.

One step further, this type of phenomenon can be treated as possessing *path dependent* characteristics, which is in contrast to the fundamental analysis emphasizing more on asset valuation. It is said that if the most general law of nature is to be chosen, then *principle of least action* should be counted for. However, it appears that the financial markets often decide to be heterogeneous from this law.This leads to the discussion in the next subsection.

6.4.3 The market is gaining entropy

In [487], the idea of using entropy as a measure of stock market volatility is proposed. The market trends to more disorder [488, 489]. In [490], a hypothesis that maximum entropy production principle governs the stock returns was proposed. While the Shannon entropy yields exponential equilibrium distributions, Tsallis entropy yields power-law distributions which is related to fractional calculus. A truly large system tends to be complex [491, 492], and disorder can be expected.

More intuitively, for the sake of the following reasons: 1) the increase in the amount of participants, 2) convenient availability to information, and 3) the improvement of participants' knowledge level, the conventional advantages of institutional traders become weak, such as the timely accessibility to breaking news and the privilege of viewing the market depth, etc. Hence, a single factor which could dominate the market is no longer as dominant as before. The number of participants who do not follow conventional routines are increasing. The system is gaining complexity and unpredictability, therefore, it is becoming more and more disorder. Thus, anomalous events happen more and more often. For example, a good earnings report and financial guidance of a company may drive a sell-off of its stock, e.g. Jakk Pacific on Oct 23, 2014, or Foot Locker on Nov 21, 2014. More examples can be observed in the commodity markets.

These evidence and reasoning imply that the market is gaining entropy. This does not necessarily mean a bull or bear market, but may indicate a more volatile and unpredictable market in which profiting becomes harder. This leads to the following discussion about extreme events.

Description 3 (Extreme events)**.** *There is no officially precise definition of extreme events. Often, it refers to the events with an occurrence of the most unusual percentage in human's historical records.*

For instance, the flash mob, variant Jasmine Revolution, "occupy wall street" and the recent "occupy center" in Hongkong are social extreme events; the well-known El Niño phenomenon is an example of the extreme weathers. More extreme events can be found in [493] and the "Book of extremes" [225]. In the PM Magazine, Dr. Linda Kiltz states:

> "This sense of powerlessness is part of the motivation behind the Occupy Wall Street protests that started in September 2011 in New York City and are spreading across the nation to such cities as Boston, Chicago, Denver, Seattle, and Washington D.C. While these groups are not flash mobs, they are using social media to organize, communicate, and raise awareness on a number of issues. As the use of social media increases, the potential for more flash mobs that are used for political protest and for criminal purposes is likely to increase."

For these types of unexpected events, the extent of randomness is controversial. From outsiders' point of view, they are thoroughly random. However, on the other hand, to the organizers, these events are deterministic because they planned the events and knew those would happen in advance, although they might not foresee the scale and influence. This

brings us back to the original question about whether the market is predictable, which is similar to the doubt: if there exists an prophet who can see the future. The answer to this question can be referred to the principle of entropy increase. Murphy's law is often cited as a form of the second law of thermodynamics (the law of entropy) because both are predicting a tendency to a more disorganized state [489]. This is one of the motivations to cite Murphy's law in the beginning of the chapter.

If there exists a Maxwell demon who could generate negative entropy such that the disorder could be drained and the universe could be made deterministic, then, does this fall into a kind of predictability. Or, if there exists a wise man like the Laplace demon [494], who possesses the knowledge of the position, velocity, forces, etc, of all the atoms in the universe, then, he/she could predict the future. Unfortunately, this has been proven impossible because the data processing capability for such a demon exceeds the limit obtained from the max entropy of the universe, light speed, and the elapse time of information transmitted through a Planck length. Similarly in the stock market, if one knows every single participant's current action and the action plan for the next time period, then, he/she could predict the market. However, the fact is that given today's huge number of participants and high frequency of trading, it is impossible. Any prediction turns out to be a form of gambling as in Nash's prisoner dilemma. Encouragingly, the coming of the big data era could partially realize this "delusion" to a small extent. Benefited from this technology, novel trading indicators are invented to analyze the market momentum, for example, the sentiment interpretation of the employees of a company, the aggregated user sentiment on social media networks, etc. Related research work can be found in [495, 496].

6.4.4 Burst, spikiness, and pump & dump

There is increasing evidence that the timing of many human activities is characterized by bursts of rapidly occurring events separated by long periods of inactivity. In [497], it is shown that the burst nature of human behavior is a consequence of a decision-based queuing process: when individuals execute tasks based on some perceived priority, the timing of the tasks will be heavy tailed.

Bursts and spikiness can be observed occasionally on the price charts of small-cap penny stocks. Following a burst, there is usually a decay which appears like pumping-and-dumping an inflammable balloon. Usually, analysts employ technical tools based on Fibonacci sequence to project the stabilization level of the price or the potential next spike. The Fibonacci sequence has a wide application in chart analysis, for example, the Fibonacci projection, the Fibonacci fan line and the Fibonacci retracement.

Description 4 (Fibonacci sequence)**.** *In mathematics, the Fibonacci sequence is the numbers in the following integer sequence,*

$$F_n = F_{n-1} + F_{n-2} \quad (n > 2). \tag{6.7}$$

It is well known that when $n \to \infty$, the ratio of the adjacent two numbers in the Fibonacci sequence converges to the golden ratio, φ,

$$\lim_{n\to\infty} \frac{F_{n-1}}{F_n} = \varphi = 0.61803\cdots, \tag{6.8}$$

and it has a property that

$$\lim_{n\to\infty} \frac{F_{n-m}}{F_n} = \varphi^m. \tag{6.9}$$

By empirically viewing the shape, the decay can be often better fitted by inverse power law rather than exponential law. Curiosity may rise the question that whether or not the combination of the golden ratio with fractional calculus is useful in this case as a projection tool. Hence, the fitting of some stock price burst data is attempted using the α-stable distribution pdf curves, with $\alpha = \varphi$ and β, γ, δ fitted automatically. Note: there may or may not be any principles in the background, and the legal issues are not addressed here. Only the shapes in the charts are analyzed and a gallery of fitting is generated for research documentation, as exhibited in figure 6.11.

6.4.5 A Hurst exponent based technical indicator

6.4.5.1 Self-similarity and Hurst estimates

It is commonly adopted that most technical indicators and candlestick patterns can be applied on any time scale of an underlying security or index, because analysts believe that the stock price charts are fractal and self-similar [498]. For example, the candlestick patterns can be applied on 5-min chart, hourly chart, daily chart and monthly chart, etc. The Hurst exponent is an effective measure of the long term memory and self-similarity of a time series, and is usually used to analyze stock returns, $r_t = log(P_t) - log(P_{t-1})$.

Description 5 (Hurst exponent)**.** *The Hurst exponent is used as a measure of long-term memory of time series. It relates to the autocorrelations of the time series, and the rate at which these decrease as the lag between pairs of values increases. [479]*

The fractal dimension is sometimes used as another inspector of self-similarity. The major definitions of fractal dimension use Hausdorff-Besicovitch Dimension or the box-counting.

Description 6 (Fractal Dimension)**.** *The fractal dimension, also referred to as capacity dimension, is a ratio providing a statistical index of complexity comparing how detail in a pattern (strictly speaking, a fractal pattern) changes with the scale at which it is measured [499].*

$$d_{cap} = -\lim_{n\to\infty} \frac{\ln N_n}{\ln L_n}, \tag{6.10}$$

where N_n is the number of solid boxes and L_n is the length of a side of a hole.

It is well known that for the Menger Sponge, the capacity dimension is $d_{cap} = \log_3 20 \approx 2.727$. In [500], Bayraktar *et. al* estimated the fractal dimension of the Standard & Pool 500 (S&P500) index using Wavelet Analysis. Using Matlab 1D, 2D and 3D Box-counting, the fractal dimension of S&P 500 index from year 2010 to 2015 can be computed, as shown in figure 6.12.

Many fundamental analysts criticize the technical analysis to be a self-fulfilling prophecy, as many people's pursuit of the analyzing rules makes the rules more robust. All technical

traders adjust their positions by anchoring at the alleged critical price levels, which eventually makes the levels given by technical analysis seemingly justified. This may be one of the factors that makes the stock return data possess self-similarity.

6.4.5.2 The proposed technical indicator

Many studies can be found in the literature regarding the use of Hurst exponent for financial market analysis [501]. In this subsection, a novel way of using the Hurst exponent in the form of a technical indicator is presented.

Description 7 (Technical indicators)**.** *In technical analysis, a technical indicator is a mathematical calculation based on historic price, volume information, or open interest of futures contracts, that aims to forecast financial market direction.*

There are more than 100 types of technical indicators for chart analysis [502]. They are generally classified into 4 categories:

1. Momentum, such as stochastic (%K,%D), Relative Strength Index (RSI), Aroon Index;
2. Trend, such as MACD, Average True Range (ATR);
3. Volume, such as VWAP;
4. Overlays, such as Bollinger Bands, Parabolic SAR, etc.

Inspired by the principle of the center oscillation type indicators, similar calculation technique is applied to the proposed Hurst exponent based indicator. Let one Hurst estimation evaluate more points and the other evaluate less, then, a plot of two crossing curves can be generated. The recommended default numbers of points are 200 and 50, which respectively, are approximately the number of trading sessions per year, and the industrial convention for checking moving-average crossovers. To demonstrate, the application of this indicator to the VIX index and the S&P 500 index are shown below as examples.

Description 8 (VIX)**.** *Introduced in 1993, the Chicago Board Options Exchange's S&P 500 volatility index (VIX) provides a snapshot of expectations about future stock market volatility.*

VIX is usually used to gauge fear and greed in the market and is one of the market breath. Hence, it is also known as the fear index, which generally moves in the opposite direction to the overall stock market. The mathematical computation of VIX can be found in [503]. Figure 6.13 shows the running Hurst estimation on the VIX derivative. To the author's knowledge, there has not been such discussion in the literature. It can be seen from this figure that when the running Hurst exponent (blue curve) diverges far from the overall value (red curve), there is a relatively larger spike following.

This indicator does not signal a buy/sell point, yet, it implies how far the current performance of an underlying security resides from its normal behavior performance.

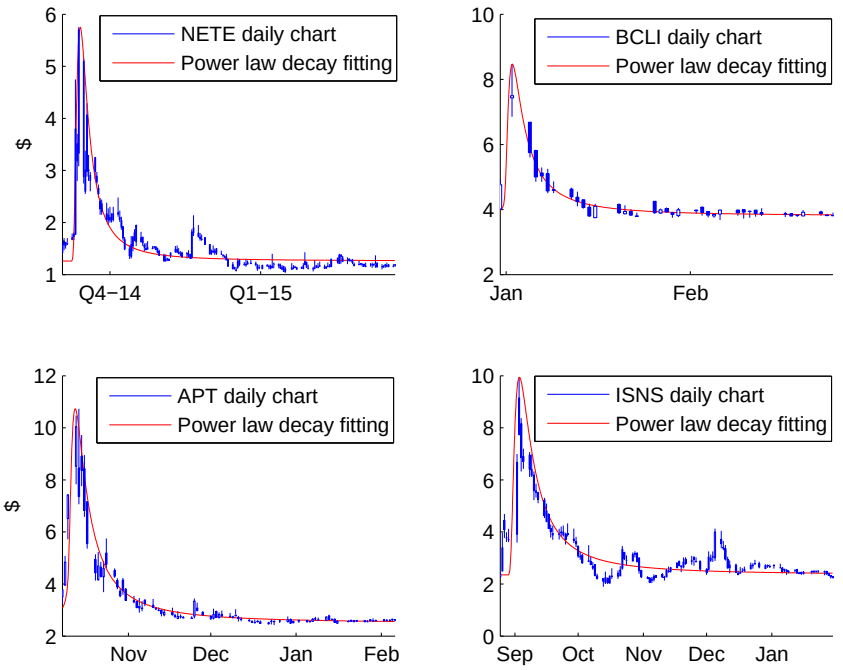

(a) Sample 1-4.

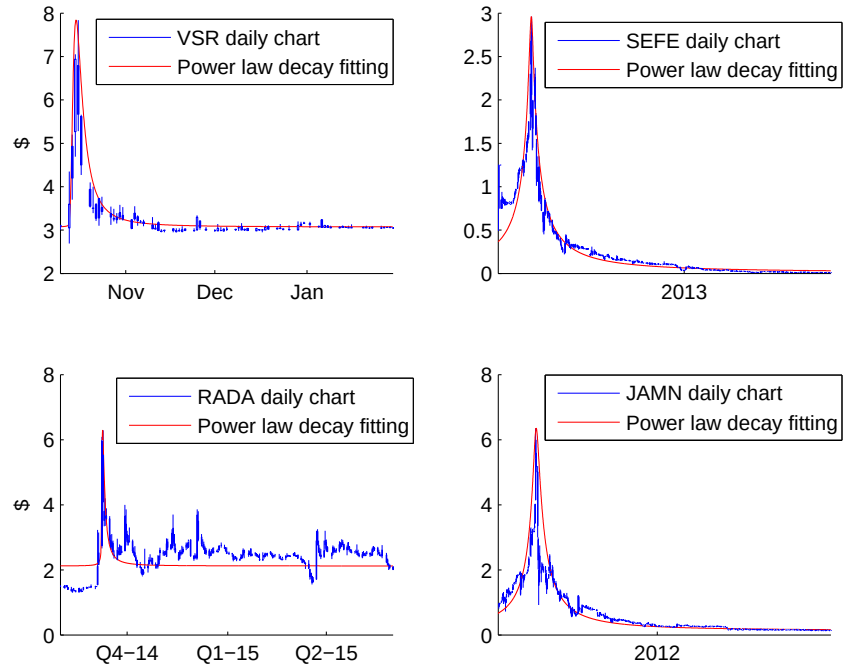

(b) Sample 5-6.

Figure 6.11: A gallery of fitting the decay after bursts using power law decay curves.

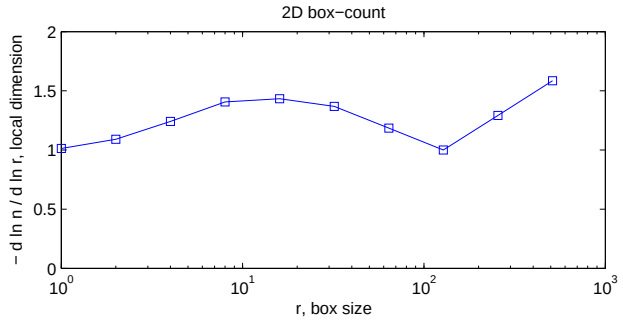

Figure 6.12: The fractal dimension of spy.

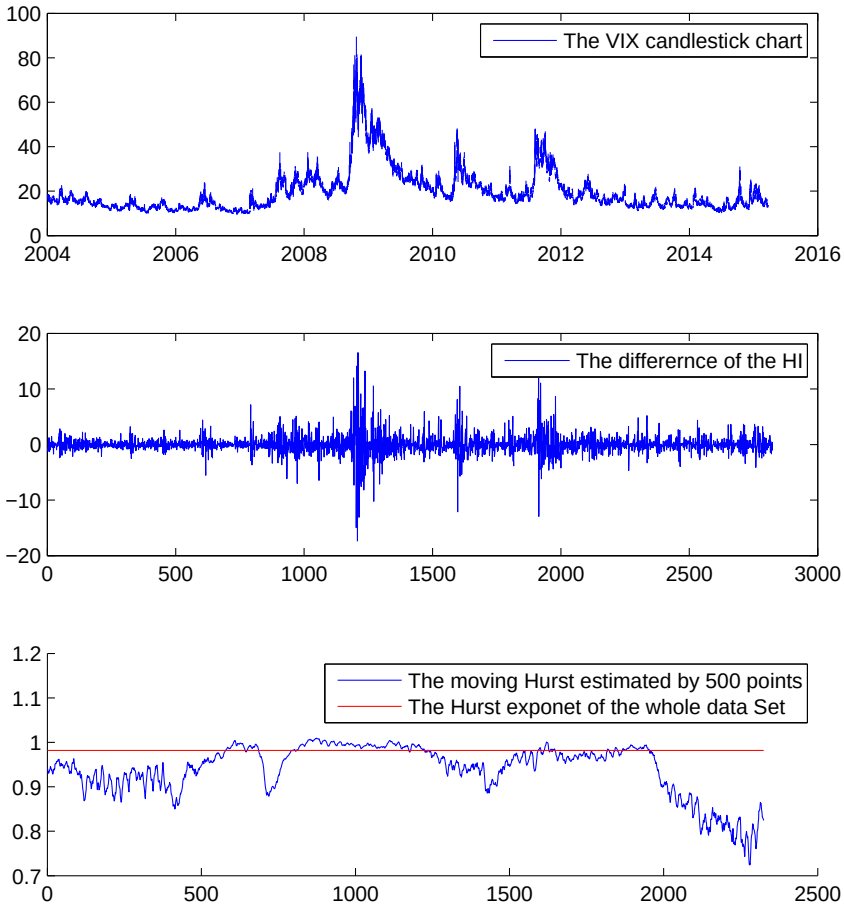

Figure 6.13: The VIX index daily chart and the running Hurst estimation of its derivative.

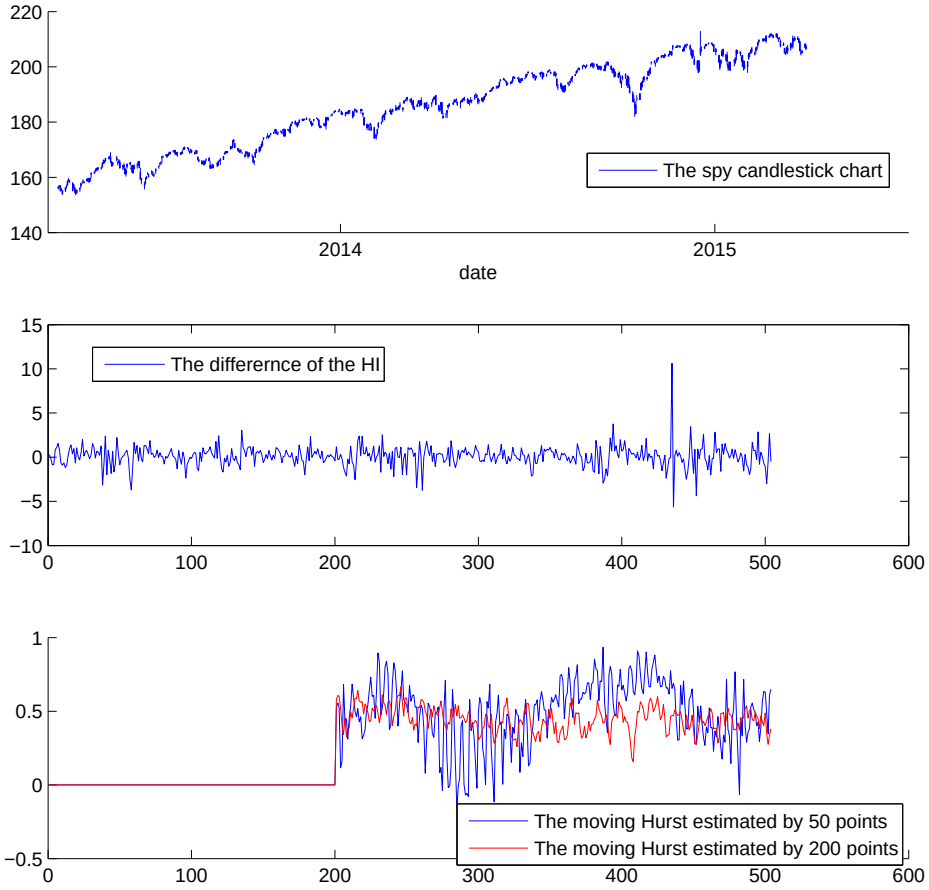

Figure 6.14: Applying the proposed technical indicator on SPY.

Chapter 7

Summary and Future Work

> A lifetime of glory is worth a moment of pain.
>
> — Laura Hillenbrand, *Unbroken*

A longer-term of benefits for system performance is worth a moment of fractional order modeling and control.

7.1 Summary

As expressed throughout the forgoing chapters, the intention and passion of this dissertation is to provide a turnkey solution for fractional order modeling and control of industrial processes. To summarize, the overall workflow for dealing with a process using the proposed FO modeling and control methodology is briefly listed below:

1. Obtain the historical data of the object process if available; review the behavior and determine the control objective, I/O constraints and potential difficulties. If no historical data is available, perform simple tests, such as ramping up the input gradually, to grasp an initial impression of the process.
2. Depending on the extent of nonlinearity, design suitable input excitation in terms of frequency, amplitude and shape. Section 3.4.2 can be refereed to for the design process.
3. After reviewing the process response to the designed inputs, determine the model structure to be used. A selection from the "model pool" in sections 3.2 and 3.4 can be made.
4. For MIMO processes, determine the number of inputs and outputs, and quantify the input-output paring and loop interactions using the acquired data. Section 3.5 can be used as a guide for this procedure.
5. With the selected model structure, model parameters can be identified using the listed methods in section 3.3, such as least squares and relay feedbacks. If these two methods are not enough, refer to the cited references therein.

6. Now that the model is obtained, a validation can be performed by examining and comparing the model output and actual output under the same input signals. If the non-model-based control laws are to be used, e.g. the FO ESC in section 4.4 or the FOPID in 4.5, then, modeling is not a necessary step and the above three steps can be skipped.
7. Next, determine the applicable control type according to the performance requirements, for example, time optimality, steady-state tracking accuracy, disturbance rejection, least loop interaction or minimal overshoot, etc.
8. Finally, the controller can be designed by following the corresponding procedures in section 4.5.1 to 4.5.

With the word "fractional order" appearing more than 100 times in this context, readers might feel tired of hearing and talking about it. Don't be terrified because this is just the beginning. As claimed by many authors of the cited books, this is just the beginning of a voyage to a vast ocean, just the beginning of a long road to a broad plane. Given sufficient time, fractional order modeling techniques are destined to be the inevitable way of characterizing the nature.

7.2 Future work

Fractional calculus opens up a whole new arena for modern controls. The topics covered in this dissertation are just like a toe of a giant, and there is a much bigger portion of interesting topics to be explored and many problems to be solved. Some potential research opportunities have been identified in the main chapters. They are briefly stated here as a summary.

Fractional order Rayleigh differential equation

To the author's knowledge, there is not yet deep investigation of the fractional order Rayleigh differential equation available in the literature. While four possible forms are proposed in section 2.2.1.2, questions are still open with regard to the following topics: whether there are other possible forms; which form has physical meaning so that real data support can be obtained, etc. Moreover, it is known that the classic integer order Van der Pol equation can be derived from the integer order Rayleigh's differential equation, while the fractional order VDP cannot be derived from the corresponding FO Rayleigh's differential equation. However, what variant FODEs can be derived from the FO Rayleigh's differential equation is to be studied.

Fractional order feedback linearization

The discussion on the feedback linearization of nonlinear FO processes is very limited in the literature. Even definitions are not given. Hence, definitions, preliminary theorems, the design rules for control laws, and a particular case study are given in sections 3.4.3 and 5.5, under certain assumptions. Nevertheless, due to mathematical difficulty in dealing with the nested fractional order derivatives, no generalized results are obtained. Hence, the feedback linearization of more classes of FO nonlinear processes can be another further

research opportunity. More experimental results or practical implementation evaluation are also expected.

Embedded RIOTS for FOCP and FO MPC

As introduced in section 4.3, RIOTS is a powerful numerical tool for solving traditional optimal control problems. Tricaud *et. al* extended the use of RIOTS to FOCPs. Zhao *et. al* pushed the use of RIOTS to the model predictive control of a fractional order thermal process simulation. Li *et. al* implemented the RIOTS based MPC on an hardware-in-the-loop temperature control experimental platform which had fractional order dynamics. With this step-by-step advancement, a good foundation is established for approaching the ultimate goal, i.e. an *embedded RIOTS* for both integer and fractional order optimal and predictive controls. The next move towards this goal is to implement the RIOTS on micro-controllers or DSPs or FPGAs for stand-alone application. This is motivated by the sponsoring industrial project of equipment temperature control. To realize this goal, the FPGA realization of FO models reviewed in chapter 1 can be used. Besides, the conversion of the RIOTS algorithm onto DSPs and the online model adjustment for fractional order MPC need to be accomplished, which could expand this goal to a huge project involving tremendous development and debugging efforts. However, once these are achieved, much more practical benefits to the industry can be expected.

MESABox apps for fractional order control tutorial

Section 6.2 introduced the development of MESABox for mechatronics course teaching and control system tutorial. In addition to the three MESABox apps shown in the app gallery, students are encouraged to develop their own control apps and integrate them into the gallery so that more apps can be demonstrated for the next year education. For example, a student from the last year class created an Arduino-driven pond game board using the components in the MESABox. Currently, the available three demonstrating apps are based on "black box" models using PID feedback control. To better help students with understanding the dynamics, mathematical models could be built. While existing work can be found in the literature using conventional approaches, e.g. the modeling and control of a floating ball inside a tube in [504], it is worth trying the discussed fractional order modeling techniques, e.g. employing the fractional Bernoulli equation for modeling, etc. The modeling of the existing hardware setups for the corresponding apps could also be designed as lab modules for students to learn and practice the nonlinear fractional order system identification.

Optimal parameter tuning for FO SM ESC

Parameter tuning of many types of controllers is not an easy task, and it is sometimes tricky, especially for the sliding mode based ESC. It is shown in section 5.7 that the parameters of the SM ESC have big impact on the performance. Including the fractional order reaching law will add more tuning nobs to be determined, which makes the tuning even harder. Therefore, the problem of finding the optimal set of parameter values for the FO SM ESC arises. Some researchers consider this problem as a multi-objective optimization problem. For example, [505] presented the tuning of FO controllers using PSO for a four tank level process. In [506],

Abdelhamid *et. al* also used the PSO algorithm to design the FO SM controller for a class of nonlinear commensurate order systems. On the other hand, the way of solving this problem is not unique, and the enumerated two methods do not claim "optimality". There is still work to be done on this research direction.

"Heavy-tailed" randomization based multi objective optimization

The above discussed topic promotes the demand of multi-objective optimization in the fractional order controls field. Conventionally, meta-heuristic algorithms are often used to fulfill the task. Most meta-heuristic algorithms rely on the random number generation based on Gaussian or unform distributions. However, it has been evidenced by literature that heavy-tailed distributions could provide better performance in many scenarios. The Lévy flight based PSO described in section 6.1 is one such example. While some algorithms are tested with the heavy-tailed distributions for particular cases, there has not been systematic investigation to show how the randomness acts on different algorithms for different types of problems. For example, for the multi-objective optimization of a class of non-smooth functions, whether there is a unique combination of parameters for an α-stable distribution based random search algorithm is uncertain. These questions may be NP (nondeterministic polynomial time) or NP hard that can not be proven analytically.

Power efficient fractional order control

The power efficiency is always a big concern in control engineering, but the research on fractional order control has not covered this topic intensively. One of the very few studies is carried out by Tavazoei *et. al* [90], and another is the power efficiency of indoor lighting control by Yin *et. al* [49], as mentioned in section 4.4. Nevertheless, the power and energy considered in these research are in the mathematical point of view, e.g. the indicator of the energy consumption takes a quadratic form of the voltage. This is similar to the thinking in Lyapunov functions which usually use quadratic forms of the system states as the indicator of the system energy and it is not necessarily the practical energy in the sense of physics. Hence, the topic of power efficiency is planned to be further investigated in terms of the actual product of voltage and current. Hardware, such as the non-invasive current sensor using inductive coupler, is prepared to perform the experiment on the Peltier based temperature control platform described in section 5.1. The results will be a valuable contribution to the FO control research community.

Other control schemes to be extended to fractional order

Besides the control schemes discussed in chapter 4, there are many more that can be implanted with "fractional order", or be potentially used on fractional order systems, such as the computed torque control, preview control, load balancing control, matrix fraction description (MFD) [507], fractional order run-to-run control, fractional order adaptive control [362], etc.

All in all, there are just so many opportunities in this exciting research field, which provides infinite hope to the future industry.

"We were home.
How do you pick up the threads of an old life?
How do you go on,
when in your heart,
you begin to understand,
there is no going back?
There are somethings that time cannot mend
some hurts that go too deep...
that have taken hold"
— J.R.R Tolkien, (in The Lord of the Rings)

References

[1] R. Borkar, M. Bohr, and S. Jourdan, "Advancing Moore's law - the road to 14 nm," Intel Corp. 14 nm FinFET product announcement presentation, Aug 2014.

[2] A. Tepljakov, "Fractional-order calculus based identification and control of linear dynamic systems," Master's thesis, Tallinn University of Technology, Estonia, 2011.

[3] S. Dine, J. Jolly, and J. Guillon, "Coupled power and plasma impedance measurements in a VHF capacitive discharge in hydrogen," Archive in Laboratoire de Physique et Technologie des Plasmas Ecole Polytechnique, Palaiseau, France.

[4] F. L. Lewis, *Applied Optimal Control and Estimation*. Prentice-Hall, 1992, ch. 1: Introduction to Modern Control Theory.

[5] S. Y. Nof, Ed., *Springer Handbook of Automation*. Springer, 2009.

[6] H. Janocha, *Actuators: Basics and Applications*. Springer, 2004.

[7] Funakubo, *Actuators for Control*, ser. Precision Machinery and Robotics. CRC Press, 1991, vol. 2.

[8] C. A. Smith and A. B. Corripio, *Principles and Practice of Automatic Process Control*. John Wiley & Sons, Inc., 2006.

[9] Stanford Nano-fabrication Facility, "Oxford ICP 100 dry etcher," [Online] http://snf.stanford.edu/, 2015.

[10] T. P. A. Laboratory, "ICP plasma through argon in the GEC reactor," [Online] (University of Texas at Dallas) http://www.utdallas.edu/~overzet/PALpict.htm, 2015.

[11] G. W. Bohannan, "Analog realization of a fractional control element - revisited," in *Proc. of the 41st IEEE Intl. Conference on Decision and Control (CDC), Tutorial Workshop 2: Fractional Calculus Applications in Automatic Control and Robotics*, Las Vegas, NV, 2002.

[12] ——, "Analog fractional order controller in temperature and motor control applications," *Journal of Vibration and Control*, vol. 14, no. 9, pp. 1487–1498, 2008.

[13] J. A. T. Machado, I. S. Jesus, A. Galhano, J. B. Cunha, and J. K. Tar, *Electrical Skin Phenomena: A Fractional Calculus Analysis*. Springer, 2013, ch. 5, pp. 305–322.

[14] G. Catania and S. Sorrentino, *Analytical modelling and experimental identification of viscoelastic mechanical systems*. Springer, 2013, ch. 6, pp. 403–416.

[15] M. D. Paola, F. P. Pinnola, and M. Zingales, "Fractional differential equations and related exact mechanical models," *Computers and Mathematics with Applications*, vol. 66, pp. 608–620, 2013.

[16] A. Chauchois, D. Didier, A. Emmanuel, and D. Bruno, "Use of noninteger identification models for monitoring soil water content," *Measurement Science and Technology*, vol. 14, pp. 868–874, 2003.

[17] R. L. Magin, *Fractional calculus in bioengineering*. Begell House Inc., 2006.

[18] T. J. Freeborn, "A survey of fractional-order circuit models for biology and biomedicine," *IEEE Journal on Emerging and Selected Topics in Circuits and Systems*, vol. 3, no. 3, pp. 416–424, 2013.

[19] J. Sabatier, O. P. Agrawal, and J. A. T. Machado, *Advances in Fractional Calculus - Theoretical Developments and Applications in Physics and Engineering*. Springer, 2007.

[20] K. S. Miller and B. Ross, *An Introduction to the Fractional Calculus and Fractional Differential Equations*, 1st ed. New York, NY, USA: Wiley-Interscience, 1993.

[21] K. Oldham and J. Spanier, *The Fractional Calculus: Theory and Application of Differentiation and Integration to Arbitrary Order*. New York, NY, USA: Academic Press, 1974.

[22] D. Valério and J. S. da Costa, *Advances in Fractional Calculus: Theoretical Developments and Applications in Physics and Engineering.* Springer, 2007, ch. Identification of fractional models from frequency data, pp. 229–242.

[23] W. Mitkowski, J. Kacprzyk, and J. B. (Editors), *Advances in the theory and application of non-integer order systems.* Springer, 2013.

[24] H. W. Bode, *Network Analysis and Feedback Amplifier Design.* New York: D. Van Nostrand Company, Inc., 1945.

[25] M. Axtell and M. E. Bise, "Fractional calculus applications in control systems," in *Proc. of the Nat. Aerospace and Electronic Conf.*, New York, NY, 1990, pp. 563–566.

[26] R. L. Bagley and R. A. Calico, "Fractional order state equations for the control of viscoelastically damped structure," *Journal of Guidance*, vol. 14, no. 2, pp. 304–310, 1989.

[27] I. Podlubny, "Fractional-order systems and $PI^{\lambda}D^{\mu}$ controllers," *IEEE Transactions on Automatic Control*, vol. 44, no. 1, pp. 208–214, 1999.

[28] I. Petráš, "Stability of fractional-order systems with rational orders: A survey," *Fractional Calculus & Applied Analysis*, vol. 12, no. 3, pp. 269–298, 2009.

[29] I. Podlubny, I. Petráš, B. M. Vinagre, P. O'Leary, and L. Dorčák, "Analogue realizations of fractional-order controllers," *Nonlinear Dynamics*, vol. 29, pp. 281–296, 2002.

[30] L. Brančík, J. Valsa, E. Gonzalez, J. Terpak, I. Petras, and L. Pivka, "Analogue realization of fractional-order dynamical systems," *Entropy*, vol. 15, no. 10, pp. 4199–4214, 2013.

[31] I. Petráš, L. Brančík, I. Podlubny, J. Terpak, and P. O'Leary, "Implementation of fractional-order controllers on PLC," in *Proc. of the International Carpathian Control Conference (ICCC)*, Miskolc, Hungary, 2005, pp. 141–144.

[32] E. A. Gonzalez, J. Y. Hung, L. Brančík, J. Terpak, and I. Petráš, "Posicast control of a class of fractional-order processes," *Central European Journal of Physics*, vol. 11, no. 6, pp. 868–880, 2013.

[33] I. Petráš, *Fractional-Order Nonlinear Systems: Modeling, Analysis and Simulation.* China: Springer Science & Business Media, Jointly published by Higher Education Press, 2011.

[34] D. Sierociuk, A. Dzieliński, G. Sarwas, I. Petráš, I. Podlubny, and T. Skovranek, "Modeling heat transfer in heterogeneous media using fractional calculus," in *Proc. of the ASME International Design Engineering Technical Conferences & Computers and Information in Engineering Conference (IDETC/CIE)*, Washington, DC, USA, Aug 2011.

[35] C. A. Monje, Y. Chen, B. M. Vinagre, D. Xue, and V. Feliu, *Fractional order Systems and Controls: Fundamentals and Applications.* Springer, 2010.

[36] Y. Chen, Petráš, and D. Xue, "Fractional order control - a tutorial," in *Proc. of the 2009 American Control Conference, (ACC '09)*, St. Louis, MO, USA, June 2009, pp. 1397–1411.

[37] Y. Chen and K. L. Moore, "Discretization schemes for fractional-order differentiators and integrators," *IEEE Transactions on Circuits and Systems - I:Fundamental Theory and Applications*, vol. 49, no. 3, pp. 363–367, 2002.

[38] Y. Li, H. Sheng, and Y. Chen, "Impulse response invariant discretization of a generalized commensurate fractional order filter," in *Proc. of the 8th World Congress on Intelligent Control and Automation*, Jinan, China, 2010, pp. 191–196.

[39] ——, "Analytical impulse response of a fractional second order filter and its impulse response invariant discretization," *Signal Processing*, vol. 91, no. 3, pp. 498–507, 2011.

[40] H. Sheng, Y. Chen, and T. Qiu, *Fractional Processes and Fractional-Order Signal Processing.* Springer, 2012.

[41] H. Li, Y. Luo, and Y. Chen, "A fractional order proportional and derivative (FOPD) motion controller: Tuning rule and experiments," *IEEE Transactions on Control Systems Technology*, vol. 18, no. 2, pp. 516–520, 2010.

[42] Y. Luo and Y. Chen, "Fractional-order [proportional derivative] controller for robust motion control: Tuning procedure and validation," in *Proc. of the American Control Conference (ACC)*, St. Louis, Missouri, USA, 2009, pp. 1412–1417.

[43] C. A. Monje, B. M. Vinagre, Y. Chen, V. Feliu, P. Lanusse, and J. Sabatier, "Optimal tunings for fractional $PI^{\lambda}D^{\mu}$," *Fractional Derivatives an Their Applications, Part. 3: Systems analysis, implementation and simulation, systems identification and control, UBooks*, vol. 2809, pp. 675–686, 2005.

[44] C. A. Monje, A. J. Calderon, B. M. Vinagre, V. Feliu, and Y. Chen, "On fractional PI^{λ} controllers: some tuning rules for robustness to plant uncertainties," *Nonlinear Dynamics*, vol. 38, pp. 369–381, 2004.

[45] Y. Chen, D. Xue, and T. Bhaskaran, "Practical tuning rule development for fractional order proportional and integral controllers," *Journal of Computational and Nonlinear Dynamics*, vol. 3, no. 2, pp. 498–507, 2008.

[46] I. Suárez, B. M. Vinagre, A. J. Calderón, C. A. Monje, and Y. Chen, "Using fractional calculus for lateral and longitudinal control of autonomous vehicles," *A Chapter in the Lecture Notes in Computer Science (LNCS), Springer Verlag*, vol. 2809, pp. 337–348, 2003.

[47] Y. Luo, T. Zhang, B. Lee, C. Kang, and Y. Chen, "Disturbance observer design with Bode's ideal cut-off filter in hard-disc-drive servo system mechatronics," *Mechatronics*, vol. 23, no. 7, pp. 856–862, 2013.

[48] ——, "Fractional-order proportional derivative controller synthesis and implementation for hard-disk-drive servo system," *IEEE Transactions on Control Systems Technology*, vol. 22, no. 1, pp. 281–289, 2014.

[49] C. Yin, B. Stark, Y. Chen, and S. Zhong, "Adaptive minimum energy cognitive lighting control: integer order vs fractional order strategies in sliding mode based extremum seeking," *Mechatronics*, vol. 23, pp. 863–872, 2013.

[50] C. Yin, Y. Chen, and S. Zhong, "Fractional-order sliding mode based extremum seeking control of a class of nonlinear system," *Automatica*, vol. 50, pp. 3173–3181, 2014.

[51] Z. Jiao, Y. Chen, and I. Podlubny, *Distributed Order Dynamic Systems: Stability, Simulation, Applications and Perspectives*. SpringerBrief, Springer-Verlag, 2012.

[52] Y. Li and Y. Chen, "Stability analysis of fractional order universal adaptive stabilization," in *New Trends in Nanotechnology and Fractional Calculus Applications*, vol. 5. Springer, 2009, pp. 357–368.

[53] Z. Jiao and Y. Chen, "Stability of fractional-order linear time-invariant systems with multiple noncommensurate orders," *Computers & Mathematics with Applications*, vol. 64, no. 10, pp. 3053–3058, 2012.

[54] Y. Li, Y. Chen, and I. Podlubny, "Mittag-Leffler stability of fractional order nonlinear dynamic systems," *Automatica*, vol. 45, no. 8, pp. 1965–1969, 2008.

[55] J. Liang, Y. Chen, B. M. Vinagre, and I. Podlubny, "Identification of a fractional linear diffusion-wave equation from noisy boundary measurements," in *Proc. of the 1st IFAC Symposium on Fractional Differentiation and its Applications*, Bordeaux, France, 2004.

[56] C. Yin, S. Dadras, S. Zhong, and Y. Chen, "Control of a novel class of fractional-order chaotic systems via adaptive sliding mode control approach," *Applied Mathematical Modelling*, vol. 37, no. 4, pp. 2469–2483, 2013.

[57] H. Malek, S. Dadras, and Y. Chen, "A fractional order maximum power point tracker: Stability analysis and experiments," in *Proc. of the 51st Annual Conference on Decision and Control (CDC)*, Maui, Hawaii, USA, 2012, pp. 6861–6866.

[58] Y. Luo and Y. Chen, *Fractional order motion controls*. John Wiley & Sons, Inc., 2012.

[59] The CRONE Team, "The CRONE toolbox homepage," Internet, http://www.ims-bordeaux.fr/CRONE/toolbox, Feb/2014.

[60] A. Oustaloup, P. Melchior, P. Lanusse, O. Cois, and F. Dancla, "The CRONE toolbox for Matlab," in *Proc. of the Computer-Aided Control System Design (CACSD), IEEE International Symposium on*, 2000, pp. 190–195.

[61] A. Oustaloup, X. Moreau, and M. Noulllant, "From fractal robustness to non integer approach in vibration insulation: the CRONE suspension," in *Proc. of the 36th Conference on Decision & Contro*, San Diego, California, USA, Dec 1997.

[62] A. Oustaloup, B. Mathieu, and P. Lanusse, "The CRONE control of resonant plants: application to a flexible transmission," *European Journal of Control*, vol. 1, no. 2, pp. 113–121, 1995.

[63] A. Oustaloup, X. Moreau, and M. Noulllant, "The CRONE suspension," *Control Engineering Practice*, vol. 4, no. 8, pp. 1101–1108, 1996.

[64] R. Malti, M. Aoun, J. Sabatier, and A. Oustaloup, "Tutorial on system identification using fractional differentiation models," in *Proc. of the 14th IFAC Symposium on System Identification*, Newcastle, Australia, 2006.

[65] R. Malti, S. Victor, and A. Oustaloup, "Advances in system identification using fractional models," *Journal of Computational and Nonlinear Dynamics*, vol. 3, no. 2, pp. 021 401–1–7, 2008.

[66] S. Victor and R. Malti, "Model order identification for fractional models," in *Proc. of the 2013 European Control Conference (ECC)*, Zärich, Switzerland, 2013.

[67] R. Malti, J. Sabatier, and H. Akçay, "Thermal modeling and identification of an aluminum rod using fractional calculus," in *Proc. of the 15th IFAC Symposium on System Identification (SYSID)*, Saint-Malo, France, 2009, pp. 958–963.

[68] J. D. Gabano and T. Poinot, "Fractional modelling and identification of thermal systems," *Signal Processing*, vol. 91, no. 3, pp. 531–541, 2011.

[69] A. Benchellal, T. Poinot, and J.-C. Trigeassou, "Fractional modelling and identification of a thermal process," *Journal of Vibration and Control*, vol. 14, no. 9, pp. 1403–414, 2008.

[70] M. Tenoutit, N. Maamri, and J.-C. Trigeassou, "An identification procedure for the tuning of a robust fractional controller," in *Proc. of the 6th Workshop on Fractional Differentiation and Its Applications, Part of 2013 IFAC Joint Conference*, Grenoble, France, 2013, pp. 367–372.

[71] S. Victor, R. Malti, H. Garnier, and A. Oustaloup, "Parameter and differentiation order estimation in fractional models," *Automatica*, vol. 49, pp. 926–935, 2013.

[72] A. Maachou, R. Malti, P. Melchior, J.-L. Battaglia, A. Oustaloup, and B. Hay, "Nonlinear thermal system identification using fractional Volterra series," *Control Engineering Practice*, vol. 29, pp. 50–60, 2014.

[73] R. Malti, X. Moreau, F. Khemane, and A. Oustaloup, "Stability and resonance conditions of elementary fractional transfer functions," *Automatica*, vol. 47, no. 11, pp. 2462–2467, 2011.

[74] N. Maamri, J. C. Trigeassou, and D. Mehdi, "A frequency approach to the stability of fractional differential equations with time delays," in *Proc.of the European Control Conference*, Budapest, Hungary, 2009, pp. 1614–1619.

[75] J. Sabatier, C. Farges, and J.-C. Trigeassou, "A stability test for non-commensurate fractional order systems," *Systems & Control Letter*, vol. 62, pp. 739–746, 2013.

[76] M. Moze, J. Sabatier, and A. Oustaloup, "LMI tools for stability analysis of fractional systems," in *Proc. of the 20th ASME International Design Engineering Technical Conferences & Computers and Information in Engineering Technical Conference, (IDETC/CIE)*, Long Beach, CA, USA, Sep 2005, pp. 1–9.

[77] D. Valério and J. S. da Costa, "Time-domain implementation of fractional order controllers," *IEE Proc.-Control Theory Appl.*, vol. 152, no. 5, pp. 539–552, 2005.

[78] ——, "Identifying digital and fractional transfer functions from a frequency response," *Int. J. Control*, vol. 84, pp. 445–457, 2011.

[79] ——, "Ninteger: a non-integer control toolbox for MatLab," in *Proc. of the 1st IFAC Workshop on Fractional Differentiation and Applications*, Bordeaux, France, 2004, pp. 208–213.

[80] D. Valério, *An Introduction to fractional control*, ser. IET Control Engineering Series 91. The Institution of Engineering and Technology, 2013.

[81] J. L. Adams and T. T. Hartley, "Finite-time controllability of fractional-order systems," *Journal of Computational and Nonlinear Dynamics*, vol. 3, no. 2, pp. 021 402–021 402–5, 2008.

[82] T. T. Hartley and C. F. Lorenzo, "A frequency-domain approach to optimal fractional-order damping," *Journal of Nonlinear Dynamics*, vol. 38, pp. 69–84, 2004.

[83] ——, "Optimal fractional-order damping," in *Proc. of the ASME 2003 Design Engineering Technical Conferences and Computers and Information in Engineering Conference (DETC/CIE)*, Chicago, IL, 2003, pp. 563–566.

[84] C. F. Lorenzo and T. T. Hartley, "Energy considerations for mechanical fractional-order elements," in *Proc. of the ASME 2013 Design Engineering Technical Conferences and Computers and Information in Engineering Conference (DETC/CIE)*, Portland, OR, 2013.

[85] T. T. Hartley and C. F. Lorenzo, "Fractional-order system identification based on continuous order-distributions," *Signal processing*, vol. 83, pp. 2287–2300, 2003.

[86] ——, "Dynamics and control of initialized fractional order systems," *Nonlinear Dynamics*, vol. 29, pp. 201–233, 2002.

[87] J. Hicks, R. Gruich, A. Oldja, D. Myers, T. T. Hartley, R. Veillette, and I. Husain, "Ultracapacitor energy management and controller development for a series-parallel 2x2 hybrid electric vehicle," in *Proc. of the IEEE Vehicular Propulsion and Power Conference*, Arlington, TX, USA, 2007.

[88] C. Jiang, T. T. Hartley, J. E. Carletta, and R. J. Veillette, "A systematic approach for implementing fractional-order operators and systems," *IEEE Journal on Emerging and Selected Topics in Circuits and Systems*, vol. 3, no. 3, pp. 301–312, 2013.

[89] M. S. Tavazoei, "From traditional to fractional PI control," *IEEE Industrial Electronics Magazine*, pp. 41–51, 2012.

[90] M. Tavakoli-Kakhki, M. Haeri, and M. S. Tavazoei, "Study on control input energy efficiency of fractional order control systems," *IEEE Journal on Emerging and Selected Topics in Circuits and Systems*, vol. 3, no. 3, pp. 475–482, 2013.

[91] M. S. Tavazoei and M. Tavakoli-Kakhki, "Minimal realizations for some classes of fractional order transfer functions," *IEEE Journal on Emerging and Selected Topics in Circuits and Systems*, vol. 3, no. 3, pp. 313–321, 2013.

[92] Z. Liao, P. Cheng, and W. Yong, "Subspace identification for commensurate fractional order systems using instrumental variables," in *Proc. of the 30th Chinese Control Conference (CCC)*, Yantai, China, 2011.

[93] Z. Liao, Z. Zhu, S. Liang, C. Peng, and Y. Wang, "Subspace identification for fractional order Hammerstein systems based on instrumental variables," *International Journal of Control, Automation and Systems*, vol. 10, no. 5, pp. 947–953, 2012.

[94] W. Li, C. Peng, and Y. Wang, "Identifying the fractional order systems with frequency responses: A maximum likelihood algorithm," in *Proc. of the 2011 IEEE CIE International Conference on Radar*, vol. 2, 2011, pp. 1943–1948.

[95] Z. Liao, C. Peng, and Y. Wang, "A frequency-domain identification algorithm for MIMO fractional order systems with time delay in state," *Manufacturing Science and Technology*, vol. 383, pp. 4397–4404, 2011.

[96] S. Liang, S.-G. Wang, and Y. Wang, "Representation and LQR of exact fractional order systems," in *Proc. of the IEEE 53rd Annual Conference onDecision and Control (CDC)*, Dec 2014, pp. 6908–6913.

[97] Y. Wei, Y. Hu, L. Song, and Y. Wang, "Tracking differentiator based fractional order model reference adaptive control: The $1 < \alpha < 2$ case," in *Proc. of the IEEE 53rd Annual Conference onDecision and Control (CDC)*, Los Angeles, CA, Dec 2014, pp. 6902–6907.

[98] X. Zhou, Y. Wei, S. Liang, and Y. Wang, "Positive real lemmas for fractional order systems," in *Proc. of the IEEE 53rd Annual Conference onDecision and Control (CDC)*, Dec 2014, pp. 6914–6919.

[99] J. Lu, Y. Chen, and W. Chen, "Robust asymptotical stability of fractional-order linear systems with structured perturbations," *Computers & Mathematics with Applications*, vol. 66, no. 5, pp. 873–882, 2013.

[100] J. Lu and Y. Chen, "Robust stability and stabilization of fractional-order interval systems with the fractional order α: The $0 < \alpha < 1$ case," *IEEE Transactions on Automatic Control*, vol. 55, no. 1, pp. 152–158, 2010.

[101] X. J. Wen, Z. M. Wu, and J. G. Lu, "Stability analysis of a class of nonlinear fractional-order systems," *IEEE Transactions on Circuits and Systems-II*, vol. 55, no. 11, pp. 1178–1182, 2008.

[102] D. Matignon, "Stability results for fractional differential equations with applications to control processing," in *Computational Engineering in Systems Applications*, Lille, France, 1996, pp. 963–968.

[103] ——, "Stability properties for generalized fractional differential systems," *ESAIM: Proc*, vol. 5, pp. 145–158, 1998.

[104] ——, "Generalized fractional differential and difference equations: stability properties and modelling issues," *ESAIM: Proc*, vol. 5, 1998.

[105] C. Bonnet and J. Partington, "Coprime factorizations and stability of fractional differential systems," *Systems & Control Letters*, vol. 41, no. 3, pp. 167–174, 2000.

[106] H. S. Ahn and Y. Chen, "Necessary and sufficient stability condition of fractional-order interval linear systems," *Automatica*, vol. 44, no. 11, pp. 2985–2988, 2008.

[107] S. E. Hamamci, "An algorithm for stabilization of fractional-order time delay systems using fractional-order PID controllers," *IEEE Transactions on Automatic Control*, vol. 52, no. 10, pp. 1964–1969, 2007.

[108] A. Dzieliński and D. Sierociuk, "Stability of discrete fractional order state-space systems," *Journal of Vibration and Control*, vol. 14, no. 9, pp. 1543–1556, 2008.

[109] R. Stanislawski and K. J. Latawiec, "Stability analysis for discrete-time fractional-order LTI state-space systems. Part I: New necessary and sufficient conditions for the asymptotic stability," *Bulletin of the Polish Academy of Sciences: Technical Sciences*, vol. 61, no. 2, pp. 353–361, 2013.

[110] ——, "Stability analysis for discrete-time fractional-order LTI state-space systems. Part II: New stability criterion for fd-based systems," *Bulletin of the Polish Academy of Sciences: Technical Sciences*, vol. 61, no. 2, pp. 365–370, 2013.

[111] C. Hwanga and Y.-C. Cheng, "A numerical algorithm for stability testing of fractional delay systems," *Automatica*, vol. 42, no. 5, pp. 825–831, 2006.

[112] M. Buslowicz, "Stability of linear continuous-time fractional order systems with delays of the retarded type," *Bulletin of the Polish Academy of Sciences: Technical Sciences*, vol. 56, no. 4, pp. 319–324, 2008.

[113] M. Ikeda and S. Takahashi, "Generalization of Routh's algorithm and stability criterion for non-integer integral system," *Electronics and Communications in Japan*, vol. 60, no. A(2), pp. 41–50, 1977.

[114] M. Buslowicz, "Frequency domain method for stability analysis of linear continuous-time state-space systems with double fractional orders," *Theory & Appl. of Non-integer Order Syst*, vol. LNEE 257, pp. 31–39, 2013.

[115] A. Ruszewski, "Stability conditions of fractional discrete-time scalar systems with pure delay," *Pomiary Automatyka Robotyka*, pp. 340–344, 2013.

[116] ——, "Stability conditions of fractional discrete-time scalar systems with two delays," *Theory & Appl. of Non-integer Order Syst*, vol. LNEE 257, pp. 53–64, 2013.

[117] M. Buslowicz, "Robust stability of positive discrete-time linear systems of fractional order," *Bulletin of the Polish Academy of Sciences: Technical Sciences*, vol. 58, no. 4, pp. 567–572, 2011.

[118] H. S. Ahn, Y. Chen, and I. Podlubny, "Robust stability test of a class of linear time-invariant interval fractional-order system using Lyapunov inequality," *Applied Mathematics and Computation*, vol. 187, pp. 27–34, 2007.

[119] I. Petráš, Y. Chen, and B. M. Vinagre, "Robust stability test for interval fractional order linear systems," *Unsolved Problems in Mathematical Systems and Control Theory*, pp. 208–211, 2009.

[120] H. S. Ahn and Y. Chen, "Conservatism-free robust stability check of fractional-order interval linear systems," in *Proc. of the 17th IFAC World Congress*, Seoul, Korea, 2008, pp. 15 256–15 261.

[121] Y. Q. Chen, H.-S. Ahn, and I. Podlubny, "Robust stability check of fractional order linear time invariant systems with interval uncertainties," in *Proc. of the 2005 IEEE International Conference on Mechatronics and Automation*, vol. 1, July 2005, pp. 210–215.

[122] A. G. Radwan, A. M. Soliman, A. S. Elwakil, and A. Sedeek, "On the stability of linear systems with fractional-order elements," *Chaos, Solitons and Fractals*, vol. 40, pp. 2317–2328, 2009.

[123] M. Buslowicz, "Stability of continuous-time linear systems described by state equation with fractional commensurate orders of derivatives," *Przeglad Elektro-Techniczny*, vol. ISSN 0033-2097, pp. 17–20, 2012.

[124] Z. Jiao and Y. Chen, "Stability analysis of fractional-order systems with double noncommensurate orders for matrix case." *Fractional Calculus and Applied Analysis, An Int. J. for Theory and Applications*, vol. 14, no. 3, pp. 436–453, 2011.

[125] F. Merrikh-Bayat, "Stability of fractional-delay systems: A practical approach," *New Trends in Nano-technology and Fractional Calculus Applications, Z. B. Guvenc and J. A. T. Machado and D. Baleanu (ed.)*, pp. 163–170, 2010.

[126] F. Merrikh-Bayat and M. Afshar, "Extending the root-locus method to fractional-order systems," *Journal of Applied Mathematics*, vol. 2008, no. Article ID: 528934, 2008.

[127] F. Merrikh-Bayat, M. Afshar, and M. Karimi-Ghartemani, "Extension of the root-locus method to a certain class of fractional-order systems," *ISA Transactions*, vol. 48, pp. 48–53, 2009.

[128] J. A. T. Machado and A. M. Galhano, "A computational approach for obtaining the root locus of fractional systems," in *Proc. of the 2011 ENOC*, Rome, Italy, Jul 2011.

[129] J. A. T. Machado, "Root locus of fractional linear systems," *Commun Nonlinear Sci Numer Simulat*, vol. 16, pp. 3855–3862, 2011.

[130] A. M. Lopes and J. A. T. Machado, "Root locus practical sketching rules for fractional-order systems," *Abstract and Applied Analysis*, vol. 2013, no. Article ID 102068, 2013.

[131] J. A. T. Machado, "A gallery of root locus of fractional systems," in *Proc. of the ASME 2013 International Design Engineering Technical Conferences and Computers and Information in Engineering Conference (IDETC/CIE)*, Portland, OR, USA, Aug 2013.

[132] A. De and S. Sen, "Root locus method for any fractional order commensurate system," in *Proceeding of the 2011 IEEE Students' Technology Symposium*, IIT, Kharagpur, India, Jan 2011.

[133] M. D. Patil, V. A. Vyawahare, and M. K. Bhole, "A new and simple method to construct root locus of general fractional-order systems," *ISA Transactions*, vol. 53, pp. 380–390, 2014.

[134] R. Malti, S. Victor, A. Oustaloup, and H. Garnier, "An optimal instrumental variable method for continuous-time fractional model identification," in *Proceddings of the 17th IFAC World Congress*, Seoul, South Korea, 2008.

[135] A. Narang, "Identification and control of fractional and integer order systems," Ph.D. dissertation, University of Alberta, Canada, 2012.

[136] J. Lin, T. Poinot, S. T. Li, and J. C. Trigeassou, "Identification of non-integer order systems in frequency domain," *J. Control Theory Appl*, vol. 25, pp. 517–520, 2008.

[137] R. Caponetto, G. Dongola, L. Fortuna, and I. Petráš, *Fractional Order Systems: Modelling and Control Applications*. World Scientific, 2010.

[138] K. Barbé, O. J. O. Rodriguez, W. V. Moer, and L. Lauwers, "Fractional models for modeling complex linear systems under poor frequency resolution measurements," *Digital Signal Processing*, vol. 23, pp. 1084–1093, 2013.

[139] S. Das, *Functional Fractional Calculus for System Identification and Controls*. Berlin, Heidelberg: Springer-Verlag, 2008.

[140] R. Tanwar, "Analog realization of fractional order circuits," Master's thesis, Thapar University, India, 2013.

[141] M. Khanra, J. Pal, and K. Biswas, "Reduced order approximation of MIMO fractional order systems," *IEEE Journal on Emerging and Selected Topics in Circuits and Systems*, vol. 3, no. 3, pp. 451–458, 2013.

[142] S. Oh and Y. Hori, "Realization of fractional order impedance by feedback control," in *Proc. of the 33rd Annual Conference of the IEEE Industrial Electronics Society (IECON)*, Taipei, Taiwan, 2007.

[143] D. Heleschewitz and D. Matignon, "Diffusive realisations of fractional integro differential operators: structural analysis under approximation," in *Proceedings of 5th IFAC Conference on System Structure and Control*, vol. 2, Nantes, France, 1998, pp. 243–248.

[144] T. Poinot and J. C. Trigeassou, "A method for modelling and simulation of fractional systems," *Signal Processing*, vol. 83, pp. 2319–2333, 2003.

[145] R. S. Barbosa and J. A. T. Machado, "Implementation of discrete-time fractional-order controllers based on LS approximations," *Acta Polytechn Hung*, vol. 3, no. 4, pp. 5–22, 2006.

[146] P. Lanusse and J. Sabatier, "PLC implementation of a CRONE controller," *Fract Calc Appl Anal*, vol. 14, no. 4, p. 505C522, 2011.

[147] Q. Chen, T. Chen, H. Yu, J. Song, and D. Liu, "Lateral control for autonomous parking system with fractional order controller," *Journal of Software*, vol. 6, no. 6, pp. 1075–1081, 2011.

[148] P. Duch, M. Łaski, S. Błaszczyk, and P. Ostalczyk, "The variable, fractional-order discrete-time PD controller in the IISv1.3 robot arm control," *Central European Journal of Physics*, vol. 11, no. 6, pp. 750–759, 2013.

[149] I. Pan and S. Das, *Intelligent Fractional Order Systems and Control: An Introduction.* Springer, 2012.

[150] I. Podlubny, *Fractional differential equations.* Academic Press, 1999.

[151] G. W. Leibniz, *Mathematische Schiften.* Georg Olms Verlagsbuch-handlung, 1692.

[152] M. Kline, *Mathematical Thought from Ancient to Modern Times.* Oxford University Press, 1990, vol. 1.

[153] X. Gu, "Paradox and mathematics teaching (in chinese)," Research and Practice on Teaching and Education, 2003.

[154] E. Snapper, "The three crises in mathematics: Logicism, intuitionism and formalism," *Mathematics Magazine*, vol. 52, pp. 207–216, 1979.

[155] J. T. Machado, V. Kiryakova, and F. Mainardi, "Recent history of fractional calculus," *Commun Nonlinear Sci Numer Simulat*, vol. 16, pp. 1140–1153, 2011.

[156] J. C. Prajapati and A. K. Shukla, "Decomposition of generalized Mittag-Leffler function and its properties," *Advances in Pure Mathematics*, vol. 2, pp. 8–14, 2012.

[157] V. B. L. Chaurasia and S. C. Pandey, "On the fractional calculus of generalized Mittag-Leffler function," *SCIENTIA Series A: Mathematical Sciences*, vol. 20, pp. 113–122, 2010.

[158] A. K. Shukla and J. C. Prajapati, "On a generalization of Mittag-Leffler function and its properties," *J. Math. Anal. Appl*, vol. 336, pp. 797–811, 2007.

[159] G. Jumarie, "Laplace's transform of fractional order via the Mittag-Leffler function and modified Riemann-Liouville derivative," *Applied Mathematics Letters*, vol. 22, pp. 1659–1664, 2009.

[160] L. G. Romero and L. L. Luque, "K-Weyl fractional derivative, integral and integral transform," *Int. J. Contemp. Math. Sciences*, vol. 8, no. 6, pp. 263–270, 2013.

[161] S. Das and I. Pan, *Fractional order signal processing: Introductory Concepts and Applications.* Springer Brief, 2012.

[162] H. M. Ozaktas, Z. Zalevsky, and M. A. Kutay, *The Fractional Fourier Transform.* John Wiley & Sons, 2001.

[163] V. A. Narayanana and K. Prabhu, "The fractional Fourier transform: theory, implementation and error analysis," *Microprocessors and Microsystems*, vol. 27, pp. 511–521, 2003.

[164] Y. Chen, R. Sun, and A. Zhou, "An improved Hurst parameter estimator based on fractional Fourier transform," *Telecommun. Syst.*, vol. 43, no. 3, p. 197C206, 2010.

[165] A. Bultheel and H. Martínez-Sulbaran, "Computation of the fractional Fourier transform," *Applied and Computational Harmonic Analysis*, vol. 16, no. 3, pp. 182–202, 2004.

[166] ——, "Calculation of the fractional Fourier transform," [Online] http://nalag.cs.kuleuven.be/research/software/FRFT/, 2004.

[167] B. M. Vinagre and V. Feliu, "Optimal fractional controllers for commensurate order systems: A special case of the Wiener-Hopf method," in *Proc. of the 39th IEEE Conference on Decision and Control (CDC)*, Sydney, Australia, 2000.

[168] F. Mainardi and P. Pironi, "The fractional Langevin equation: Brownian motion revisited," *Extracta Mathematicae*, vol. 11, no. 1, pp. 140–154, 1996.

[169] B. V. der Pol and J. V. der Mark, "Frequency demultiplication," *Nature*, vol. 120, pp. 363–364, 1927.

[170] R. E. Mickens, "Analysis of nonlinear oscillators having non-polynomial elastic terms," *Journal of Sound and Vibration*, vol. 255, no. 4, pp. 789–792, 2002.

[171] ——, "Fractional Van der Pol equations," *Journal of Sound and Vibration*, vol. 259, no. 2, pp. 457–460, 2003.

[172] E. Pereira, C. Monje, B. Vinagre, and F. Gordillho, "Matlab toolbox for the analysis of fractional order systems with hard nonlinearities," in *Proceedings of the 1st IFAC Workshop on Fractional Differentiation and Its Applications (FDA'04)*, Bordeaux, France, 2004, pp. 214–219.

[173] R. S. Barbosa, J. A. T. Machado, I. M. Ferreira, and J. K. Tar, "Dynamics of the fractional-order Van der Pol oscillator," in *Proc. of the IEEE International Conference on Computational Cybernetics(ICCC'04)*, Vienna, Austria, 2004.

[174] G. Diaz and C. F. M. Coimbra, "Nonlinear dynamics and control of a variable order oscillator with application to the Van der Pol equation," *Nonlinear Dynamics*, vol. 56, pp. 145–157, 2009.

[175] R. S. Barbosa, B. M. Vinagre, and A. J. Calderón, "Analysis of the Van der Pol oscillator containing derivatives of fractional order," *Journal of Vibration and Control*, vol. 13, no. 9-10, pp. 1291–1301, 2007.

[176] M. S. Tavazoei, M. Haeri, M. Attari, S. Bolouki, and M. Siami, "More details on analysis of fractional-order Van der Pol oscillator," *Journal of Vibration and Control*, vol. 15, no. 6, pp. 803–819, 2009.

[177] J. W. Strutt, *(Lord Rayleigh), The Theory of Sound*. Dover Publication, reprint, 1945.

[178] P. Arena, R. Caponetto, L. Fortuna, and D. Porto, "Chaos in a fractional order Duffing system," in *Proceedings of ECCTD*, Budapest, Hungary, 1997, pp. 1259–1262.

[179] M. Borowiec, G. Litak, and A. Syta, "Vibration of the Duffing oscillator: Effect of fractional damping," *Shock and Vibration*, vol. 14, pp. 29–36, 2007.

[180] Z.-M. Ge and C.-Y. Qu, "Chaos in a fractional order modified Duffing system," *Chaos, Solitons and Fractals*, vol. 34, pp. 262–291, 2007.

[181] J. Cao, C. Ma, H. Xie, and Z. Jiang, "Nonlinear dynamics of Duffing system with fractional order damping," *ASME J.Comput. Nonlinear Dyn*, vol. 5, no. 4, pp. 1012–1018, 2010.

[182] R. Zhang, W. Xu, G. Yang, and Q. Han, "Response of a Duffing-Rayleigh system with a fractional derivative under Gaussian white noise excitation," *Chin. Phys. B*, vol. 24, no. 2, pp. 020 204–020 204–5, 2015.

[183] J. Hristov, "An exercise with the He's variation iteration method to a fractional Bernoulli equation arising in a transient conduction with a non-linear boundary heat flux," *International Review of Chemical Engineering*, vol. 4, no. 5, pp. 489–497, 2012.

[184] K. R. Hedrih, "Dynamics of multi-pendulum systems with fractional order creep elements," *Journal of Theoretical and Applied Mechanics*, vol. 46, no. 3, pp. 483–509, 2008.

[185] D. Baleanu, J. H. Asad, and I. Petráš, "Fractional-order two-electric pendulum," *Romanian Reports in Physics*, vol. 64, no. 4, pp. 907–914, 2012.

[186] E. Anli and I. Ozkol, "Classical and fractional-order analysis of the free and forced double pendulum," *Engineering*, vol. 2, pp. 935–949, 2010.

[187] R. Gorenflo, F. Mainardi, D. Moretti, G. Pagnini, and P. Paradisi, "Discrete random walk models for space-time fractional diffusion," *Chemical Physics*, vol. 284, no. 1-2, pp. 521–541, 2002.

[188] ——, "Fractional calculus and continuous-time fractional diffusion," *Chem. Phys.*, vol. 284, pp. 521–544, 2002.

[189] R. Metzler and J. Klafter, "The random walk's guide to anomalous diffusion: a fractional dynamics approach," *Physics Reports*, vol. 339, pp. 1–77, 2000.

[190] R. Klages, G. Radons, and I. M. Sokolov, Eds., *Anomalous Transport: Foundations and Applications*. Wiley-VCH Verlag GmbH & Co. KGaA, 2008.

[191] T. M. Atanacković, S. Pilipović, B. Stanković, and D. Zorica, *Fractional Calculus with Applications in Mechanics: Vibrations and Diffusion Processes*. John Wiley & Sons, Inc., 2014.

[192] S. Kumar, D. Kumar, S. Abbasbandy, and M. Rashidi, "Analytical solution of fractional Navier-Stokes equation by using modified Laplace decomposition method," *Ain Shams Engineering Journal*, vol. 5, pp. 569–574, 2014.

[193] V. B. L. Chaurasia and D. Kumar, "Solution of the time-fractional Navier-Stokes equation," *Gen. Math. Notes*, vol. 4, no. 2, pp. 49–59, 2011.

[194] L. Dorčák, I. Petráš, I. Koštial, and J. terpák, "Fractional-order state space models," in *Proc. of the International Carpathian Control Conference (ICCC)*, Malenovice, Czech Republic, May 2002.

[195] J. C. Trigeassou, N. Maamri, J.Sabatier, and A.Oustaloup, "A Lyapunov approach to the stability of fractional differential equations," *Signal Processing*, vol. 91, pp. 437–445, 2011.

[196] C. Li and F. Zhang, "A survey on the stability of fractional differential equations," *Eur. Phys. J. Special Topics*, vol. 193, pp. 27–47, 2011.

[197] M. S. Tavazoei and M. Haeri, "A proof for non existence of periodic solutions in time invariant fractional order systems," *Automatica*, vol. 45, pp. 1886–1890, 2009.

[198] M. S. Tavazoei, "A note on fractional-order derivatives of periodic functions," *Automatica*, vol. 46, pp. 945–948, 2010.

[199] M. Yazdani and H. Salarieh, "On the existence of periodic solutions in time-invariant fractional order systems," *Automatica*, vol. 47, pp. 1834–1837, 2011.

[200] E. Kaslik and S. Sivasundaram, "Non-existence of periodic solutions in fractional-order dynamical systems and a remarkable difference between integer and fractional-order derivatives of periodic functions," *Nonlinear Analysis: Real World Applications*, vol. 13, pp. 1489–1497, 2012.

[201] L. M. B. C. Campos, "On the solution of some simple fractional differential equations," *Internat. J. Math. & Math. Sci.*, vol. 13, no. 3, pp. 481–496, 1990.

[202] N. V. Zhukovskaya and A. A. Kilbas, "Solving homogeneous fractional differential equations of Euler type," *Differential Equations*, vol. 47, pp. 1714–1725, 2011.

[203] M. Khanra, J. Pal, and K. Biswas, "Formulation of Euler-Lagrange equations for fractional variational problems," *J. Math. Anal. Appl*, vol. 272, pp. 368–379, 2002.

[204] M. A. E. Herzallah and D. Baleanu, "Fractional Euler-Lagrange equations revisited," *Nonlinear Dynamics*, vol. 69, pp. 977–982, 2012.

[205] T. Błszczyk and M. Ciesielski, "Fractional Euler-Lagrange equations - numerical solutions and applications of reflection operator," *Scientific Research of the Institute of Mathematics and Computer Science*, vol. 9, pp. 17–24, 2010.

[206] W. R. Evans, "Graphical analysis of control systems," *American Institute of Electrical Engineers, Transactions of the*, vol. 67, no. 1, pp. 547–551, 1948.

[207] A. M. Krall, "The root locus method: a survey," *Transactions of the American Institute of Electrical Engineers*, vol. 61, no. 1, pp. 547–551, 1948.

[208] M. K. Ghartemani and F. M. Bayat, "Necessary and sufficient conditions for perfect command following and disturbance rejection in fractional order systems," in *Proc. of the 17th World Congress IFAC*, Soul, Korea, Jul 2008, pp. 364–369.

[209] H. M. Farkas and I. Kra, *Riemann Surfaces*, 2nd ed. New York: Springer-Verlag, 1980.

[210] D. Xue and Y. Chen, *System Simulation Techniques with Matlab and Simulink*. John Wiley & Sons, Ltd., 2014.

[211] R. M. Corless and D. J. Jeffrey, "Graphing elementary Riemann surface," *SIGSAM Bulletin*, vol. 32, no. 1, pp. 11–17, 1998.

[212] Z. Li, "Fractional order root locus," [online] (Matlab Central) http://www.mathworks.com/matlabcentral/fileexchange/50458, 2015.

[213] F. Merrikh-Bayat, "Root-locus plot of fractional order systems," [Online] (Matlab Central) http://www.mathworks.com/matlabcentral/fileexchange/20577, 2008.

[214] M. Tavazoei and M. Tavakoli-Kakhki, "Compensation by fractional-order phase-lead/lag compensators," *Control Theory Applications, IET*, vol. 8, no. 5, pp. 319–329, March 2014.

[215] J. C. Trigeassou and N. Maamri, "A new approach to the stability of linear fractional systems," in *Proc. of the 6th International Multi-Conference on Systems, Signals and Devices (SSD)*, Djerba, Tunisia, 2009.

[216] A. C. McBride and G. F. Roach, Eds., *Fractional Calculus*, ser. Research Notes in Mathematics. Boston-London-Melbourne: Longman Sc & Tech, 1985, vol. 214.

[217] M. Tabatabaei and M. Haeri, "CRA based control of non-minimum phase fractional order systems," in *Proc. of the 2012 IEEE International Conference on Control Applications (CCA)*, Dubrovnik Croatia, Oct 2012.

[218] Z. Li, T. Zhao, and Y. Chen, "A low cost research platform for modeling and control of multi-input multi-output fractional order dynamic systems," in *Proc. of the International conference on fractional differentiation and its applications (ICFDA)*, Catania, Italy, 2014.

[219] R. C. Dorf and R. H. Bishop, *Modern Control Systems*, 12th ed. Prentice Hall, 2010.

[220] D. M. Rowe, Ed., *CRC Handbook of Thermoelectrics*. CRC Press, 1995.

[221] J. D. Gabano, T. Poinot, and H. Kanoun, "Identification of a thermal system using continuous linear parameter-varying fractional modelling," *IET Control Theory and Applications*, vol. 5, no. 7, pp. 889–899, 2011.

[222] M. S. Tavazoei, "Time response analysis of fractional-order control systems: A survey on recent results," *Fractional Calculus and Applied Analysis*, vol. 17, no. 2, pp. 440–461, 2014.

[223] B. J. West, *Where Madicine Went Wrong*. World Scientific Publishing Company, 2006.

[224] B. J. West, M. Turalska, and P. Grigolini, *Complex Networks: From Social Crises to Neuronal Avalanches*. Wiley-VCH Verlag GmbH & Co. KGaA, 2014, pp. 509–524.

[225] T. G. Lewis, *Book of Extremes: Why the* 21^{st} *Century Isn't Like the* 20^{th} *Century?* Switzerland: Springer, 2014.

[226] Z. Ding, C. W. Granger, and R. F. Engle, "A long memory property of stock market returns and a new model," *Journal of Empirical Finance 1*, pp. 83–106, 1993.

[227] B. G. Malkiel, *A Random Walk down Wall Street*, 7th ed. W. W. Norton & Company, 1999.

[228] Z. Li and Y. Chen, "Identification of linear fractional order systems using the relay feedback approach," in *Proc. of the 2014 American Control Conference (ACC)*, Portland, OR, USA, 2014.

[229] D. Valério and J. S. da Costa, "Time-domain implementatio of fractional order controllers," *Control Theory and Applications, IEE Proceedings* -, vol. 152, no. 5, pp. 539–552, Sept 2005.

[230] N. Yousfi, P. Melchior, C. Rekik, N. Derbel, and A. Oustaloup, "Design of centralized CRONE controller combined with MIMO-QFT approach applied to non-square multivariable systems," *Int. J. Comput. Appl*, vol. 45, pp. 6–14, 2012.

[231] A. Tepljakov, E. Petlenkov, and J. Belikov, "FOMCON: Fractional-order modeling and control toolbox for Matlab," in *Proc. of the 18th International Conference "Mixed Design of Integrated Circuits and Systems"*, Gliwice, Poland, 2011.

[232] T. Prabhakar, "A singular integral equation with a generalised Mittag-Leffler function in the kernel," *Yokohama Math. J*, vol. 19, pp. 7–15, 1971.

[233] B. Barrowes, "Generalized hypergeometric function," [Online] (Matlab Central) http://www.mathworks.com/matlabcentral/fileexchange/5616, 2005.

[234] J. Huntley, "Generation of random variates," [Online] (Matlab Central) http://www.mathworks.com/matlabcentral/fileexchange/35008, 2012.

[235] F. R. de Hoog, J. Knight, and A. Stokes, "An improved method for numerical inversion of Laplace transforms," *SIAM Journal on Scientific Computing*, vol. 3, no. 3, pp. 357–366, 1982.

[236] J. Liang, "Control of linear time-invariant distributed parameter systems: from interger order to fractional order," Master's thesis, Utah State University, 2005.

[237] J. Valsa and L. Brančík, "Fractional order state equations for the control of viscoelastically damped structure," *International Journal of Numerical Modelling: Electronic Networks, Devices and Fields*, vol. 11, no. 3, pp. 153–166, 1998.

[238] L. Brančík, "An improved numerical inversion of two-dimensional Laplace transforms with application to transient analysis of transmission lines," in *Proceedings EDS'99 Brno*, Czech Republic, 1999.

[239] ——, "Utilization of quotient-difference algorithm in FFT-based numerical ILT method," in *Proc. of the 11th International Czech-Slovak Scientific Conference Radioelektronika*, Czech Republic, 2001.

[240] H. Sheng, Y. Li, and Y. Chen, "Application of numerical inverse Laplace transform algorithms in fractional calculus," *Journal The Franklin Institu te*, vol. 348, pp. 315–330, 2011.

[241] I. Petráš, "Digital fractional order differentiator/integrator - IIR type," [Online] (Matlab Central) http://www.mathworks.com/matlabcentral/fileexchange/3672, 2003 (updated 2011).

[242] ——, "Digital fractional order differentiator/integrator - FIR type," [Online] (Matlab Central) http://www.mathworks.com/matlabcentral/fileexchange/3673, 2003 (updated 2011).

[243] ——, "Digital fractional order differentiator/integrator - new IIR type," [Online] (Matlab Central) http://www.mathworks.com/matlabcentral/fileexchange/31358, 2011.

[244] Y. Chen and B. M. Vinagre, "A new IIR-type digital fractional order differentiator," *Signal processing*, vol. 83, pp. 2359–2365, 2003.

[245] Y. Chen, "Impulse response invariant discretization of fractional order integrators/differentiators," [Online] (Matlab Central) http://www.mathworks.com/matlabcentral/fileexchange/21342, 2008.

[246] D. Xue, Y. Chen, and D. Atherton, *Linear feedback control - analysis and design with Matlab*. Society for Industrial and Applied Mathematics, 2009.

[247] A. Oustaloup, F. Levron, B. Mathieu, and F. M. Nanot, "Frequency-band complex noninteger differentiator: Characterization and synthesis," *IEEE Trans. on Circ. and Sys. - I: Fundamental Theory And Applications*, vol. 47, no. 1, pp. 25–39, 2000.

[248] F. M. Bayat, "Fractional differentiator," [Online] (Matlab Central) http://www.mathworks.com/matlabcentral/fileexchange/13858, 2007.

[249] Jonathan, "Fractional derivative," [Online] (Matlab Central) http://www.mathworks.com/matlabcentral/fileexchange/45982, 2014.

[250] D. Xue and Y. Chen, *Modeling, Analysis and Design of Control Systems in Matlab and Simulink*. World Scientific, 2014.

[251] G. Papazafeiropoulos, "Fractional differentiation and integration," [Online] (Matlab Central) http://www.mathworks.com/matlabcentral/fileexchange/45877, 2014.

[252] T. M. Marinov, N. Ramirez, and F. Santamaria, "Fractional integration toolbox (FIT)," [Online] (Santamaria Lab) http://www.cbi.utsa.edu/FIT, 2013.

[253] ——, "Fractional integration toolbox," *Fractional Calculus & Applied Analysis*, vol. 16, no. 3, pp. 670–681, 2013.

[254] I. Petráš, "Discrete fractional-order PID controller," [Online] (Matlab Central) http://www.mathworks.com/matlabcentral/fileexchange/33761, 2011.

[255] N. Lachhab, F. Svaricek, F. Wobbe, and H. Rabba, "Fractional order PID controller (FOPID) - toolbox," in *Proc. of the 2013 European Control Conference (ECC)*, Zuich, Switzerland, 2013, pp. 3694–3699.

[256] P. Apkarian and D. Noll, "Nonsmooth H_∞ synthesis," *IEEE Transactions on Automatic Control*, vol. 51, no. 1, pp. 71–86, 2006.

[257] E. Pisoni, A. Visioli, and S. Dormido, "An interactive tool for fractional order PID controllers," in *Proc. of the IECON '09. 35th Annual Conference of IEEE*, 2009.

[258] J. L. Guzman, K. J. Astrom, S. Dormido, T. Hagglund, M. Berenguel, and Y. Piguet, "Interactive modules for PID control," *IEEE Control Systems Magazine*, vol. 28, no. 5, pp. 118–134, 2008.

[259] I. Podlubny, "Mittag-Leffler function," [Online] (Matlab Central) http://www.mathworks.com/matlabcentral/fileexchange/8738, 2005.

[260] S. Mukhopadhyay, "Mittag-Leffler function, m-file, cmex DLL, and S-function," [Online] (Matlab Central) http://www.mathworks.com/matlabcentral/fileexchange/20731, 2008.

[261] Y. Chen, "Generalized Mittag-Leffler function," [Online] (Matlab Central) http://www.mathworks.com/matlabcentral/fileexchange/20849, 2008.

[262] R. Garrappa, "The Mittag-Leffler function," [Online] (Matlab Central) http://www.mathworks.com/matlabcentral/fileexchange/48154, 2014.

[263] Juraj, "Numerical inversion of Laplace transforms in Matlab," [Online] (Matlab Central) http://www.mathworks.com/matlabcentral/fileexchange/32824, 2011.

[264] Y. Chen, "Oustaloup-recursive-approximation for fractional order differentiators," [Online] (Matlab Central) http://www.mathworks.com/matlabcentral/fileexchange/3802, 2003.

[265] C. Tricaud, "Solution of fractional optimal control problems," [Online] (Matlab Central) http://www.mathworks.com/matlabcentral/fileexchange/22196, 2009.

[266] D. Sierociuk, "Fractional States-Space Toolkit (FSST)," [Online] http://www.ee.pw.edu.pl/~dsieroci/fsst/fsst.htm, 2003.

[267] I. Podlubny, "Matrix approach to discrete fractional calculus," *Factional Calculus and Applied Analysis*, vol. 29, no. 4, pp. 281–296, 2000.

[268] C. Tricaud and Y. Chen, "Solution of fractional order optimal control problems using SVD-based rational approximations," in *Proc. of the 2009 American Control Conference (ACC)*, St. Louis, MO, USA, 2009, pp. 1430–1435.

[269] A. Dzieliński and D. Sierociuk, "Simulation and experimental tools for fractional order control education," in *Proceedings IFAC World Congress*, Seoul, Korea, 2008, pp. 11 654–11 659.

[270] C. F. Lorenzo and T. T. Hartley, "Variable order and distributed order fractional operators," *Nonlinear Dynamics*, vol. 29, no. 1, pp. 57–98, 2002.

[271] I. Podlubny, "Matrix approach to discretization of ODEs and PDEs of arbitrary real order," [Online] (Matlab Central) http://www.mathworks.com/matlabcentral/fileexchange/22071, 2008.

[272] D. Sierociuk, "Fractional variable order derivative Simulink toolkit," [Online] (Matlab Central) http://www.mathworks.com/matlabcentral/fileexchange/38801, 2012.

[273] D. Valério, "Variable order derivatives," [Online] (Matlab Central) http://www.mathworks.com/matlabcentral/fileexchange/24444, 2009.

[274] I. Petráš, *Engineering Education and Research Using Matlab*. InTech, 2011, ch. Fractional Derivatives, Fractional Integrals, and Fractional Differential Equations in Matlab, pp. 239–264.

[275] G. Germano, "Mittag-Leffler random number generator," [Online] (Matlab Central) http://www.mathworks.com/matlabcentral/fileexchange/19392, 2008 (updated 2014).

[276] D. Chen, Y. Chen, and D. Xue, "Digital fractional order Savitzky-Golay differentiator," *IEEE Transactions on Circuits and Systems - II: Express Briefs*, vol. 58, no. 11, pp. 758–762, 2011.

[277] I. S. Jesus, "Fractional electrical impedances in botanical elements," *Journal of Vibration and Control*, vol. 14, no. 9-10, pp. 1389–1402, 2008.

[278] I. Goychuk, "Fractional diffusion modeling of ion channel gating," *Phys. Rev. E*, vol. 70, 2004.

[279] F. Mainardi, "Fractional calculus: some basic problems in continuum and statistical mechanics," in *Fractals and Fractional Calculus in Continuum Mechanics*. New York: Springer, 1997, pp. 291–348.

[280] O. Cois, A. Oustaloup, T. Poinot, and J. L. Battaglia, "Fractional state variable filter for system identification by fractional model," in *Proc. of the 6th IEEE European Control Conference (ECC)*, Porto, Portugal, 2001.

[281] D. Sierociuk and I. Petráš, "Modeling of heat transfer process by using discrete fractional-order neural networks," in *Proc. of the 16th International Conference on Methods and Models in Automation and Robotics (MMAR)*, Aug 2011, pp. 22–25.

[282] C. Zener, "Elasticity and anelasticity of metals," *University of Chicago Press*, 1948.

[283] G. Catania and S. Sorrentino, "Analytical modelling and experimental identification of viscoelastic mechanical systems," in *Advances in Fractional Calculus: Theoretical Developments and Applications in Physics and Engineering*, J. Sabatier, Ed. Springer, 2007, pp. 403–441.

[284] F. Mainardi and R. Gorenflo, "Time-fractional derivatives in relaxation processes: a tutorial survey," *Fractional Calculus and Applied Analysis*, vol. 10, no. 3, pp. 207–308, 2007.

[285] P. J. Torvik and R. Bagley, "On the appearance of the fractional derivatives in the behavior of real materials," *J. Appl. Mech*, vol. 51, pp. 294–298, 1984.

[286] H. Sheng and Y. Chen, "Optimal distributed-order fractional damping," in *Proceedings of FDA'10. The 4th IFAC Workshop Fractional Differentiation and its Applications.*, Badajoz, Spain, 2010.

[287] Y. Naranjani, Y. Sardahi, Y. Chen, and J.-Q. Sun, "Multi-objective optimization of distributed-order fractional damping," *Communications in Nonlinear Science and Numerical Simulation*, vol. 24, no. 1, pp. 159–168, 2015.

[288] O. Ozgen, S. Sumengen, M. Kallmann, C. F. Coimbra, and S. Balcisoy, "Simulating colliding flows with fractional derivatives," *Computer Animation and Virtual Worlds (CAVW)*, vol. 24, pp. 511–523, 2013.

[289] E. D. Brown, O. Ozgen, and M. Kallman, "Simulating shear thickening fluids with fractional derivatives," Fractional Calculus Day at MESA Lab, UC Merced, [Online] https://mechatronics.ucmerced.edu/sites/mechatronics.ucmerced.edu/files/page/documents/fractionalcalculusday_ebrown.pdf, Jun 2013.

[290] M. A. Lieberman and A. J. Lichtenberg, *Principles of Plasma Discharges and Materials Processing*, 2nd ed. John Wiley & Sons, 2005.

[291] D. A. Gurnett and A. Bhattacharjee, *Introduction to Plasma Physics: with Space and Laboratory Applications*. Cambridge University Press, 2005.

[292] S. E. Frier, "Using a plasma torch to clean your teeth," *The Economist print edition*, 2009.

[293] A. C. Wu, M. A. Lieberman, and J. P. Verboncoeur, "A method for computing ion energy distributions for multifrequency capacitive discharges," *J. Appl. Phys.*, vol. 101, no. 5, pp. 056 105–056 105–3, 2007.

[294] V. Uchaikin and R. Sibatov, *Fractional Kinetics in Solids: Anomalous Charge Transport in Semiconductors, Dielectrics and Nanosystems*. World Scientific Publishing Company, 2013.

[295] B. P. Wood, A. Lieberman, and A. J. . Lichtenberg, "Stochastic electron heating in a capacitive RF discharge with non-Maxwellian and time-varying distributions," *IEEE Transactions on Plasma Science*, vol. 23, no. 1, pp. 89–96, 1995.

[296] D. Summers and R. M. Thorne, "The modified plasma dispersion function," *Phys. Fluids B*, vol. 8, no. 3, pp. 1835–1847, 1991.

[297] K. S. Cole and R. H. Cole, "Dispersion and absorption in dielectrics - I. alternating current characteristics," *J. Chem. Phys.*, vol. 9, pp. 341–352, 1941.

[298] R. R. Nigmatullin and Y. E. Ryabov, "Cole-Davidson dielectric relaxation as a self-similar relaxation process," *Phys. Solid State*, vol. 39, no. 1, pp. 87–90, 1997.

[299] L. Ljung, *System Identification: Theory for the User*. Prentice-Hall, Inc., 1999.

[300] M. Muddu, A. Narang, and S. C. Patwardhan, "Development of ARX models for predictive control using fractional order and orthonormal basis filter parametrization," *Ind. Eng. Chem. Res.*, vol. 48, no. 19, pp. 8966–8979, 2009.

[301] ——, "Reparametrized ARX models for predictive control of staged and packed bed distillation columns," *Control Engineering Practice*, vol. 18, no. 2, pp. 114–130, 2010.

[302] T. Poinot and J. C. Trigeassou, "Parameter estimation of fractional models: application to the modeling of diffusive systems," in *Proc. of the The 15th IFAC World Congress*, Barcelona, Spain, 2002.

[303] H. Garnier and L. Wang, Eds., *Identification of Continuous-time Models from Sampled Data*. London: Springer-Verlag, 2008, ch. Refined Instrumental Variable Identification of Continuous-time Hybrid Box-Jenkins Models, pp. 91–131.

[304] P. S. Kokoszka and M. S. Taqqu, "Fractional ARIMA with stable innovations," *Stochastic Processes and Their Applications*, vol. 60, pp. 19–47, 1995.

[305] J. Mikleš and M. Fikar, Eds., *Process Modelling, Identification, and Control*. Berlin Heidelberg: Springer-Verlag, 2007.

[306] K. S. Holkar and L. M. Waghmare, "An overview of model predictive control," *International Journal of Control and Automation*, vol. 3, no. 4, pp. 47–64, 2010.

[307] K. M. Vu, Ed., *The ARIMA and VARIMA Time Series: Their Modelings, Analyses and Applications*. Ottawa, Canada: AuLac Technologies Inc, 2007.

[308] M. Viano, C. Deniau, and G. Oppenheim, "Continuous-time fractional ARMA processes," *Statistics & Probability Letters*, vol. 21, pp. 232–336, 1994.

[309] J. Schoukens, R. Pintelon, and Y. Rolain, *Mastering System Identification in 100 Exercises*. John Wiley & Sons, 2012.

[310] R. Pintelon and J. Schoukens, *System Identification: A Frequency Domain Approach*, 2nd ed. Wiley-IEEE Press, 2012.

[311] S. Oukacine, T. Djamah, S. Djennoune, R. Mansouri, and M. Bettayeb, "Multi-model identification of a fractional nonlinear system," in *Proc. of the 6th Workshop on Fractional Differentiation and Its Applications*, Grenoble, France, 2013, pp. 48–53.

[312] A. Djouambi, A. Charef, and A. Voda, "Numerical simulation and identification of fractional systems using digital adjustable fractional order integrator," in *Proc. of the 2013 European Control Conference (ECC)*, Zürich, Switzerland, 2013.

[313] M. Tavakoli, M. Tavazoei, and M. Afshi, "Parameter and order estimation from noisy step response data," in *Proc. of the 6th Workshop on Fractional Differentiation and Its Applications (FDA) and IFAC Joint Conference SSSC*, France, 2013.

[314] D. Liu, T.-M. Laleg-Kirati, O. Gibaru, and W. Perruquetti, "Identification of fractional order systems using modulating functions method," in *Proc. of the 2013 American Control Conference (ACC)*, Washington, DC, USA, 2013.

[315] I. Petráš, D. Sierociuk, and I. Podlubny, "Identification of parameters of a half-order system," *IEEE Transactions on Signal Processing*, vol. 60, no. 10, pp. 5561–5566, 2012.

[316] H. Malek, Y. Luo, and Y. Chen, "Identification and tuning fractional order proportional integral controllers for time delayed systems with a fractional pole," *Mechatronics*, vol. 23, no. 7, pp. 746–754, 2013.

[317] S. Zhou, J. Cao, and Y. Chen, "Genetic algorithm-based identification of fractional-order systems," *Entropy*, vol. 15, pp. 1624–1642, 2013.

[318] L. Meng, D. Wang, and P. Han, "Identification of fractional order system using particle swarm optimization," in *Proc. of the 2012 International Conference on Machine Learning and Cybernetics*, Xi'an, China, 2012.

[319] H. Akaike, "A new look at the statistical model identification," *IEEE Transactions on Automatic Control*, vol. 19, no. 6, pp. 716–723, 1974.

[320] K. Aho, D. Derryberry, and T. Peterson, "Model selection for ecologists: the worldviews of AIC and BIC," *Ecology*, vol. 95, pp. 631–636, 2014.

[321] M. Tavakoli-Kakhki and M. S. Tavazoei, "Estimation of the order and parameters of a fractional order model from a noisy step response data," *ASME Journal of Dynamic Systems, Measurement and Control*, vol. 136, no. 3, pp. 031 020–1–7, 2014.

[322] Z. Li, "Fractional order scanning," [online] (Matlab Central) http://www.mathworks.com/matlabcentral/fileexchange/52061, 2015.

[323] C. C. Hang, K. J. Åström, and Q. G. Wang, "Relay feedback auto-tuning of process controllers - a tutorial review," *Journal of Process Control*, vol. 12, pp. 143–162, 2002.

[324] K. J. Åström, T. H. Lee, K. K. Tan, and K. H. Johansson, "Recent advances in relay feedback methods - a survey," in *Proc. of the IEEE International Conference on Systems, Man and Cybernetics (Intelligent Systems for the 21st Century)*, vol. 3, 1995.

[325] I. Boiko, *Non-parametric tuning of PID controllers: a modified relay-feedback-test approach*, ser. Series in Advances in Industrial Control. New York: Springer, 2013.

[326] J. Byeon, J. Kim, S. W. Sung, and J. Lee, "Fractional order integrator for the relay feedback identification of a process Nyquist point in the third quadrant," *Korean J. Chem. Eng.*, vol. 28, no. 12, pp. 2227–2229, 2011.

[327] J. Lee, S. Sung, and T. F. Edgar, "Integrals of relay feedback responses for extracting process information," *AIChE Journal*, vol. 53, no. 9, pp. 2329–2338, 2007.

[328] A. J. Brzezinski, S. L. Kukreja, J. Ni, and D. S. Bernstein, "Identification of sensor-only MIMO pseudo transfer functions," in *Proc. of the 50th IEEE Conference on Decision and Control and European Control Conference (CDC-ECC)*, 2011, pp. 2154–2159.

[329] J. P. Schwartz, H. H. Sawin, and T. A. Hatton, "Frequency response analysis of nonsuperimposable systems using a pseudo transfer function: application to system with coverage-dependent adsorption," *Chem. Eng. Sci.*, vol. 41, no. 3, pp. 495–510, 1986.

[330] D. P. Atherton, *The describing functions, Chapter 3, Nonlinear Control Engineering.* Van Nostrand Reinhold Company, 1982.

[331] G. J. Thaler and M. P. Pastel, *Analysis and design of nonlinear feedback control systems.* New York, USA: McGraw-Hill, Inc., 1962.

[332] K. J. Åström and T. H. Hägglund, "Automatic tuning of simple regulators with specifications on phase and amplitude margins," *Automatica*, vol. 20, no. 5, pp. 645–651, 1984.

[333] W. L. Luyben, "Derivation of transfer functions for highly nonlinear distillation column," *Ind. Eng. Chem. Res.*, vol. 26, pp. 2490–2495, 1987.

[334] S. Shen, J. Wu, and C. Yu, "Use of biased-relay feedback for system identification," *AIChE Journal*, vol. 42, no. 4, pp. 1174–1180, 1996.

[335] Q. Wang, T. Lee, and L. Chong, *Relay feedback: analysis, identification and control.* Springer, 2003.

[336] C. C. Yu, *Autotuning of PID controllers: a relay feedback approach.* Springer, 2006.

[337] K. Tan, T. L. ang, and Q. G. Wang, "Enhanced automatic tuning procedure for process control of PI/PID controllers," *AIChE Journal*, vol. 42, no. 9, pp. 2555–2562, 1996.

[338] K. J. Åström and T. H. Hägglund, *PID Controllers: Theory, Design, and Tuning*, 2nd ed. Research Triangle Park, North Carolina: Instrument Society of America, 1995.

[339] M. Vítečková and A. Víteček, *Engineering the Future.* InTech, 2010, ch. 12 Plant identification by relay method, pp. 241–256.

[340] M. Friman and K. V. Waller, "A two-channel relay for auto-tuning," *Ind. Eng. Chem. Res*, vol. 36, no. 9, pp. 2662–2671, 1997.

[341] Q. G. Wang, C. C. Hang, and B. Zou, "Low-order modeling from relay feedback," *Ind. Eng. Chem. Res*, vol. 36, no. 2, pp. 375–381, 1997.

[342] Q. Bi, Q. G. Wang, and C. C. Hang, "Relay-based estimation of multiple points on process frequency response," *Automatica*, vol. 33, no. 9, pp. 1753–1757, 1997.

[343] R. Caponetto, G. Maione, A. Pisano, M. R. Rapaić, and E. Usai, "Analysis and shaping of the self-sustained oscillations in relay controlled fractional-order systems," *Fractional Calculus and Applied Analysis*, vol. 16, no. 1, pp. 93–108, 2013.

[344] W. Li, E. Eskinat, and W. L. Luyben, "An improved autotune identification method," *Ind. Eng. Chem. Res*, vol. 30, pp. 1530–1541, 1991.

[345] S. Majhi, "Relay based identification of processes with time delay," *Journal of Process Control*, vol. 17, pp. 93–101, 2007.

[346] R. S. Barbosa and J. A. T. Machado, "Fractional describing function analysis of systems with backlash and impact phenomena," in *Proc. of the 6th International Conference on Intelligent Engineering Systems 2002*, Opatija, Croatia, 2002, pp. 521–526.

[347] O. Cois, A. Oustaloup, E. Battaglia, and J. L. Battaglia, "Non integer model from modal decomposition for time domain system identification," in *Proc. of the 12th IFAC Symposium on System Identification*, Santa Barbara, CA, USA, 2000, pp. 989–994.

[348] O. Nelles, *Nonlinear System Identification: From Classical Approaches to Neural Networks.* Berlin, Heidelberg: Springer-Verlag, 2001.

[349] S. A. Billings, *Nonlinear System Identification: NARMAX Methods in the Time, Frequency, and Spatio-Temporal Domains.* Berlin, Heidelberg: Wiley, 2013.

[350] M. Schetzen, *The Volterra and Wiener Theories of Nonlinear Systems.* Berlin, Heidelberg: Wiley, 1980.

[351] S. Hadjiloucas and R. K. H. Galvão, "Fractional order and non-linear system identification algorithms for biomedical applications," *Journal of Physics*, vol. Conference Series 490, 2nd Intl. Conf. on Mathematical Modeling in Physical Sciences, 2014.

[352] M. Aoun, R. Malti, O. Cois, and A. Oustaloup, "System identification using fractional Hammerstein models," in *Proc. of the 15th Triennial World Congress*, Barcelona, Spain, 2002, pp. 1028–1033.

[353] Y. Zhao, Y. Li, and Y. Chen, "Complete parametric identification of fractional order Hammerstein systems," in *Proc. of the 2014 International Conference on Fractional Differentiation and Its Applications (ICFDA)*, Catania, Italy, June 2014, pp. 1–6.

[354] Y. Li, L. Zhai, Y. Chen, and H. Ahn, "Fractional-order iterative learning control and identification for fractional-order Hammerstein system," in *Proc. of the 11th World Congress on Intelligent Control and Automation*, Jul 2014, pp. 840–845.

[355] L. Vanbeylen, "A fractional approach to identify Wiener-Hammerstein systems," *Automatica*, vol. 50, pp. 903–909, 2014.

[356] C. Li and Y. Ma, "Fractional dynamical system and its linearization theorem," *Nonlinear Dynmics*, vol. 71, pp. 621–633, 2013.

[357] P. Hartman, "On the local linearization of differential equations," *Proc. Am. Math. Soc.*, vol. 14, no. 4, pp. 568–573, 1963.

[358] M. A. Henson and D. D. Esborg, *Nonlinear Process Control.* Prentice Hall, 1997.

[359] V. Pommier, P. Lanusse, J. Sabatier, and A. Oustaloup, "Input-output linearization and fractional robust control of a non-linear system," in *Proc. of the 2011 European Control Conference (ECC)*, Porto, Portugal, Sep 2001.

[360] J. P. Krisch, "Fractional Israel layers," *J. Math. Phys*, vol. 47, 2006.

[361] A. A. Kilbas, H. M. Srivastava, and J. J. Trujillo, *Theory and Applications of Fractional Differential Equations.* Elsevier, 2006.

[362] Y. Li and Y. Chen, "Fractional order universal adaptive stabilization for fractional order MIMO systems," in *Proc. of the 4th IFAC Workshop Fractional Differentiation and its Applications*, Badajoz, Spain, 2010.

[363] S. Victor, P. Melchior, D. Nelson-Gruel, and A. Oustaloup, "Flatness control for linear fractional MIMO systems: thermal application," in *Proceddings of the 3rd IFAC Workshop on Fractional Differentiation and Its Application*, Ankara, Turkey, 2008, pp. 5–7.

[364] D. Matignon and B. d'Andréa Novel, "Some results on controllability and observability of finite-dimensional fractional differential systems," in *Computational Engineering in Systems Applications*, 1996, pp. 952–956.

[365] Y. Chen, H. S. Ahn, and D. Xue, "Robust controllability of interval fractional order linear time invariant systems," *Signal Processing*, vol. 86, no. 5, pp. 2794–2802, 2006.

[366] G. Acioli and P. Barros, "Evaluation and redesign of decouplers for TITO processes using relay experiment," in *Proc. of the IEEE International Conference on Control Applications (CCA)*, Denver, CO, USA, 2011.

[367] Z. Li and Y. Chen, "Ideal, simplified and inverted decoupling of fractional order TITO processes," in *Proc. of the 19th IFAC World Congress*, Cape Town, South Africa, 2014.

[368] V. Kučera, "Optimal decoupling controllers for singular systems," in *Proc. of the 2013 European Control Conference (ECC)*, Zürich, Switzerland, 2013, pp. 306–311.

[369] C. A. Lin, "Necessary and sufficient conditions for existence of decoupling controllers," *IEEE Transactions on Automatic Control*, vol. 42, no. 8, pp. 1157–1161, 1997.

[370] H. Wade, "Inverted decoupling: a neglected technique," *ISA Transactions*, vol. 36, pp. 3–10, 1997.

[371] Q. G. Wang, B. Huang, and X. Guo, "Auto-tuning of TITO decoupling controllers from step tests," *ISA Transactions*, vol. 39, pp. 407–418, 2000.

[372] P. K. Padhy and S. Majhi, "Identification of TITO processes," in *Proc. of the IEEE Intl. Conf. on Industrial Technology (ICIT)*, Mumbai, India, 2006, pp. 664–669.

[373] S. Skogestad and I. Postlethwaite, *Multivariable feedback control: analysis and design*, 2nd ed. England: John Wiley & Sons, 2007.

[374] R. Farrell and A. Polli, "Comparison of unconstrained dynamic matrix control to conventional feedback control for a first order model," *Adv. Instr. Cont. Proc., ISA Trans on*, vol. 45, no. 2, pp. 1033–1046, 1990.

[375] M. L. Darby and M. Nikolaou, "MPC: Current practice and challenges," *Control Engineering Practice*, vol. 20, pp. 328–342, 2012.

[376] P. Falugi, "Model predictive control for tracking randomly varying references," *International Journal of Control*, vol. 88, no. 4, pp. 745–753, 2015.

[377] J. L. Jerez, P. J. Goulart, S. Richter, G. A. Constantinides, E. C. Kerrigan, and M. Morari, "Embedded predictive control on an FPGA using the fast gradient method," in *Proc. of the 2013 European Control Conference (ECC)*, Zürich, Switzerland, 2013, pp. 3614–3620.

[378] C. E. GarcíA, D. M. Prett, and M. Morari, "Model predictive control: Theory and practice a survey," *Automatica*, vol. 25, no. 3, pp. 335–348, 1989.

[379] S. J. Qin and T. A. Badgwell, "A survey of industrial model predictive control technology," *Control Engineering Practice*, vol. 11, pp. 733–764, 2003.

[380] M. Romero, A. P. de Madrid, C. M. noso, and R. Hernndez, "Application of generalized predictive control to a fractional order plant," in *Proceedings of the ASMD/IDETC 07'*, Las Vegas, NV, USA, 2007, pp. 1285–1292.

[381] M. Romero, A. P. de Madrid, C. M. noso, V. Milanés, , and B. M. Vinagre, "Fractional-order generalized predictive control: Application for low-speed control of gasoline-propelled cars," *Mathematical Problems in Engineering*, vol. Article ID 895640, p. 10 pages, 2013.

[382] A. Rhouma, B. Bouzouita, and F. Bouani, "Practical application of model predictive control to fractional thermal system," in *Proc. of the 2013 Second International Conference on Informatics and Applications (ICIA)*, Sept 2013, pp. 222–227.

[383] Z. Deng, H. Cao, X. Li, J. Jiang, J. Yang, and Y. Qin, "Generalized predictive control for fractional order dynamic model of solid oxide fuel cell output power," *Journal of Power Sources*, vol. 195, pp. 8097–8103, 2010.

[384] M. Romero, A. P. de Madrid, C. M. noso, , and B. M. Vinagre, "A survey of fractional-order generalized predictive control," in *Proc. of the IEEE 51st Annual Conference on Decision and Control (CDC)*, Maui, HI, USA, Dec 2012, pp. 6867–6872.

[385] T. Zhao, Y. Chen, and Z. Li, "Fractional order nonlinear model predictive control using RIOTS_95," in *Proc. of the International Conference on Fractional Differentiation and Its Applications (ICFDA)*, Catania, Italy, 2014.

[386] W. H. Kwon and S. Han, *Receding Horizon Control*. London: Springer-Verlag, 2005.

[387] H. Fukushima, T. Kim, and T. Sugie, "Adaptive model predictive control for a class of constrained linear systems based on comparison model," *Automatica*, vol. 43, no. 2, pp. 301–308, 2007.

[388] O. P. Agrawal, "A general formulation and solution scheme for fractional optimal control problems," *Nonlinear Dynamics*, vol. 38, no. 1, pp. 323–337, 2004.

[389] C. Tricaud and Y. Chen, "Time-optimal control of systems with fractional dynamics," *International Journal of Differential Equations*, vol. Article ID 461048, p. 16 pages, 2010.

[390] ——, "An approximate method for numerically solving fractional order optimal control problems of general form," *Journal of Computers and Mathematics with Applications*, vol. 59, pp. 1644–1655, 2010.

[391] N. H. Sweilam, T. M. Al-Ajami, and R. H. W. Hoppe, "Numerical solution of some types of fractional optimal control problems," *Hindawi Publishing Corporation*, vol. 2013, no. Article ID 306237, p. 9 pages, 2013.

[392] A. Dzieliński and P. M. Czyronis, "Fixed final time and free final state optimal control problem for fractional dynamic systems - linear quadratic discrete-time case," *Bulletin of the Polish Academy of Sciences: Technical Sciences*, vol. 61, no. 3, pp. 681–690, 2013.

[393] A. Dzieliński and P. M. Czyronis, "Optimal control problem for fractional dynamic systems linear quadratic discrete-time case," *Theory & Appl. of Non-integer Order Syst*, vol. LNEE 257, pp. 87–97, 2013.

[394] O. P. Agrawal, "A quadratic numerical scheme for fractional optimal control problems," *ASME Journal of Dynamic Systems, Measurement, and Control*, vol. 130, no. 1, pp. 011 010–1–6, 2008.

[395] J. T. Betts, "SOCS: the sparse optimal control software family," Tech. Rep., 1996.

[396] O. V. Stryk, "DIRCOL: a direct collocation method for the numerical solution of optimal control problems," Tech. Rep., 1997.

[397] L. S. Jennings, M. E. Fisher, K. L. Teo, and C. J. Goh, "MISER3: software for solving optimal control problems," Tech. Rep., 1997.

[398] J. T. Betts, "Survey of numerical methods for trajectory optimization," *Journal of Guidance, Control and Dynamics*, vol. 21, no. 2, pp. 193–207, 1998.

[399] A. V. Rao, "A survey of numerical methods for optimal control," *Advances in the Astronautical Sciences*, vol. 1, pp. 497–528, 2009.

[400] B. A. Conway, "A survey of methods available for the numerical optimization of continuous dynamic systems," *J Optim Theory Appl*, vol. 152, pp. 271–306, 2012.

[401] H. S. Rodrigues, M. T. T. Monteiro, and D. F. M. Torres, *Systems Theory: Perspectives, Applications and Developments*. Nova Science Publishers, 2014, ch. Optimal Control and Numerical Software: an Overview.

[402] A. L. Schwartz, "Theory and implementation of numerical methods based on Runge-Kutta integration for solving optimal control problems," Ph.D. dissertation, EECS Department, University of California, Berkeley, 1996.

[403] K. Radhakrishnan and A. C. Hindmarsh, "Description and use of LSODE, the Livermore solver for ordinary differential equations," *NASA Reference Publ*, vol. 1327, 1993.

[404] P. Gill, W. Murray, M. Saunders, and M. Wright, "NPSOL," Stanford Business Software, Inc, 2015.

[405] A. Griewank, D. Juedes, and J. Utke, "ADOL-C: A package for the automatic differentiation of algorithms written in C/C++," Argonne National Laboratory, Dec, 1993.

[406] Y. Chen and A. Schwartz, "RIOTS_95: a MATLAB toolbox for solving general optimal control problems and its applications to chemical processes," *http://www.optimization-online.org/DB_FILE/2002/11/567.pdf*, 2002.

[407] J. Liang, R. Fullmer, and Y. Chen, "Time-optimal magnetic attitude control for small spacecraft," in *Proc. of the 43rd IEEE Conference on Decision and Control*, Atlantis, Paradise Island, Bahamas, 2004.

[408] C. Tricaud and Y. Chen, "Linear and nonlinear model predictive control using a general purpose optimal control problem solver RIOTS_95," in *Proc. of the Chinese Control and Decision Conference (CCDC) 2008*. IEEE, 2008, pp. 1552–1557.

[409] ——, "Solving fractional order optimal control problems in RIOTS_95 - a general-purpose optimal control problem solver," in *Proceedings of the 3rd IFAC Workshop on Fractional Differentiation and Its Applications*, Ankara, Turkey, 2008.

[410] A. Schwartz, E. Polak, and Y. Chen, *RIOTS_95: a Matlab Toolbox for Solving Optimal Control Problems - Version 1.0 for Windows*, 333 Quinterra Ln. Danville, CA, USA, 1997.

[411] S. H. Hosseinnia, R. Ghaderi, N. A. Ranjbar, M. Mahmoudian, and S. Momani, "Sliding mode synchronization of an uncertain fractional order chaotic system," *Comput. Appl. Math.*, vol. 59, pp. 1637–1643, 2010.

[412] M. S. Tavazoei and M. Haeri, "Synchronization of chaotic fractional-order systems via active sliding mode controller," *Phys. A*, vol. 387, pp. 57–70, 2008.

[413] S. Drakunov, U. Özgüner, P. Dix, and B. Ashrafi, "ABS control using optimum search via sliding modes," *IEEE Trans Control Syst Technol*, vol. 3, pp. 79–85, 1995.

[414] T. Oliveira, A. Peixoto, E. Nunes, and L. Hsu, "Global real-time optimization by output-feedback extremum-seeking control with sliding modes," *J the Franklin Inst*, vol. 349, pp. 1397–1415, 2012.

[415] C. Yin, Z. Li, Y. Chen, and S. Zhong, "Fractional order sliding mode control based on fractional order reaching law: reaching condition analysis and experimental validation," in *Proc. of the 2013 ASME IDETC/CIE*, Portland, OR, USA, 2013.

[416] S. L. Brunton, C. W. Rowley, S. R. Kulkarni, and C. Clarkson, "Maximum power point tracking for photovoltaic optimization using ripple-based extremum seeking control," *IEEE Trans. on Power Electronics*, vol. 25, no. 10, pp. 2531–2540, 2010.

[417] C. Yin, B. Stark, S. Zhong, , and Y. Chen, "Design global extremum seeking control with sliding mode for output-feedback tracking of nonlinear systems," in *Proc. of the 51th IEEE Conference on Decision and Control and European Control Conference (CDC-ECC)*, 2012, pp. 7113–7118.

[418] D. Valério and J. S. da Costa, "Tuning of fractional PID controllers with Ziegler-Nichols type rules," *Signal Processing*, vol. 86, no. 10, pp. 2771–2784, 2006.

[419] P. Lino and G. Maione, "Loop-shaping and easy tuning of fractional-order proportional integral controllers for position servo systems," *Asian Journal of Control*, vol. 15, no. 3, pp. 796–705, 2013.

[420] Y. Luo, Y. Chen, C. Wang, and Y. Pi, "Tuning fractional order proportional integral controllers for fractional order systems," *Journal of Process Control*, vol. 20, pp. 823–831, 2010.

[421] D. Xue and Y. Chen, "A comparative introduction of four fractional order controllers," in *Proceedings of the 4th IEEE World Congress on Intelligent Control and Automation*, Shanghai, China, 2002, pp. 3228–3235.

[422] D. Xue, C. Zhao, and Yangquan, "Fractional order PID control a DC-motor with elastic shaft: a case study," in *Proc. of the 2006 American control conference (ACC)*, Minnesota, USA, 2006, pp. 3182–3188.

[423] C. Monje, B. Vinagre, G. Santamara, and I. Tejado, "Auto-tuning of fractional order PID controllers using a PLC," in *Proc. of the 14th IEEE ETFA conference*, Palma de Mallorca, 2009.

[424] F. Padula and A. Visioli, *Advances in Robust Fractional Control*. Switzerland: Springer, 2015.

[425] M. H. Basiri and M. S. Tavazoei, "On robust control of fractional order plants: Invariant phase margin," *ASME. J. Comput. Nonlinear Dynam*, vol. 10, no. 5, pp. 263–270, 2015.

[426] V. Feliu-Batlle, R. Rivas-Perez, and F. J. Castillo-Garcia, "Robust fractional-order temperature control of a steel slab reheating furnace with large time delay uncertainty," in *Proc. of the 2014 International Conference on Fractional Differentiation and Its Applications (ICFDA)*, Catania, Italy, 2014.

[427] Y. Li, Y. Chen, H. S. Ahn, and G. Tian, "A survey on fractional-order iterative learning control," *J Optim Theory Appl*, vol. 156, pp. 127–140, 2013.

[428] H. Chao, Y. Luo, L. Di, and Y. Chen, "Roll-channel fractional order controller design for a small fixed-wing unmanned aerial vehicle," *Control Engineering Practice*, vol. 18, no. 7, pp. 761–772, 2010.

[429] Y. Luo, H. Chao, L. Di, and Y. Chen, "Lateral directional fractional order PI$^\alpha$ control of a small fixed-wing UAV: Controller designs and flight tests," *IET Control Theory and Applications*, vol. 18, no. 5, pp. 2156–2167, 2011.

[430] P. R. Barros, G. A. Júnior, and J. B. M. dos Santos, "Two-input two-output laboratory-scale temperature system based on Peltier modules," in *Proceedings of the 17th World Congress, The International Federation of Automatic Control*, Seoul, Korea, 2008.

[431] MathWorks Classroom Resources Team, "Matlab support package for Arduino (aka ArduinoIO package)," Latest update: 2013. [Online]. Available: http://www.mathworks.com/matlabcentral/fileexchange/32374

[432] B. Stark, Z. Li, B. Smith, and Y. Chen, "Take-home mechatronics control labs: a low-cost personal solution and educational assessment," in *Proc. of the 2013 ASME IDETC/CIE*, Portland, OR, 2013.

[433] Tellurex Corporation, "The most frequently asked questions about thermo-electric cooling," Technical white paper, [online] http://tellurex.com/products/multistage-thermoelectric-modules/, 2006.

[434] M. Macias and D. Sierociuk, "Fractional order calculus for modeling and fractional PID control of the heating process," in *Proc. of the 13th International Carpathian Control Conference (ICCC)*, 2012, pp. 452–457.

[435] Jippie, "How to drive a Peltier element," 2012. [Online]. Available: http://electronics.stackexchange.com/questions/28634/how-to-drive-a-peltier-element

[436] Z. Li, "I2C block for ArduinoIO Simulink package," [online] (Matlab Central) http://www.mathworks.com/matlabcentral/fileexchange/41602, 2013.

[437] R. K. Wood and M. W. Berry, "Terminal composition control of binary distillation column," *Chem. Eng. Sci.*, pp. 1707–1717, 1973.

[438] K. Srinivasan and M. Chidambaram, "An improved autotune identification method," *Chem. Biochem. Eng. Q*, vol. 18, no. 3, pp. 249–256, 2004.

[439] F. Mainardi, "Fractional relaxation and diffusion equations of distributed order," Lecture slides for the FC Day at UC Merced. [Online], http://mechatronics.ucmerced.edu/node/68, 2013.

[440] P. Bellan, *Fundamentals of plasma physics*. Cambridge University Press, 2008.

[441] C Zhang and R. Ordóñez, *Extremum-seeking control and applications: a numerical optimization-based approach*. London: Springer-Verlag, 2012.

[442] C. Zhang, L. Wong, K. Ramaswamy, J. Cruse, and H. Hanawa, "Plasma reactor with RF generator and automatic impedance match with minimum reflected power-seeking control," US Patent Application #: 2011/0009999 A1, Jan 2011.

[443] Y. M. Kagan and V. I. Perel, "Probe methods in plasma research," *Sov. Phys. Usp*, vol. 6, pp. 767–793, 1964.

[444] D. D. Blackwell, D. N. Walker, and W. E. Amatucci, "Measurement of absolute electron density with a plasma impedance probe," *Rev. Sci. Instrum*, vol. 76, pp. 023 503–1–6, 2005.

[445] A. Schwabedissen, E. Benck, and J. Roberts, "Langmuir probe measurements in an inductively coupled plasma source," *Phys. Rev. E*, vol. 55, pp. 3450–3459, 1997.

[446] S. Lynn, "Virtual metrology for plasma etch processes," Ph.D. dissertation, National University of Ireland, Maynooth, Ireland, 2011.

[447] J. V. Ringwood, S. Lynn, G. Bacelli, B. Ma, E. Ragnoli, and S. McLoone, "Estimation and control in semiconductor etch: Practice and possibilities," *IEEE Trans. on Semiconductor Manufacturing*, vol. 23, no. 1, pp. 87–98, 2010.

[448] M. A. Sobolewski, "Noninvasive monitoring of ion energy drift in an inductively coupled plasma reactor," *J. Appl. Phys.*, vol. 97, no. 3, 2005.

[449] B. V. Somov, *Plasma astrophysics. Part I: Fundamentals and Practice*. Springer, 2006.

[450] M. Jayaram, "Architecture, modeling and analysis of a plasma impedance probe," Ph.D. dissertation, Utah State University, Logan, UT, USA, 2010.

[451] V. A. Godyak, *Soviet radio frequency discharge research*. Falls Church, VA.: Delphic Associates, 1986.

[452] Y. Kim and N. Yoon, "Calculation of the reactor impedance for capacitively coupled plasma sources," *Journal of the Korean Physical Society*, vol. 55, no. 5, pp. 1855–1859, 2009.

[453] K. Ukai and K. Hanazawa, "End-point determination of aluminum reactive ion etching by discharge impedance monitoring," *J. Vac. Sci. Technol.*, vol. 16, no. 385, pp. 385–387, 1979.

[454] Advanced Energy Industries Inc., "Impedance matching," White paper, 2008.

[455] L. Besser and R. Gilmore, *Practical RF circuit design for modern wireless systems, Chapters 2 and 5*. Artech House, 2003.

[456] V. Todorow, "Impedance matching and matching networks," Applied Materials Inc. Slide tutorial, 2003.

[457] J. D. Faires and R. L. Burden, *Numerical Methods*, 3rd ed. Cengage Learning, 2004.

[458] Z. Li, "A multi-agent based approach for solving the redundancy allocation problems," Master's thesis, Department of Electrical and Computer Engineering, Temple University, Philadelphia, PA, USA, 2011.

[459] R. Bellman, *Dynamic Programming*. Princeton University Press, Dover Paperback Reprint, 2003.

[460] T. H. Cormen, C. E. Leiserson, R. L. Rivest, and C. Stein, *Introduction to Algorithms*, 3rd ed. The MIT Press, 2009.

[461] Z. Li, "Particle swarm optimization using Lévy distribution," [online] (Matlab Central) http://www.mathworks.com/matlabcentral/fileexchange/50277, 2015.

[462] J. Kennedy and R. Eberhart, "Particle swarm optimization," in *Proc. of IEEE International Conference on Neural Networks IV*, 1995, pp. 1942–1948.

[463] M. Frame and N. Cohen, *Benoit Mandelbrot: A Life in Many Dimensions*. Princeton University Press, Dover Paperback Reprint, 2003.

[464] A. M. Reynolds, "Scale-free animal movement patterns: Lévy walks outperform fractional Brownian motions and fractional Lévy motions in random search scenarios," *Journal of Physics A: Mathematical and Theoretical*, vol. 42, pp. 434 006–1–11, 2009.

[465] E. J. S. Pires, J. A. T. Machado, P. B. de Moura Oliveira, J. B. Cunha, and L. Mendes, "Particle swarm optimization with fractional-order velocity," *Nonlinear Dynamics*, vol. 61, pp. 295–301, 2010.

[466] M. Couceiro and P. Ghamisi, *Fractional Order Darwinian Particle Swarm Optimization - Applications and Evaluation of an Evolutionary Algorithm*. Springer Briefs in Applied Sciences and Technology, 2016.

[467] D. Maiti and A. Konar, "Approximation of a fractional order system by an integer order model using particle swarm optimization technique," in *Proc. of the IEEE Sponsored Conference on Computational Intelligence, Control and Computer Vision in Robotics & Automation*, 2008.

[468] EtherCAT Technology Group, "EtherCAT - the Ethernet Fieldbus," [online] http://www.ethercat.org/pdf/english/ETG_Brochure_EN.pdf, 2013.

[469] O. I. Sheluhin, S. M. Smolskiy, and A. V. Osin, *Self-Similar Processes in Telecommunications*. John Wiley & Sons, 2007.

[470] W. Willinger, M. S. Taqqu, R. Sherman, and D. V.Wilson, "Self-similarity through high-variability: statistical analysis of Ethernet LAN traffic at the source level," *Networking, IEEE/ACM Transactions on*, vol. 5, no. 1, pp. 71–86, 1997.

[471] I. T. Balsera, "Some contributions in networked control systems based on fractional calculus," Ph.D. dissertation, Universidad de Extremadura, Spain, 2011.

[472] M. S. Taqqu, *Encyclopedia of Statistical Sciences*. New York: Wiley, 1988, ch. Self-similar processes, pp. 352–357.

[473] Beckhoff Automation Corperation, "The EtherCAT products," [online] http://www.beckhoff.com/, 2014.

[474] Wireshark, "The Wireshark official homepage," [online] https://www.wireshark.org/, 2014.

[475] X. Zheng and B. M. Chen, *Stock Market Modeling and Forecasting - A System Adaptation Approach*. London: Springer-Verlag, 2013.

[476] E. Scalas, R. Gorenflo, and F. Mainardi, "Fractional calculus and continuous-time finance," *Physica A*, vol. 284, no. 1-4, pp. 376–384, 2000.

[477] A. W. Lo, "Long-term memory in stock market prices," *Econometrica*, vol. 59, no. 5, pp. 1279–1313, 1991.

[478] R. Cont, *Fractals in Engineering: New Trends in Theory and Applications, Jacques Lévy-Véhel and Evelyne Lutton (Eds.)*. Springer, 2005, ch. Long range dependence in financial markets, pp. 159–179.

[479] H. Hurst, "Long term storage capacity of reservoirs," *Transactions of the American Society of Civil Engineers*, vol. 116, pp. 770–799, 1951.

[480] M. Benoît, *The Fractal Geometry of Nature*. San Francisco: W.H. Freeman, 1983.

[481] M. Douglas, *Trading in the Zone: Master the Market with Confidence, Discipline and a Winning Attitude*. Prentice Hall Press, 2001.

[482] Hubpages, "Do 95% of all traders lose?" [Online] http://marketstudent.hubpages.com/hub/Do-95-percent-of-all-traders-lose, 2011.

[483] I. Bezek, "FXCM: This equity is nearly worthless," Seeking Alpha [Online] http://seekingalpha.com/article/2842986, 2015.

[484] W. L. Andrew and A. C. MacKinlay, *A Non-Random Walk down Wall Street*. Princeton University Press, 1999.

[485] E. Scalas, "The application of continuous-time random walks in finance and economic," *Physica A*, vol. 225, no. 5, pp. 1279–1313, 2006.

[486] V. Niederhoffer, *The Education of a Speculator*. New York: John Wiley & Sons, 1998.

[487] S. R. Bentes and R. Menezes, "Entropy: A new measure of stock market volatility?" *Journal of Econometrics*, vol. 107, pp. 291–312, 2000.

[488] E. Maasoumi and J. Racine, "Entropy and predictability of stock market returns," *Journal of Econometrics*, vol. 107, pp. 291–312, 2000.

[489] R. D. Handscombe and E. A. Patterson, *The Entropy Vector: Connecting Science and Business*. World Scientific, 2004.

[490] P. Fiedor, "Maximum entropy production principle for stock returns," *ArXiv preprint arXiv:1408.3728, Quantitative Finance MEPP*, 2014.

[491] B. J. West, *Fractional Calculus View of Complexity - Tomorrow's Science*. CRC Press, 2015.

[492] ——, *Complex Worlds: Uncertain, Unequal and Unfair*. Black Rose Writing, 2012.

[493] National Climate Data Center (NCDC), "Extreme events," [online] http://www.ncdc.noaa.gov/climate-information/extreme-events, 2015.

[494] P. S. Laplace, *A Philosophical Essay on Probabilities*, 6th ed. New York: Dover Publications Reprints, translated into English from the original French by F. W Truscott and F. L. Emory, 1951.

[495] E. D. Brown, "Analysis of Twitter messages for sentiment and insight for use in stock market decision making," Ph.D. dissertation, Dakota State University, 2014.

[496] ——, "Trade the sentiment blog," [Online] http://blog.tradethesentiment.com/, 2015.

[497] A. L. Barabási, "The origin of bursts and heavy tails in human dynamics," *Nature*, vol. 435, no. 12, pp. 207–211, 2005.

[498] T. N. Bulkowski, *Encyclopedia of Chart Patterns*. John Wiley & Sons, 2005.

[499] B. J. West, M. Bologna, and P. Grigolini, *Physics of Fractal Operators*. New York: Springer Verlag, 2003.

[500] E. Bayraktar, H. V. Poor, and K. R. Sircar, "Estimating the fractal dimension of the S&P 500 index using wavelet analysis," *Int. J. Theor. Appl. Finan*, vol. 07, p. 615, 2004.

[501] B. Qian and K. Rasheed, "Hurst exponent and financial market predictability," *Int. J. Theor. Appl. Finan*, 2007.

[502] J. J. Murphy, *Technical Analysis of The Financial Markets*. New York Institute of Finance, 1999.

[503] R. Rhoads, *Trading VIX Derivatives: Trading and Hedging Strategies Using VIX Futures, Options, and Exchange Traded Notes*. Wiley, 2011.

[504] J. L. Gamboa, "Modeling and output feedback control of a floating ball inside a tube," Master's thesis, The University of Texas At San Antonio, 2012.

[505] J. Poovarasan, R. Kayalvizhi, and M.Aramudhan, "Design of fractional order controller using particle swarm optimization for a four tank level process," *International Journal of Engineering Sciences Research IJESR*, vol. 4, no. 2, pp. 895–901, 2013.

[506] D. Abdelhamid, T. Bouden, and A. Boulkroune, "Design of fractional-order sliding mode controller (FSMC) for a class of fractional-order non-linear commensurate systems using a particle swarm optimization (PSO) algorithm," *Journal of Control Engineering and Applied Informatics*, vol. 16, no. 3, pp. 46–55, 2014.

[507] E. N. Rosenwasser and B. P. Lampe, *Multivariable computer-controlled systems: a transfer function approach*. Springer, 2006.